A METHODOLOGY TO IMPROVE THE PROACTIVE MITIGATION OF HELICOPTER ACCIDENTS RELATED TO LOSS OF TAIL ROTOR EFFECTIVENESS

A Thesis
Presented to
The Academic Faculty

By

Paola Zanella

In Partial Fulfillment
of the Requirements for the Degree
Doctor of Philosophy in the
School of Aerospace Engineering

Georgia Institute of Technology

August 2021

A METHODOLOGY TO IMPROVE THE PROACTIVE MITIGATION OF HELICOPTER ACCIDENTS RELATED TO LOSS OF TAIL ROTOR EFFECTIVENESS

Approved by:

Professor Dimitri N. Mavris
School of Aerospace Engineering
Georgia Institute of Technology

Professor Lakshmi N. Sankar
School of Aerospace Engineering
Georgia Institute of Technology

Professor J. V. R. Prasad
School of Aerospace Engineering
Georgia Institute of Technology

Mr. Charles C. Johnson
Aviation Research Division
Federal Aviation Administration

Professor Daniel P. Schrage
School of Aerospace Engineering
Georgia Institute of Technology

Date Approved: July 28$^{\text{th}}$, 2021

ACKNOWLEDGMENTS

The completion of this work could not have been possible without the guidance and assistance of many. I would like to thank my advisor, Professor Dimitri Mavris, for allowing me to be part of the Aerospace Systems Design Laboratory. He provided me the opportunity to engage in meaningful research while guiding me in refining my critical thinking. I am deeply grateful to my co-advisor, Professor J.V.R. Prasad, for teaching me the challenging art of modeling helicopter flight dynamics. His technical supervision and invaluable support were essential to the delivery of this work. I also extend my gratitude to the other members of my thesis committee. Professor Daniel Schrage for his insights in rotorcraft operations, Professor Lakshmi Sankar for his feedback in rotorcraft aerodynamics, and Mr. Charles Johnson for encouraging me to deeply explore the challenges of rotorcraft safety.

Further, I would like to thank Dr. Chengjian He, Advanced Rotorcraft Technology Inc., for his technical feedback in the use of the rotorcraft simulation model FLIGHTLAB; Mr. Mark Dreier and Dr. Albert Brand, Bell Helicopter Textron Inc., for their support towards the development of the vortex ring emitter model; Dr. Etienne Demers-Bouchard, Georgia Institute of Technology, for his assistance in furthering my understanding of rotorcraft theory; Dr. Darshan Sarojini, Georgia Institute of Technology, for his suggestions during the formulation of the research.

Finally, I gratefully acknowledge the support for this work offered by the Federal Aviation Administration under Project No. 2 “Rotorcraft Aviation Safety Information Analysis and Sharing” of the FAA Center of Excellence for General Aviation, PEGASAS (Partnership to Enhance General Aviation Safety Accessibility and Sustainability).

TABLE OF CONTENTS

LIST OF TABLES

LIST OF FIGURES

LIST OF ACRONYMS

AC	Advisory Circular
ASIAS	aviation safety information analysis and sharing
CAA	Civil Aviation Authority
CCW	counterclockwise
C&RT	classification and regression tree
FAA	Federal Aviation Administration
FDM	flight data monitoring
FOQA	flight operational quality assurance
GMM	Gaussian mixture model
HFDM	helicopter flight data monitoring
ICAO	International Civil Aviation Organization
LOC	loss of control
LTE	loss of tail rotor effectiveness
MKAD	multiple kernel anomaly detection
NN	neural network
NTSB	National Transportation Safety Board
OGE	out of ground effect
RMSE	root mean squared error
RNN	recurrent neural network
SVM	support vector machine
TR	tail rotor
TRF	tail rotor failure
VRS	vortex ring state
YR	yaw rate

NOMENCLATURE

a	2-D lift curve slope of airfoil section
A	rotor disk area
$\boldsymbol{A}$	system matrix
$\boldsymbol{C}$	influence coefficient matrix
C_{d0}	profile drag coefficient
C_L	aerodynamic rolling moment coefficient
C_M	aerodynamic pitching moment coefficient
C_{Nf}	fuselage yaw moment coefficient
$C_{Nv}, C_{N\beta}$, etc.	normalized directional static stability derivatives
C_P	power coefficient
C_{Pc}	climb power coefficient
C_{Pi}	induced power coefficient
C_{P0}	profile power coefficient
C_{Pp}	parasitic power coefficient
$C_{Q,mr}$	main rotor torque coefficient
C_T	rotor thrust coefficient
C_{T0}	rotor thrust coefficient in hover-like flow condition
C_T/σ	main rotor blade loading coefficient
C_Y	side force coefficient
f	equivalent flat-plate area
$\boldsymbol{F_m}$	blade loading vector
g	acceleration due to gravity
I_{xx}, I_{yy}, I_{zz}	moments of inertia of the helicopter about the x-, y-, and z-axes
I_{xz}	product of inertia of the helicopter about the x- and z-axes
k	empirical inflow factor
k_x, k_y	longitudinal and lateral inflow gradients

l	length of influencing vortex filament
l	distance between rotor hub and center of gravity
$\boldsymbol{L}$	inflow influence coefficient matrix
L, M, N	body-axes aerodynamic and propulsive moments
l_f	fuselage reference length
L_f, M_f, N_f	fuselage aerodynamic moments about center of gravity
l_{hf}	distance between horizontal fin center of pressure and center of gravity
L_{hf}, M_{hf}, N_{hf}	horizontal fin aerodynamic moments about center of gravity
L_{mr}, M_{mr}, Q_{mr}	main rotor moments about center of gravity
L_{tr}, M_{tr}, N_{tr}	tail rotor moments about center of gravity
l_{vf}	distance between vertical fin center of pressure and center of gravity
L_{vf}, M_{vf}, N_{vf}	vertical fin aerodynamic moments about center of gravity
L'	lift generated by a blade unit span
m	aircraft mass
$\boldsymbol{M}$	apparent mass matrix
n_b	number of rotor blades
N_v, N_β	directional static stability derivatives
p, q, r	angular velocities in body axes
r	nondimensional radial distance
$\boldsymbol{r}$	position vector of a point in space
R	rotor radius
R	vortex ring radius
r_{core}	core radius of toroidal ring cross-section
S_f	fuselage side area
S_{vf}	vertical fin side area
T	rotor thrust
$\boldsymbol{u}$	control vector
u, v, w	translational velocities in body axes

U_P	total inflow velocity at the blade element
U_T	angular speed of the blade element
V	mass flow parameter
$\boldsymbol{v_B}$	translational velocity vector in body frame
v_c	axial component of the freestream velocity
V_f	total velocity incident on fuselage
v_h	rotor induced inflow velocity in hover-like flow condition
v_i	rotor induced inflow velocity
V_{ix}, V_{iz}	velocity components induced by vortex ring
V_{tip}	rotor blade tip speed
V_{vf}	total velocity incident on vertical fin
V_x, V_z	freestream inflow velocity components
V_∞	magnitude of relative airspeed
W	aircraft weight
$\boldsymbol{x}$	state vector
X, Y, Z	body-axes aerodynamic and propulsive forces
x_B, y_B, z_B	body-fixed axes system
x_e, y_e, z_e	position vector components
X_f, Y_f, Z_f	aerodynamic forces acting on fuselage
X_{hf}, Y_{hf}, Z_{hf}	aerodynamic forces acting on horizontal fin
X_{mr}, Y_{mr}, Z_{mr}	forces acting on main rotor hub
x_p, z_p	position coordinates of vortex ring element
X_{tr}, T_{tr}, Z_{tr}	forces acting on tail rotor hub
X_{vf}, Y_{vf}, Z_{vf}	aerodynamic forces acting on vertical fin
α	angle of attack
β	blade flapping angle
Γ	vortex circulation strength
δ_p	pedal control
θ	azimuth angle of vortex ring element
θ	blade pitch angle

θ_0	main rotor collective pitch angle
θ_{0tr}	tail rotor collective pitch angle
θ_{1c}	lateral cyclic pitch angle
θ_{1s}	longitudinal cyclic pitch angle
λ	inflow ratio
λ_c	climb inflow ratio
λ_i	induced inflow ratio
$\boldsymbol{\lambda_n}$	states of the flowfield
λ_x, λ_y	longitudinal and lateral inflow ratios
λ_0	mean induced inflow ratio
μ	advance ratio
ρ	air density
σ	rotor solidity
ϕ	inflow angle of attack
ϕ, θ, ψ	Euler angles
χ	wake skew angle
ψ	blade azimuth angle

Subscripts

e	equilibrium or trim condition
f	fuselage
hf	horizontal fin
mr	main rotor
tr	tail rotor
vf	vertical fin

SUMMARY

Loss of tail rotor effectiveness (LTE) has been recognized to be a major contributing factor in several helicopter accidents where pilots lost directional control. However, it has been noticed that different definitions of this phenomenon exist in the rotorcraft community. Further, the somewhat imprecise representation of LTE in some flight training simulators has led to its low awareness, placing pilots at a much higher risk for potential accidents. One significant method to specifically address those gaps and support rotorcraft safety involves the proactive mitigation of LTE via the analysis of flight data within the Helicopter Flight Data Monitoring (HFDM) program. Through this program, the pilots receive constant flight evaluation reports to promote improved LTE risk evaluations. The main method used for flight data analysis is the detection of safety metrics, i.e., predefined hazardous flight conditions. Nevertheless, a sufficiently reliable LTE safety metric still does not exist, leading to false or missed detections that degrade the quality of the overall safety analysis.

The objective of this thesis is to formulate a methodology to enhance the detection capability of the proximity to LTE within the HFDM program. This promotes the awareness of LTE within the rotorcraft community while supporting the proactive mitigation of helicopter accidents related to this critical helicopter safety threat. An alternative approach is used to develop a more reliable LTE safety metric, using a combination of physics-based simulations and machine learning techniques. First, a physics-based investigation is performed to enhance the understanding of the nature of the LTE. A more comprehensive LTE definition is proposed and analyzed, including three different aspects that can lead to LTE behavior, i.e., loss of weathercock stability, running out of pedal (tail rotor collective) for trim, and tail rotor vortex ring state. The modeling of the flight dynamics of each phenomenon is individually

analyzed to ensure an accurate physics-based representation of LTE. Further, the parameters that support the detection of LTE are investigated to enable the recognition and classification of each LTE phenomenon in simulation results. Ultimately, a physics-based investigation of the aircraft flight envelope is combined with the application of supervised learning techniques to develop the predictive models of the different LTE phenomena. This provides the operator with a physics-based LTE safety metric designed to detect the proximity to LTE without the need for a simulation model. The methodology is implemented using a generic nonlinear helicopter simulation model. To verify the enhanced capabilities of the final methodology, the physics-based LTE safety metric is compared against the LTE metric currently used within the HFDM program. The results confirm the improved detection of the proximity to LTE, validating the overarching hypothesis of this research and satisfying the research objective.

CHAPTER 1
MOTIVATION

Rotorcraft are a unique and valuable component within our modern aviation system. Their ability to hover and take-off and land vertically, along with their good low-speed handling qualities gives them great versatility and are just some of the examples that make rotorcraft an essential element in aviation. Because of these characteristics, rotorcraft are repeatedly used within challenging operating conditions. However, reducing the accident rate of rotorcraft continues to remain a challenge. Thus, it is of remarkable value to the aerospace industry to focus on enhancing rotorcraft safety [76].

1.1 The Threat of Loss of Tail Rotor Effectiveness (LTE)

Handling qualities degradations resulting from system failures, atmospheric disturbances, loss of visual cues, and/or loss of control effectiveness may cause loss of control accidents [114]. An extensive study published by Harris et al. [68, 67] of the U.S. civil helicopter accidents shows that, even if the problem of loss of control only accounts for 15% of all helicopter accidents, this phenomenon has been growing since 1964. As shown in Figure 1.1 the number of loss of control accidents has almost doubled within the 40 years considered. Specifically, the dominance of loss of directional control about the yaw axis within all the loss of control accidents is shown to be alarming. Figure 1.2 confirms that controlling yaw is a leading problem and it seems to be particularly important for single, turbine-powered helicopters.

The tail rotor (TR) system represents an important element in several accidents related to loss of directional control. The tail rotor not only provides the anti-torque force but also gives yaw stability allowing for directional control about the

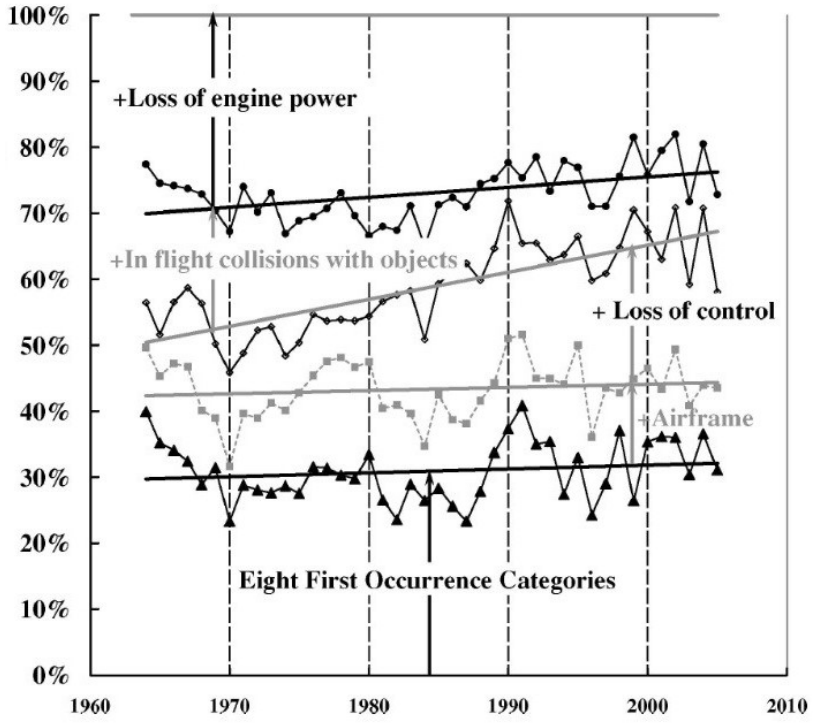

Figure 1.1: Distribution of rotorcraft accidents between 1964 to 2004 [67].

yaw axis [92, 56]. Since most helicopters in production have a single main rotor with an antitorque tail rotor configuration design, it is of the utmost importance for the rotorcraft community to enhance the level of understanding of the tail rotor system. The Safety Regulation Group of the U.K. Civil Aviation Authority (CAA) and the Defense Procurement Agency of the U.K. Ministry of Defense investigated different helicopter tail rotor failures (TRFs) [31]. The study was based on the evidence brought by the U.K. Tail Rotor Action Committee of an unacceptably high rate of TRFs compared to the airworthiness design standards. The primary objectives were to enhance the understanding of accidents related to TRFs and explore ways to reduce the accident rates. Common recovery techniques are reviewed with the formulation of improved procedures following TRF events. The types of TRFs analyzed are categorized as follows:

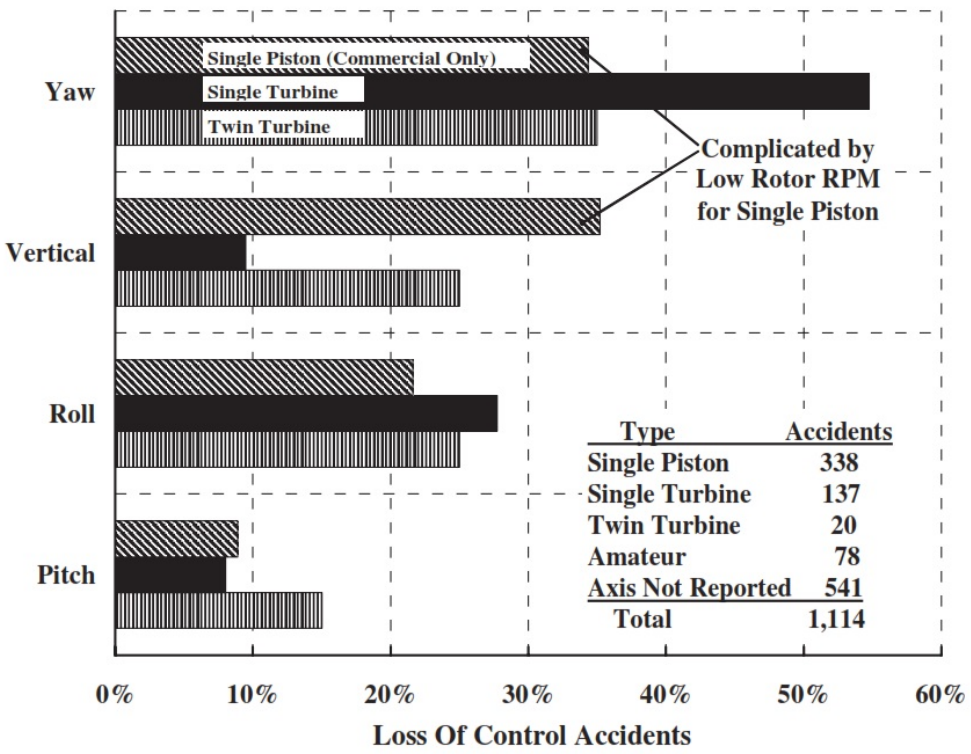

Figure 1.2: Loss of control accidents classification [67].

- the tail hit an obstacle;
- an object hit the tail;
- tail/boom structural failure;
- tail rotor drive system failure: the tail rotor drive system broke, causing complete loss of tail rotor thrust;
- tail rotor control system failure: the tail rotor control system failed, causing partial or complete loss of tail rotor thrust;
- loss of tail rotor effectiveness (LTE).

The analysis of the accidents of different fleets of aircraft reveals a consistently high rate of tail rotor failures, in the range of 9.2 to 15.8 per million flight hours, while

the failure rate requirement should not be more than 1 per million flight hours. In particular, civil and military fleets are compared. These two categories were considered because of their different operational uses. Indeed, while civil helicopters are primary used for personnel transport, military helicopters are forced to operate in more extreme areas of the flight envelope because of the high-risk flight scenarios involved. Figure 1.3 shows the profiles for civil and military helicopter fleets. With regards to the military fleet, the accidents caused by the tail hitting an obstacle and the TR drive system failure are similarly important. Specifically, they represent the most important causes of accidents for the heavy helicopter category. However, if the comparison is limited only to light military helicopters, the number one contributor of accidents related to the tail rotor is LTE, alongside the tail hitting an obstacle. The data provide a picture of the type of helicopters and operational environments that are statistically most susceptible to LTE events. Within all loss of directional control accidents related to the tail rotor system, LTE is a leading problem for small-size helicopters performing in high-risk operational conditions.

Both the Federal Aviation Administration (FAA) and the National Transportation Safety Board (NTSB) have recognized LTE to be a major contributing factor in several accidents related to loss of directional control [107, 54, 56]. Since 2004, more than 70 accidents involving LTE have been investigated. Within those accidents, a significant number of pilots were unable to recover causing several fatalities. In addition, recent statistics from the U.S. Helicopter Safety Team and the European Helicopter Safety Team confirm the occurrence of fatal accidents where the loss of control in-flight followed an LTE encounter [141, 53].

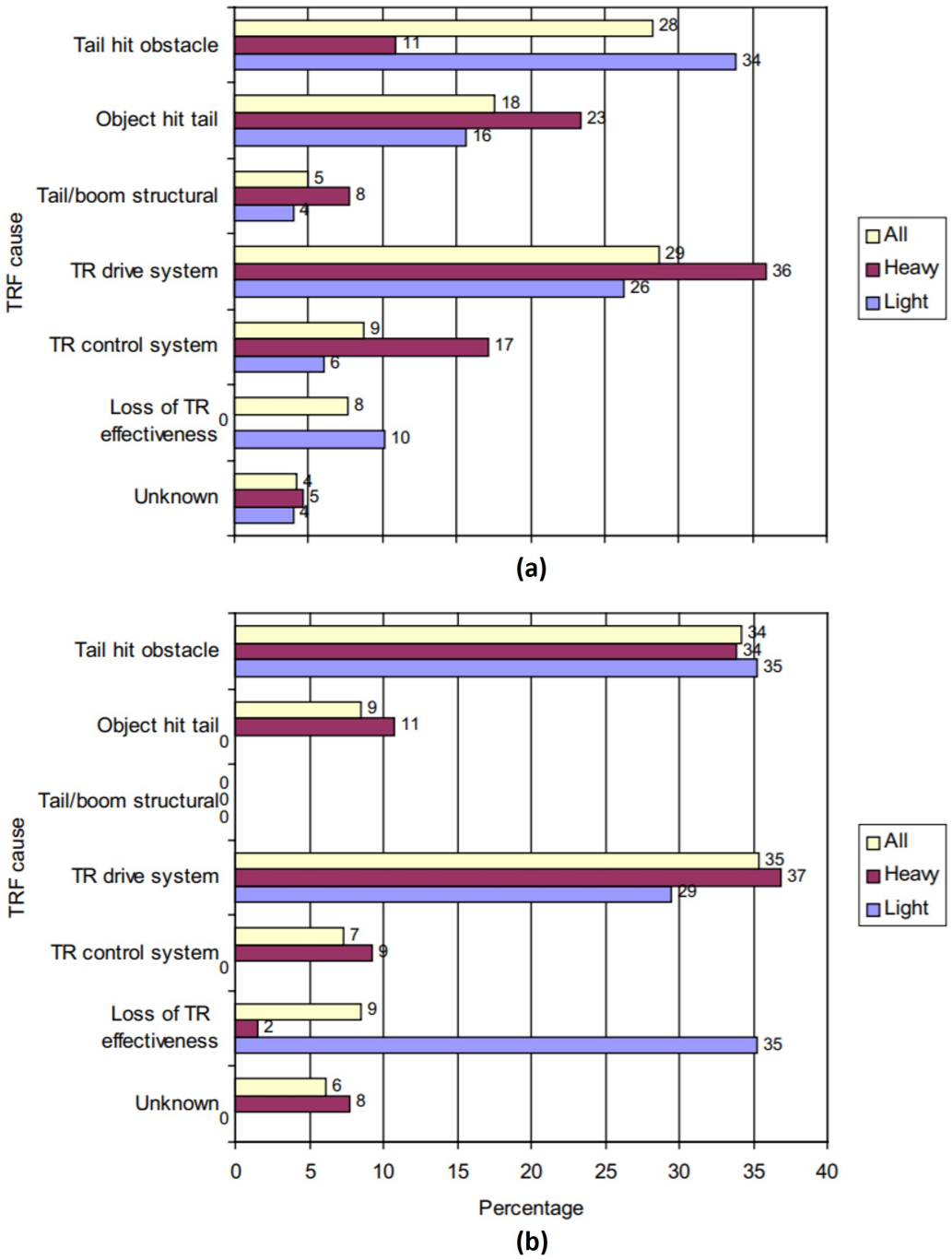

Figure 1.3: Distribution of causes for tail rotor failure [31]. (a) Civil helicopter fleet. (b) Military helicopter fleet.

1.2 Historical Benchmarks

In addressing the danger that this phenomenon still represents nowadays within the rotorcraft community, it is helpful to review its historical background. The U.S. Army first identified the phenomenon in 1978 as tail rotor stall, after numerous and similar accidents involving OH-58 helicopters [138]. An unanticipated rapid yaw rate seemed to occur during low-speed operative conditions, leading to loss of directional control of the aircraft. The tail rotor seemed to fail on providing the necessary antitorque thrust, while no mechanical malfunction was noticed, and no limitation was exceeded. The recommended recovery was to reduce the antitorque pedal and the collective while applying forward cyclic to increase speed. However, this did not solve the problem. Several accidents related to loss of directional control involved the OH-58 and 206 series helicopters, while the investigations could not find any maintenance or mechanical issues.

Prompted by safety concerns, between 1982 and 1984, the U.S. Army formed a Joint Special Study Group to conduct wind tunnel tests and flight tests on the phenomenon. A discovery was revealed: the tail rotor did not stall, and it was possible to recover from it. The new recovery procedure recommended the simultaneous application of full antitorque pedal and forward cyclic [130]. By then, the Army referred to the phenomenon as loss of tail rotor effectiveness. Promptly, the study results were divulged by Bell Helicopters, which referred to the phenomenon as unanticipated yaw triggered by low-speed flight characteristics. Indeed, Bell specified that the name loss of tail rotor effectiveness was misleading since the tail rotor systems had exhibited the capability to produce thrust during all approved flight regimes [7, 8, 140].

Though, despite all of those efforts, the accident rates related to this phenomenon did not reduce. Therefore, in response to this negative trend, in 1995 the FAA issued the Advisory Circular (AC) 90-95 [54], which currently still represents the

main document available on the topic. Within this document both names were used, unanticipated yaw and loss of tail rotor effectiveness. The main purpose of the AC 90-95 was to enhance the understanding of the phenomenon and promote its awareness among pilots. Unfortunately, even after this effort, a significant LTE accident rate persisted. Between 2004 and 2014, the NTSB investigated 55 accidents involving LTE in which the pilots were not able to stop the fast yaw rate caused by the encountering of this dangerous phenomenon. Because of these alarming data, in 2017 the NTSB issued a Safety Alert [107] to promote awareness within the pilot community. It is evident that, after nearly 40 years from its discovery, LTE remains an unresolved problem within the rotorcraft community and more efforts are needed to mitigate future accidents.

1.3 From LTE Ambiguities to LTE Accidents

It has been noticed that within the aviation community there is a lack of understanding and a variety of opinions about this phenomenon. Different names and definitions have been used throughout the years. Loss of tail rotor effectiveness [138, 139, 130, 140, 54], unanticipated yaw [7, 8], running out of pedal, loss of directional control [126] are just some examples. While the FAA categorizes it as a dangerous aerodynamic condition, the CAA refers to it as a tail rotor failure [31], mentioning that no mechanical malfunction is involved. It is evident how this lack of consistency led to confusion and misunderstandings within the rotorcraft community. Further complicating matters is that pilots are often not well enough trained to predict and mitigate this anomalous event. Many variations of recovery techniques have been found within the literature [54, 56, 32], raising doubts between pilots on what maneuver to apply in the critical flight condition. Furthermore, because of the risks involved, training for LTE is rarely done during real flights. The only way for pilots to practice recovery techniques is in simulators. However, as stated by the NTSB [107]

and the U.S. Helicopter Safety Team [141], some of the flight simulation tools do not accurately represent the physical dynamics of this flight condition. That may have contributed to misleading training and a propensity to recover from unrealistic conditions in the simulator giving pilots a false sense of security in the actual aircraft. The consequences of those issues are highlighted by the European Helicopter Safety Team, which confirms how pilot disorientation during LTE events is a major contributing factor to LTE accidents [53]. Even worse, pilots are often unaware of the proximity to LTE events encountered in-flight, placing them at a much higher risk for potential accidents. Because of those reasons, it is evident that improved efforts are needed to improve the understanding of this complex phenomenon and support the mitigation of LTE accidents.

1.4 Summary

Both the FAA and the NTSB have recognized LTE to be a major contributing factor in several civil helicopter accidents where the pilot lost control of the aircraft. However, even if multiple helicopter accident investigations have been attributed to LTE, it has been noticed that within the rotorcraft community there is a lack of understanding and a variety of opinions about this phenomenon. Different names and definitions have been used throughout the years leading to confusion and misunderstandings. Because of the risks involved, training for LTE is rarely done during real flights. Further, some of the flight training simulators do not accurately represent the different LTE phenomena. Because of those reasons, pilots are often not adequately trained to anticipate and mitigate LTE events. After nearly 40 years from its discovery, LTE remains an unresolved problem within the rotorcraft community and more efforts are needed to mitigate future accidents. Improved knowledge and awareness are the first steps towards prevention and consequently reduction of the LTE accident rate [56]. Hence, this research aims to provide a methodology to support the

proactive mitigation of helicopter accidents related to loss of tail rotor effectiveness. The following chapters are organized as follows:

- Chapter 2 presents the problem formulation, which leads to the motivating research question and the main research objective.
- Chapter 3 details the methodology formulation, in which the research questions and the hypotheses are articulated.
- Chapter 4 describes the experimentation phase and the results obtained.
- Chapter 5 presents the final methodology and the testing of the overarching hypothesis.
- Chapter 6 summarizes the important contributions of this research and the recommendations for future work.

CHAPTER 2
PROBLEM FORMULATION

2.1 LTE Characterization

Most helicopters in production have a single main rotor with a tail rotor configuration design. With a single main rotor helicopter, the presence of an antitorque system becomes essential. By Newton's Third Law, the main rotor rotation causes a torque reaction on the fuselage that, if not countered by an antitorque force, would cause the helicopter body to turn in the opposite direction of the main rotor rotation. The tail rotor system not only provides that antitorque force but also gives yaw stability and allows for directional control about the yaw axis [92, 56].

Because of the changes in wind direction and velocity, the required tail rotor thrust in actual flight has to be continuously modified to maintain heading. However, both gusty and steady winds from specific wind azimuth regions may alter the angle and/or speed of the airflow through the tail rotor leading to loss of tail rotor effectiveness (LTE). As detailed by the FAA [54]:

"LTE is a critical, low-speed aerodynamic flight characteristic which can result in an uncommanded rapid yaw rate that does not subside of its own accord and, if not corrected, can result in the loss of aircraft control."

Significant ambiguity surrounds the nature of this phenomenon. As detailed in Chapter 1, within the literature different names and definitions are found, together with inconsistent descriptions of recovery techniques. Even flight training simulators do not represent this condition well enough. All these ambiguities lead to misleading pilot's training and low awareness during flights. The dramatic consequences are seen in the number of LTE accidents. Between 2004 and 2014, the National Transporta-

tion Safety Board investigated more than 50 accidents in which LTE was recognized to be a strong contributing factor [107]. Within those accidents, a significant number of pilots were unable to recover when the helicopter encountered LTE, in most cases due to the inappropriate recovery attempts and the low altitude conditions. The flight conditions that seem to be particularly susceptible to LTE involve low airspeed maneuvers, particularly when the wind conditions are difficult to establish while flying.

Numerous flight and wind tunnel tests [54, 130] have shown that LTE is not caused by a mechanical malfunction, and it may happen in any single main rotor helicopter. Also, it is not necessarily related to a control margin insufficiency, as enough anti-torque control was still available during several tests. It was also demonstrated that the tail rotor does not stall, and it is possible to recover from it. However, if an incorrect or slow pilot response is applied, the yaw rate may rapidly increase to the point of no possible recovery.

The results obtained by the Joint Special Study Group [7, 8, 140] have identified certain wind azimuth regions that can lead to loss of tail rotor effectiveness. Specifically, the study established that weathercock stability, tail rotor vortex ring state, and main rotor vortex interaction with the tail rotor are key contributing factors of this complex phenomenon [54]. The results of a comprehensive wind tunnel test on an OH-58 KIOWA scale model [154], shown in Figure 2.1, well visualize the wind azimuths responsible for those dangerous flight conditions.

During the test, the aircraft yaw moment was measured while rotating the model at a fixed yaw rate. A fixed collective pitch of the tail rotor blades, together with a constant low wind speed within the tunnel allowed to investigate the resulting yaw moment fluctuations, mainly caused by the effects of the wind variations through the tail rotor. It was seen how specific relative wind conditions are more likely to trigger LTE, altering the angle and/or the speed of the airflow through the tail rotor.

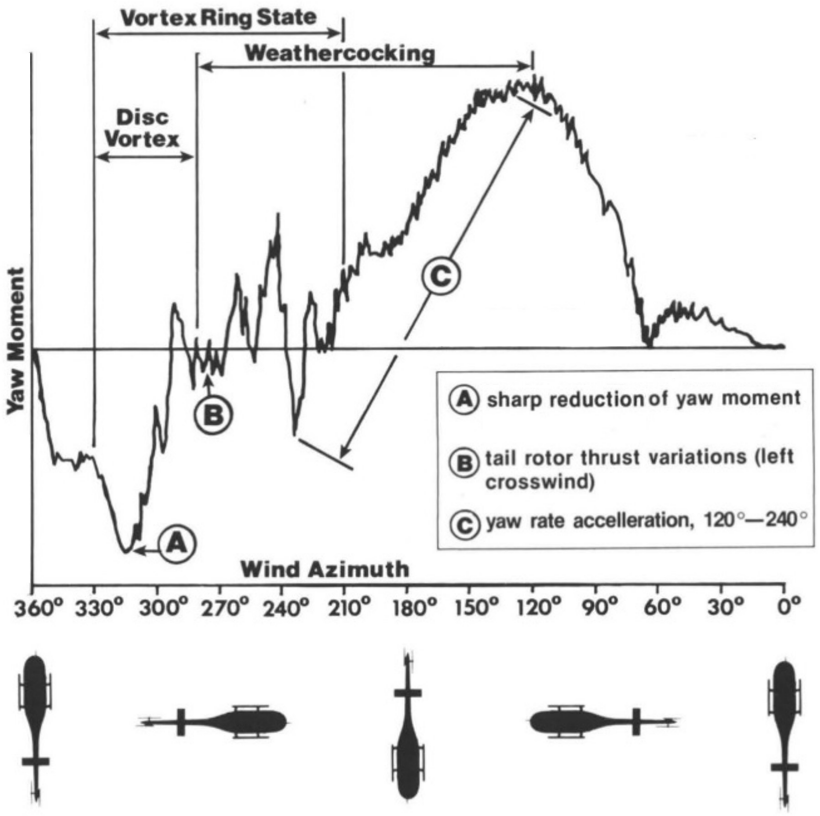

Figure 2.1: Yaw moment characteristics of the OH-58 for variation of wind azimuth at constant wind velocity (modified from [130]).

Despite the test did not involve a trim flight condition (the sum of the moments was never equal to zero), the trend of the yaw moment was used as an indication of the pilot pedal workload variation. The wind azimuth regions shift depending on the wind condition and they may overlap, causing the most pronounced tail rotor thrust variations in the overlapping areas. It was observed that pilots should always be aware of the changes in wind conditions and avoid critical flight scenarios where the tail rotor thrust fluctuations are present.

The wind azimuth region characterized by relative tailwinds from 120° to 240°, as in Figure 2.2, may cause LTE events related to the loss of weathercock stability of the aircraft. During those scenarios, the tailwinds may attempt to weathervane the aircraft away from the equilibrium flight condition leading to LTE like behavior.

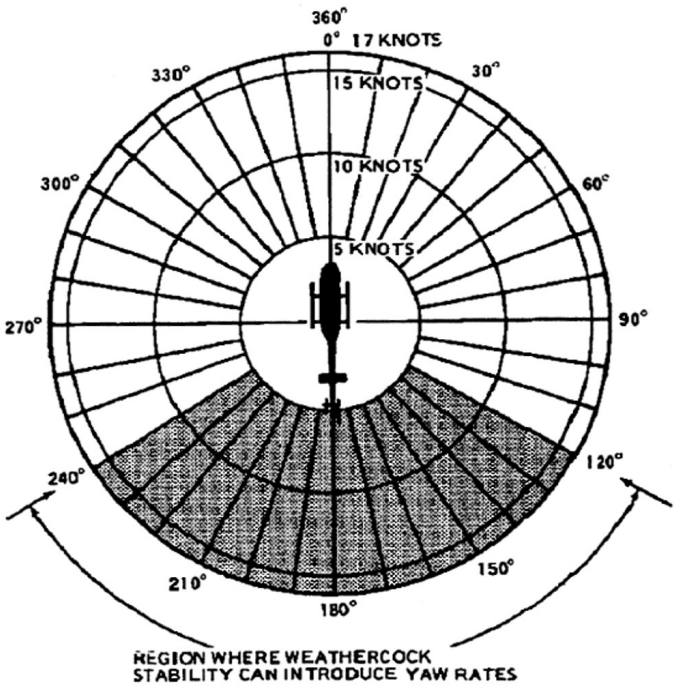

Figure 2.2: Wind azimuth region of weathercock stability [54].

An uncommanded turn may occur, depending upon the wind direction, unless a resisting pedal input is made. These kind of tailwinds are a yaw rate accelerator and if a yaw rate has been previously established, it will be rapidly accelerated in the same direction. The helicopter can be operated safely if proper attention is given to maintaining control. However, rapid and continuous pedal movements are necessary, greatly increasing the pilot workload [54].

The main rotor vortex interference is another phenomenon recognized as a contributor to LTE behavior. Many studies of the main rotor wake in quartering flight have shown that the vortices created by the main rotor influence the tail rotor thrust because they can strongly influence the inflow conditions [83, 20]. The FAA recognizes the impact of the main rotor-to-tail rotor interaction during quartering flight to the left or during hovering with low-speed wind from a wind azimuth of about 300°. When the main rotor vortex wake is blown into the tail rotor by the rela-

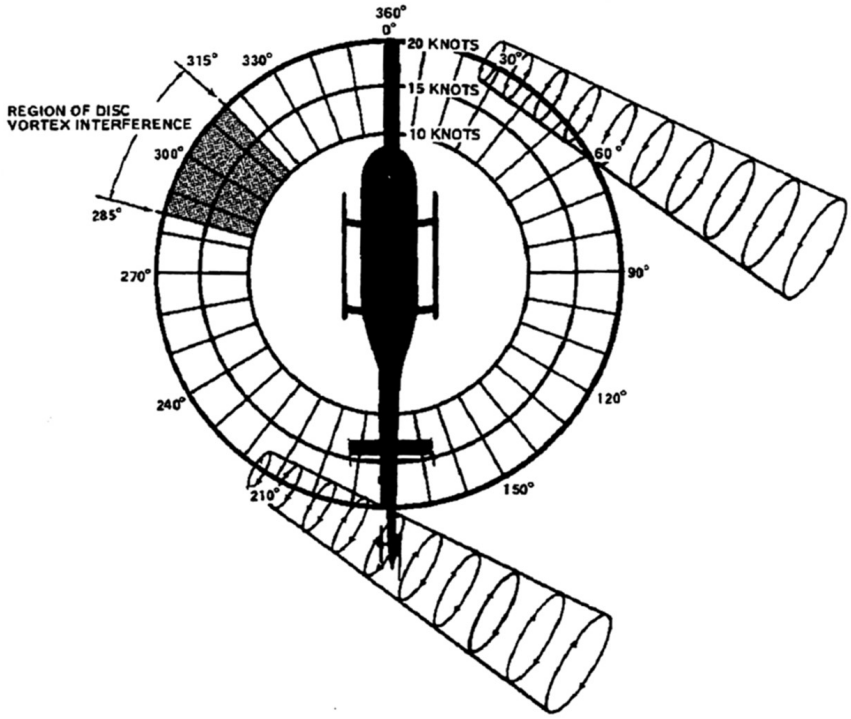

Figure 2.3: Wind azimuth region of main rotor vortex interaction with the tail rotor [54].

tive wind, as shown in Figure 2.3, the tail rotor operates in an extremely turbulent environment [148, 85].

While the flight tests conducted by both the U.S Army and the FAA revealed the left quartering flight to be a dangerous wind azimuth, Ellin [51] describes the quartering flight to the right, as shown in Figure 2.4, as a more critical condition. The tail rotor is exposed to a powerful effect of the advancing rotor blade tip vortices which reduces the tail rotor control margins. During this phenomenon, commonly known as the phenomenon of running out of pedal, the tail rotor may not produce enough thrust to ensure directional control of the aircraft. If a right yaw rate is allowed to increase, it may be dramatically accelerated by the phenomenon of loss of weathercock stability leading to loss of directional control. The inconsistency in the definition of the most critical wind azimuth region responsible for the LTE events related to the main rotor-to-tail rotor interaction reveals an additional LTE ambiguity

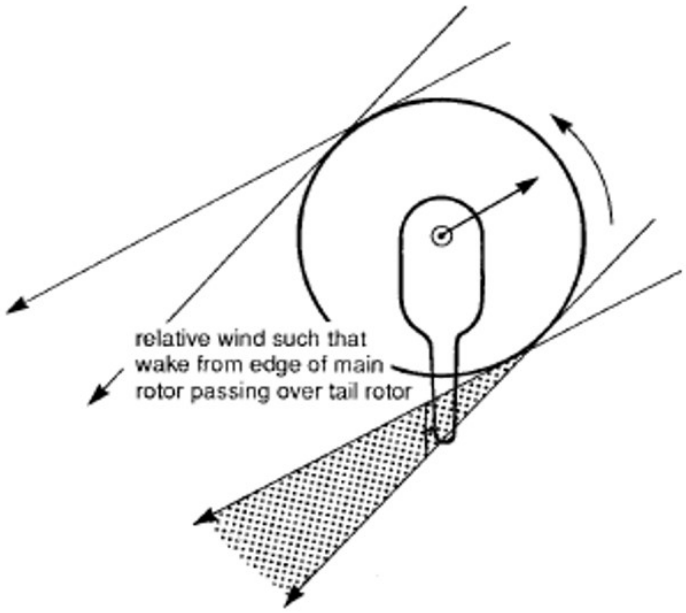

Figure 2.4: Tail rotor in right quartering flight [114].

that needs further investigation.

Finally, the wind azimuth region characterized by relative crosswind with azimuth between 210° to 330°, as shown in Figure 2.5, may cause the tail rotor to operate in vortex ring state (VRS) flow conditions leading to LTE like behavior. VRS at the tail rotor may develop while hovering in left crosswind, during sideward flights to the left while maintaining low forward speeds, or even during a hover turn to the right. During those scenarios, the rotor induced inflow is opposed by a crosswind creating a non-uniform and unsteady environment. Significant thrust fluctuations are present which cause continuous yaw variations. Rapid and continuous pedal inputs are needed to compensate for the changes in tail rotor thrust during VRS. This greatly increases pilot workload, as shown in Figure 2.6, which describes the pedal activity during a left sideward flight of a Hughes AH-64 [122]. Flight tests revealed that maintaining heading with relative crosswinds from the left is very difficult and that smooth pedal corrective actions are essential to compensate for the incessant yaw variations. However, LTE may occur if the pilot overcontrols the helicopter [54].

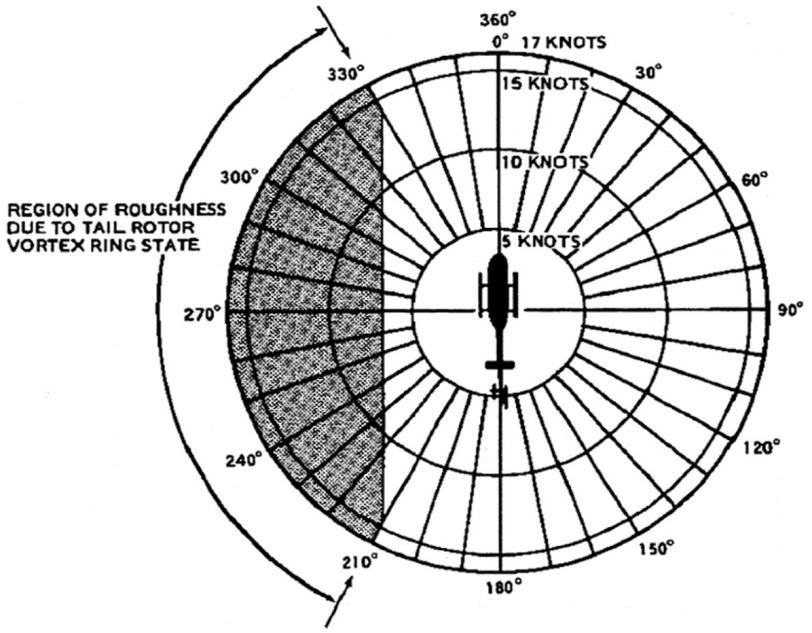

Figure 2.5: Wind azimuth region of tail rotor vortex ring state [54].

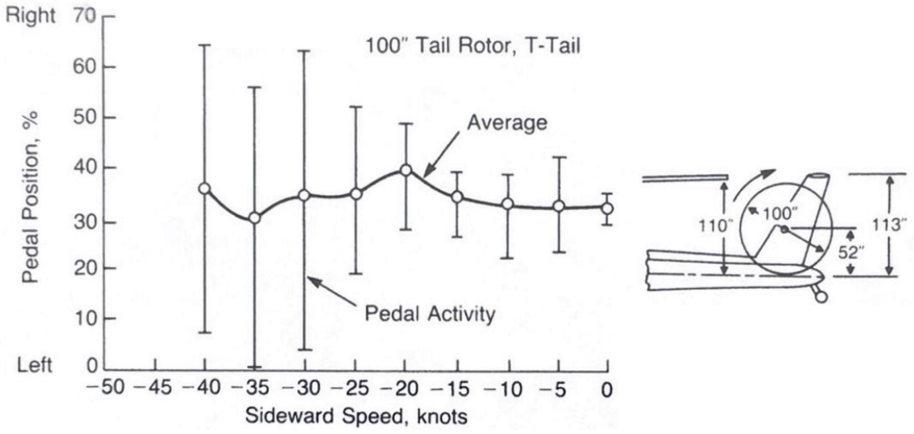

Figure 2.6: Pedal activity in left sideward flight of Hughes AH-64 [122].

2.2 Ongoing LTE Preventive Strategies

From 2004, the NTSB investigated more than 70 accidents involving LTE. Within those accidents, a significant number of pilots were unable to proactively recognize the onset of LTE and recover when the helicopter encountered the unanticipated yaw. The existing methods for LTE prevention, mitigation, and detection are presented.

The bowtie analysis of LTE accident scenarios and the proximity to LTE detection within the flight data monitoring program represent the ongoing strategies to promote better awareness of LTE within the pilots' community and improve the preventive LTE risk evaluations during flight. It will be shown that the knowledge gaps that surround the LTE phenomenon greatly affect the efficacy of the existing proactive mitigation techniques and that improved efforts are needed to mitigate LTE accidents.

2.2.1 Bowtie Analysis of LTE Accident Scenarios

The identification of the most important accident scenarios is the first step towards future safety developments. To promote pilot awareness of the multiple scenarios that may trigger a certain type of flight hazard, the bowtie methodology is often used to obtain a better overview of the situation in which certain risks are present [95]. The strength of this methodology lies in its tradeoff between efficacy and simplicity. The diagram has the bow-tie shape making the risk visualization particularly intuitive for the reader, an example is given by Figure 2.7. Risk in the bowtie methodology is elaborated by the relationship between hazards, top events, threats, and consequences. The hazard defines the context of the diagram describing the desired state which is interrupted by the top event. This event happens before damage occurs and it is possible to recover from it. On the left part of the diagram, the threats are visualized in blue. Each one of them can cause the top event independently. Instead, on the right, the consequences are visualized within red boxes. Each one describes a different scenario in which the damage occurs. The power of this diagram lies in the fact that proactive and reactive risk management are clearly distinguished within the diagram, respectively on the left and right side of the top event, providing all the scenarios in a single picture. Barriers are used to display what measures an organization has in place to control the risks. Preventive barriers prevent the top event from happening while recovery barriers mitigate the consequences. The effectiveness

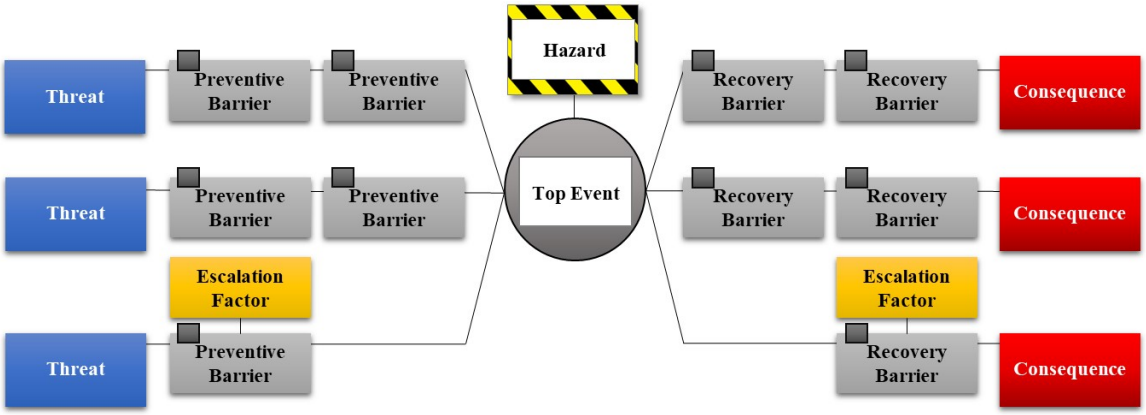

Figure 2.7: Example of bowtie diagram.

rating of a barrier is depicted using an intuitive color scale from green through red. Escalation factors, in yellow, are conditions that lead to increased risk by defeating or reducing the effectiveness of a barrier.

Because of the large number of accident scenarios that led to LTE, Zanella et al. [158] developed a bowtie diagram to support LTE risk assessment, risk management and, risk communication within the helicopter community. As visualized in Figure 2.8, the diagram aims to give pilots a schematic summary of all the dangerous flight scenarios, enhancing their ability to quickly recognize the proximity to LTE and increase their chance of survival. It is an easy-to-read picture with a clear relationship between the threats that may lead to LTE, and the potential consequences of the LTE occurrence. The diagram was built after reviewing several fatal accidents related to LTE and identifying the most significant safety hazards that may potentially lead to an LTE encounter. The diagram refers specifically to single rotor helicopters with counterclockwise rotation of the main rotor. Several proactive barriers are identified to help prevent the safety threat from triggering LTE. Instead, in the case of an LTE occurrence, reactive barriers are visualized to help the pilot avoid a fatal collision. The most significant barriers are linked to one or more escalation factors that may reduce the effectiveness of the specific barrier and compromise flight performance.

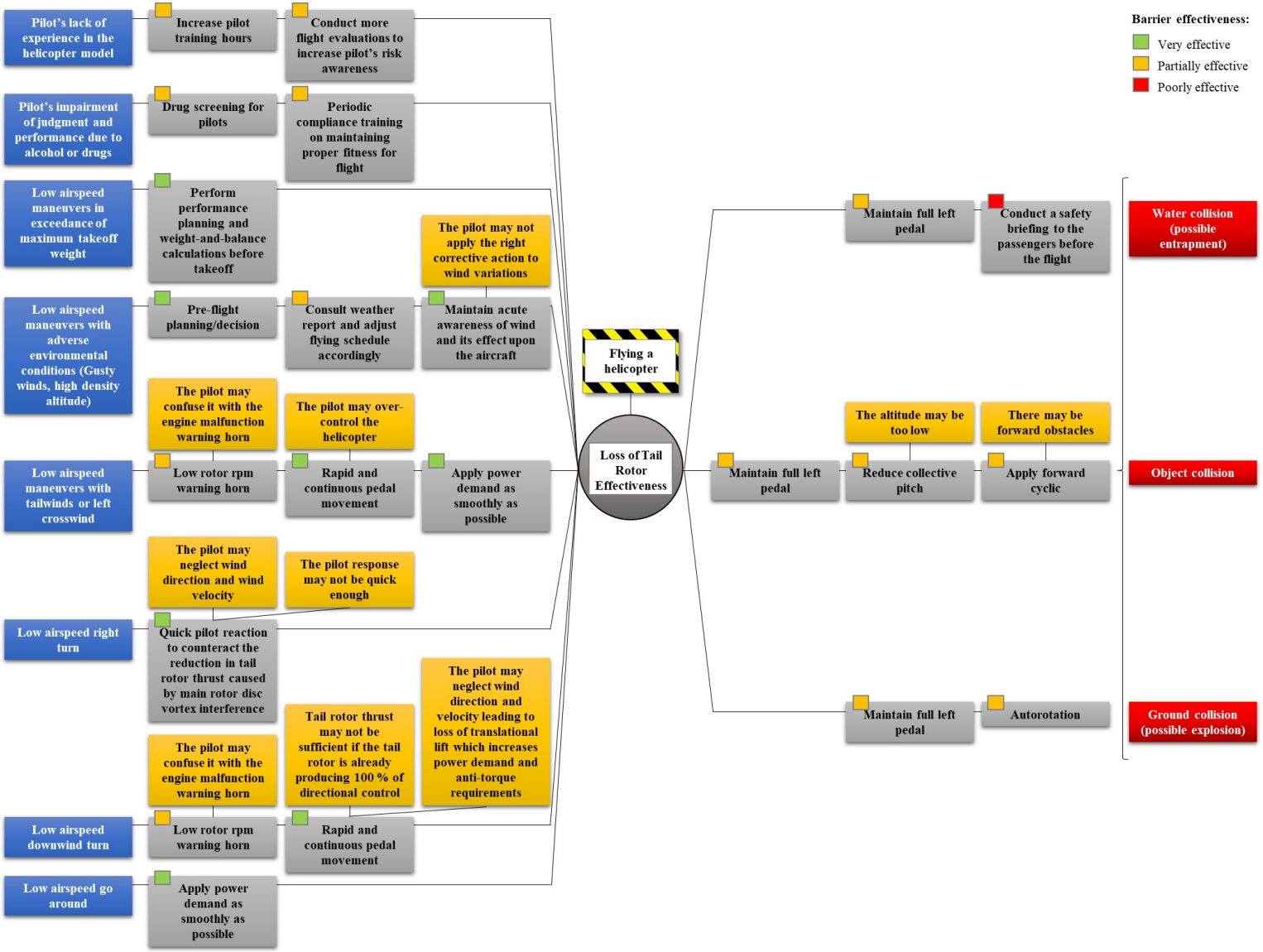

Figure 2.8: Loss of tail rotor effectiveness bowtie diagram [158].

The dangerous flight scenarios that may lead to LTE are identified as follows:

- *Pilot's lack of total experience in flying helicopters*

  The pilot's experience is an essential factor that may heavily influence flight performance. An increment of pilot training hours and flight report evaluations may enhance pilot's risk awareness decreasing the chance of LTE accidents.

- *Pilot's impairment of judgment and performance due to alcohol or drugs*

  Compliance training on maintaining proper fitness for flight is necessary. Increased attention and education on the benefits of using a fitness for flight checklist and on the dangers of flying while under the influence of drugs or alcohol could prevent this issue from reoccurring.

- *Low airspeed flight in proximity or exceedance of maximum takeoff weight*

  It is required for the pilot to ensure flight operations within the safe flight envelope of the aircraft. Performing proper performance planning and weight-and-balance calculations before takeoff is of fundamental importance to prevent the triggering of LTE events.

- *Low airspeed maneuvers with adverse environmental conditions*

  Gusty winds and/or high density altitude conditions increase the pilot's workload and may lead to a pilot's failure to maintain directional control. Note that density altitude increases as field elevation, temperature, and/or humidity increase, compromising the overall flight performance. Consulting weather reports and adjusting flying schedules accordingly is an essential part of a proper preflight planning. Also, it is fundamental for the pilot to maintain acute awareness of the wind and its effect upon the aircraft.

- *Low airspeed maneuvers with tailwinds or left crosswinds*

  Winds from critical wind azimuth regions increase the pilot's workload and

may lead to loss of aircraft control. Rapid and continuous pedal movements are necessary to maintain directional control with particular attention to not over-control the helicopter. Also, power demand should be applied as smoothly as possible to not cause uncommanded yaws.

- *Low airspeed right turns*

  The main rotor vortex interference has a strong impact on the tail rotor thrust produced. It is very important for the pilot to not neglect wind direction and wind velocity, and to always react with a quick response to any relative wind variation.

- *Low airspeed downwind turns*

  Rapid and continuous pedal movements are required to maintain helicopter control. Note that relative tailwinds cause high-power flight conditions and may lead to scenarios in which the tail rotor may not produce enough thrust to maintain directional control. The pilot may neglect wind direction and velocity leading to loss of translational lift which increases power demand and anti-torque requirements.

- *Low airspeed go-around*

  The fast application of collective pitch at low airspeed may trigger LTE. This threat becomes even more dangerous while the helicopter is in a high-power demand situation. Power demand should be applied as smoothly as possible to not cause uncommanded yaws.

In case of an LTE occurrence, several reactive barriers are identified to help the pilot avoid the fatal collision. As recommended in the FAA Advisory Circular 90-95, if unanticipated yaw occurs the pilot should maintain full anti-torque pedal input, opposite to the direction of the yaw. When allowed, simultaneously move cyclic forward to increase speed until the recovery is completed. A collective pitch reduction will aid

in arresting the yaw rate but may cause an excessive rate of descent. The decision to reduce collective must be based on the pilot's assessment of the altitude available for recovery. If the spin cannot be stopped and ground contact is imminent, an autorotation may be the best course of action. The pilot should maintain full anti-torque pedal until the spin stops, then adjust to maintain heading [54]. A safety briefing to the passengers shall be conducted before each flight but it may not be effective in preventing fatalities, due to the challenge of escaping from water entrapment or an explosion after a ground collision.

The LTE bowtie diagram promotes improved LTE risk evaluations and proactive identification of dangerous scenarios while flying. However, the large number of factors that influence LTE increase the difficulty for pilots to proactively avoid the hazard. Further, the diagram is rule-based, established by many domain experts' estimations. However, the qualitative and subjective nature of those rules limits the capabilities of this strategy to efficiently prevent and mitigate LTE accidents. Hence, the next sections will give more quantitative insights on the ongoing risk mitigation efforts related to LTE.

2.2.2 LTE Detection Within the Flight Data Monitoring (FDM) Program

Operational flight data are essential not only for accident investigations but also to provide insights towards safety developments. The systematic collection and analysis of flight data to support aviation safety is known as flight data monitoring (FDM) program. Also known as the flight operational quality assurance (FOQA) program, it has been rapidly expanding as a safety culture because of its numerous benefits. The CAA defines the FDM program as "the pro-active and non-punitive use of digital flight data from routine operations to improve aviation safety" [33]. It has been recognized by the NTSB and the CAA as one of the most promising technological efforts for safety improvements in aviation [106, 33]. Figure 2.9 illustrates the typical FDM

process [33]. The first step consists of collecting flight data by a removable quick access recorder, e.g., videotape, disk, memory card, wireless system. FDM data is then used to perform different kinds of analyses like event detection routine, operations measurement, airworthiness investigation, and incident investigation. Following, a validation and risk assessment of the event is performed by domain experts. Next, the level of risk of the event detected is determined and corrective actions are considered to minimize the risk of future hazards. Recommendations are initiated to the departments of flight training and safety and, if appropriate, to airports, clients, and aircraft manufacturers to enhance safety reporting and awareness [75]. To support the expansion of this safety practice, the International Civil Aviation Organization (ICAO) and the NTSB encourage the installation of on-board flight data recorders to support routine safety analyses. Furthermore, due to an increased interest in

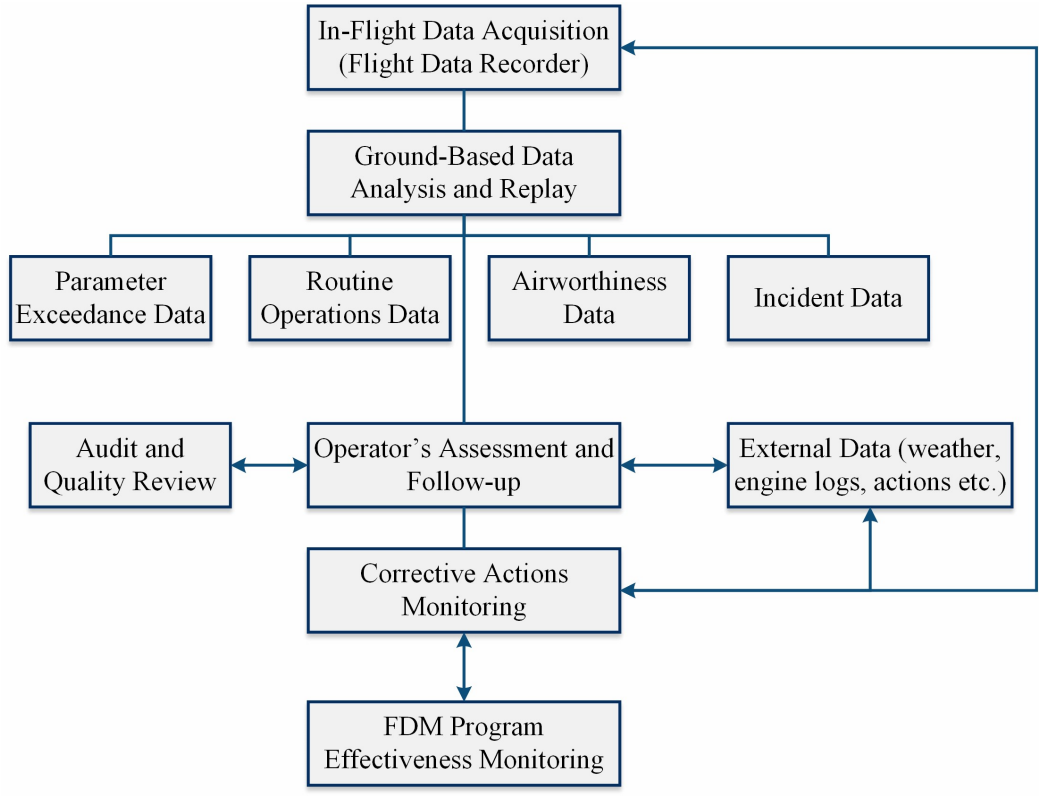

Figure 2.9: Typical flight data monitoring process [33].

data-sharing to promote aviation safety, the FAA assisted in the development of a data-sharing network called aviation safety information analysis and sharing (ASIAS). This is promoted through a collaborative partnership between government and industry. A virtual shared platform is available to each operator to collect flight data and develop secure safety analyses to support risk mitigation efforts. The ASIAS program provides the framework that multiple operators use to obtain and share safety-related, de-identified flight data. Those efforts, together with the rising number of operators participating in the FDM program, as shown in Figure 2.10, have allowed for the ASIAS program to expand its pool of data to support improved safety analyses of aggregate operations. While in the past, safety analysts had to rely their research on limited past accidents information, nowadays the database includes also the flight data of routine operations, with a vast number of flight procedures of multiple and diverse aircraft. The application of the FDM program to commercial aviation has been leading to a significant reduction in accident rates during the past few decades, allowing operators to identify, assess, and tackle multiple operational risks and emerg-

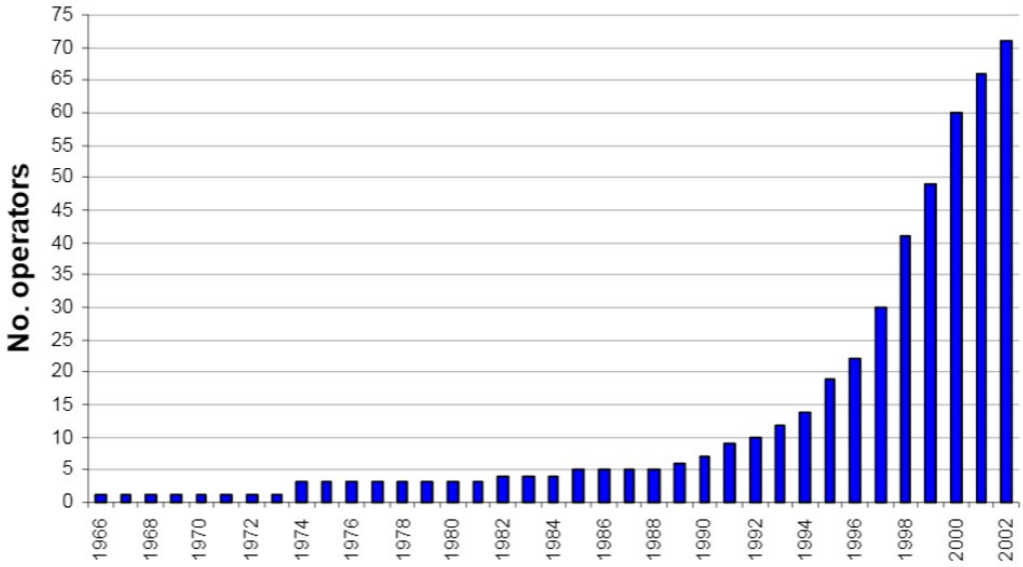

Figure 2.10: Historical growth of operators participating to a flight data monitoring program [58].

ing safety concerns [150]. Because of these reasons, the same idea has been applied to rotorcraft and it has been named the helicopter flight data monitoring (HFDM) program. This expansion is providing meaningful contributions facilitating risk-based decision-making for helicopter operators [33, 142, 71, 30].

Safety metric detection is the main method of analysis used, comparing flight data to a large safety metric database which includes predefined hazardous flight conditions and different levels of proximity to events. Through this event detection strategy, the operators can develop improved safety analyses promoting flight safety [30, 57]. However, if the safety metric is not well established, it may lead to false and missed detections, reducing the reliability of the entire flight analysis. As a result, pilots may not be aware of the risks encountered while flying. Because of this, domain experts constantly fine-tune the accuracy of the safety metrics to ensure reliable flight analyses.

To provide improved LTE detections within the HFDM environment, Zanella et al. [158] developed a filter-based LTE safety metric able to detect different levels of proximity to LTE. The metric is based on the approach of exceedance detection, detecting events using predefined constraints. The definition of those constraints is based on the critical flight conditions identified by the review of accident reports and experts' estimations. Figure 2.11 presents the filter-based framework that defines the LTE safety metric. This framework is currently implemented in the HFDM Research website for ASIAS supported by the Helicopter Association International and the Federal Aviation Administration and allows helicopter operators to conduct post-flight analyses and investigate flight data to promote pilots' awareness of the proximity to LTE. Predefined dangerous wind azimuth regions are identified based on the qualitative estimations of subject matter experts. Note that no further validation was performed on the detection results. The medium-risk level of proximity to LTE is related to the relative wind conditions. The high-risk level of proximity to LTE

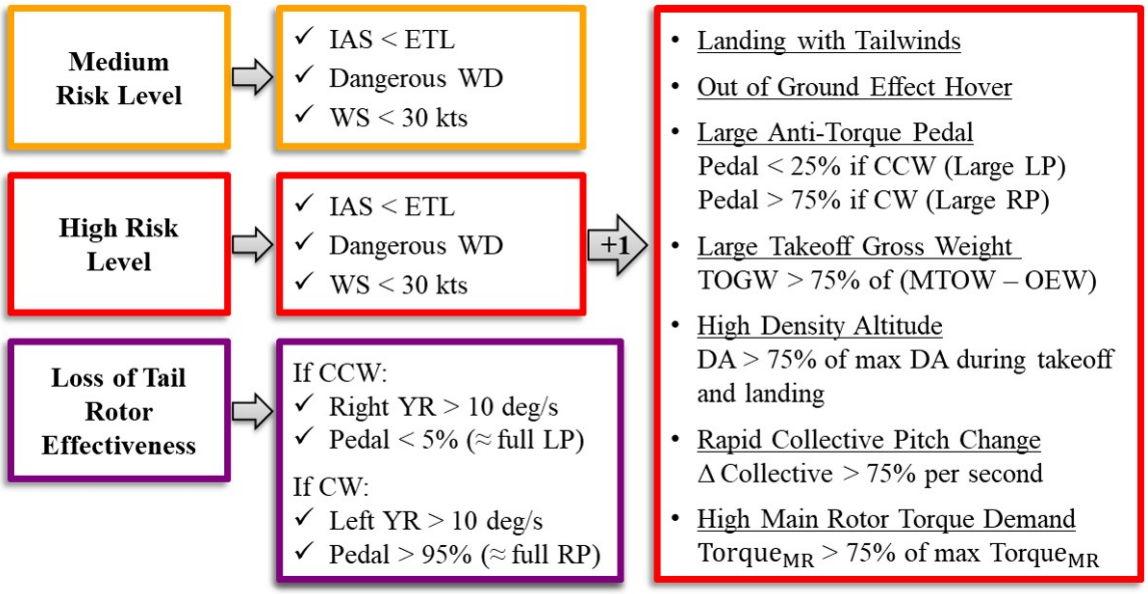

Figure 2.11: Filter-based framework currently used to detect the proximity to LTE within the HFDM program [158].

is detected if other than the constraints that define medium-risk level, at least one constraint of any remaining (underlined) conditions is simultaneously satisfied for at least one second. Those conditions include flight data thresholds that may cause high-power demand situations. Indeed, while reviewing LTE accident reports it was noted that high-power phases of flight are an important factor that may trigger an LTE event. Hence, out of ground effect (OGE) hover, landing with tailwinds, high takeoff weight, high density altitude, rapid power applications, and situations where high torque demand or small pedal control margin is used are all included in the safety metric. Finally, an LTE event is detected if the combination of yaw rate (YR) and the pedal control input is satisfied, as shown in Figure 2.11. Assuming a counterclockwise (CCW) rotation of the main rotor, the right yaw rate should be greater than 10 deg/s and pedal used lower than 5% (almost full left pedal). However, the pedal control input may not be appropriate or fast enough to correct the unanticipated yaws. Hence, this LTE safety metric does not allow for the detection of LTE events caused by pilot's disorientation leading to possible missed detections. It is noted that

for a proper application of the safety metric, several input parameters are needed to detect the different levels of proximity to LTE. However, some of those parameters, e.g., the flight control parameters, are often not available within the recorded flight data. This greatly hinders the accuracy of the detection of the proximity to LTE making the safety metric less applicable within the HFDM environment.

Even if this approach is an improvement towards an efficient proactive mitigation of LTE accidents, the threshold values that define the current LTE safety metric are not fully accurate. Indeed, the level of impact on LTE of each influencing factor was established using pilots' subjective evaluations, hindering the reliability of the detection. Hence, improved efforts are needed for a more reliable definition of LTE safety metric to enable more accurate flight analyses within the HFDM program.

2.3 Safety Analysis Approaches Within the FDM Program

One significant method to promote rotorcraft safety involves the systematic collection and analysis of flight data through the flight data monitoring program. It has been observed that the LTE safety metric currently used needs to be improved to provide more accurate safety analyses. Enhancing the accuracy of safety metrics and the ability of the FDM program on assessing the risk experienced during specific flight conditions has been the focus of several recent studies. Hence, an overview of the safety analysis approaches, and the safety metric quantification methods used within the FDM program is presented. It will be shown that both data-driven approaches and physics-based approaches present drawbacks that hinder the development of an enhanced safety metric that allows an accurate prediction of LTE within the HFDM environment.

2.3.1 Data-Driven Approaches

Exceedance Detection

Exceedance detection is one of the most common methods of safety metric identification currently used within the FDM program, and it is the approach currently used to define the LTE safety metric. This approach is based on a set of parameter constraints that define the safety metric of interest. If one or more recorded flight variables exceed any of the thresholds previously specified over a specific amount of time, an exceedance is detected [75, 33]. The application of this method is promoted by the FAA Advisory Circular 120-82 [55], which provides multiple events definitions for air carriers that operate primarily under part 121 or 135. An example of event names and descriptions is provided in Table 2.1.

The exceedance detection method is also used by Wilborn and Foster [149] after defining the loss of control (LOC) envelope in commercial transport aircraft. First, they developed a quantitative loss of control criteria with the union of five envelopes. Each envelope is defined by two different states, as shown in Table 2.2. Then, they defined two risk levels of loss of control as a function of the number of exceeded envelopes. Exceedance detections may correspond to aggressive maneuvers dangerously close to the boundary of LOC. If two out of five envelopes are exceeded, the event

Table 2.1: Examples of event exceedences used by the FAA (modified from [55]).

Event name	Event description	Basic event definition
Operating ceiling exceeded	An event to detect operation of the aircraft above its certificated maximum operating altitude	Altitude $>$ x feet for x seconds
Engine failure	An event to detect in-flight engine failure/shutdown	Air/ground switch= air, oil pressure $<$ x psi, fuel flow $<$ x pph, exhaust gas temperature $<$ x degrees

Table 2.2: Summary of loss of control envelopes (modified from [149]).

Name of envelope	First state	Second state
Adverse aerodynamics	Angle of attack	Sideslip angle
Unusual attitude	Bank angle	Pitch angle
Structural integrity	Velocity	Load factor
Dynamic pitch control	Dynamic pitch angle	Percent pitch control
Dynamic roll control	Dynamic roll angle	Percent roll control

named "borderline LOC" is detected, while an actual LOC event occurs when three or more envelope thresholds are exceeded simultaneously.

Exceedance detection is a simple and popular monitoring technique of known and predefined events. However, it requires the input of subject matter experts with enough background knowledge of the occurrence to correctly define the safety metric and consequently obtain an adequate detection. If the safety metric is not well defined, it may lead to false or missed detections degrading the quality of the overall safety analysis.

Statistical Analysis

Statistical analysis is an additional class of data-driven approaches, which has been widely used within safety aviation research for the exploration of event frequency within large flight databases. This approach focuses on hazard detection within flight data and the synthesis of the results in the form of distributions. This reveals to the operator the frequency at which certain flight parameters are exceeded within a certain period. Hence, statistical analysis can be used to monitor the safety performance of the overall fleet giving an overview of the possible negative trends of operational performance. Distributions of parameter exceedance frequency allow for monitoring, providing an additional capability over exceedance detection. As an example, this method was used by Puranik et al. [124] for the analysis of approach and landing

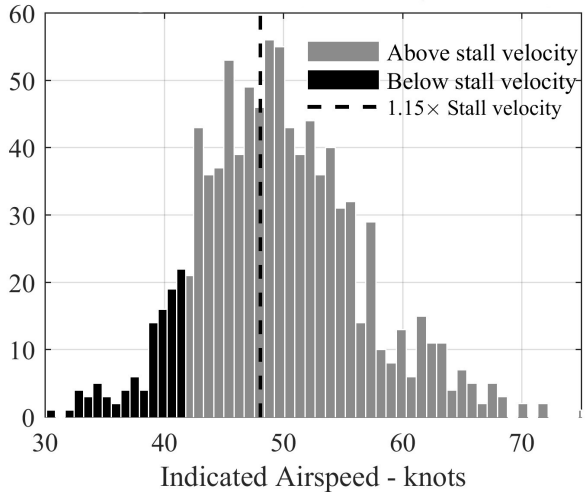

Figure 2.12: Distribution of touchdown velocity [124].

maneuvers for general aviation aircraft. As shown in Figure 2.12, the distribution of touchdown indicated airspeeds for a set of training flights of a Cessna C172S was used to obtain more insights about important parameters during the phases of flight considered. The definition of the hazard flight envelope must be reliable to minimize the number of false and missed detections and maximize the reliability of the monitoring task. However, even if this approach does not involve a significant computational effort, it is purely retrospective, restraining the monitoring of past flight data and limiting the improvements of safety analyses.

Anomaly Detection through Machine Learning Techniques

With the increasing use of flight data recorders, a vast amount of recorded data became available. Meanwhile, computing power rapidly evolved spurring the development of new advanced data analysis techniques. Within this environment, machine learning became a popular field of study focused on the development of computer learning algorithms able to use data to obtain intelligent actions. A vast literature review on machine learning is provided by [90, 100, 70, 152]. Machine learning techniques are divided into different categories depending on their purpose. This section

provides an introduction to the main groups of learning approaches largely used within aviation safety research.

A predictive model, as the name implies, provides predictions of output values after going through a learning training process of the relationship between input-output values of a specific dataset. Since clear learning instructions are provided, the process of training a predictive model is called supervised learning. In other words, the supervised learning algorithm aims to optimize the predictive model to find the combination of values, called features, that give the target output. The models involved may be categorized as probabilistic, if Bayesian methods are used, or deterministic if no randomness is involved. Furthermore, based on the desired output different learning techniques may be preferable to others, for example, classification is used for discrete outputs while numerical prediction deals with continuous results.

Descriptive models, instead, are known for their potential of finding structure or patterns in a given dataset. Specific techniques, like clustering or pattern recognition, may be used on a vast dataset to reorganize the input data in a more useful way. Since only input data are needed and no mapping between input and output is created, this approach is also known as unsupervised learning. Because the aviation industry urges on mitigating emerging issues within large flight datasets, unsupervised learning techniques are often preferred for their ability on detecting abnormal operations for which predefined detection criteria still do not exist. Though the support of domain experts is needed to complete the detection analysis with meaningful insights to minimize missed and false alerts, it is important to notice that the choice of the learning technique and the subsequent algorithm is a function of different factors, such as the dataset size, the type of parameters involved, also called features, and the characteristics of the anomaly that is intended to be detected. Following, a literature review on the most popular machine learning methods used in aviation safety is provided.

Budalakoti et al. [23] developed a method called SequenceMiner, to help the safety experts identifying abnormalities of pilot inputs used to control the autopilot system of commercial aircraft. This method stands for its capability to detect and characterize anomalies within a large set of discrete symbol sequences. A sequence is defined as the set of switches that the airline pilot flips during a landing phase. Two main steps define the detection of anomalous sequences. First, sequences are clustered using a distance-based similarity measure and anomalous sequences are identified. An outlier analysis follows to provide an explanation of the anomalies detected, through easy-to-read indicators. SequenceMiner represents an innovative approach not only for discovering significant safety events within discrete aircraft data but also for its capability of describing why the discrete sequences detected are anomalous.

An important contribution has been given by Bay and Schwabacher [5]. They developed an algorithm called Orca that can treat both discrete (binary) and continuous features for anomaly detection within aviation datasets. The algorithm created is based on the kth nearest neighbor approach. More precisely, for each point the average distance to the k nearest neighbors is calculated and the top t points with the largest resultant are considered outliers. Unfortunately, its use becomes very inconvenient within large datasets because of the too high computational time due to potential quadratic time complexity. An improved version named the iOrca was developed by Bhaduri et al. [10] to improve the method efficiency while providing the same anomaly detection results. The advanced sequential method resulted up to an order of magnitude faster than the previous version.

Within aviation safety, the approach of combining different machine learning algorithms to obtain better performance has been rapidly spreading. Das et al. [37] developed the multiple kernel anomaly detection (MKAD) method to detect potential flight anomalies within a vast dataset of worldwide operations of commercial fleets. The algorithm was created from two baseline anomaly detection algorithms, Orca and

SequenceMiner, to combine their performance into a single method. The detection is based on the multiple kernel learning theory, using the one-class support vector machine (SVM) which is a semi-supervised machine learning technique. One-class SVM has been chosen for its ability to combine both discrete and continuous variables from different data sources. MKAD method was shown to be reliable in predicting anomalies detection in heterogeneous data sources and robust enough against the existing baseline algorithms.

Li et al. [97, 96] developed a novel clustering method named ClusterAD-Flight, which detects abnormal flights within routine airline operations. This method supports proactive risk management with no predefined anomaly criteria. Three main steps characterize the method as shown in Figure 2.13. First, the time series flight data is transformed into high-dimensional vectors. Then, dimensional reduction is applied to address the problem of data sparsely distributed across dimensions and multicollinearity. Finally, the cluster analysis defines clusters, or groups of proximate vectors, and abnormal flights, or standalone vectors. Through the analysis of flight data provided by Boeing and Airbus, it has been shown that ClusterAD-Flight is more sensitive in identifying abnormal patterns of continuous parameters than the

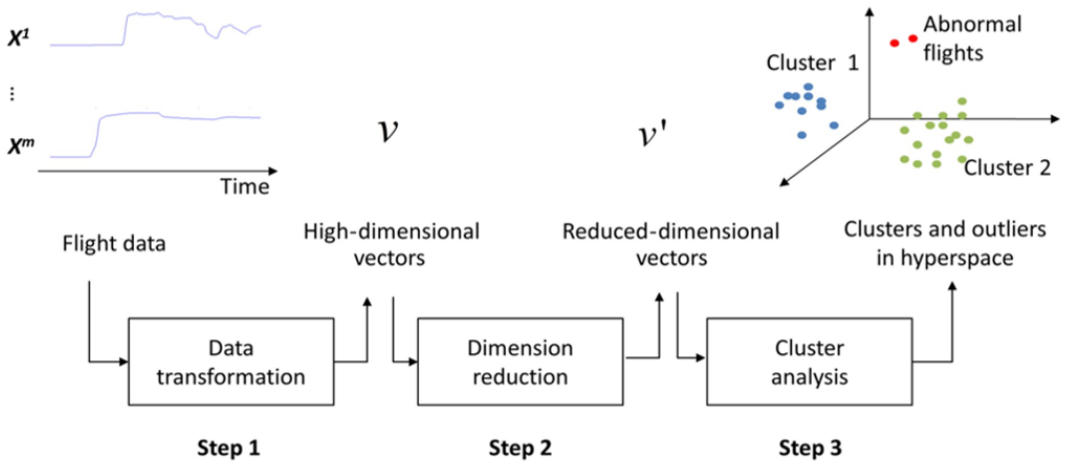

Figure 2.13: ClusterAD-Flight process [96].

traditional exceedance detection method. However, those abnormalities need to be referred to domain experts for following reviews to determine their operational implications. Also, the method is limited to the analysis of only take-off and approach phases.

Multiple studies compare ClusterAD-Flight, MKAD, and exceedance detection analysis methods on common aviation datasets. It has been shown that both ClusterAD-Flight and MKAD perform better than the traditional exceedance detection approach. Though, while the former is more effective in identifying abnormal patterns of continuous features, the latter is more sensitive to discrete flight parameters. As a limitation, each abnormality detected needs to be referred to domain experts for following reviews to determine their operational implications. Also, the analysis is restricted to few specific phases of flight of very similar commercial aircraft [36, 96].

Flight operators record new flight data every day and the computational cost to update the clustering analysis including data as they accumulate is very expensive. Hence, an adaptive online clustering-based method was developed by Zhao et al. [160] to allow real-time update of clusters as new flight data are recorded by the operators and included in the analysis. The method is based on the Gaussian mixture model (GMM), a probabilistic model that represents normally distributed clusters. An offline GMM calculates the cluster model parameters, while an online GMM updates the previous parameters of the existing clusters based on the new dataset. A constraining limitation is the inability of the method to create new clusters as more flight data are included. New data are assigned only to already existing clusters, neglecting new patterns caused by the introduction of new technologies. Also, the method does not include the inputs of airline safety experts on the anomaly detection results limiting the power of this application.

With regards to the predictive models used in aviation safety, a vast classification analysis of aviation historical data was performed by Babic et al. [2]. The goal of this

study was to develop a cost-effective model to proactively identify the occurrences of potential accidents. Multiple decision tree algorithms were used and compared to provide an easy to read classification. Also, an ensemble learning classifier called random forest approach was used. Its ability to create a multitude of decision trees at training time enhances the output accuracy while complicating the tree structure interpretability.

Another vast comparison between prediction models was done by Stolzer and Halford [134]. The scope of their work was to create a tool able to identify anomalous rates of fuel consumptions within the fleet, to improve operational efficiency and safety. Classification and regression trees (C&RT) models and neural networks (NNs) architectures, were tested against traditional regression methods to predict fuel burns within FOQA data. It has been shown that both C&RT and NNs outstand the predictive performance of the traditional methods. However, while NNs results are of difficult interpretation, the dendrograms produced by C&RT enable the analyst to understand the key factors that contribute to the results, mapping the relationship between features and outcomes.

Recurrent neural networks (RNNs) have been used by Nanduri and Sherry [105] to detect well-known anomalies within flight datasets. RNNs differ from standard NNs by using their internal memory to process sequences of inputs. This study aims to address the limitations of MKAD method, such as the need for dimensional reduction preprocess, the poor sensitivity towards short durations of anomalous patterns, and the inability to detect anomalies in features that are derivable from features present in the feature vector. Their superior performance was proven compared to the MKAD method. Indeed, while RNNs detect 8 out of 11 anomalies, MKAD was able to detect only 6 of them. RNNs have been used for their capability of handling both continuous and discrete time series data. Further, after the training process, the resulting predictive models can be used for real-time anomaly detection onboard the

aircraft.

In the context of helicopter risk detection within HFDM data, Gavrilovski [61] developed a methodology to improve monitoring capabilities of adverse rotorcraft flight conditions within flight datasets. A multilayer perceptron neural network with several hidden layers was used to perform regression on the nonlinear response of the helicopter simulation data. This approach allowed for an accurate representation of the outputs preserving the characteristics of the simulation analysis results. This study enabled hazard detection within HFDM databases, to predict operating conditions that contribute to rotorcraft accidents. However, as already mentioned, NN architectures are difficult to interpret not allowing for an easy understanding of the input-output relationship.

As already discussed, machine learning techniques are widely used within aviation research. Specifically, descriptive and predictive modeling capabilities have been used for anomaly detection within large flight datasets. However, most of the literature concerns commercial aviation datasets. There are notable differences between rotorcraft and commercial aircraft operations. Commercial airplanes usually follow a routine pattern with a strong similarity between profiles within the same phase of flight. Instead, as explained by Gavrilovski et al. [62], the mission profiles of rotorcraft operations are not enough homogeneous. For example, operations involving search and rescue, medical transport, or tourism all feature very different mission characteristics. This explains why rotorcraft mission profiles are so different from each other, making the analysis difficult in terms of a systematic comparison between phases of flight. Also, while the definition of phases of flight of commercial airplanes is well established, rotorcraft phases of flight remain not well defined in the literature. Chin et al. [29] supported this effort proposing a process for rotorcraft phases of flight identification. The detection is based on guidelines found in literature and the estimations of domain matter experts. Furthermore, the heterogeneity of flight

data recording devices represents a big challenge within rotorcraft aviation. Not all helicopters have the same equipment, resulting in not uniform recordings of flight parameters. The NTSB has recommended spreading and standardizing the use of flight data recorders onboard helicopters [106]. This lack of consistency limits the comparison between similar flight profiles and hinders the accumulation of sufficient flight data that would allow for knowledge discovery through machine learning techniques.

2.3.2 Physics-Based Approaches

A physics-based model is typically built up from first principles using many a priori assumptions about the vehicle characteristics. During a simulation, the model is required to predict the aircraft response from a specific set of inputs. While sufficient information about the aircraft is required, no flight data is needed to build the model [114]. Within the literature, different levels of model complexity exist. From the approximated point mass model to the most complete nonlinear helicopter model, different tradeoffs between model complexity and simulation accuracy may be chosen depending on the requirements.

Even if building the model can be very labor intensive, physics-based approaches are essential for many applications. Contrary to the data-driven techniques, a physics-based model can predict aircraft performance and dynamic behaviors even before the aircraft has been built. Often no flight data is available for the analysis of conditions at the boundaries of the flight envelope and flight tests are too expensive and dangerous to perform. Hence, physics-based simulations are used to predict the aircraft response in those critical conditions to facilitate several activities such as performance analysis, design and certification, handling qualities research, and safety training.

Harrison [69] used the physics-based model of a general aviation fixed-wing aircraft to define the flight envelope of loss of control conditions. Further, the model supported the investigation of new mitigation techniques at the boundaries of the flight envelope.

Since the flight conditions analyzed in this work are far from nominal and cannot be well approximated by linear models, a nonlinear dynamic model was chosen to assure an accurate representation of the upset conditions during loss of control incidents.

With regards to rotorcraft physics-based simulations, Gavrilovski [61] used several models to improve the understanding of some dangerous conditions that contribute to current helicopter accident rates. The analysis focused on vortex ring state, autorotation, and tipover conditions. Several levels of fidelity were considered, from static performance models to nonlinear dynamic simulations. As shown in Figure 2.14, a two dimensional dynamic model was used to study the lateral behavior of a helicopter on the ground for the tipover analysis. Further, the same study was performed using a three-dimensional dynamic model which accounted for the rolling motion. Finally, the sophisticated nonlinear dynamic model implemented in the simulation software FLIGHTLAB was used to validate the previous models. It was shown how lower fidelity models allow for a general understanding of the condition, while a more com-

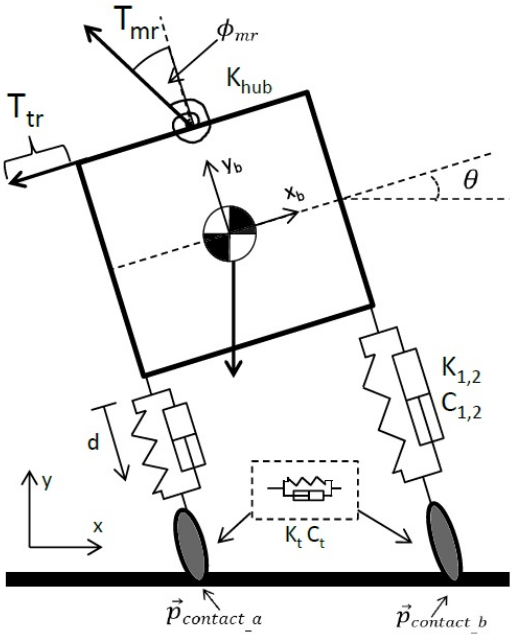

Figure 2.14: Two dimensional tipover model [61].

plex helicopter model gives more detailed and accurate results. Improved detection capabilities were demonstrated compared to the existing techniques used within the HFDM program.

Okuno and Kawachi [112, 111] built a rigid-body dynamic model to investigate helicopter safety procedures following power failure. The rigid body dynamic model has three degrees of freedom, as shown in Figure 2.15. Important aerodynamic characteristics were included such as the blade rotor stall effects and the main rotor vortex ring, with modified versions of the blade element theory and momentum theory, respectively. A good correlation was demonstrated between the predicted height-velocity curve and the flight tests, demonstrating how the success in emergency landings mainly depends on the pilot's collective inputs, wind speed, and landing site characteristics. However, some differences were observed in the results because of the model assumptions. Bottasso et al. [14] studied the trajectory optimization for rotorcraft vehicles, including pilot-in-the-loop effects. The dynamics of a generic medium size helicopter were simulated using the software FlightLab. The model is based on three-dimensional rigid body dynamics, computing rotor forces and moments using blade element theory and uniform inflow. A power balance equation calculates the

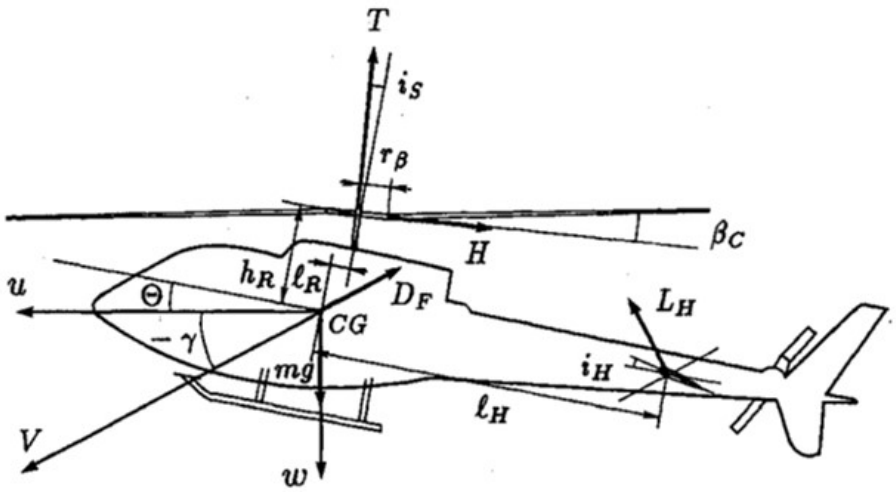

Figure 2.15: Helicopter physics-based model representation [112].

power available and the rotor torque to the rotor speed rate. Quasi-steady flapping dynamics with a linear aerodynamic damping correction is used to derive rotor attitude. Also, the model includes corrections for compressibility effects and downwash angle variation due to the main rotor interactions. To capture for performance loss due to human limitations, the addition of a simple delay in the control application was preferred to the more sophisticated modeling of the musculoskeletal system using multibody dynamics. Improved accuracy in the results was achieved while showing the potential for solutions obtained with simpler and less laborious physics-based models.

2.4 Summary and Observations

The numerous accidents involving LTE and the inability of pilots to recognize and avoid the proximity to LTE suggests that this phenomenon still represents a less-understood phenomenon within the rotorcraft community. Different names and definitions can be found in the literature, together with the inconsistent descriptions of the most critical flight conditions that may lead to LTE behavior. Even some flight training simulators do not accurately represent it, potentially contributing to a misleading pilot's training and low awareness during flights. The dramatic consequences are seen in the number of LTE accidents reported by the NTSB [107]. Because of the critical flight scenarios developed during LTE events, the ongoing strategies aim to promote better awareness of LTE within the pilots' community to support the proactive mitigation of LTE accidents.

The LTE bowtie analysis [158] provides pilots with a schematic summary of all the dangerous flight scenarios that lead to fatal LTE accidents in the past, enhancing their ability to quickly recognize the proximity to LTE and increase their chance of survival. This safety practice is easy to apply and does not require a significant amount of flight data or computational effort. However, because of its retrospective nature

and its strict correlation to the specific accident scenarios, it is not a powerful enough approach for the prediction of negative trends of potential safety issues related to LTE. Also, the large number of factors that influence LTE increase the difficulty for pilots to proactively avoid the hazard. Finally, because of its qualitative characteristics, the LTE bowtie diagram has limited capabilities to efficiently prevent and mitigate LTE accidents. Therefore, the rotorcraft industry has been moving towards a more quantitative approach to mitigate more efficiently potential accidents related to LTE.

The detection of the proximity to LTE within the HFDM program represents an improvement towards quantitative flight data assessments related to LTE. Through this program, pilots become aware of the proximity to LTE that occurred during the flight, training on improving their proactive LTE risk evaluations. However, the threshold values that define the current LTE safety metric [158] are not fully accurate since they are based on pilots' subjective evaluations, hindering the full reliability of the detection. Also, the metric does not account for the human factor component. In fact, during an LTE event, the failed application of the correct pedal control recovery would lead to a missed detection. Also, it is noted that for a proper application of the safety metric, several input parameters are needed to detect the different levels of proximity to LTE. However, some of those parameters, e.g., the flight control parameters, are often not available within the recorded flight data. This greatly hinders the accuracy of the detection of the proximity to LTE making the safety metric less applicable within the HFDM environment. Hence, improved efforts are needed for a more reliable definition of LTE safety metric to avoid false or missed detections and enable more accurate flight analyses.

Within the FDM program several safety analysis approaches are employed, depending on the information available and the characteristics of the hazard that is meant to be analyzed. Data-driven approaches, e.g., statistical analysis and anomaly detection through machine learning techniques, rely on the use of flight data to in-

vestigate flight conditions. Though, helicopter flight operations have several pitfalls that hinder the accumulation of sufficient flight data to perform analysis. The lack of homogeneity of recorders and several differences between helicopter mission profiles does not allow to gather consistent data to analyze. Further, because of the rarity of LTE events, the amount of flight data capturing this phenomenon is extremely limited. Since this flight condition is particularly dangerous, it is very difficult to perform flight tests to gather data for further investigations. Further, some of the flight simulation tools do not accurately represent the LTE phenomenon hindering the accumulation of flight data related to LTE.

Physics-based simulations are often used to investigate the aircraft response during dangerous flight scenarios, allowing for the exploration of phenomena for which sufficient flight data is not available. Even if building the model can be very labor intensive, physics-based models are essential for many applications such as performance analysis, design and certification, handling qualities research, and safety training. Often no flight data is available for the analysis of conditions at the boundaries of the flight envelope and flight tests are too expensive and dangerous to perform, therefore physics-based approaches can be used to replicate and analyze critical flight scenarios. However, the ambiguities surrounding the physics of LTE hinder the application of this type of approach. Also, because of the complexity involved in performing physics-based simulations, there is the necessity to provide the operator with a tool designed to analyze flight data and easily detect the proximity to LTE without the need for a simulation model. Hence, an alternative approach is needed to enhance the detection accuracy of the proximity to LTE within the HFDM program.

2.5 Research Objective

The ongoing strategies that support the proactive mitigation of LTE accidents revealed several pitfalls. In particular, it has been observed that a more reliable defini-

tion of LTE safety metric is needed to avoid false and missed detections of proximity to LTE. Further, because of the limitations provided by the current techniques used within the FDM program, an alternative approach is needed to improve the detection accuracy of the proximity to LTE. Hence, the motivating question of this research is:

How can a more accurate LTE safety metric be developed to enable a more reliable prediction of proximity to LTE within the HFDM program?

Motivated by this question, the main research objective is defined as follows:

Formulate a methodology to improve the detection capability of the proximity to LTE within the HFDM program and support the proactive mitigation of helicopter accidents related to LTE.

To achieve the main objective the following sub-objectives will be tackled:

- Enhance the understanding of the physics of the different LTE phenomena.
- Investigate what are the assumptions and theories that the helicopter simulation model should include to adequately represent the different LTE phenomena.
- Enhance the understanding of the factors that mainly influence the proximity to LTE.
- Improve the current investigative approach used for helicopter accidents involving LTE phenomena.
- Evaluate what gaps still exist that prevent a more reliable proximity to LTE detection to guide future research in rotorcraft safety.

CHAPTER 3
METHODOLOGY FORMULATION

3.1 Approach Overview

The methods used within the FDM program present several drawbacks that hinder the development of a more accurate LTE safety metric. Specifically, data-driven approaches cannot be directly used because of the limited availability of flight data related to LTE. Also, the ambiguities surrounding the fundamental nature of LTE hinder the correct physics-based modeling and simulation of this phenomenon. Hence, an alternative approach is sought to enhance the detection accuracy of the proximity to LTE within the HFDM program. This will not only improve the understanding of the factors that may influence the proximity to LTE but also promote LTE awareness within the rotorcraft community to support the proactive mitigation of helicopter accidents related to LTE.

Figure 3.1 illustrates an overview of the approach used to formulate the methodology. First, it is necessary to analyze the physics of LTE to enhance the understanding of this less-understood phenomenon. This is accomplished through a physics-based approach based on the work published by Zanella et al. [159]. Because of the ambiguities surrounding the fundamental nature of LTE, it is essential to investigate each LTE phenomenon, i.e., loss of weathercock stability, running out of pedal for trim, and vortex ring state at the tail rotor. The different physics-based models needed to adequately represent those conditions must be analyzed to ensure an accurate representation of LTE. Further, the parameters that enable the detection of those conditions must be found to classify each LTE phenomenon within the simulation results. However, there is the necessity to provide the operator with a tool

designed to analyze flight data and easily detect the proximity to LTE without the need for a simulation model. Hence, a method is sought to enable a fast and reliable identification of LTE events within the HFDM environment.

Machine learning represents a promising approach to develop computer learning algorithms able to use data to obtain intelligent actions. A vast literature review on machine learning is provided by [90, 100, 70, 152]. The choice of the learning technique and the subsequent algorithm is a function of different factors, such as the dataset size, the type of parameters involved, and the characteristics of the anomaly that is intended to be detected. Considering the lack of helicopter flight data related to LTE, it is observed that predictive models represent an advantageous approach to identify LTE within flight data. A predictive model estimates the output values after going through a learning training process of the relationship between the input-output values of a specific dataset. Since clear learning instructions are provided, the process of training a predictive model is called supervised learning. In other words, the supervised learning algorithm aims to optimize the predictive model to find the combination of values that give the target output.

The new LTE safety metric will be a predictive model that relate to each of the LTE phenomena and allow for the identification of their proximity within flight data. To build the model, a dataset that includes the different types of LTE occurrences is needed. Since it is known how to represent LTE through physics-based simulations, a dataset can be created simulating each LTE phenomenon using the appropriate simulation model. After going through the learning training process of the relationship between the initial test conditions and the results of the predefined physics-based simulations, different prediction functions are created for each LTE phenomenon. Ultimately, appropriate boundaries must be defined to detect the proximity to the different types of LTE events. The resulting LTE safety metric, i.e., the comprehensive model that predicts LTE events and proximity to LTE, will encompass the

different predictive models obtained. This metric will be evaluated against the current filter-based metric used within the HFDM program, to test if the proposed methodology provides an improved detection of the proximity to LTE to better support the mitigation of helicopter accidents related to LTE. During the development of the proposed methodology, the following assumptions are considered:

- *The helicopter design parameters are known*

  If some of the design parameters of the helicopter considered are not available, the user may use published design parameters of a similar helicopter configuration to obtain an approximated result.

- *The LTE safety metric will be based on out of ground effect flight scenarios*

  The methodology creates a more applicable framework for future developments which may involve the addition of in ground effects to improve the accuracy of proximity to LTE predictions.

- *The required flight data for the detection of the proximity to LTE is available*

  The methodology will focus on enabling the more accurate detection of proximity to LTE within the HFDM program, assuming that the necessary flight data is available.

- *The methodology performance is measured in terms of false alerts and missed detections*

  The performance of the system will be compared to the current method used with the HFDM program, evaluating false and missed detections.

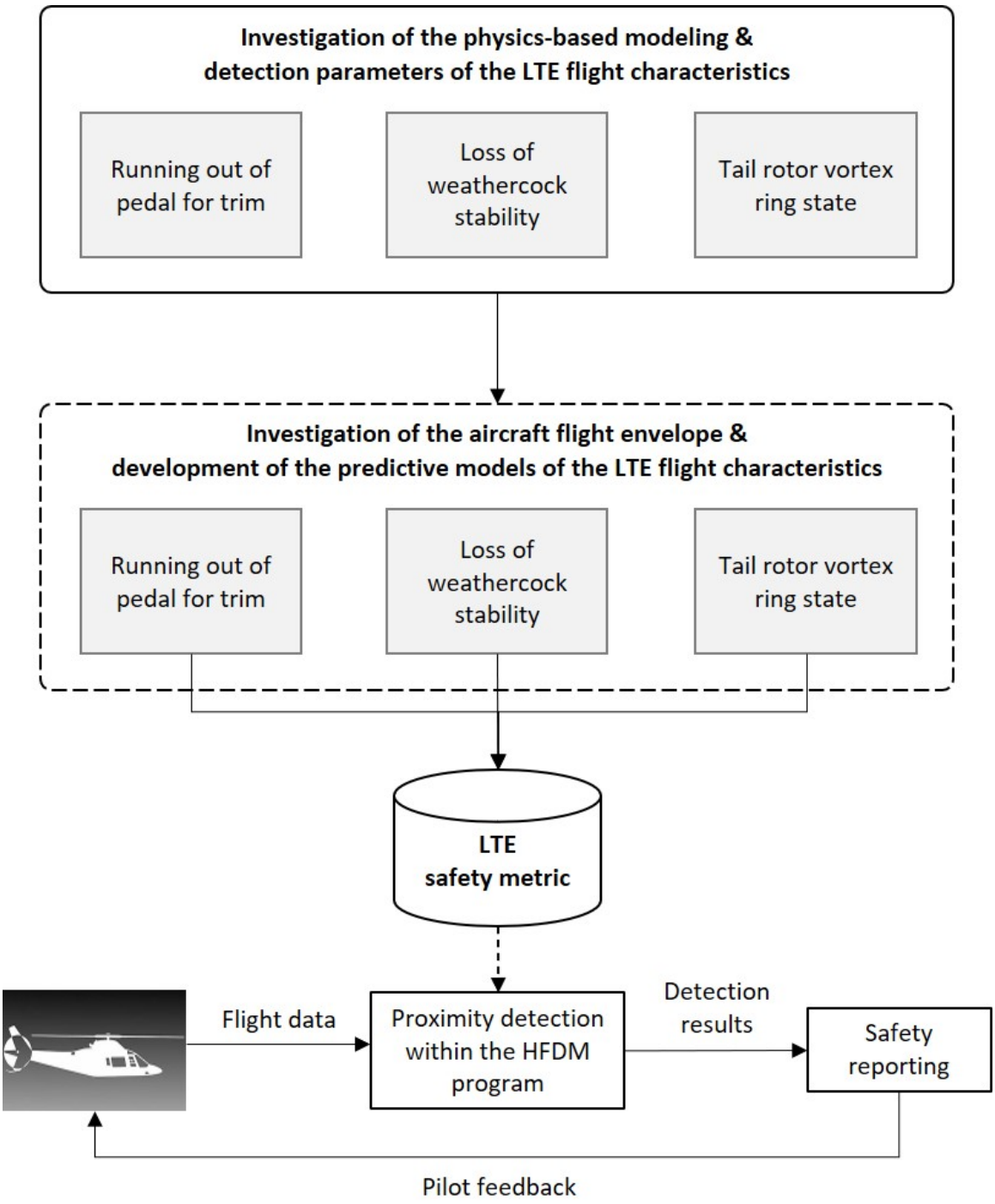

Figure 3.1: Overview of research approach.

3.2 Helicopter Simulation Model

Because of the lack of flight data including LTE events, a physics-based approach is sought to investigate the different LTE phenomena. This section describes the baseline simulation model used within this research.

3.2.1 An Overview

The analysis of rotorcraft flight dynamics requires a mathematical model able to replicate the behavior of the aircraft in flight. It is often used in conceptual design, the early phase of the design process, to investigate mission requirements, aircraft design constraints, and performance estimations. The simulation model must be able not only to perform trim estimation and stability analysis, but also should capture the response of the aircraft to pilot's controls and external atmospheric disturbances. Aerodynamic and structural effects highly influence the rotorcraft dynamics, often involving non-linear phenomena, making the problem even more complex. Throughout this work, the vehicle can be treated by making the following assumptions:

1. Rigid body motion
2. Constant body mass, m
3. The Earth is considered as the inertial reference frame

Because small flight speeds and short flight times are considered, the listed assumptions are considered to be valid. The basic vehicle model has 6 degrees of freedom, 3 translational, and 3 rotational, and it is characterized by a state vector of 12 components, formed by the translational velocities, angular velocities, attitude angles, and body position. Those quantities are referred to a system of body-fixed axes centered at the aircraft's center of mass, with x_B pointing towards the nose of the aircraft, y_B towards the right hand side of the vehicle is seen from behind, and

z_B that completes the right-handed orthogonal frame. The state vector $\boldsymbol{x}$ is defined as:

$$\boldsymbol{x} = \{u, v, w,\ p, q, r, \phi, \theta, \psi, x_e, y_e, z_e\} \tag{3.1}$$

where u, v and w are the body-axes translational velocities; p, q and r are the body-axes angular velocities; ϕ, θ and ψ are the Euler angles; and x_e, y_e, and z_e the components of the position vector relative to a fixed point on earth. As the state vector changes at each time step of the simulation, the objective of the vehicle motion model is to determine the 12 states of the aircraft with time.

The body dynamics is governed by the Newton's laws, which relate the applied loads to the translational and rotational accelerations. The translational dynamics is given by Newton's second law which determines the body-axes translational acceleration components:

$$\dot{u} = -\left(wq - vr\right) + \frac{X}{m} - g\ sin\theta \tag{3.2}$$

$$\dot{v} = -\left(ur - wp\right) + \frac{Y}{m} + g\ cos\theta\ sin\phi \tag{3.3}$$

$$\dot{w} = -\left(vp - uq\right) + \frac{Z}{m} + g\ cos\theta\ cos\phi \tag{3.4}$$

where X, Y, and Z are the aerodynamic and propulsive force components in the body frame which include the contributions from the different aircraft components. The rotational dynamics is expressed by the Newton-Euler equation, that defines the body-axes angular acceleration components:

$$I_{xx}\dot{p} = +I_{xz}\left(\dot{r} + pq\right) + \left(I_{yy} - I_{zz}\right)qr + I_{yz}\left(q^2 - r^2\right) + I_{xy}\left(\dot{q} - rp\right) + L \tag{3.5}$$

$$I_{yy}\dot{q} = +I_{xz}\left(r^2 - p^2\right) + \left(I_{zz} - I_{xx}\right)rp + I_{xy}\left(\dot{p} + qr\right) + I_{yz}\left(\dot{r} - pq\right) + M \tag{3.6}$$

$$I_{zz}\dot{r} = +I_{xz}\left(\dot{p} - qr\right) + \left(I_{xx} - I_{yy}\right)pq + I_{yx}\left(p^2 - q^2\right) + I_{yz}\left(\dot{q} + rp\right) + N \tag{3.7}$$

where L, M, and N are the aerodynamic and propulsive moment components in the

body frame which include the contributions from the different aircraft components, and I_{xx}, I_{yy}, etc., are the fuselage moments of inertia about the reference axes.

The time derivatives of the attitude angles and the position vector are determined using kinematic relationships. The body attitude rates are obtained from measurements of the body angular rates using an iterative solution that is initialized using the ground orientation of the vehicle:

$$\dot{\phi} = p + (\sin\phi \tan\theta)\ q + (\cos\phi \tan\theta) \tag{3.8}$$

$$\dot{\theta} = \cos\phi\ q - \sin\phi\ r \tag{3.9}$$

$$\dot{\psi} = (\sin\phi \sec\theta)\ q + (\cos\phi \sec\theta)\ r \tag{3.10}$$

The vehicle position $[x_e, y_e, z_e]$ is expressed with reference to the inertial reference frame, and its derivative is computed using a rotation matrix that transforms the translational velocity vector in the body reference frame, i.e., $\boldsymbol{v_B} = [u, v, w]$, to the inertial reference frame. Hence, 12 first-order ordinary differential equations form the basic vehicle model. Those equations are integrated in time using a given initial state vector, and the appropriate values of aerodynamic and propulsive forces and moments expressed in the body-reference frame. The basic vehicle model is similar for both fixed wing and rotorcraft. The differences rely on the calculation of the aircraft forces and moments, and here hides the real complexity of the problem.

As shown in Figure 3.2, a single rotor helicopter is a system of interacting components, including the main and tail rotors, the fuselage, and the empennage. For each of those subsystems, the body-axes components of forces and moments must be determined. First, the loads are computed using the local coordinate system of each component, and then they are transformed to the body-axes of the aircraft using appropriate transformation matrices. By summing the contributions from all the helicopter components, the total aerodynamic and propulsive loads about the center

of mass of the vehicle can be established. Talbot et al. [136] give a great overview of this process while describing the mathematical model of a single main rotor helicopter developed at Ames Research Center and used to advance the development of design criteria in future helicopters. Including the aerodynamic loads of the aircraft within the vehicle simulation model, it is possible to compute the aircraft flying qualities and investigate phenomena for which flight data is not available. Figure 3.3 illustrates the main components of a single rotor helicopter model, giving a high-level view of the baseline simulation model used within this research.

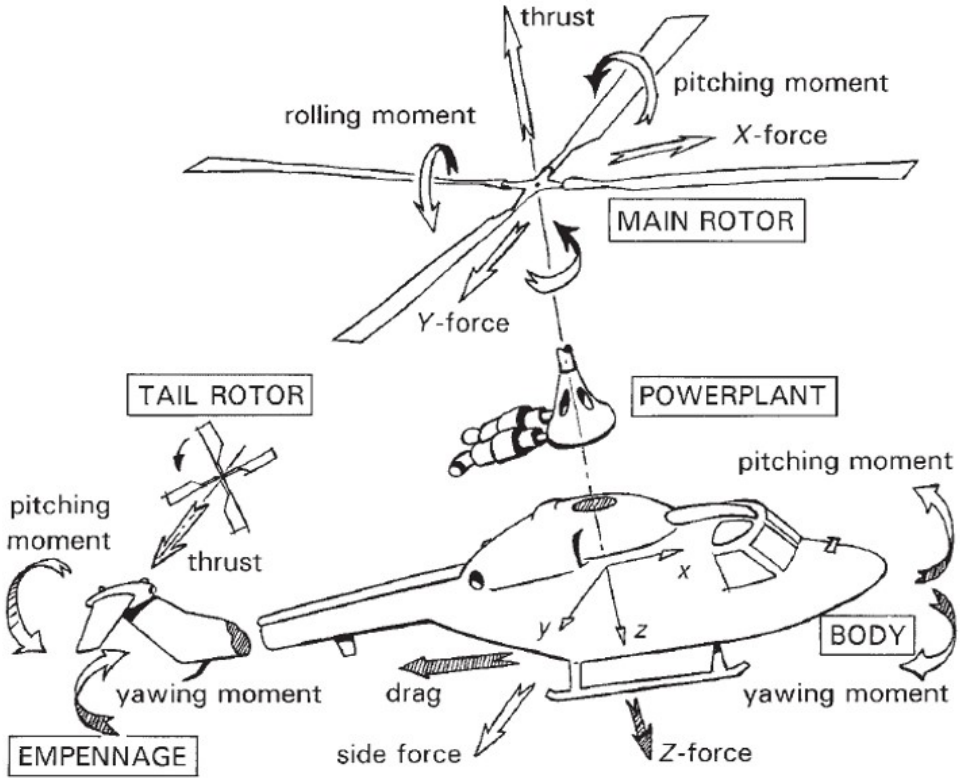

Figure 3.2: Helicopter subcomponents [114].

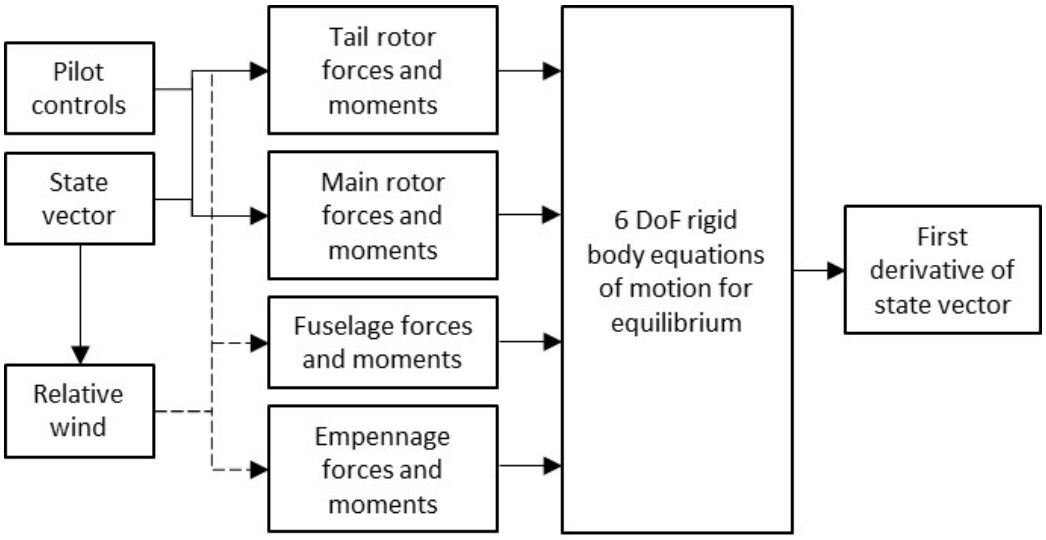

Figure 3.3: Main elements of a single rotor helicopter model.

3.3 Modeling of Loss of Weathercock Stability

Because of the ambiguities surrounding the fundamental nature of LTE, it is essential to investigate each LTE phenomenon. This section describes the physics-based modeling of the phenomenon of loss of weathercock stability. It will be shown that an experiment is required to establish what inflow model is needed to ensure its accurate representation.

3.3.1 The Physics

Directional static stability, also called the weathercock stability, is related to the yaw moment reaction about the center of gravity of the vehicle due to a sideward gust disturbance. If the yaw moment reaction from the vehicle to an external wind gust is such that it tends to yaw the helicopter back to its equilibrium position, it is considered as a statically stable reaction. On the contrary, if the yaw moment reaction is such that it tends to yaw the helicopter away from its equilibrium position, it is considered as a statically unstable reaction.

Aerodynamically, a lateral movement of the aircraft along the positive body y axis

is equivalent to a sideward gust, i.e., a change in wind magnitude, from the pilot's right. However, if we assume small perturbations, the variation in lateral speed v can also be related to a change in sideslip angle β, i.e., a change in wind azimuth, as shown by the following equation:

$$\Delta\beta \approx \ tan\ \Delta\beta \ = \frac{\Delta v}{u} \tag{3.11}$$

where u is the translational velocity of the aircraft. It is noted how the sideslip angle is equivalent to the wind azimuth as they both describe the body yaw orientation relative to air. It is inferred that both wind magnitude and wind azimuth are important variables that may heavily impact the weathercock stability of an aircraft.

The yaw moment reaction from the aircraft is the result of the contributions from the different helicopter subsystems. The main influences are from the tail rotor, the vertical fin, and the fuselage [114]. Each of the helicopter components generates a yaw moment about the center of gravity of the vehicle that will vary with the relative wind conditions. The aerodynamic loads generated by the fuselage and vertical fin are complex non-linear functions of relative airspeed and direction. They are often based on empirical curve fittings of wind tunnel test results that have been carried out for a range of dynamic pressures and aerodynamic angles [151, 13]. Assuming similar fluid dynamics at the test and the simulated flight conditions, each force and moment can be estimated using the aerodynamic coefficients measured during the wind tunnel tests and defined as a function of the angle of attack and the sideslip angle. The fuselage side force coefficient, C_{Yf}, is used to measure the side force at the fuselage reference point, which is defined as:

$$Y_f = \frac{1}{2}\rho V_f^2 C_{Yf} S_f \tag{3.12}$$

where ρ is the air density, V_f is the incident velocity, and S_f is the fuselage side area.

The yaw moment coefficient, C_{Nf}, is used to calculate the yaw moment developed at the fuselage reference point, i.e.:

$$N_f = \frac{1}{2}\rho V_f^2 C_{Nf} S_f l_f \tag{3.13}$$

where l_f is the fuselage reference length. In general, N_f is destabilizing because of the greater fuselage area ahead of the aircraft center of gravity. The vertical fin side force coefficient, C_{Yvf}, obtained from the wind tunnel measurements, is used to calculate the side force generated by the vertical fin, i.e.:

$$Y_{vf} = \frac{1}{2}\rho V_{vf}^2 C_{Yvf} S_{vf} \tag{3.14}$$

where V_{vf} is the incident velocity, and S_{vf} is the fin side area. Figure 3.4 shows the aerodynamic force in body axis frame acting on the vertical fin. The yaw moment developed by the vertical fin is computed as:

$$N_{vf} = Y_{vf} l_{vf} \tag{3.15}$$

where l_{vf} is the distance between the vertical fin center of pressure and the center of gravity of the aircraft. The vertical fin is an essential element for directional static stability. It is often called the vertical stabilizer as, in most cases, it provides a significant contribution to the directional stability of the aircraft. It is noted how a lower dynamic pressure causes the fuselage and the vertical fin to develop a smaller yawing moment, influencing the weathercock stability of the aircraft much less. Low-speed conditions cause the vertical fin to lose its critical role in providing the restoring yaw moments to external disturbances.

From the literature, low airspeeds provide an enabling environment for LTE. Hence, they are of particular importance to this study. A key contribution to di-

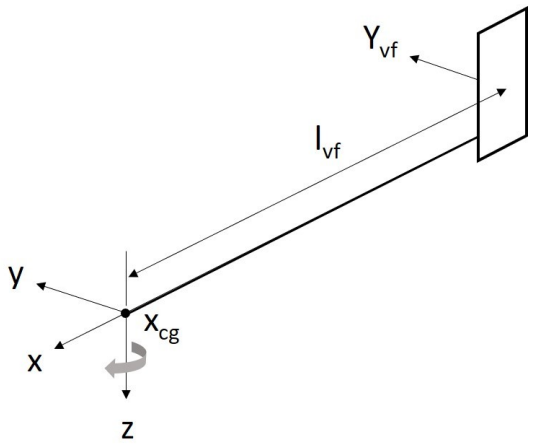

Figure 3.4: Vertical fin subsystem.

rectional static stability at low airspeeds is given by the tail rotor. The yaw moment developed by the tail rotor N_{tr} is directly proportional to the thrust generated T_{tr} through the simple equation:

$$N_{tr} = T_{tr} l_{tr} \tag{3.16}$$

where l_{tr} is the distance between the tail rotor hub and the center of gravity where the body frame is fixed, as depicted in Figure 3.5. Since the T_{tr} points towards the positive y axis of the vehicle, the resulting N_{tr} is negative and causes a left yaw. In the case of a canted tail rotor configuration, only the side force component of the

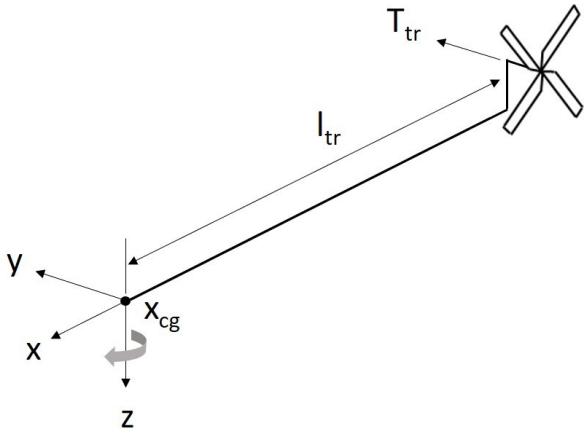

Figure 3.5: Tail rotor subsystem.

thrust would affect the yaw moment magnitude. From blade element analysis, the thrust produced by the rotor is expressed by:

$$T_{tr} = \rho V_{tip,tr}^2 C_{T,tr} A_{tr} \tag{3.17}$$

where $V_{tip,tr}$ is the tail rotor blade tip speed, $C_{T,tr}$ the tail rotor thrust coefficient, and A_{tr} the tail rotor disk area. T_{tr} can be assumed to be equal to the sum of the lift contributions produced by each blade element. Figure 3.6 illustrates the aerodynamic environment at a typical blade element. The lift produced by the blade element can be defined in non-dimensional form by the lift coefficient c_l. This is a function of the effective angle of attack α of the blade element, which is given by:

$$\alpha = \theta - \phi \approx \theta - \frac{U_P}{U_T} \tag{3.18}$$

where θ is the blade pitch angle and ϕ is the relative inflow angle which can be assumed to be defined as the ratio between the perpendicular and the tangential components of the relative airflow velocity. Considering the hover case, U_T is the angular speed of the blade element, and U_P is the total inflow velocity at the blade section which is defined as:

$$U_P = v_c + v_i + r\dot{\beta} \tag{3.19}$$

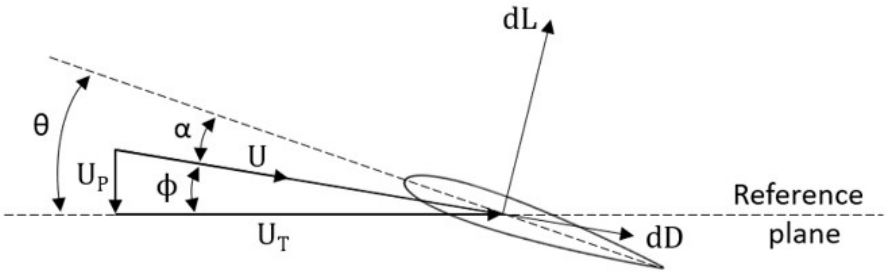

Figure 3.6: Incident velocities at the blade element.

where v_c is the axial component of the freestream velocity, v_i is the induced inflow velocity, and $r\dot{\beta}$ is the flapping rate induced velocity in which r is the blade element location along the blade and β is the blade flapping angle. It is noted how the effective angle of attack at each blade section is a function of the key variables θ, v_c, and v_i. The blade pitch angle is directly related to the pilot pedal control applied. The axial component of the freestream velocity is a function of the relative wind conditions at the tail rotor plane. The induced inflow velocity, also called downwash, is the flowfield induced by the rotor, and, from momentum theory, it is inversely proportional to the mass flow through the rotor. The accuracy of induced velocity prediction in the analysis depends on the inflow model used. Several models allow for the calculation of the induced inflow over the rotor disk based on distinct theories and assumptions. However, which of those models is the most appropriate to accurately replicate the weathercock stability of the aircraft is still unclear.

3.3.2 Research Question 1 and Hypothesis

The rotor induced inflow, also called downwash, is the flowfield induced by the rotor. The accuracy of its representation depends on the inflow model used, impacting the prediction of the tail rotor loadings and, consequently, the simulation of the helicopter's directional stability. Hence, it is essential to investigate the inflow model needed for the proper simulation of loss of weathercock stability. The following research question is formulated:

What assumptions and theories should the tail rotor inflow model include to adequately represent the phenomenon of loss of weathercock stability?

To identify the types of inflow models needed for this study, a few observations are made:

- The investigation of loss of weathercock stability is sought, involving the study

of helicopter flight dynamics.

- The phenomenon of loss of tail rotor effectiveness is defined as a low-speed flight characteristic [54].
- It is assumed that only out of ground effect flight scenarios are considered in the development of the final LTE safety metric.

To investigate the aircraft flight dynamics during out of ground effect low-speed flight conditions, an inflow model that provides a good tradeoff between modeling accuracy and computational time is needed. A comprehensive review of inflow models intended for this specific set of applications is given in Appendix A.1. It is observed that models that involve a linear gradient distribution of the inflow along the rotor blade provide an appropriate prediction of the rotor inflow for applications involving helicopter flight dynamics. Those models are often used in rotorcraft flight simulators because of their better correlation with the available experimental data [26].

Several experimental tests confirm that the operational environment of the tail rotor is affected by the turbulent aerodynamic interaction with the main rotor wake [4, 137, 35]. Low-speed quartering flight conditions reveal to be the most critical and difficult to predict. As illustrated in Figure 3.7, within specific wind azimuth regions the tail rotor is impacted by the tip vortices trailed from the edges of the main rotor disk. The formation of this type of vortices is described in more detail by Heyson [72] and Brocklehurst [19]. The tail rotor performance can be significantly degraded by the velocity field induced by the main rotor tip vortices, impacting the directional stability of the aircraft. Therefore, the following hypothesis is formulated:

If the tail rotor inflow is represented by a linear gradient distribution along the tail rotor blade while accounting for the aerodynamic interference from the main rotor vortex wake, then the impact of external atmospheric disturbances on the representation of the loss of weathercock stability phenomenon will be more realistic.

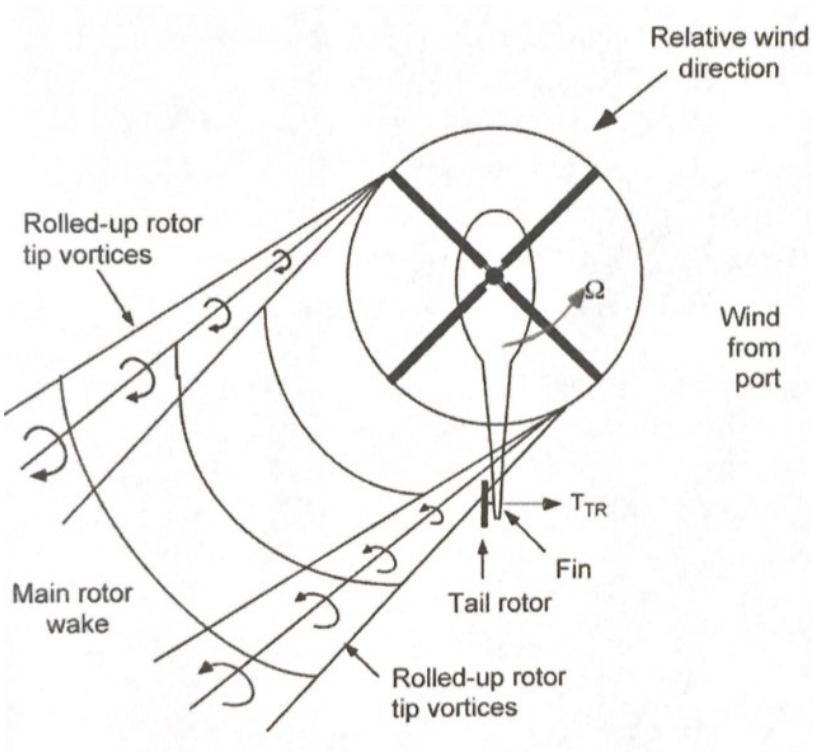

Figure 3.7: Aerodynamic interaction between tail rotor and main rotor tip vortices during quartering flight [92, 143].

To test this hypothesis and ensure an appropriate level of accuracy in the representation of this phenomenon, an investigation on the impact of the inflow modeling on the loss of weathercock stability of the aircraft is needed.

3.3.3 Formulation of Experiment 1

It has been observed that for a particular helicopter configuration in ambient conditions, the tail rotor blade pitch angle, the inflow model used for the tail rotor, and the relative wind conditions are essential variables that should be considered while analyzing the weathercock stability of the aircraft. To ensure a causal effect between the change in relative wind conditions and the resulting tail rotor thrust variations, the blade pitch angle needs to be constant throughout the investigation. With regards to the wind conditions considered, constant settings of wind magnitude are needed

while varying the wind azimuth to ensure a unique relationship between lateral speed change Δv and yaw moment reaction ΔN from the aircraft. This type of analysis is usually accomplished during wind tunnel tests. The aircraft model is pinned at the aerodynamic center with all degrees of freedom fixed except for the yaw motion, and it is forced to spin at a fixed body yaw rate while being subjected to constant wind magnitude coming from the tunnel. The moments and forces generated from the aircraft reaction to the change in wind azimuth are then recorded at the aerodynamic center of the vehicle. An example of this study was performed by the LTE Joint Special Study Group in the attempt to investigate the critical flight characteristics of LTE [154].

This experiment aims to replicate the above controlled environment using a physics-based simulation model to investigate the impact of the inflow model used on the aircraft weathercock stability. Models with different levels of fidelity have been selected. The models are characterized by a low computational effort to enable a fast and reliable investigation of the flight dynamics of the vehicle through rotorcraft simulation. First, a uniform inflow is considered because of its simplicity. Specifically, momentum theory is used to derive the induced inflow as a constant value over the rotor disk [92]. The thrust coefficient is calculated using the simplified rotor model derived by Bailey [3]. Second, a linear inflow gradient along the rotor blade is assumed. This is a popular assumption used in rotorcraft flight dynamics as it gives a good representation of the inflow, calculating the inflow gradients that a uniform model fails to predict. Pitt-Peters dynamic inflow model is used as its results compare well with the experimental data. This model is derived using an acceleration potential approach, by modeling the rotor as an actuator disk. It represents the flow over the rotor disk in terms of three inflow states while accounting for the geometric skew of the wake [121]. The tail rotor thrust is calculated coupling the inflow dynamics with a blade element model that accounts for 11 blade elements [92]. Lastly, the aerodynamic interaction

of the main rotor wake with the tail rotor is considered. Pitt-Peters model is extended to calculate the velocity induced by the main rotor vortex wake at any arbitrary point in the flow field. Specifically, the geometric relationship between the main and tail rotor is considered to quantify the interference [118]. This approach is initially applied while using momentum theory at the tail rotor. Then, the Pitt-Peters model is used to increase the accuracy of the tail rotor inflow dynamics.

3.4 Modeling of Running Out of Pedal for Trim

The next LTE event considered is the phenomenon of running out of pedal (tail rotor collective) for trim. This section describes the physics-based models required to accurately simulate it. It will be shown that an experiment is required to establish what inflow model is needed to achieve an accurate representation of this phenomenon.

3.4.1 The Physics

The tail rotor system provides thrust that is necessary for balancing the main rotor torque, providing yaw stability and directional control [92, 56]. The amount of thrust produced is controlled by the pilot through the pedals, which vary the collective pitch angle of the tail rotor blades. Some flight scenarios require the pilot to apply a large amount of pedal control to maintain equilibrium. For example, during low-speed high power conditions, a large main rotor torque is developed, and a high anti-torque thrust is needed to achieve directional equilibrium. This is obtained using a large amount of anti-torque pedal. However, if the pedal is not enough to develop the necessary tail rotor thrust, then the aircraft undergoes an uncommanded yaw. It is observed that the running out of pedal phenomenon is related to the yaw moment developed by the tail rotor to maintain directional equilibrium. Hence, it is essential to consider the aircraft yaw balance to calculate the pedal control needed.

Figure 3.8 illustrates the aerodynamic forces and moments in the body axis system

that are acting on a helicopter in free flight. The aircraft subsystems that provide a significant contribution to the directional equilibrium are the main rotor, the tail rotor, the vertical fin, and the fuselage. The yaw moment balance is achieved by summing the moments with respect to the aircraft center of gravity. Hence, the equation for directional equilibrium is:

$$Q_{mr} - Y_{mr}l_{mr} - T_{tr}l_{tr} - Y_{vf}l_{vf} + N_f - Y_f l_f = 0 \tag{3.20}$$

The contributions provided by the fuselage and the vertical fin have already been detailed in the previous section. A summary of the most important considerations is provided here. The aerodynamic loads generated by the fuselage and the vertical fin are complex non-linear functions of relative airspeed and direction. They are often defined as functions of the angle of attack and the sideslip angle using empirical curve fittings of wind tunnel test data. It has been observed that at low dynamic pressures

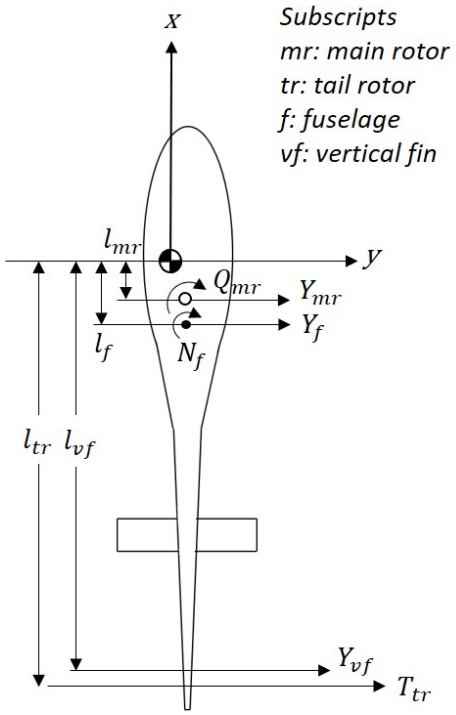

Figure 3.8: Aerodynamic loads acting on a helicopter in free flight (top view).

those two components develop small yaw moments. At low airspeeds, the tail rotor represents the key contribution for yaw moment balance.

By Newton's Third Law, the main rotor rotation causes a torque reaction on the fuselage that, if not countered by an antitorque force, would cause the helicopter body to turn in the opposite direction of the main rotor rotation. Hence, the yaw balance equation also includes the main rotor torque, Q_{mr}, which is defined as:

$$Q_{mr} = \rho V_{tip,mr}^2 C_{Q,mr} R_{mr} A_{mr} \tag{3.21}$$

where ρ is the air density, $V_{tip,mr}$ is the main rotor blade tip speed, $C_{Q,mr}$ is the main rotor torque coefficient, R_{mr} is the main rotor radius, and A_{mr} is the main rotor disk area. The torque coefficient is equivalent to the power coefficient which can be defined as:

$$C_P = C_{Pi} + C_{P0} + C_{Pp} + C_{Pc} \tag{3.22}$$

where C_{Pi} is the induced power coefficient related to the ideal power required to hover, C_{P0} is the profile power coefficient related to the power required to overcome the viscous losses at the rotor, C_{Pp} is the parasitic power coefficient related to the power required to overcome the drag of the helicopter, and C_{Pc} is the climb power coefficient related to the power required to increase the gravitational potential of the helicopter. Using the energy balance approach, the main rotor torque can be calculated using the dimensionless coefficient of the main rotor power required, i.e.:

$$C_{P,mr} = \frac{C_{T,mr}^2}{2\sqrt{\mu^2 + \lambda^2}} + \frac{\sigma C_{d0}}{8}\left(1 + 4.65\mu^2\right) + \frac{1}{2}\mu^3 \frac{f}{A} + \lambda_C C_{T,mr} \tag{3.23}$$

where μ is the main rotor advance ratio, λ is the main rotor inflow ratio, σ is the main rotor solidity, C_{d0} is the profile drag coefficient of the airfoils that make up the main rotor blades, f is the equivalent flat-plate area, A is the main rotor disk area,

λ_c is the dimensionless climb rate, and $C_{T,mr}$ is the main rotor thrust coefficient.

While knowing the main rotor torque, and the yaw moments developed by the fuselage and vertical fin, the yaw balance equation allows to calculate the tail rotor thrust required to maintain equilibrium, T_{tr}. From this, the tail rotor thrust coefficient is computed as:

$$C_{T,tr} = \frac{T_{tr}}{\rho V_{tip,tr}^2 A_{tr}} \tag{3.24}$$

After calculating the tail rotor thrust coefficient, a simplified approach can be used to estimate the tail rotor collective pitch angle, $\theta_{0,tr}$. An equation for the steady value of the rotor thrust coefficient can be derived from blade element theory while neglecting the non-steady effects responsible for vibratory loads. The normal force at each blade element is expressed as a function of the air velocity components and the pitch angle. This force is then integrated over the entire blade span, averaged over one rotor revolution, and multiplied by the number of blades, constructing the equation:

$$\mathrm{C}_{T\,\mathrm{tr,steady}} = \frac{\sigma_{tr} a_{tr}}{4\pi} \int_{\psi=0}^{2\pi} \int_{r=0}^{1} [U_T^2 \theta - U_T U_P] dr d\psi \tag{3.25}$$

After deriving the above equation, the collective pitch angle for a tail rotor with untwisted blades is defined as follows:

$$\theta_{0,tr} = \frac{\frac{6C_{T,tr}}{\sigma_{tr} a_{tr}} + \frac{3}{2}\lambda_{tr}}{1 + \frac{3}{2}{\mu_{tr}}^2} \tag{3.26}$$

where μ_{tr} is the tail rotor advance ratio, and λ_{tr} is the tail rotor inflow ratio. The tail rotor advance ratio is defined as:

$$\mu_{tr} = \frac{V_\infty cos\alpha_{tr}}{V_{tip,tr}} \tag{3.27}$$

where V_∞ is the relative airspeed, and α_{tr} is the angle of attack of the tail rotor disk.

The tail rotor inflow ratio, λ_{tr}, includes the freestream inflow and the induced inflow components, and it is obtained using:

$$\lambda_{\text{tr}} = \mu_{tr}\ tan\alpha_{tr} + \lambda_{\text{i,tr}} \tag{3.28}$$

It is noted how the tail rotor collective pitch angle is a function of the tail rotor thrust coefficient, the relative wind magnitude and direction, and the inflow model used for the rotor modeling. Several models allow for the calculation of the induced inflow over the rotor disk based on distinct theories and assumptions. However, it is still unclear which of those models is the most appropriate to accurately estimate the collective pitch angle of the tail rotor during yaw moment balance.

3.4.2 Research Question 2 and Hypothesis

The tail rotor collective pitch angle needed to maintain directional equilibrium is impacted by the accuracy of the inflow model used. Because this angle is directly linked to the pilot's pedal input, an investigation on the impact of the inflow modeling on the pedal control needed for yaw balance is necessary to ensure an appropriate level of accuracy in the representation of the running out of pedal phenomenon. The following research question is formulated:

What assumptions and theories should the tail rotor inflow model include to adequately represent the phenomenon of running out of pedal for trim?

To identify the types of inflow models needed, similar observations made during the analysis of the phenomenon of loss of weathercock stability can be considered for this study. To investigate the aircraft flight dynamics during out of ground effect low-speed flight conditions, a good tradeoff between model accuracy and computational time is needed. A comprehensive review of inflow models intended for this specific set of applications is given in Appendix A.1. It is observed that models that involve a

linear gradient distribution of the inflow along the rotor blade provide an appropriate prediction of the rotor inflow for applications involving helicopter flight dynamics. Those models are often used in rotorcraft flight simulators because of their better correlation with the available experimental data [26].

Several experimental tests confirm that the operational environment of the tail rotor is affected by the turbulent aerodynamic interaction with the main rotor wake [147, 148, 94]. Low-speed quartering flight conditions reveal to be the most critical and difficult to predict. Within specific wind azimuth regions, the tail rotor is impacted by the tip vortices trailed from the edges of the main rotor disk. The tail rotor performance can be significantly degraded by the velocity field induced by the main rotor tip vortices, impacting the pedal control margin [51, 6]. Therefore, the following hypothesis is formulated:

If the tail rotor inflow is represented by a linear gradient distribution along the tail rotor blade while accounting for the aerodynamic interference from the main rotor vortex wake, then the representation of the phenomenon of running out of pedal for trim will be more realistic.

To test this hypothesis and ensure an appropriate level of accuracy in the simulation of the running out of pedal phenomenon, an investigation on the impact of the inflow modeling on the pedal control needed for equilibrium is needed.

3.4.3 Formulation of Experiment 2

It has been observed that the yaw balance analysis is necessary to investigate the running out of pedal phenomenon. However, to calculate the pedal control needed to hold a helicopter in equilibrium, the yaw moment generated by the other aircraft components must be known. Because of the significant amount of crosscoupling between forces and moments, a comprehensive equilibrium analysis of the aircraft is

needed. A helicopter is in equilibrium if the sum of all the forces and moments acting on the vehicle is zero:

$$\sum \boldsymbol{F} = \mathbf{0} \tag{3.29}$$

$$\sum \boldsymbol{M} = \mathbf{0} \tag{3.30}$$

Those relationships define the 6 equations that describe the motion of the helicopter while the forces and moments acting on the aircraft are balanced. While the yaw balance equation has been detailed in the previous section, a brief review of the equilibrium equations is provided here. Figure 3.9 illustrates the aerodynamic loads in the body axis system acting on the helicopter in free flight.

The force equilibrium in the longitudinal direction is:

$$X_{mr} + X_{tr} + X_{hf} + X_{vf} + X_f = W sin\theta \tag{3.31}$$

For the lateral force balance, the tail rotor thrust must be included giving:

$$Y_{mr} + T_{tr} + Y_{vf} + Y_f = -W sin\phi \; cos\theta \tag{3.32}$$

The force balance in the vertical direction leads to:

$$Z_{mr} + Z_{tr} + Z_{hf} + Z_{vf} + Z_f = -W cos\theta \; cos\phi \tag{3.33}$$

The equation for lateral moment equilibrium with respect to the center of gravity of the aircraft is:

$$R_{mr} + Y_{mr}h_{mr} + Z_{mr}y_{mr} + T_{tr}h_{tr} + Y_{vf}h_{vf} + Y_f h_f + R_f = 0 \tag{3.34}$$

Summing the pitching moments about the center of gravity of the aircraft leads to

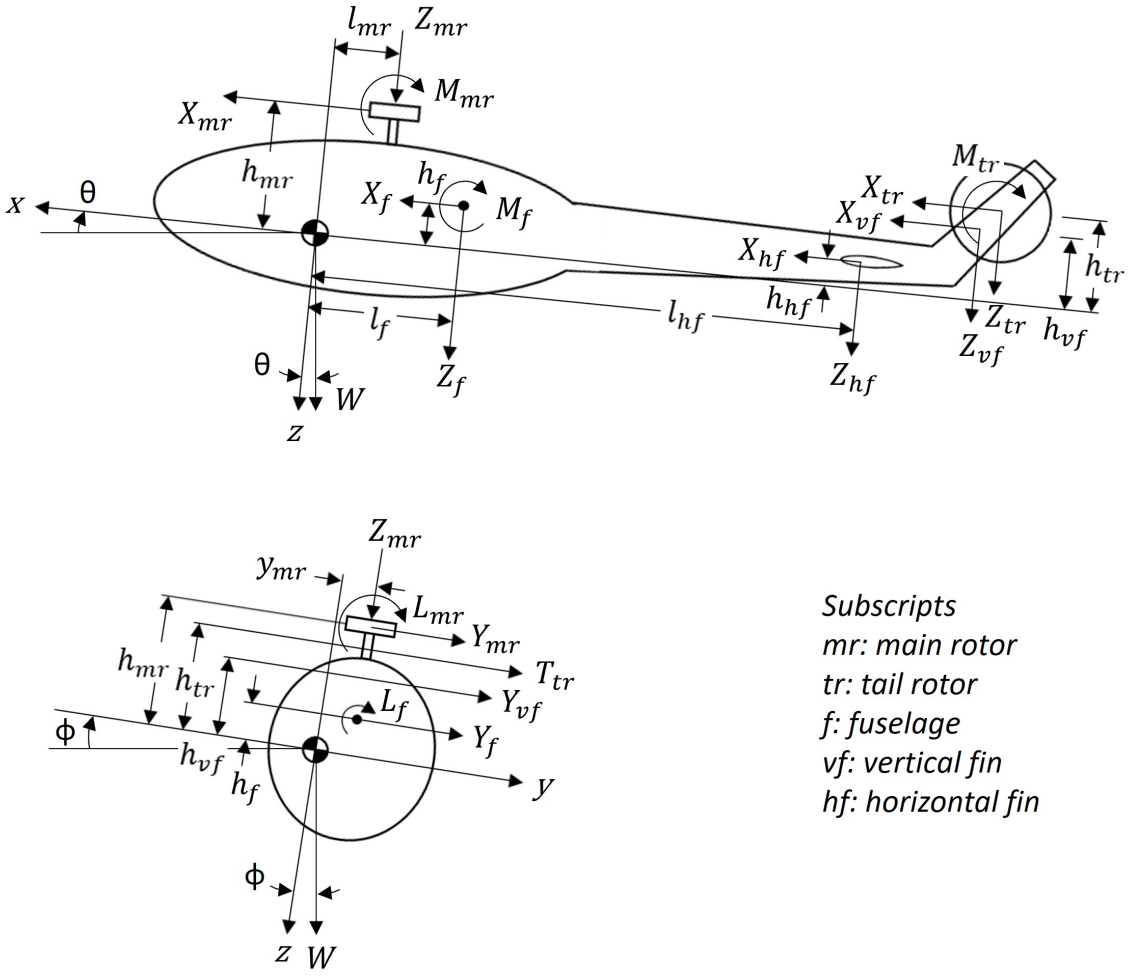

Figure 3.9: Aerodynamic loads acting on a helicopter in free flight (side and rear view).

the longitudinal moment balance equation:

$$M_{mr} - X_{mr}h_{mr} + Z_{mr}l_{mr} + M_{tr} - X_{tr}h_{tr} + Z_{tr}l_{tr} - X_{hf}h_{hf} + Z_{hf}l_{hf} + \\ -X_{vf}h_{vf} + M_f + Z_f l_f - X_f h_f = 0 \tag{3.35}$$

For completion, the yaw balance equation (Eq. 3.20) is repeated here:

$$Q_{mr} - Y_{mr}l_{mr} - T_{tr}l_{tr} - Y_{vf}l_{vf} + N_f - Y_f l_f = 0$$

Solving this set of nonlinear algebraic equations leads to the calculation of the control positions required to hold the helicopter in equilibrium. The controls available to the pilot are the main rotor collective, the longitudinal and lateral cyclic, and the pedals. This approach is usually referred to as the trim problem.

It has been observed that the axial component of the freestream velocity at the tail rotor plays an important role in the estimation of the required collective pitch angle of the tail rotor for trim. This velocity is a function of the relative wind conditions at the rotor plane. Hence, it is important to investigate the effect of the relative wind on the amount of pedal control needed to maintain equilibrium. This can be accomplished through a series of trim simulations that involve different sideslip angles and airspeeds. A similar simulation was performed by Ellin [50, 51], to establish the critical azimuth regions influenced by the interaction of the main rotor vortex wake with the tail rotor.

This experiment aims to investigate the impact of the inflow modeling on the tail rotor performance, to identify the most appropriate model for an accurate running out of pedal representation. The same models selected for the weathercock stability investigation have been chosen, because of their different levels of accuracy and low computational effort. First, a uniform inflow is considered because of its simplicity. Specifically, momentum theory is used to derive the induced inflow as a constant value

over the rotor disk [92]. The thrust coefficient is calculated using the simplified rotor model derived by Bailey [3]. Second, a linear inflow gradient along the rotor blade is assumed. This is a popular assumption used in rotorcraft flight dynamics as it gives a good representation of the inflow, calculating the inflow gradients that a uniform model fails to predict. Pitt-Peters dynamic inflow model is used as its results compare well with the experimental data. This model is derived using an acceleration potential approach, by modeling the rotor as an actuator disk. It represents the flow over the rotor disk in terms of three inflow states while accounting for the geometric skew of the wake [121]. The tail rotor thrust is calculated coupling the inflow dynamics with a blade element model that accounts for 11 blade elements [92]. Lastly, the aerodynamic interaction of the main rotor wake with the tail rotor is considered. Pitt-Peters model is extended to calculate the velocity induced by the main rotor vortex wake at any arbitrary point in the flow field. Specifically, the geometric relationship between the main and tail rotor is considered to quantify the interference [118]. This approach is initially applied while using momentum theory at the tail rotor. Then, the Pitt-Peters model is used to increase the accuracy of the tail rotor inflow dynamics.

3.5 Modeling of Tail Rotor Vortex Ring State

The last LTE event analyzed is the phenomenon of vortex ring state at the tail rotor. This section describes the physics-based models required to accurately simulate it. It will be shown that an experiment is needed to verify the impact of this phenomenon on the directional control of the helicopter and investigate its contribution to the LTE phenomenon.

3.5.1 The Physics

In axial flight, a rotor operates in different working states based on its vertical descent rate. A notional summary is provided in Figure 3.10. During climb or high descent

rates, the flow through the rotor is relatively uniform. However, before the condition of ideal autorotation, the complex phenomenon of vortex ring state develops and involves strong vortex interactions and wake distortions.

For an operating rotor, each blade trails a vortex sheet along its span with a concentrated vortex at the tip of the blade. Both the vortex sheet and the tip vortex convect downstream of the rotor in a helical motion. During normal working states (i.e. hover and climb) and windmill brake states, the wake is well organized forming a smooth contracting cylindrical column below and above the rotor, respectively. In those cases, a well-defined slipstream boundary expands downstream of the rotor, and a definite control volume around the rotor and its wake can be established. Because of

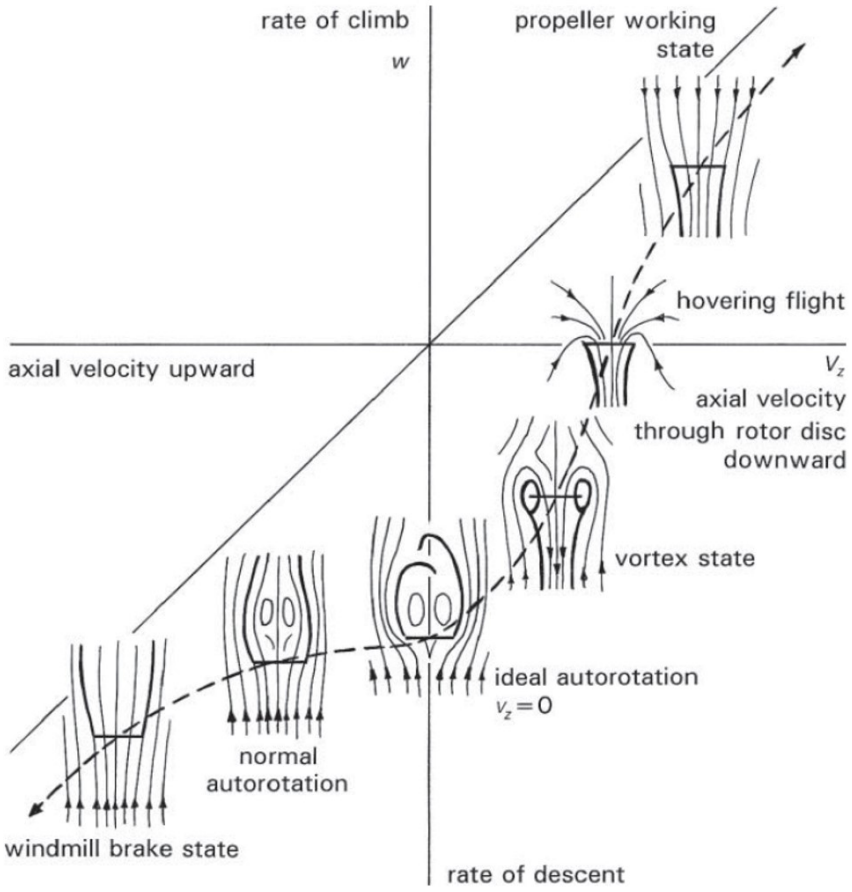

Figure 3.10: Rotor working states in axial flight [114].

this, momentum theory represents a good tool to calculate basic rotor performance, adequately approximating the effect induced by the sum of contributions of each vortex in the wake. However, at low descent rates, the freestream velocity causes the rotor wake to compress closer to the rotor. Because of the more complex flow patterns involved, a distinct slipstream boundary ceases to exist and momentum theory becomes invalid [66]. To investigate this flight condition, a theory that is applicable even in the presence of wake distortions is needed.

Because the greatest gradient in bound circulation occurs at the blade tip, the tip vortices have been determined to be the most dominating part of the rotor wake [92]. They follow helical paths forming distinct vortex filaments that are sometimes visible through natural condensation effects. Because of their main role, the impact of the tip vortices in proximity to the rotor is of primary importance and must not be neglected. Each tip vortex induces a tangential (swirl) velocity at any point in the field that decreases inversely with radial distance from the vortex core, as depicted by the 2-D velocity profile of Figure 3.11. The Biot-Savart law can be used to calculate

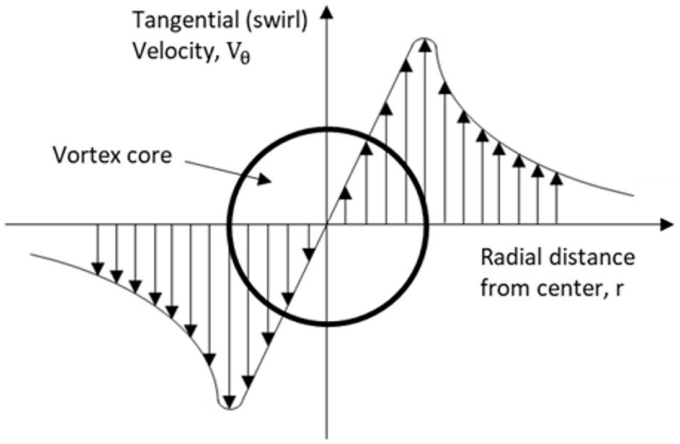

Figure 3.11: Tip vortex 2-D tangential velocity profile.

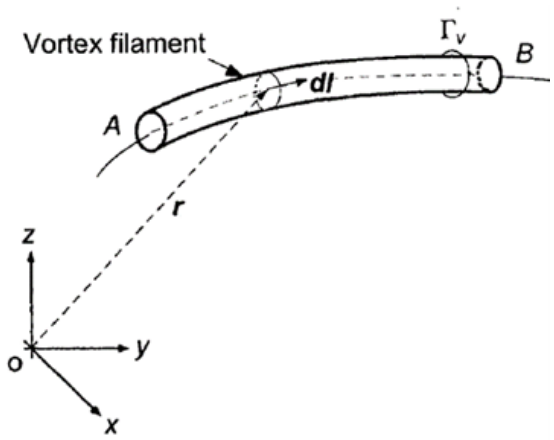

Figure 3.12: Evaluation of the velocity induced by a vortex filament using the Biot-Savart law (modified from [92]).

the velocity induced by the vortex at any point P in the field:

$$d\boldsymbol{v}_i = \frac{\Gamma}{4\pi} \frac{d\boldsymbol{l} \times \boldsymbol{r}}{(|\boldsymbol{r}|^2 + r_{core}^2)^{\frac{3}{2}}} \tag{3.36}$$

where Γ is the vortex strength, $d\boldsymbol{l}$ is the segment of the vortex filament, $\boldsymbol{r}$ is the distance from $d\boldsymbol{l}$ to the point P, and r_{core} is the core radius of the toroidal ring cross-section. The Biot-Savart law is schematically visualized in Figure 3.12. The vortex strength Γ can be easily estimated using the Kutta-Joukowski theorem which states that:

$$\mathrm{L}' = \rho \, v \, \Gamma \tag{3.37}$$

where L' is the lift generated by a blade unit span, ρ the air density, and v the air velocity. Hence, it is noted that the velocity induced by the vortex, the vortex strength, the vortex core radius, and how those properties change with time are all important factors that greatly impact the rotor performance. The velocity induced by an entire tip vortex filament is computed by numerical integration over the whole filament, while the cumulative effect of the several filaments is obtained through the superposition principle. Hence, the velocity induced by the wake vorticity at the rotor

can be approximated to be the sum of the contributions of the tip vortex filaments.

Appendix A.2 gives an overview of the experimental and physics-based investigations present in the literature that relate to vortex ring state. Several studies describe that during a descent flight condition, the vortex filaments compress and accumulate causing an increase in the resulting induced velocity at the rotor. The vortices co-rotate and influence each other leading to significant wake distortions [17]. Because of the mutual interaction between the vortices, additional compression of the helical wake causes the tip vortices to radially expand away from the rotor. For conservation of vorticity, while the diameter of the vortex filaments increases, the ability to propel themselves downward decreases. This leads the vortex filaments to recirculate beneath the rotor forming a toroidal structure of corotating vortex filaments. Brand et al. [18] extensively investigated this phenomenon, recognizing the importance of wake vorticity and its self-organization during a descent flight. The characterizing feature of VRS was found to be the organized accumulation of vortex wake that highly increases the induced inflow penalizing the rotor performance. The rotor induced inflow increases as the vortex ring grows, impacting the aerodynamic environment at the rotor blade sections.

At each blade element section, while the collective pitch angle is maintained constant, the increased inflow velocity, $U_P^{'}$, causes the effective angle of attack to reduce to the value $\alpha^{'}$, as shown in Figure 3.13. Because the rotor thrust is a function of the angle of attack at the blade element, the rotor undergoes a remarkable thrust loss that leads to a significant increase in descent rate. The rotor falls in its own wake causing the wake filaments to transit above the rotor. This loss of thrust stability, at constant rotor collective pitch, is the direct consequence of the vortex ring formation in proximity to the rotor and represents the main VRS event. When the tail rotor is under the influence of numerous corotating wake filaments, a sudden decrease in tail rotor thrust occurs causing an uncommanded right yaw of the helicopter [91].

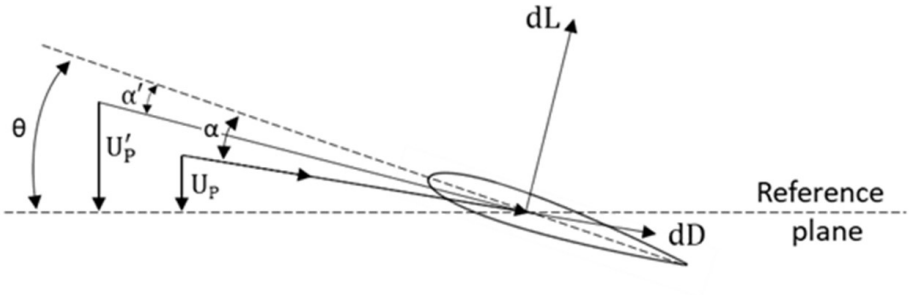

Figure 3.13: Aerodynamic environment at the blade element during a VRS event.

Viewing the helicopter from behind, the tail rotor is subjected to a descent like flow condition, for example, in presence of relative winds from the left. The freestream flow goes from left to right through the tail rotor, impacting the net rotor inflow and the rotor performance.

From the literature, conflicting theories exist about the effectiveness of the tail rotor during this flight condition [38]. Specifically, it is unclear if in presence of vortex ring flow states at the tail rotor a pedal control input, i.e., increase in tail rotor collective pitch, always provides the expected thrust increase to reestablish directional control. The existence of the phenomenon of pedal control reversal during tail rotor vortex ring state is uncertain, hindering the understanding of this LTE event. Hence, a further investigation is needed to clarify this research gap, to promote the awareness of LTE within the rotorcraft community.

3.5.2 Research Question 3 and Hypothesis

Tail rotor vortex ring state is a dangerous phenomenon that strongly impacts the tail rotor performance and may lead to loss of directional control. It is essential to fully understand the nature of this flight condition to promote its awareness within the rotorcraft community. Because of the ambiguities surrounding the effectiveness of the tail rotor during this LTE event, the following research question is formulated:

Can the phenomenon of pedal control reversal occur, during flight conditions involving vortex ring flow states at the tail rotor?

Appendix A.2 provides an overview of the experimental tests and physics-based investigations related to the phenomenon of vortex ring state. Several studies involving VRS at the main rotor reveal that an attempted recovery, i.e., increase in rotor blade collective pitch angle, not only may not be effective in reestablishing equilibrium conditions but may also increase the descent rate of the aircraft [78, 79, 135]. This reverse effect suggests the presence of the phenomenon of collective control reversal during vortex ring flow states at the main rotor, which is defined by the following condition:

$$\frac{\partial T}{\partial \theta_0} \leq 0 \tag{3.38}$$

where T is the rotor thrust and θ_0 is the main rotor blade collective pitch angle. While during normal operating conditions an application of collective control results in an increase in main rotor thrust, during descent flights in VRS the thrust developed may decrease because of the collective control reversal phenomenon. Due to the similarity between the fundamental physics of the main rotor and tail rotor, it is inferred that during a tail rotor VRS event a pedal control reversal phenomenon may occur, i.e.:

$$\frac{\partial T}{\partial \delta_p} \leq 0 \tag{3.39}$$

where δ_p is the pilot's pedal control which is directly linked to the tail rotor blade collective pitch angle. Because of this phenomenon, an attempted pedal control recovery may not provide the expected tail rotor thrust variation, leading to potential loss of control. Hence, the following hypothesis is formulated:

If during flight conditions involving vortex ring flow states at the tail rotor, the tail rotor thrust remains the same or diminishes after a pedal control application, i.e.,

increase in tail rotor blade collective pitch angle, then the existence of the pedal control reversal phenomenon is confirmed.

To test this hypothesis and ensure an appropriate understanding of this phenomenon, an investigation on the pedal control effectiveness during VRS is needed.

3.5.3 Formulation of Experiment 3

It has been described that the phenomenon of vortex ring state is characterized by strong wake distortions. The rotor wake is formed by a vortex sheet and a tip vortex filament continuously emitted by each rotating blade. During a descent flight, the vortices that form the rotor wake compress and accumulate in proximity to the rotor. To accurately investigate vortex ring state, a theory that models the impact of the wake vorticity on the rotor performance is needed.

Vortex methods properly represent the transportation of vorticity throughout the flow field relative to the rotor. They often assume an incompressible potential flow, with all the vorticity concentrated within the finite elements of the vortex wake. To estimate the total velocity induced at a specific point of the flow field, the Biot-Savart law is applied for each discretized vortex element, and the superposition principle is used to sum the different contributions. Often, the vorticity trailed by each blade is assumed to be represented by numerous vortex filaments each divided into hundreds of segments. Because the computational expense rapidly increases with the number of finite segments considered, several approximations can be made to reduce the complexity of the rotor wake, as described by Leishman [92]. It was noted that the rotor wake is dominated by the blade tip vortices, because of the greater variation of bound circulation in proximity to each blade tip. Hence, it is assumed that the entire vorticity of the blade is trailed from the blade tip, neglecting the bound circulation gradient along the blade span. To help decrease the computational expense while retaining an adequate level of physical accuracy, a simple vortex ring model

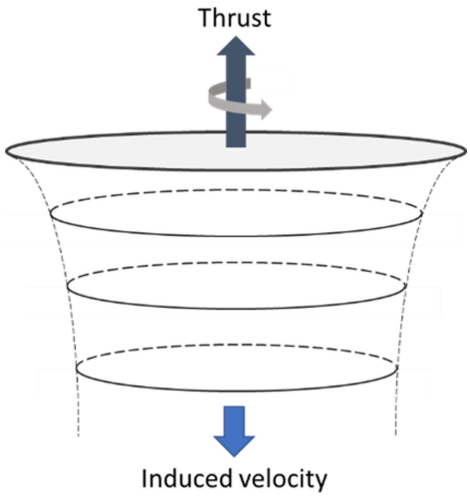

Figure 3.14: Approximation of rotor wake into a series of vortex rings convecting downstream.

is considered where one vortex ring represents the trailed wake of each blade and is emitted after every rotor blade revolution. As depicted in Figure 3.14, the rotor wake is approximated by a series of vortex rings that can contract or expand radially while moving downstream with respect to the rotor. The performance analysis of a rotor in pure axial flight is an advantageous approach because of its simplicity. An axisymmetric flow is assumed, constraining each ring to be centered at the rotor's vertical axis. The wake self-organization and the time-varying vortex accumulation in proximity to the rotor are essential to simulate the vortex ring behavior and its influence on the rotor's aerodynamics. The ring emitter model allows for a simple estimation of the vortex ring motion during the simulated descent. Each ring motion is influenced not only by the surrounding velocity field induced by the other rings but also by the self-induced velocity provided by the ring itself. Hence, it is important to accurately estimate the cumulative velocity induced by all the rings at any point in the flow field. This is accomplished by applying the Biot-Savart law, simplified by the axisymmetric flow assumption. Only the motion along the radial and vertical axes of the rotor is needed to fully describe the ring dynamics. Figure 3.15 illustrates

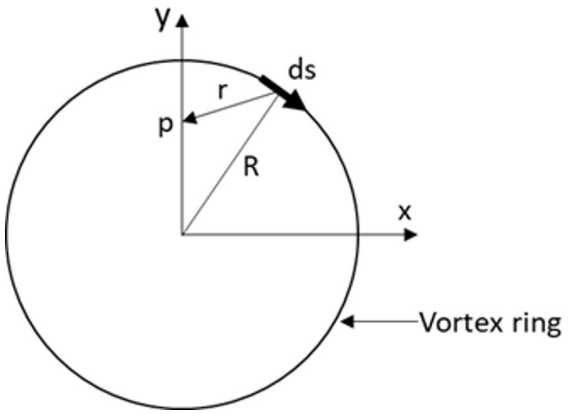

Figure 3.15: Geometry of a vortex ring (top view).

the geometry of a vortex ring of radius R and centered about the vertical axis of the rotor. Hence, the induced velocities at point p are obtained by integrating the Biot-Savart law over the circumference of the ring:

$$V_{ix} = \frac{\Gamma}{4\pi} \int_0^{2\pi} \frac{(Rz_p cos\theta)\ d\theta}{(L^2 - 2Rx_p cos\theta)^{\frac{3}{2}}} \tag{3.40}$$

$$V_{iz} = \frac{\Gamma}{4\pi} \int_0^{2\pi} \frac{(R^2 - Rx_p cos\theta)\ d\theta}{(L^2 - 2Rx_p cos\theta)^{\frac{3}{2}}} \tag{3.41}$$

where the parameter L is defined as $L^2 = R^2 + x_p^2 + z_p^2 + r_{core}^2$. The axial component of the induced velocity, V_{iz}, is not only responsible for impacting the axial velocity of the close by rings, but it also represents the self-induced velocity of the vortex ring itself. The radial component of the induced velocity, V_{ix}, impacts the radial deformation of the neighboring rings, contracting or expanding their diameter. Because the fluid is assumed to be inviscid, the vortex circulation can be considered constant throughout the vortex ring life. Hence, if the radius of the toroidal ring is stretched by the radial velocity induced by the nearby rings, the size of the vortex ring cross-section must change as a function of time.

It has been measured that the maximum value of the vortex swirl velocity is just

10% of the velocity at the tip of the rotor blade [103]. This suggests that the flow can be treated as incompressible, and hence the volume of the toroidal ring can be assumed to be constant over time. The radius of the toroidal vortex changes, as it is influenced by the radial component of the induced velocity. From the conservation of the ring volume, the core radius of the ring cross-section at each time step is thus obtained:

$$r_{core,t+\Delta t} = r_{core,t}\sqrt{\frac{R_t}{R_{t+\Delta t}}} \tag{3.42}$$

Each vortex ring strength Γ can be assumed to be related to the average thrust produced by one blade as follows:

$$\Gamma = \frac{T}{n_b R \rho V_{tip}} \tag{3.43}$$

where V_{tip} is the velocity at the tip of the rotor blade. A lift model is needed to estimate the rotor loading. The rotor thrust can be easily calculated by coupling the ring emitter model with a blade element model. As depicted in Figure 3.16, at each blade element the feedback loop of the inflow dynamics provides the downwash contribution to the effective blade incidence. The blade pitch is an independent input controlled by the pilot. Usually, the feedback loop of the blade dynamics is included to estimate the blade flapping perturbation on the blade incidence. However, in this

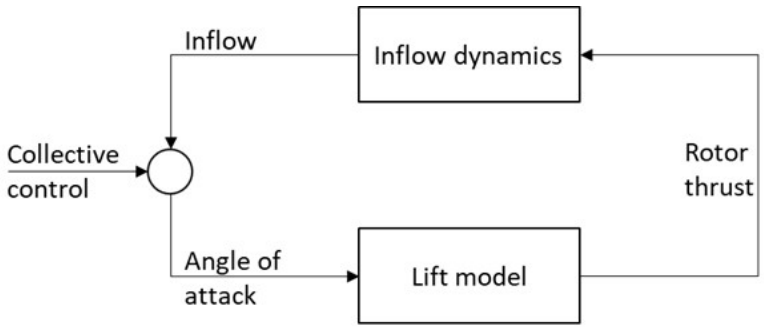

Figure 3.16: Modeling breakdown of inflow dynamics and rotor lift.

investigation the blade motion can be neglected because of the axisymmetric flow assumption. Hence, the thrust coefficient can be calculated using:

$$C_T = \frac{1}{2}\sigma a \int_{r=0}^{1} \left(\theta r^2 - \lambda r\right)\ dr \tag{3.44}$$

Numerous VRS investigations have been carried out in a wind tunnel environment. However, this test condition provides a controlled wind tunnel flow that remains independent from the rotor thrust generated. This affects the dynamics of the wake vorticity trailed by the rotor. As reported by the flow visualizations of Drees and Hendal [42], this test condition induces the development and dissipation of the vortex ring around the rotor causing high load fluctuations. Brand et al. [18] compared this approach to a free-flight vertical descent and observed how the wind-tunnel simulation leads to a non-realistic representation of VRS. While the vortex ring is approaching the rotor, the induced velocity increases, negatively impacting the effective angle of attack at the blade section. This induces a decrease in rotor thrust that should further increase the rotor descent rate. However, this dynamic is not well represented in a wind tunnel environment as the wind tunnel flow is independent of the rotor thrust. Hence, a free axial descent needs to be simulated, allowing the axial freestream component at the rotor to change as a function of the velocity induced by the vortex ring. The tail rotor is subjected to a free descent like flow condition, for example, while the aircraft is flying sideward to the left. Viewing the helicopter from behind, the freestream flow goes from left to right through the tail rotor, impacting the net rotor inflow and the rotor performance. For simplicity, this analysis investigates an isolated tail rotor in axial sideward motion to the left. A series of blade collective pitch reductions are used to replicate the free descent like flow condition at the tail rotor.

It is noted that this approach includes the most important elements needed for

this study. The vortex ring properties and the impact induced on the rotor performance are estimated at each time step of the simulation to ensure an accurate representation of the transportation of wake vorticity. It is critical to consider that in a time-marching simulation certain time integration approaches lead to numerical instabilities [11, 12]. However, the use of an advanced numerical scheme can negatively impact the computational expense. Karpatne et al. [84] suggest that higher order Runge-Kutta methods are needed to solve the ordinary differential equations that predict the motion of the vortex rings. Additionally, it is observed that sufficient vortex rings must be modeled to capture enough wake vorticity [18]. This increases the processing time as the square of the number of rings, because of the calculations of the velocity induced on each ring. Hence, it is important to find a balance between numerical method accuracy and number of rings, to provide accurate simulations while maintaining an affordable computational time. After ensuring that an accurate time-marching simulation is being applied, the existence of the control reversal phenomenon at the tail rotor during a VRS event is investigated. An attempted recovery through a sudden increase in tail rotor collective pitch is introduced and the resulting rotor performance is analyzed.

3.6 Detection of Loss of Weathercock Stability

After the physics-based investigation of the three types of LTE events, an appropriate approach for the detection of each of those phenomena needs to be determined, offering the capability to flag LTE events in simulation results. While a parameter to detect the phenomenon of running out of pedal for trim has already been identified, a more detailed analysis is required for the other two LTE phenomena. This section describes the approach used to detect the loss of weathercock stability of the helicopter. It will be shown that an experiment is needed to establish the appropriate parameter able to accurately predict the directional static stability of the helicopter.

3.6.1 Detection Flag Estimation

A common approach to study the aircraft stability characteristics is based on linear system theory [114, 123, 43]. Specifically, in presence of small external disturbances or control changes, the helicopter behavior can be described as a linear perturbation about the trim condition. Consider the helicopter equations of motion expressed in the nonlinear form:

$$\dot{\boldsymbol{x}} = \boldsymbol{f}(\boldsymbol{x}, \boldsymbol{u}) \tag{3.45}$$

The state vector $\boldsymbol{x}$ is defined as:

$$\boldsymbol{x} = \{u, v, w,\ p, q, r, \phi, \theta, \psi, x_e, y_e, z_e\}$$

where u, v and w are the body-axes translational velocities; p, q and r are the body-axes angular velocities; ϕ, θ and ψ are the Euler angles; and x_e, y_e, and z_e the components of the position vector relative to a fixed point on earth.

The control vector $\boldsymbol{u}$ is defined by the main rotor collective pitch angle θ_0, the longitudinal cyclic pitch angle θ_{1s}, the lateral cyclic pitch angle θ_{1c}, and the tail rotor collective pitch angle θ_{0tr}:

$$\boldsymbol{u} = \{\theta_0, \theta_{1s}, \theta_{1c}, \theta_{0tr}\} \tag{3.46}$$

Using small perturbation theory, the nonlinear helicopter model can be linearized about an equilibrium point $(\boldsymbol{x_e}, \boldsymbol{u_e})$ using the Taylor series expansion, as follows:

$$\boldsymbol{f}\left(\boldsymbol{x}, \boldsymbol{u}\right) = \boldsymbol{f}\left(\boldsymbol{x_e}, \boldsymbol{u_e}\right) \ + \ \left.\frac{\partial \boldsymbol{f}}{\partial \boldsymbol{x}}\right|_{\boldsymbol{x_e}, \boldsymbol{u_e}} \left(\boldsymbol{x} - \boldsymbol{x_e}\right) \ + \ \left.\frac{\partial \boldsymbol{f}}{\partial \boldsymbol{u}}\right|_{\boldsymbol{x_e}, \boldsymbol{u_e}} \left(\boldsymbol{u} - \boldsymbol{u_e}\right) + h.o.t. \tag{3.47}$$

Because of the linearity assumption, each partial derivative is obtained while keeping constant the other degrees of freedom. An important assumption is that all the aerodynamic loadings, i.e. external forces X, Y, Z and moments L, M, N from

the different components of the vehicle, can be expressed as analytic functions of the motion of the aircraft about the trim condition. For example, the yawing moment can be written as:

$$N = N_e + \frac{\partial N}{\partial u}\delta u + \frac{\partial N}{\partial v}\delta v + \cdots + \frac{\partial N}{\partial \theta_0}\delta\theta_0 + \frac{\partial N}{\partial \theta_{1s}}\delta\theta_{1s} + \ldots, etc. \tag{3.48}$$

The partial derivatives are usually referred to as:

$$\frac{\partial N}{\partial u} = N_u \ , \qquad \frac{\partial N}{\partial \theta_0} = N_{\theta_0} \ , \quad etc. \tag{3.49}$$

Because this analysis does not involve any perturbation in the control inputs and the position of the aircraft with respect to earth, the control vector components, and the position states can be assumed constant. Also, the yaw attitude can be ignored, since when it is perturbed from its equilibrium value it does not give rise to any change in forces and moments on the vehicle. Also, the development of a linear model of a fixed wing aircraft is assumed, where the xz-plane of symmetry exists and the products of inertia terms I_{xy} and I_{yz} are zero. For a helicopter, the xz-plane is not a plane of symmetry because of the presence of the tail rotor. However, this assumption is often used since the effect of the terms relating to the products of inertia I_{xy} and I_{yz} are usually small. Neglecting the higher order terms, and considering $\boldsymbol{x} = \boldsymbol{x} - \boldsymbol{x_e}$, the linearized equations describing the perturbed motion about a trim condition can be written as:

$$\dot{\boldsymbol{x}} = \boldsymbol{A}\boldsymbol{x} \tag{3.50}$$

Where $\boldsymbol{A}$ is denoted as the system matrix and it is derived from the partial derivatives of the nonlinear function $\boldsymbol{f}$, i.e.:

$$\boldsymbol{A} = \left(\frac{\partial \boldsymbol{f}}{\partial \boldsymbol{x}}\right)_{\boldsymbol{x}=\boldsymbol{x_e}} \tag{3.51}$$

Note that the system matrix $\boldsymbol{A}$ is a function of the equilibrium and must be computed for each equilibrium flight condition. However, the computation of the matrix is quick, offering an affordable approach to investigate a high number of flight scenarios. The system matrix can be written in the form:

$$\boldsymbol{A} = \begin{bmatrix} \boldsymbol{A_{lon}} & \boldsymbol{A_{lon-lat}} \\ \\ \boldsymbol{A_{lat-lon}} & \boldsymbol{A_{lat}} \end{bmatrix} \tag{3.52}$$

where $\boldsymbol{A_{lon-lat}}$ and $\boldsymbol{A_{lat-lon}}$ are coupling matrices which give rise to the response coupling between longitudinal and lateral dynamics. The elements of the matrix $\boldsymbol{A}$ can be written in the expanded form:

$$\boldsymbol{A_{lon}} = \begin{bmatrix} \dfrac{X_u}{m} & \dfrac{X_w}{m} - q_e & \dfrac{X_q}{m} - w_e & -g\cos\theta_e \\ \\ \dfrac{Z_u}{m} + q_e & \dfrac{Z_w}{m} & \dfrac{Z_q}{m} + u_e & -g\cos\phi_e \sin\theta_e \\ \\ M_u & M_w & M_q & 0 \\ \\ 0 & 0 & \cos\theta_e & 0 \end{bmatrix}$$

$$\boldsymbol{A_{lon-lat}} = \begin{bmatrix} \frac{X_v}{m} + r_e & \frac{X_p}{m} & 0 & \frac{X_r}{m} + v_e \\ \frac{Z_v}{m} - p_e & \frac{Z_p}{m} - v_e & -g\sin\phi_e\cos\theta_e & \frac{Z_r}{m} \\ M_v & M_p - 2p_e I_{xz} I_{yy} & 0 & M_r - 2r_e I_{xz} I_{yy} \\ & -r_e(I_{xx} - I_{zz})I_{yy} & & -p_e(I_{xx} - I_{zz})I_{yy} \\ 0 & 0 & 0 & -\sin\theta_e \end{bmatrix}$$

$$\boldsymbol{A_{lat-lon}} = \begin{bmatrix} \frac{Y_u}{m} - r_e & \frac{Y_w}{m} + p_e & \frac{Y_q}{m} & -g\sin\phi_e\sin\theta_e \\ C_{L_u} & C_{L_w} & C_{L_q} + k_1 p_e - k_2 r_e & 0 \\ 0 & 0 & \sin\phi_e\tan\theta_e & 0 \\ C_{N_u} & C_{N_w} & C_{N_q} - k_1 r_e - k_3 p_e & 0 \end{bmatrix}$$

$$\boldsymbol{A_{lat}} = \begin{bmatrix} \frac{Y_v}{m} & \frac{Y_p}{m} + w_e & g\cos\phi_e\cos\theta_e & \frac{Y_r}{m} - u_e \\ C_{L_v} & C_{L_p} + k_1 q_e & 0 & C_{L_r} - k_2 q_e \\ 0 & 1 & 0 & \cos\phi_e\tan\theta_e \\ C_{N_v} & C_{N_p} - k_3 q_e & 0 & C_{N_r} - k_1 q_e \end{bmatrix}$$

where the partial derivatives of the aerodynamic loadings are written in the following normalized form:

$$C_{Lv} = \frac{I_{zz}}{I_{xx}I_{zz} - I_{xz}^2} L_v + \frac{I_{xz}}{I_{xx}I_{zz} - I_{xz}^2} N_v \tag{3.53}$$

$$C_{Nv} = \frac{I_{xz}}{I_{xx}I_{zz} - I_{xz}^2} L_v + \frac{I_{xx}}{I_{xx}I_{zz} - I_{xz}^2} N_v \tag{3.54}$$

I_{xx} and I_{zz} are the roll and yaw product of inertia terms and I_{xz} is the roll/yaw moment of inertia. The k constants in the inertia terms are given by:

$$k_1 = \frac{I_{xz}(I_{zz} + I_{xx} - I_{yy})}{I_{xx}I_{zz} - I_{xz}^2} \tag{3.55}$$

$$k_2 = \frac{I_{zz}\left(I_{zz} - I_{yy}\right) + I_{xz}^2}{I_{xx}I_{zz} - I_{xz}^2} \tag{3.56}$$

$$k_3 = \frac{I_{xx}\left(I_{yy} - I_{xx}\right) - I_{xz}^2}{I_{xx}I_{zz} - I_{xz}^2} \tag{3.57}$$

It is observed that the system matrix $\boldsymbol{A}$ includes terms of two different natures. The first type consists of inertial and gravitational terms, that can be computed analytically from the equations of motion. The second type consists of partial derivatives arising from the aerodynamic loadings. In general, accurate analytical expressions for the derivatives of aerodynamic forces and moments may not be possible. Hence, they may be estimated through appropriate numerical perturbation schemes, such as using positive and negative perturbations from trim:

$$N_u = \frac{\partial N}{\partial u} = \frac{N\left(u_e + \Delta u\right) - N(u_e - \Delta u)}{2\Delta u} \tag{3.58}$$

The partial derivatives of the aerodynamic loadings can be used to predict the static stability of the system. One of those derivatives is N_v, which is associated with the directional static stability of the aircraft. It is related to the variation of yaw moment N about the center of gravity of the vehicle due to a perturbation in sideward velocity

v along the body y axis, and it is defined as follows:

$$\frac{\Delta N}{\Delta v} \approx \frac{\partial N}{\partial v} = N_v \tag{3.59}$$

Because of the perturbation in sideward velocity, the aircraft may exhibit a yaw moment reaction that initiates the aircraft's tendency to yaw back to the initial equilibrium position. This is known as a statically stable behavior, and it is usually identified by a positive value of N_v [114]. Contrarily, when the change in N causes the vehicle to yaw away from its equilibrium position, then the aircraft is said to be statically unstable for that particular flight condition, and it is generally recognized by a negative value of N_v [114]. This parameter has been effectively used to predict the static stability of the aircraft at different forward speeds. However, the Federal Aviation Administration states that the weathercock stability of the helicopter is heavily affected by relative tailwinds, leading to an LTE like behavior [54]. Since it is unclear if the derivative N_v is still reliable in rearward flight conditions, a stability analysis that involves relative tailwinds is needed. The most appropriate parameter able to accurately predict the directional static stability of the helicopter must be established.

3.6.2 Research Question 4 and Hypothesis

The phenomenon of weathercock stability is heavily affected by relative tailwinds, leading to an LTE like behavior [54]. Hence, the identification of a reliable detection parameter for this flight characteristic is essential to provide an accurate prediction of LTE within flight data. Because of the research gap involving the prediction of rotorcraft stability for flight scenarios with relative tailwinds, the following research question is formulated:

What parameter should be used to reliably predict the weathercock stability of the

helicopter even in presence of flight scenarios with relative tailwinds?

The derivative N_v is related to the yaw moment reaction about the center of gravity of the vehicle due to a perturbation in sideward velocity v along the body y axis. For small perturbations, the variation in lateral speed v can also be related to a change in sideslip angle β, i.e., a change in wind azimuth, as shown by the following equation:

$$\frac{\Delta v}{u} = tan\ \Delta\beta \approx \Delta\beta \tag{3.60}$$

where u is the translational velocity of the aircraft along the longitudinal body axis. Hence, N_v can be expressed as follows:

$$N_v = \frac{\partial N}{\partial v}\ \approx \frac{\partial N}{\partial \beta}\ \frac{1}{u} = \frac{N_\beta}{u} \tag{3.61}$$

where N_β is related to the yaw moment reaction about the center of gravity of the vehicle due to a change in sideslip angle. Considering that the tail rotor is the key contribution to the static directional stability of the helicopter [15] and that the relative wind conditions at the tail rotor may be affected by the main rotor vortex wake interaction for certain sideslip angles [51], it is inferred that:

$$N_\beta = N_v\ V_{x,tr} \tag{3.62}$$

where $V_{x,tr}$ is the edgewise component of the freestream velocity at the tail rotor. It is observed that by definition N_β has the capability to differentiate between relative headwinds and tailwinds and may be a more comprehensive parameter to detect the directional static stability of the helicopter for different flight scenarios. Therefore, the following hypothesis is formulated:

If the directional static stability derivative that relates to the sideslip angle is computed,

then a reliable prediction of the weathercock stability of the helicopter, even in presence of flight scenarios with relative tailwinds, will be achieved.

To test this hypothesis and ensure an appropriate level of accuracy in the detection of this phenomenon, an investigation on the directional static stability derivatives of the aircraft is needed.

3.6.3 Formulation of Experiment 4

It has been observed that linear system theory is an affordable approach to approximate the aircraft stability characteristics. After solving the trim problem, the helicopter equations of motion can be linearized to compute the system matrix, which includes the partial derivatives of the aerodynamic loadings. This experiment aims to investigate the directional static stability derivatives of the aircraft to establish which parameter accurately predicts the weathercock stability of the helicopter. To analyze both forward and rearward flights, a series of simulations that involve different sideslip angles and airspeeds are used. It has been observed that the system matrix obtained from linearization is a function of the equilibrium and must be computed for each equilibrium flight condition. Hence, the trim problem needs to be solved for each flight scenario, followed by the stability analysis. The system matrix provides the stability derivative N_v, from which N_β can be derived.

3.7 Detection of Tail Rotor Vortex Ring State

To investigate the physics of VRS, it has been observed that a vortex method is needed to properly simulate the strong wake distortions typical of the VRS phenomenon. However, a significant disadvantage of vortex methods is the high computational expense due to the many vortex elements required to represent the rotor wake at each time step of the simulation. Hence, a more affordable method is needed to provide a rapid but still reliable detection of VRS events. This section describes the

approach used to detect the proximity to VRS at the tail rotor. It will be shown that an experiment is needed to verify the impact of the main rotor vortex interaction with the tail rotor on the detection results.

3.7.1 Boundary Criteria Definition

An affordable method is sought to provide a fast detection of the proximity to VRS at the tail rotor. Empirical methods provide an advantageous approach for real-time simulations since they neglect the time-marching representation of the rotor wake. Experimental results are often combined with an analytical approach to provide a valid representation of the rotor inflow in the VRS flight regime and appropriate VRS boundary estimations. Appendix A.2 describes different empirical models that have been developed to fit this purpose. However, their applicability is often reduced because of the limited set of experimental data used.

An empirical inflow model that is frequently used to detect VRS events and simulate the VRS influence on helicopter flight dynamics is provided by Johnson [81]. The model is an empirical extension of momentum theory and it was developed using several experimental data available in the literature. Specifically, it is based on a collection of wind tunnel test data, e.g., Castles and Grey [25], Yaggy and Mort [155], Empey and Ormiston [52], Betzina [9] and the flight test results of Taghizad et al. [78, 79, 135]. The model estimates the VRS boundary such that it encloses most of the experimental results available, providing a more comprehensive boundary criteria definition. As detailed in Appendix A.2, those limits surround the negative slope of the total inflow curve as a function of descent velocity, which is recognized as the direct cause of the instability during a VRS event and allows for the simulation of the negative damping of the aircraft seen in real flight tests. A good correlation was found with the flight test results of Taghizad et al. [78, 79, 135]. The model assumes a uniform inflow over the rotor disk, and it allows to easily calculate the induced inflow

and the VRS boundary given the edgewise and axial components of the freestream inflow. Because of its simplicity and versatility, Johnson's model has been chosen to detect VRS flight conditions at the tail rotor. A complete description of the model is provided by Johnson [81]. Note that only the application of the stability boundary definition is necessary to detect VRS, offering a quick implementation. Appropriate functions define the upper and lower VRS limits as a function of the normalized edgewise component of the freestream inflow, V_x/v_h, and the normalized axial component of the freestream inflow, V_z/v_h. It is observed that the freestream inflow, i.e., the relative wind condition at the rotor, is the key element needed for the detection of VRS events. This depends on both the external wind conditions and the vehicle motion. In the case of the tail rotor, an additional element that may significantly impact the freestream inflow is the aerodynamic interference from the main rotor vortex wake. However, from the VRS studies described in Appendix A.2, it is observed that the impact of this type of interaction on the tail rotor VRS boundary has never been investigated.

3.7.2 Research Question 5 and Hypothesis

The phenomenon of vortex ring state at the tail rotor critically impacts the helicopter directional stability in low-speed flight. It is necessary to provide an accurate estimation of the VRS stability boundary at the tail rotor to ensure accurate safety analyses of flight data. Because of the research gap involving the impact of the main rotor-to-tail rotor interaction on the predicted VRS boundary, the following research question is formulated:

Should the aerodynamic interference from the main rotor vortex wake be included in the computation of the VRS stability boundary of the tail rotor?

Several experimental tests confirm that the operational environment of the tail rotor

is affected by the turbulent aerodynamic interaction with the main rotor wake [147, 148, 94]. Low-speed quartering flight conditions reveal to be the most critical and difficult to predict. Within specific wind azimuth regions, the tail rotor is impacted by the tip vortices trailed from the edges of the main rotor disk. Flight tests show that the tail rotor performance can be significantly degraded by the velocity field induced by the main rotor tip vortices, impacting the directional stability of the aircraft [1, 108]. Therefore, the following hypothesis is formulated:

If the aerodynamic interference from the main rotor vortex wake is included, then the detection of the VRS phenomenon at the tail rotor will be more realistic.

To test this hypothesis and ensure an appropriate level of accuracy in the detection of this phenomenon, an investigation on the impact of the main rotor wake interference on the vortex ring state stability boundary of the tail rotor is needed.

3.7.3 Formulation of Experiment 5

To investigate the reliability of the VRS detection, the tail rotor needs to be subjected to a descent like flow condition. A series of trim simulations that involve different sideslip angles and airspeeds are used to reproduce a variety of relative wind conditions at the tail rotor. Only flight conditions with negative sideslip angles are of interest. Hence, to reduce the computational effort, the investigation focuses on the flight scenarios that induce a freestream inflow going from left to right through the tail rotor when the helicopter is viewed from behind. It has been observed that Johnson's model is an appropriate approach to detect VRS at the tail rotor because of its quick and reliable evaluations. Hence, after obtaining the edgewise and axial components of the freestream inflow at the tail rotor it is possible to determine if the simulated flight condition is within the VRS boundary. This experiment aims to investigate the impact of the main rotor-to-tail rotor interference on the VRS boundary of the tail

rotor, to establish what is the inflow model needed to achieve a more reliable VRS detection. Initially, the tail rotor inflow is modeled using a linear inflow gradient along the tail rotor blade. Then, the same set of simulations are repeated including the aerodynamic interference from the main rotor wake.

3.8 Development of the LTE Safety Metric

The modeling of the physics of the LTE phenomena has been described, providing the essential elements needed to accurately simulate LTE events. Specifically, three phenomena are recognized as contributors to LTE behavior, i.e., loss of weathercock stability, running out of pedal (tail rotor collective control) for trim, and tail rotor vortex ring state. Further, an appropriate approach for the detection of each of those phenomena has been determined, offering the capability to flag LTE events in simulation results. However, it is observed that the detection parameters needed to identify the LTE phenomena are usually not recorded during normal flight operations, hindering the direct detection of the LTE occurrences within flight data. Also, there is the necessity to provide the operator with a tool designed to analyze flight data and easily detect the proximity to LTE without the need for a simulation model. Hence, a method is sought to enable a fast and reliable identification of LTE events within the HFDM environment.

Machine learning represents a promising approach to develop computer learning algorithms able to use data to obtain intelligent actions. A vast literature review on machine learning is provided by [90, 100, 70, 152]. The choice of the learning technique and the subsequent algorithm is a function of different factors, such as the dataset size, the type of parameters involved, and the characteristics of the anomaly that is intended to be detected. Considering the lack of helicopter flight data related to LTE, it has been discussed how predictive models represent an advantageous approach to identify LTE within flight data. A predictive model estimates the output values

after going through a learning training process of the relationship between the input-output values of a specific dataset. Since clear learning instructions are provided, the process of training a predictive model is called supervised learning. In other words, the supervised learning algorithm aims to optimize the predictive model to find the combination of values that gives the target output.

The LTE safety metric is a predictive model that must identify the proximity to LTE within flight data. To build the model, a dataset that includes the different types of LTE occurrences is needed. Since it is known how to represent LTE through physics-based simulations, a dataset can be created simulating each LTE phenomenon using the appropriate simulation model. After going through the learning training process of the relationship between the initial test conditions and the results of the predefined physics-based simulations, a prediction model is created for each LTE phenomenon. Ultimately, appropriate boundaries must be defined to detect the proximity to LTE. The approach used to obtain the LTE safety metric can be summarized in two main steps:

- the investigation of the aircraft flight envelope, which involves the selection of the flight scenarios and the computation of the physics-based simulation results;
- the development of the predictive models of the three LTE phenomena, which involves the creation of the prediction functions of the LTE detection parameters and the definition of the proximity to the different LTE events.

The LTE safety metric, i.e., the comprehensive model that predicts LTE events and proximity to LTE, is formed by the collection of the predictive models obtained. The approach is illustrated in Figures 3.17 - 3.19, where each diagram relates to an LTE phenomenon and defines one of the three components needed to construct the LTE safety metric. Note that different research questions still need to be investigated to obtain the final methodology.

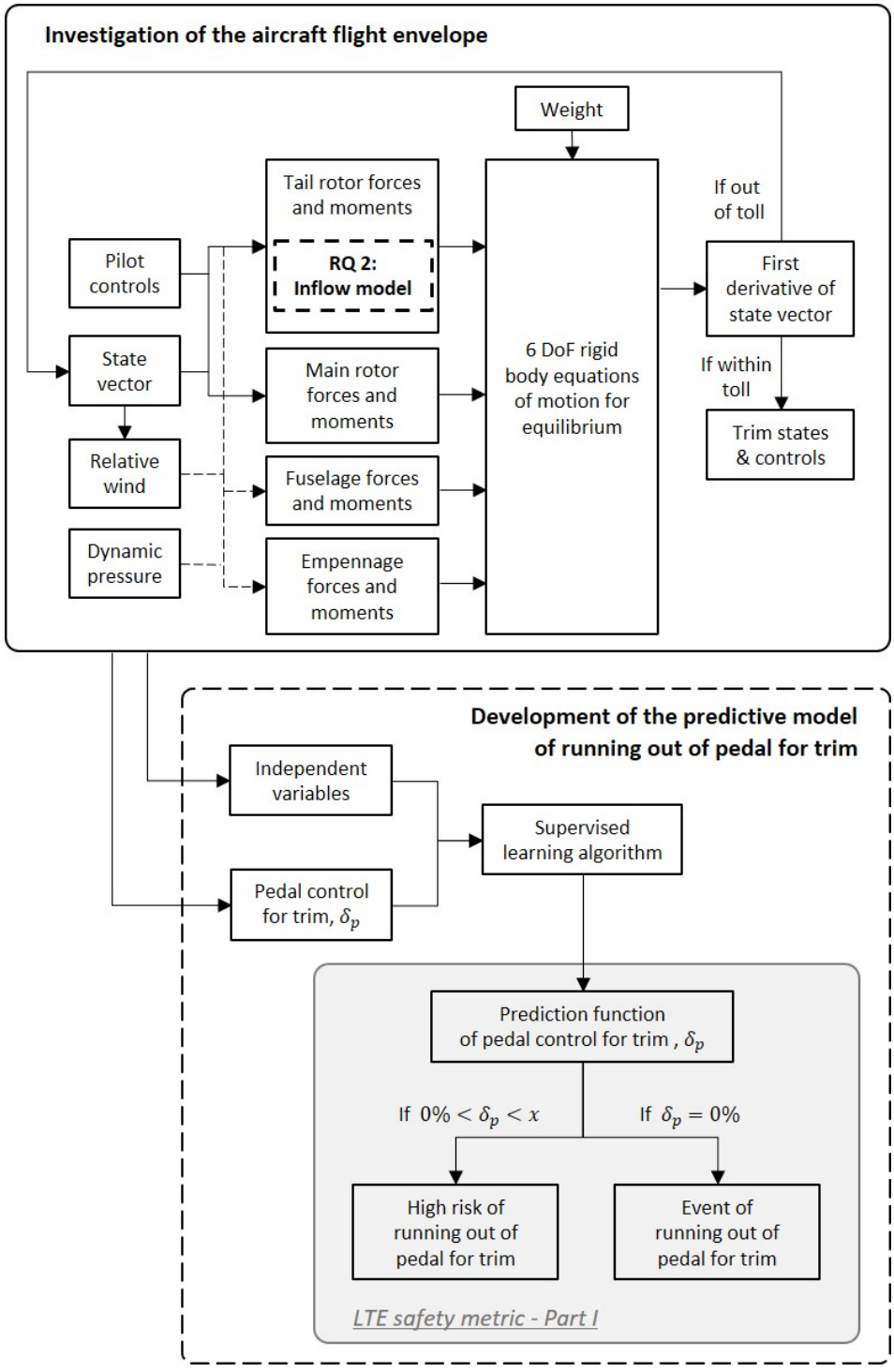

Figure 3.17: Approach to obtain the predictive model of the LTE phenomenon of running out of pedal for trim.

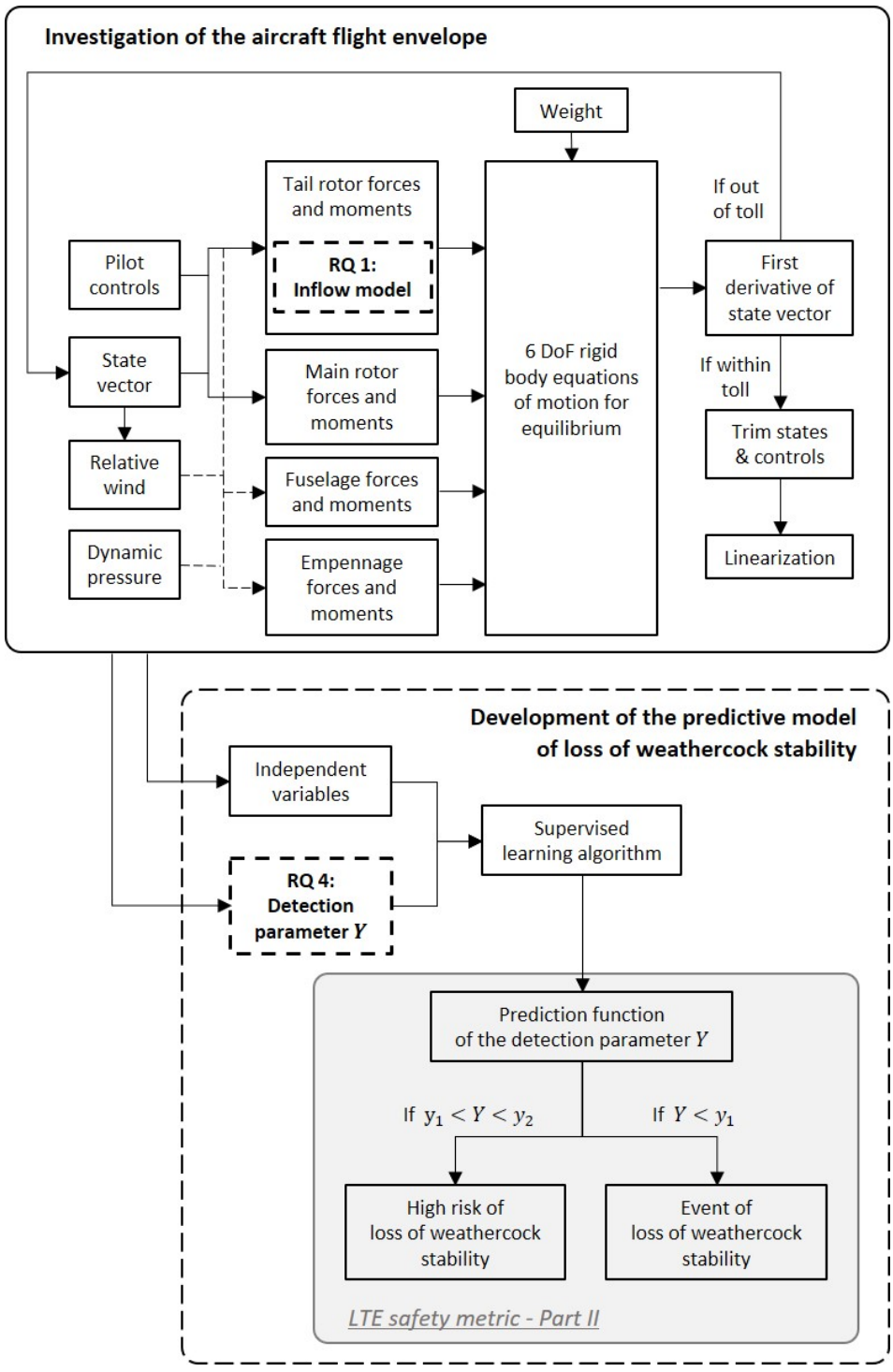

Figure 3.18: Approach to obtain the predictive model of the LTE phenomenon of loss of weathercock stability.

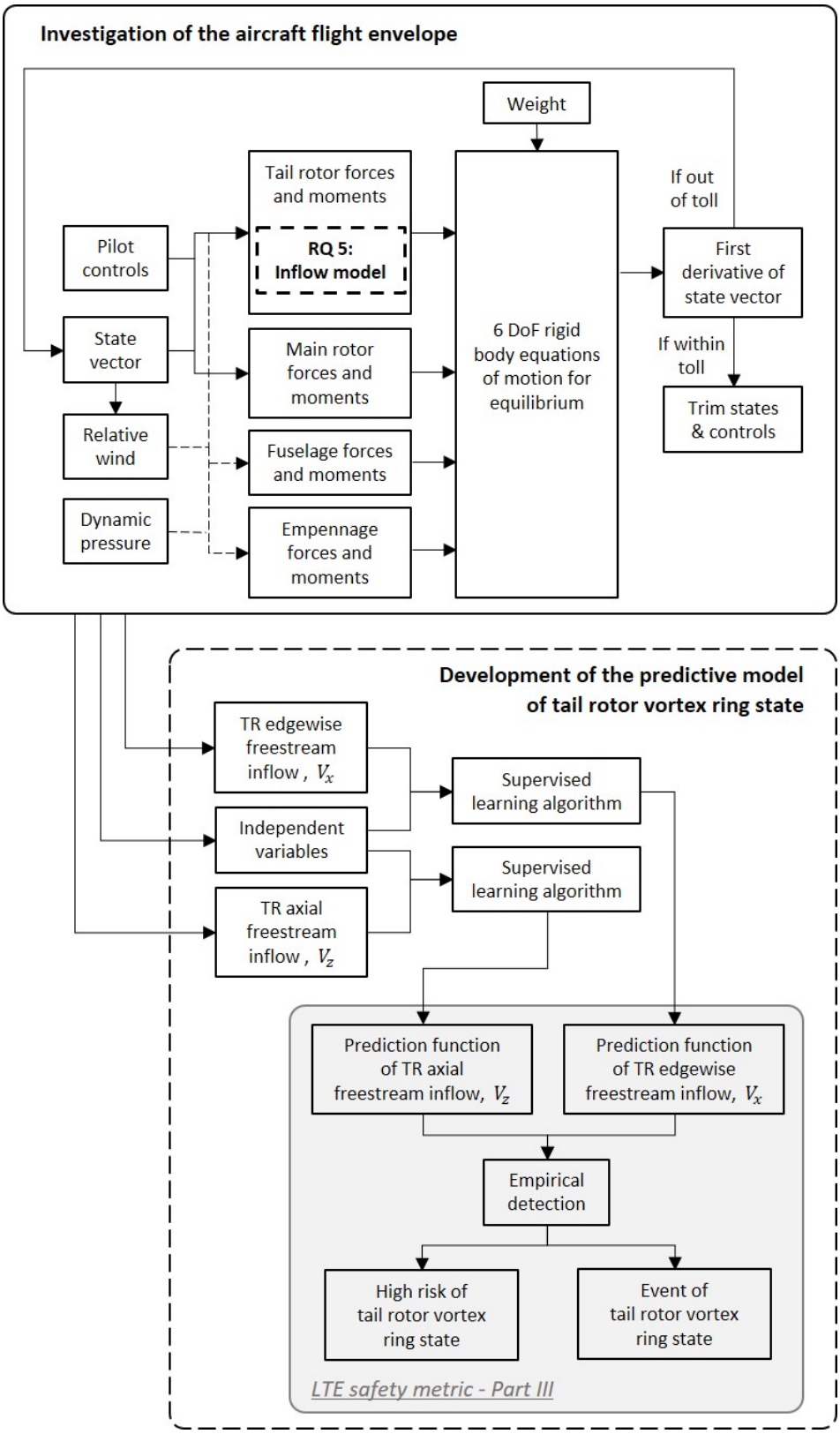

Figure 3.19: Approach to obtain the predictive model of the LTE phenomenon of tail rotor vortex ring state.

3.8.1 Investigation of the Aircraft Flight Envelope

Selection of the flight test scenarios

A set of aircraft weights and flight test conditions needs to be determined to explore the flight envelope of the helicopter. This selection determines the conditions and the ranges over which the resulting model will be applicable. It has been observed that the aircraft airspeed and the sideslip angle are essential variables that must not be neglected. To build a predictive model that encompasses a vaster area of the helicopter flight envelope, the aircraft weight, and the density altitude should also be considered as simulation input variables. Note that, since LTE is a low-speed flight characteristic, the study of a reduced airspeed range decreases the total computational cost of the investigation.

Computation of the physics-based simulation results

The predefined flight envelope needs to be investigated. The simulation model needs to include the appropriate models previously described to accurately represent each LTE phenomenon (Experiment 1, 2, and 5 will clarify what inflow model should be used at the tail rotor). It has been observed that the approaches selected to detect the three LTE phenomena involve equilibrium flight conditions. Hence, a trim simulation is performed for each combination of input variables. Additionally, in the case of the weathercock stability phenomenon, a linearization analysis is needed after solving each trim problem. The parameters recorded after the convergence of each simulation include the independent variables and the simulation output needed to develop the prediction function of the detection parameter of the LTE phenomenon considered.

3.8.2 Development of the Predictive Models of the LTE Phenomena

Creation of the prediction functions of the LTE detection parameters

Different parameters have been selected to detect the three LTE phenomena. The predictive models of the detection parameters of the three types of LTE events need to be developed. Each model is represented by a prediction function which is created through the learning training process of the relationship between the test conditions that define the specific flight scenarios, and the detection parameter of the specific LTE phenomenon. Note that the prediction functions need to be trained with input parameters that are usually available within the operators' flight data. Also, those parameters may be made non-dimensional to allow the application of the final model on flight data of different helicopter sizes, while considering the same aircraft configuration.

Several alternatives of supervised learning algorithms that involve numeric prediction are available in the literature. A common approach used to develop surrogate models is the response surface methodology [104]. This is a collection of statistical and mathematical techniques, such as simple and multiple linear regression, that can be used to explore the influence of the independent variables on the response. However, the design of a good response surface methodology study and its interpretability may become less straightforward when nonlinearities are involved. Since, the modeling of helicopter flight characteristics often involves nonlinear relationships between the inputs and outputs of the simulation model, more advanced machine learning methods are often sought. Data partitioning represents a more flexible approach that can effectively describe nonlinear relationships while providing a good balance between prediction accuracy and interpretability. It is useful in exploring relationships between inputs and outputs, providing partition diagrams that are easy to read. Decision Trees and Bootstrap Forest are some examples of this more recent data mining

approach. However, when the complexity of the model increases the resulting diagram may become too difficult to understand. From the literature, it is observed that neural network architectures are frequently used in complex environments of aviation research [86]. Even if they are difficult to interpret and do not allow for an easy understanding of the input-output relationship, their powerful learning method often provides an accurate prediction of nonlinear functions, offering a favorable approach to be applied within the flight data monitoring program [61]. To ensure an accurate approximation of the true functions of the LTE detection parameters, different models can be developed and compared evaluating the appropriate adequacy measures.

Definition of the proximity to the LTE phenomena

After defining the prediction functions of the three LTE phenomena, predefined thresholds must be set on the predicted parameters to allow for the detection of the LTE events and proximity to LTE events within flight data. For the phenomenon of running out of pedal for trim, a zero value of the pilot's pedal control for trim represents the ineffectiveness of the tail rotor in providing the necessary thrust for trim. This is identified as a running out of pedal for trim event. The risk of running out of pedal for trim can be defined by a predefined interval of the detection parameter that approaches the threshold of the running out of pedal for trim event. In the case of loss of weathercock stability, a negative value of its detection parameter (static stability derivative that will be identified in Experiment 4) characterizes a statically unstable flight condition which can potentially lead to an LTE like behavior. It is noted that while a small negative value of its detection parameter represents a more neutral behavior of the aircraft in response to external disturbances, a large negative value is of particular concern. Hence, events of loss of weathercock stability are considered to be characterized only by large negative values of its detection parameter. The risk of loss of weathercock stability can be defined by a predefined interval of the static

stability derivative that approaches the threshold of the loss of weathercock stability event. With regards to the tail rotor vortex ring state phenomenon, the freestream inflow components at the tail rotor are used to detect the stability boundary defined by Johnson [81]. This approach identifies tail rotor vortex ring state events. The risk of tail rotor vortex ring state can be defined by a predefined interval of the detection parameters that approaches the threshold of the tail rotor vortex ring state event.

Hence, the predictive model of each LTE phenomenon is formed by the prediction function of the specific detection parameters and the appropriate definition of risk thresholds. The collection of the three predictive models defines the final LTE safety metric, i.e., the comprehensive model that predicts LTE events and proximity to LTE. While the definitions of the three types of LTE events do not change, the proximity to LTE thresholds may vary between different types of flight operations. The estimation of those thresholds should be left accessible to the operator, to provide flexibility in the risk management of post-flight analyses.

3.9 Summary of Research Formulation

A comprehensive summary of the research is provided in Figure 3.20. During the formulation of the methodology five research gaps have been identified, hindering the direct application of the proposed approach. Each gap has been related to a research question for which a hypothesis and an experiment have been formulated. The experiments will be implemented in the next chapter to substantiate the related hypotheses and clarify the research gaps. This will lead to the overarching hypothesis of this thesis that will be tested comparing the new LTE safety metric against the current metric used within the HFDM program. This final experiment will verify the improved results obtained with the proposed methodology, answering the motivating question of this research and satisfying the research objective.

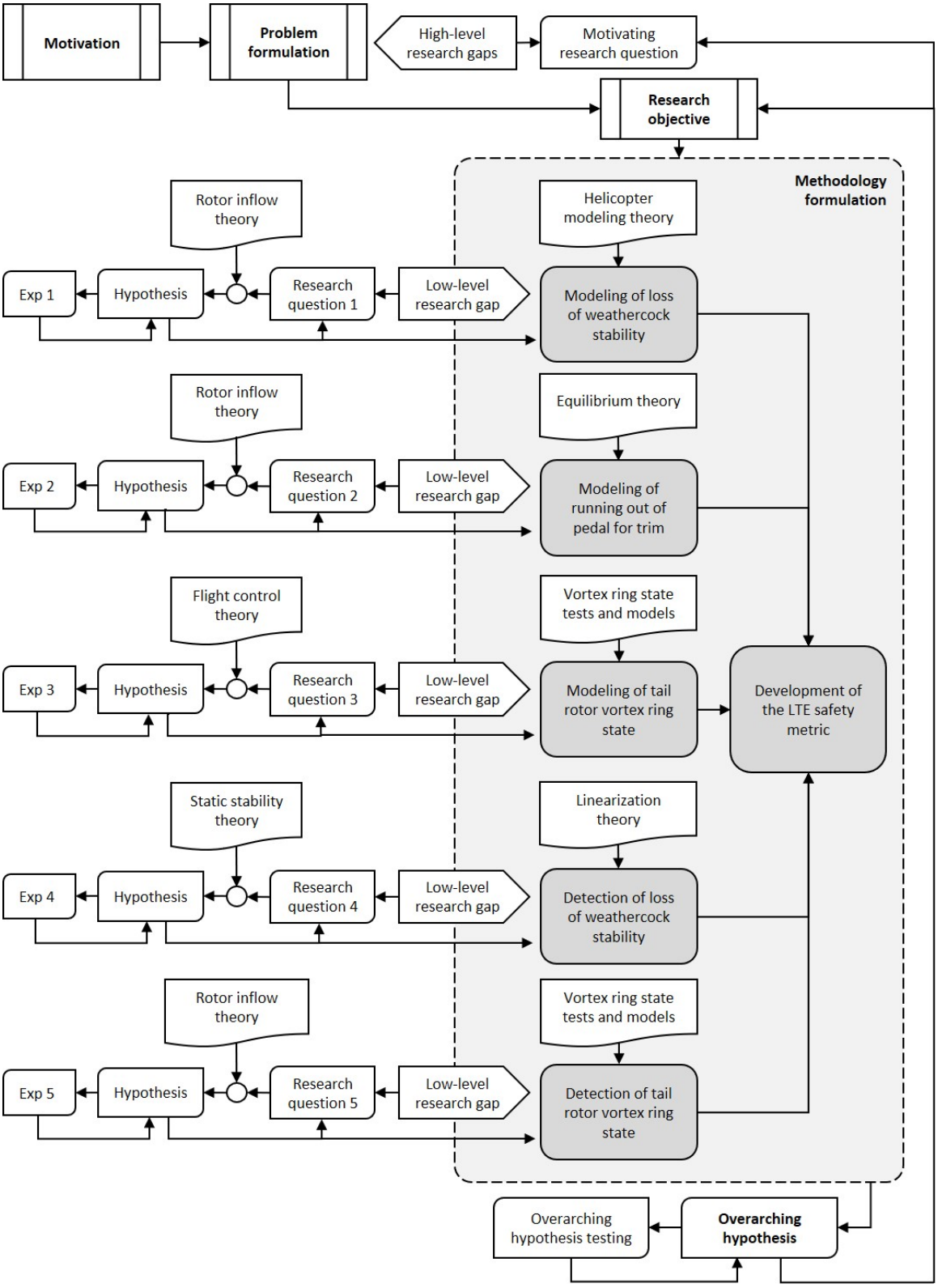

Figure 3.20: Summary of research formulation.

CHAPTER 4
EXPERIMENTATION AND RESULTS

4.1 The Simulation Model FLIGHTLAB

A rotorcraft simulation model is required to test the hypotheses formulated and the final methodology proposed. Specifically, the physics-based modeling of helicopter flight dynamics is needed to solve trim problems and stability analyses. A component-based calculation of the aerodynamic loads acting on the aircraft is necessary to assess the contribution of each helicopter subsystem. Also, a selective model fidelity is needed to compare and assess the impact of different inflow models on the representation of LTE.

Numerous software for rotorcraft modeling and simulation have been developed. A historical overview is provided by Johnson [82]. Between the available options, the simulation model FLIGHTLAB is considered for its state-of-the-art features. This aircraft modeling and simulation software was created by Advanced Rotorcraft Technology, Inc. to enable real-time analyses for flight dynamics and handling qualities applications [44, 45, 46]. It provides a predefined library of generic components which have been successfully validated, offering the reliable modeling of aerodynamic, control, structural, and propulsion systems [47]. Also, it supports selective fidelity modeling ensuring traceability and commonality between simulations. A friendly user graphic interface allows for fast and easy analyses while reducing the chance of human error. Currently, the software is widely used in industry and academia to simulate and analyze the behavior of a wide range of existing aircraft and to support the design and testing of new aircraft configurations [48]. Therefore, the rotorcraft simulation model FLIGHTLAB is used to accomplish most of the experimentation phase of this

research. A generic helicopter configuration with a counterclockwise rotation of the main rotor is assumed.

4.2 Experiment 1: Simulation of Loss of Weathercock Stability

The phenomenon of loss of weathercock stability relates to the variation of the aircraft yaw moment with the change in relative wind conditions and it is a function of the induced velocity at the tail rotor disk. To ensure an appropriate level of accuracy in the representation of this phenomenon, an investigation of the impact of the inflow modeling is needed. A physics-based simulation of a wind tunnel test is performed to create a causal effect between the variation of wind conditions and the resulting change in tail rotor thrust. The results are compared with the wind tunnel test results presented by Wood [154].

4.2.1 Experiment Setup

The rotorcraft simulation model FLIGHTLAB is used to accomplish this analysis. A generic helicopter configuration with a counterclockwise rotation of the main rotor is modeled. To replicate the controlled airstream characteristic of a wind tunnel environment, the wind is simulated to have a fixed direction with a constant wind magnitude. Any direction may be used, however, a headwind represents a convenient starting condition. The impact of 10 m/s wind is used to investigate the impact of the inflow model accuracy on the weathercock stability of the aircraft while standard sea level conditions are used. Every helicopter's degree of freedom is constrained except for the yaw motion which is controlled throughout the simulation. A constant body yaw rate r is imposed until a complete 360 deg yaw is performed. The controlled change in yaw causes the variation of the sideslip angle. A small r of 2 deg/s is used to not significantly impact the freestream velocity at the tail rotor. Note that 2 deg/s of yaw rate corresponds to roughly 0.25 m/s of freestream inflow through the

tail rotor which is very small compared to the assumed wind magnitude of 10 m/s. This makes the simulation quasi-steady, with the wind being the main influence on the yaw moment reaction developed by the aircraft. An illustration of the simulated scenario is given in Figure 4.1.

Because of its simplicity, the uniform induced inflow derived from momentum theory is initially used for the tail rotor to make first considerations on the results obtained. The helicopter is first trimmed in such condition to find the equilibrium states and controls, and then the quasi-steady simulation is performed to calculate the reaction loads from the aircraft. The process is repeated using different inflow models, i.e., the Pitt-Peters inflow model, uniform inflow with the aerodynamic interference from the main rotor wake, and Pitt-Peters model with the aerodynamic interference from the main rotor wake. The forces and yaw moments developed by the tail rotor, vertical fin, and fuselage are recorded as the sideslip angle continuously changes due

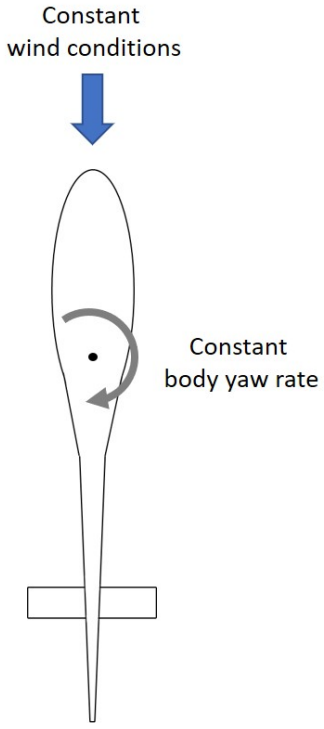

Figure 4.1: Simulated wind tunnel scenario.

to the imposed small yaw rotation. It is important to keep in mind that during the quasi-steady simulation, the helicopter loses its equilibrium condition. Consequently, the forces and moments acting on the vehicle do not balance each other while the sideslip angle is changing. It has been already discussed how the sideslip angle and the wind azimuth represent the same aerodynamic angle. For convenience, the wind azimuth variable is used for the visualization of the results.

4.2.2 Results

The fuselage, the vertical fin, and the tail rotor are the helicopter subcomponents that mainly influence the aircraft weathercock stability. Figure 4.2 presents a comprehensive comparison of the yaw moments reactions from the different helicopter subcomponents while being impacted by a wind magnitude of 10 m/s. The sum of those contributions results in the yaw moment developed by the aircraft. Considering

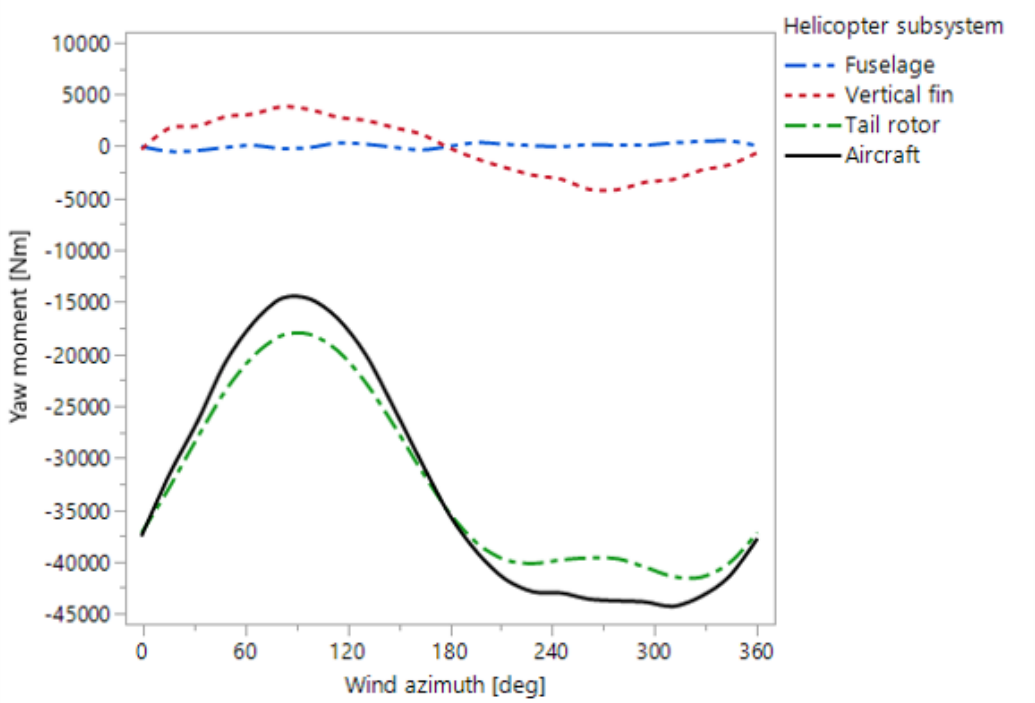

Figure 4.2: Comparison of yaw moments developed by the influencing helicopter subsystems.

an equilibrium flight condition with relative winds from 0 deg, if an external disturbance causes the wind azimuth to increase, the vertical tail experiences a higher angle of attack. This develops an aerodynamic force perpendicular to the relative airspeed that causes a positive yaw moment reaction, yawing back the aircraft to the initial equilibrium position, i.e. hover with headwinds. In this case the vertical fin has a stabilizing effect, represented by a positive slope of the yaw moment versus the wind azimuth. Instead, starting from an equilibrium condition with relative winds from 180 deg, if the wind azimuth increases the reaction side force experienced by the vertical fin develops a negative body yaw moment that initiates the tendency of the aircraft to yaw away from the equilibrium position. This is recognized as a destabilizing effect, represented by a negative slope of the yaw moment curve. The yaw moment developed by the tail rotor varies with the wind azimuth because of the change in freestream velocity at the rotor plane, influencing the resulting thrust produced. It is evident that the tail rotor is the key contribution to the static directional stability of the helicopter. In fact, it resembles the yaw moment developed by the aircraft. This result agrees with the wind tunnel test findings published by the U.S. Army Joint Special Study Group [154].

It is noted how the most critical directional static instability corresponds to the flight conditions with relative tailwinds. The yaw moment developed by the tail rotor is directly proportional to the thrust which depends on the inflow velocity at the blade section. It is important to analyze the source of the yaw moment variation, as shown in Figure 4.3. When the wind azimuth shifts from 0 to 90 deg, the axial component of the freestream inflow of the tail rotor suddenly increases, overcoming the decrease of the induced inflow. This results in a greater total inflow which, at fixed tail rotor collective pitch, causes the thrust to decrease, triggering an uncommanded right yaw. As already mentioned, this corresponds to a statically stable contribution as the aircraft is yawing back to the initial equilibrium position. Hence, the rotor

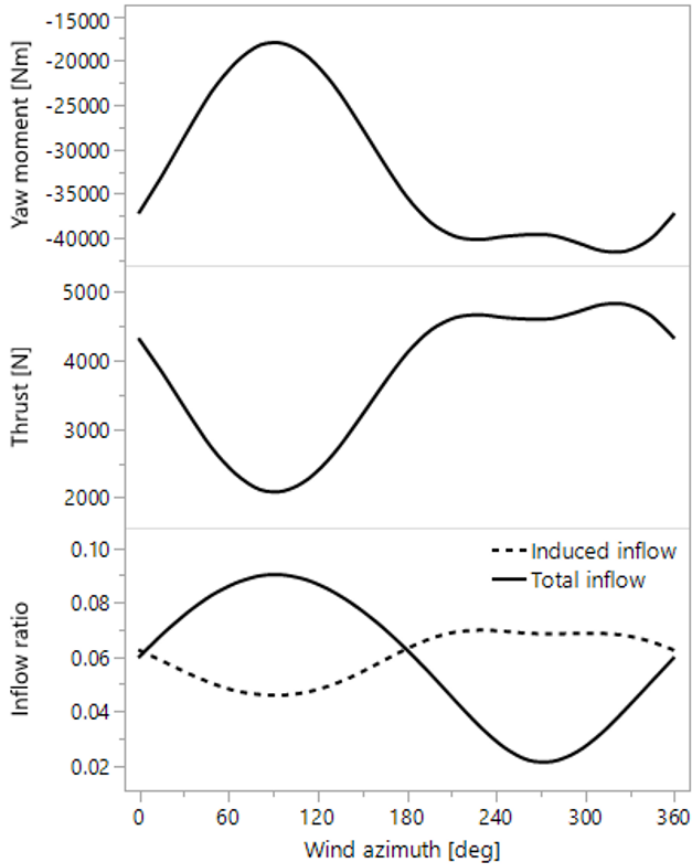

Figure 4.3: Important tail rotor parameters that influence the yaw moment developed by the tail rotor.

inflow is the leading variable that, affected by the change in wind azimuth, triggers the final yaw moment reaction. Specifically, the induced inflow is of particular interest as its accuracy may widely vary based on the modeling assumptions made.

Until this point, the results were obtained while modeling the tail rotor inflow using a uniform inflow model derived from simple momentum theory. However, this work investigates the effect of different inflow models on the weathercock stability of the aircraft. As previously described, Pitt-Peters inflow model is used to account for a more accurate representation of the non-uniform gradient distribution of the inflow along the tail rotor blade. Further, the aerodynamic interference of the main rotor vortex wake is accounted for, first while using momentum theory and then while

applying the Pitt-Peters inflow model. Figure 4.4 shows the comparison between the resulting yaw moment developed by the tail rotor as a function of wind azimuth while using different modeling techniques for the tail rotor inflow. The weathercock stability characteristics can be inferred by the slope of each yaw moment curve.

It is observed that the resulting yaw moment significantly changes only when the aerodynamic interference from the main rotor wake is included in the tail rotor inflow calculation. This was expected as the main rotor downwash has a strong impact on the relative wind conditions at the tail rotor plane, consequently influencing the tail rotor thrust developed. During right quartering flight conditions, the main rotor wake introduces a significant in-plane velocity component at the tail rotor disk [50, 51]. Because of the top-forward tail rotor rotation, the dynamic pressure at the tail rotor is reduced causing a reduction in the effective angle of attack at the blade section. This causes the tail rotor to produce less thrust for the same blade pitch setting, leading the aircraft to develop a less negative yaw moment reaction. Hence,

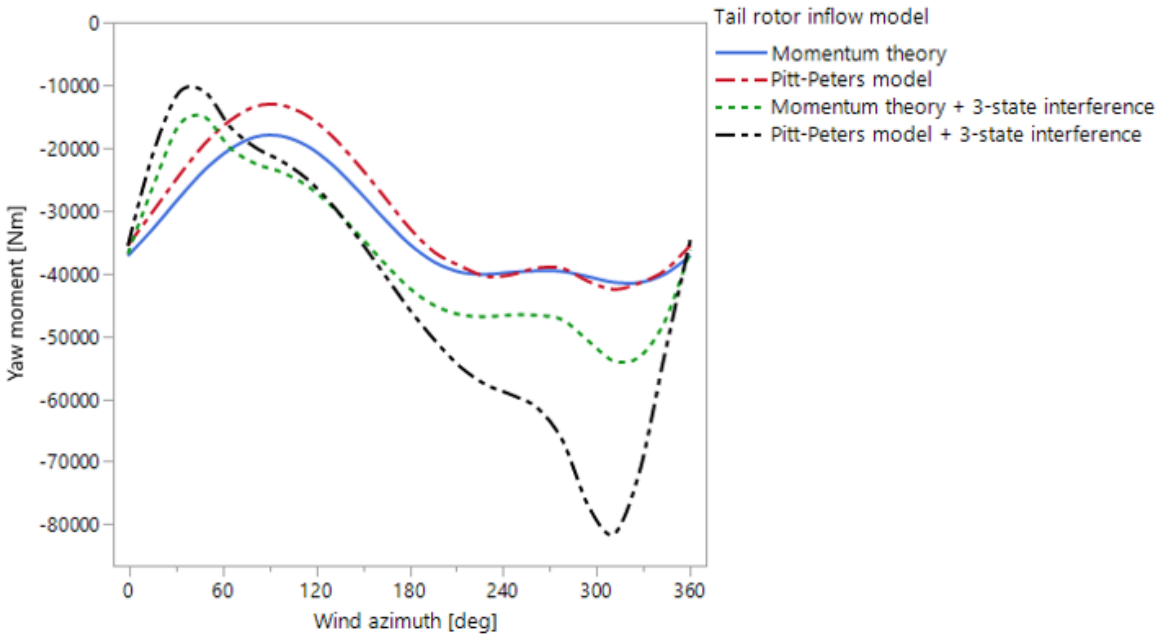

Figure 4.4: Comparison of yaw moments developed by the tail rotor while using different inflow models.

the slope of the yaw moment curve increases representing a more positive weathercock stability of the aircraft. During left quartering flight conditions, the main rotor wake still causes a decrease in dynamic pressure at the tail rotor plane, however, this effect is overtaken by the out-of-plane velocity component induced by the retreating main rotor blades. The counterclockwise rotation of the main rotor causes a strong downwash that induces the tail rotor in a more severe descent like flow condition, i.e., increased freestream flow going from left to right through the tail rotor when the helicopter is viewed from behind, significantly increasing the tail rotor thrust. This effect is greater when the model accuracy increases and includes the prediction of the inflow gradient along the tail rotor blade.

The results agree with the findings obtained by the LTE Joint Special Study Group and published by Wood [154]. A wind tunnel test was performed to investigate the critical wind azimuth regions that may lead to LTE. During the test, the yaw moment of a OH-58 KIOWA scale model was measured using a fixed yaw rate, a fixed collective pitch of the tail rotor blades, and a constant low wind speed within the tunnel. Hence, the resulting yaw moment fluctuations were mainly caused by the effects of the wind variations through the tail rotor. The contributions of the aircraft body, tail rotor, and main rotor aerodynamic interaction were considered separately. Figure 4.5.a shows that the tail rotor is the key contribution to the static directional stability of the helicopter. Figure 4.5.b confirms that aerodynamic interference from the main rotor wake has a strong impact on the tail rotor thrust developed.

Hence, it is observed that the weathercock stability of the aircraft is better represented by using the augmented Pitt-Peters inflow model at the tail rotor, validating the hypothesis formulated in Section 3.3.2. A significant static directional instability is present not only for flights under the impact of relative tailwinds but also while the main rotor vortex wake alters the flow through the tail rotor. Because of this instability, a lateral perturbation will attempt to weathervane the aircraft away from

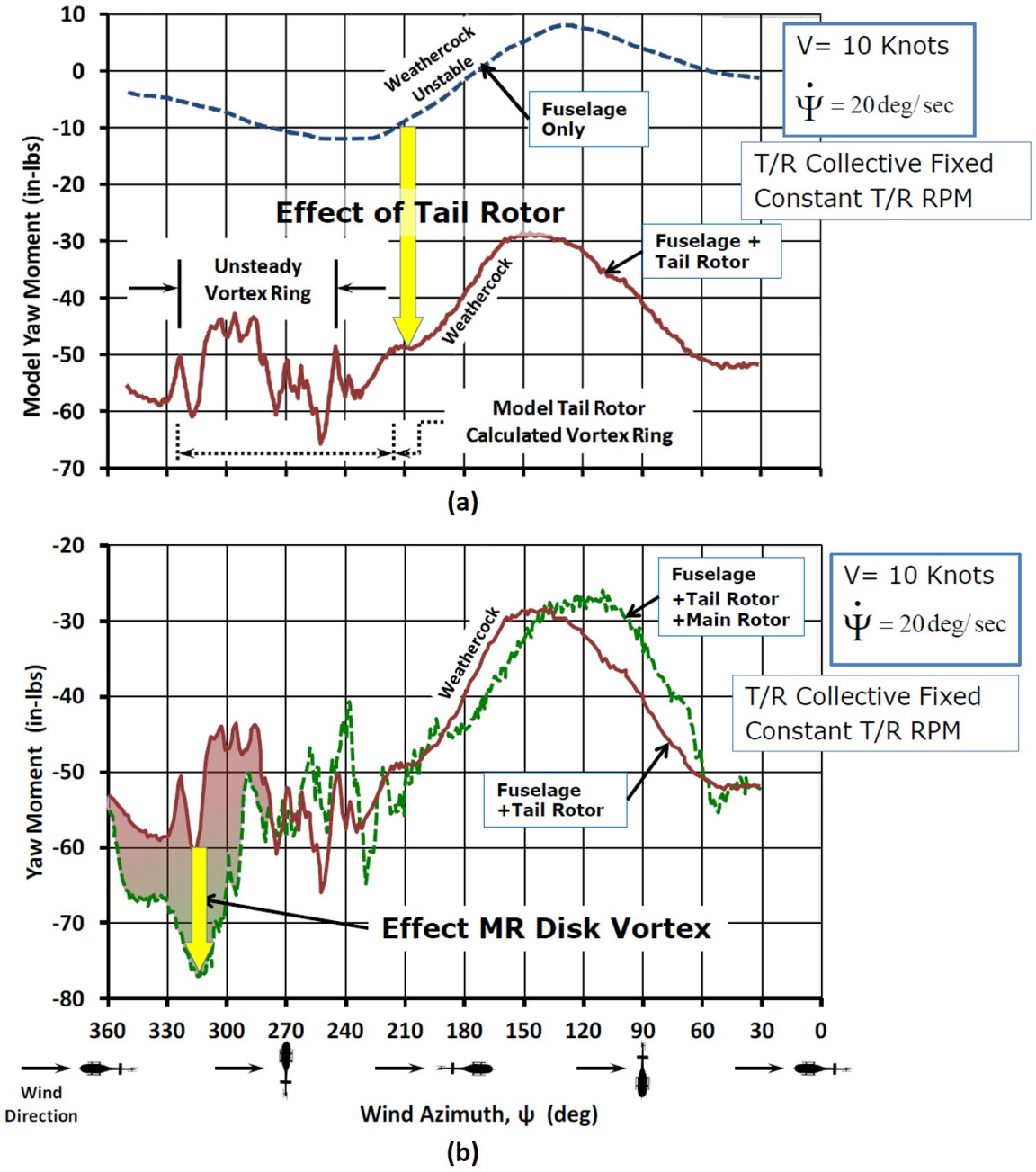

Figure 4.5: Results of LTE wind tunnel investigation published by Wood [154].

the initial flight condition, leading to LTE like behavior. Also, a sufficient amount of pedal control may not be available to reestablish another equilibrium condition. This represents another aspect of the loss of tail rotor effectiveness phenomenon, and it is further investigated in the next section.

4.3 Experiment 2: Simulation of Running Out of Pedal for Trim

The tail rotor collective pitch angle needed to maintain directional equilibrium is impacted by the accuracy of the inflow model used. Because this angle is directly linked to the pilot's pedal input, an investigation on the impact of the inflow modeling on the pedal control needed for yaw balance is necessary to ensure an appropriate level of accuracy in the representation of the running out of pedal phenomenon. Because of the significant amount of crosscoupling between forces and moments, a comprehensive equilibrium analysis of the aircraft is performed. The results are compared with the flight test measurements of Lynx Mk 5 published by Padfield [114].

4.3.1 Experiment Setup

The rotorcraft simulation model FLIGHTLAB is used to model a generic helicopter configuration with a counterclockwise rotation of the main rotor. The investigation is carried out through a series of trim analyses. For each equilibrium condition, the helicopter is in a free level flight at standard sea level conditions. The entire range of sideslip angles is explored, including forward and rearward flights, while the yaw attitude of the aircraft is maintained constant. It is noted that equivalent results would be obtained if the simulation involved a hover scenario with winds from different wind azimuths. After several iterations, it was observed that a sideslip angle interval of 5 deg between each simulation provides a good tradeoff between accuracy and computational time. The impact of 5, 10, and 15 m/s airspeeds is investigated. The trim solution is reached numerically to find the minimum of the set of nonlin-

ear equations that define the trim problem within some predefined constraints. The trim convergence criteria were set to be 0.012 m/s^2 in translational acceleration and 0.01 rad/s^2 in angular acceleration. The pedal control needed to maintain the equilibrium flight is recorded after the iteration converges. Initially, the tail rotor inflow is modeled by simple momentum theory. Then, the process is repeated using different inflow models, i.e., the Pitt-Peters inflow model, simple momentum theory with the aerodynamic interference from the main rotor wake, and the Pitt-Peters model with the aerodynamic interference from the main rotor wake.

4.3.2 Results

The calculation of the pedal control needed for trim flight is affected by the modeling of the tail rotor inflow dynamics. Figure 4.6 shows the pedal control requirements to sustain equilibrium at different relative wind conditions while modeling the tail rotor inflow using a uniform inflow model derived from simple momentum theory. The results are visualized using the Cartesian and the polar coordinate systems, offering an intuitive visualization. As a reference, a pedal control of 0% corresponds to full left pedal while 100% of pedal control is full right pedal. Note that a nonlinear relationship exists between the pedal control requirements for trim and the relative wind conditions tested. Of particular interest is the sideward flight to the right, which significantly reduces the pedal control margin. This is mostly caused by the weathercocking action of the tail rotor. The increase of the net inflow through the tail rotor causes a decrease in the angle of attack at each blade element, which leads to a reduction of the thrust produced. To sustain trim, an increase in the tail rotor collective pitch is necessary, which is accomplished by applying more left pedal.

Similar pedal control requirements are obtained when the tail rotor inflow is modeled using a linear inflow gradient over the blades. Figure 4.7 illustrates the pedal control margins measured while using the Pitt-Peters inflow model. The control limits

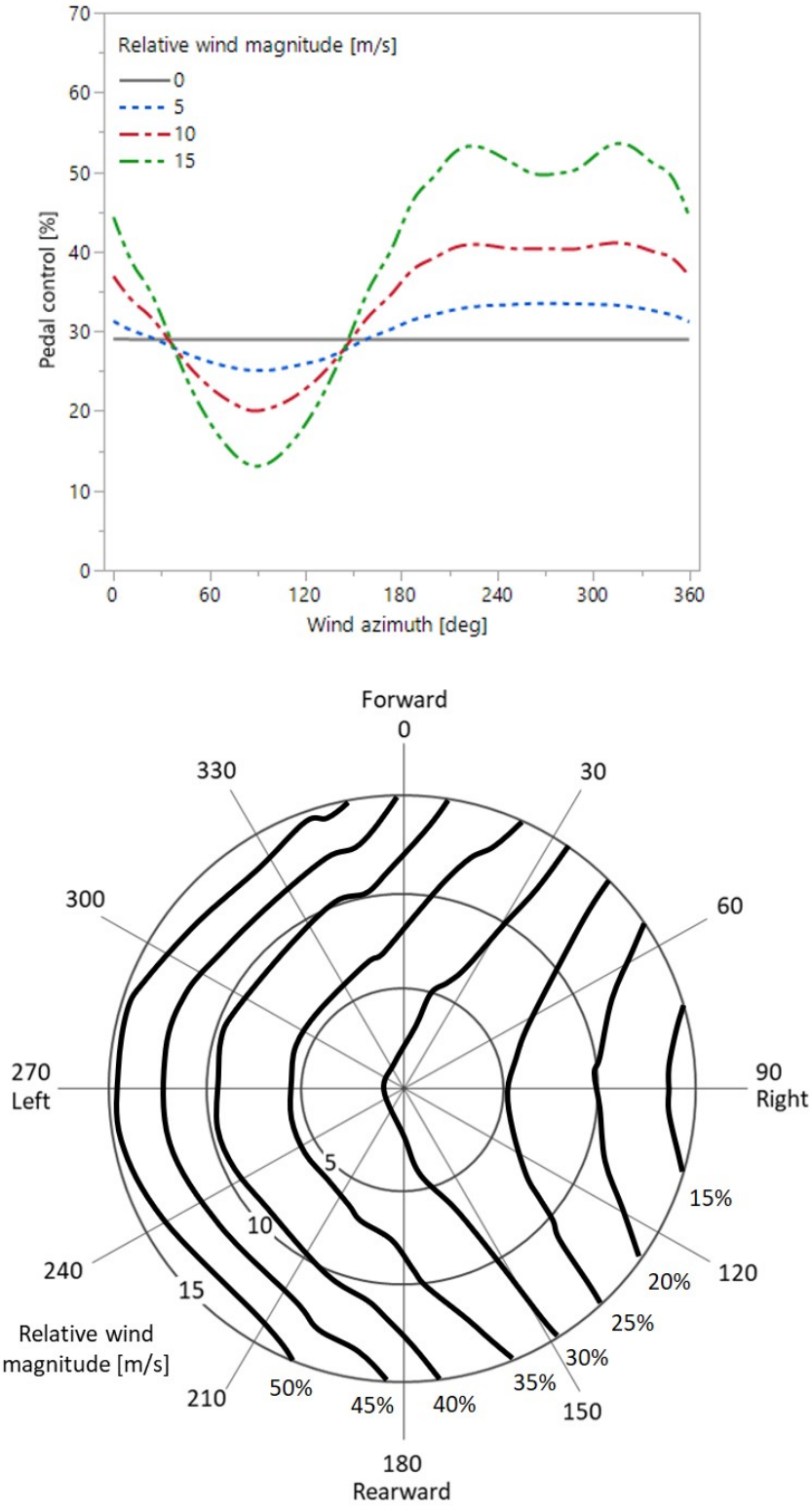

Figure 4.6: Pedal control requirements for trim flight at different relative wind conditions while the tail rotor inflow is modeled using momentum theory (Cartesian and polar visualization).

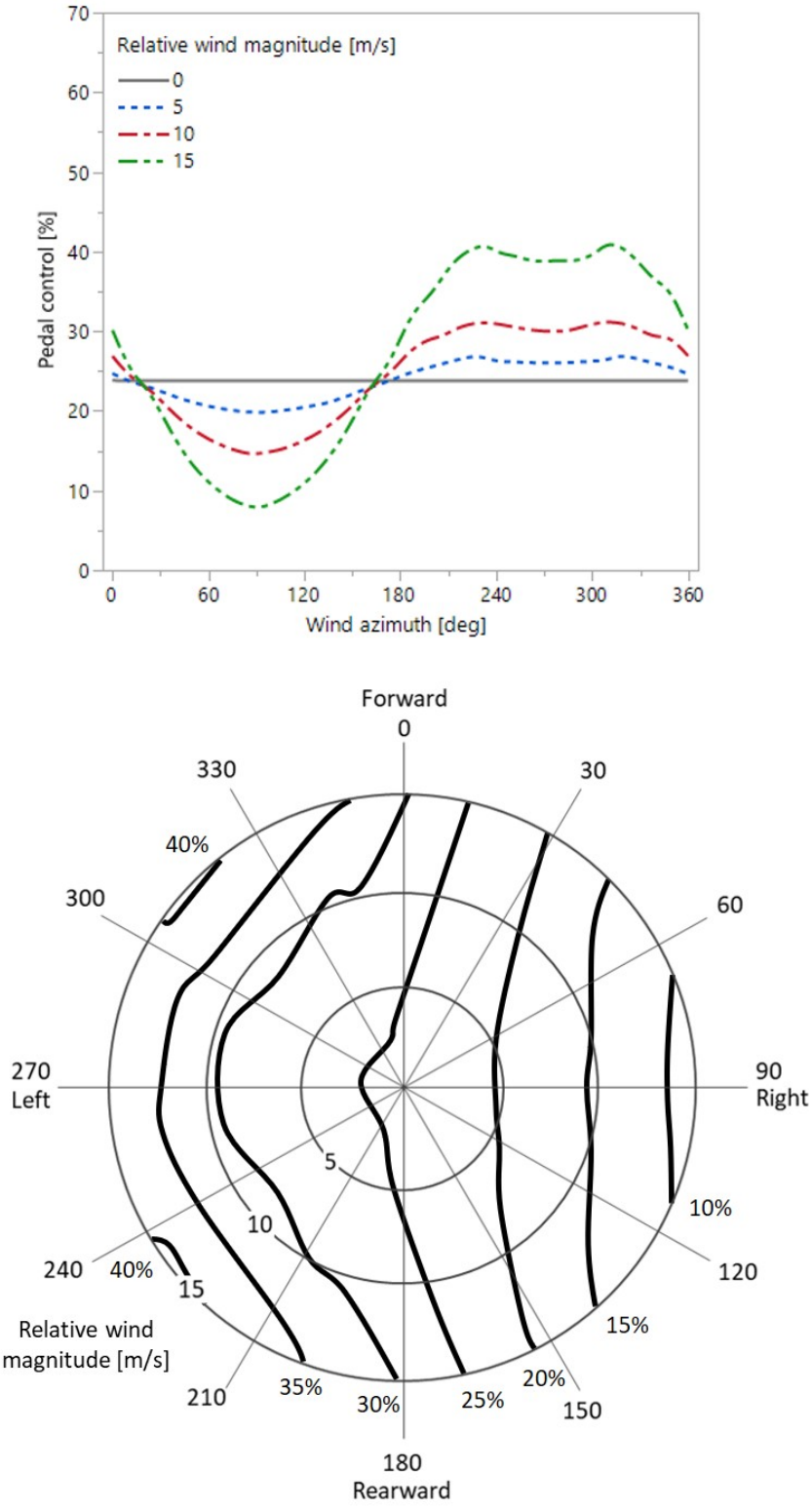

Figure 4.7: Pedal control requirements for trim flight at different relative wind conditions while using the Pitt-Peters inflow model at the tail rotor (Cartesian and polar visualization).

are smaller compared to the one identified using the uniform inflow model, showing more critical flight scenarios. However, it is observed that the most dangerous wind azimuth region remains the same, i.e., sideward flight to the right.

The distribution of the pedal control requirements for trim flight greatly changes when the inflow model used for the tail rotor is augmented with the aerodynamic interaction from the main rotor wake. This was expected as the main rotor downwash has a strong impact on the relative wind conditions at the tail rotor plane. Figures 4.8 and 4.9 show the results obtained using the momentum theory and the Pitt-Peters inflow model, both augmented with the main rotor-to-tail rotor interference. The control limits found while using the augmented Pitt-Peters inflow model are smaller compared to the one identified using the augmented uniform inflow model, revealing a more critical flight envelope. However, it is observed that the most dangerous wind azimuth region remains the same, i.e., quartering flight to the right. During this flight scenario, the main rotor wake introduces a significant in-plane velocity component at the tail rotor disk. Because of the top-forward tail rotor rotation, the dynamic pressure at the tail rotor is reduced causing a reduction in the effective angle of attack at the blade section. This leads the tail rotor to produce less thrust for the same tail rotor blade pitch setting. Hence, a greater left pedal is needed to sustain equilibrium in flight, reducing the pedal control margin. Using the helicopter configuration with a mass of 7500 kg and at sea level conditions, the smallest pedal control is 4% during a quartering flight to the right at 15 m/s of airspeed, as shown in Figure 4.9. A more critical flight scenario, e.g. higher mass and/or higher density altitude will decrease the pedal control margin often exhibiting the running out of pedal phenomenon. This is shown in Figure 4.10 which presents the trim results for the aircraft with a mass of 8000 kg and at a density altitude of 3000 m. The pedal control margins agree with the flight test measurements published by Padfield [114] and given in Figure 4.11. Hence, it is observed that a more realistic representation of the phenomenon of running out of

pedal for trim is obtained when the tail rotor inflow is represented by a linear gradient distribution along the tail rotor blade augmented with the aerodynamic interference from the main rotor vortex wake, validating the hypothesis formulated in Section 3.4.2. The insufficient pedal available during a quartering flight to the right will cause an uncommanded right yaw that confirms the ineffectiveness of the tail rotor in providing the necessary thrust for trim.

It is noted that the FAA [54] and the NTSB [107] do not acknowledge the quartering flight to the right as a critical condition, and focus only on the quartering flight to the left. During this scenario, even if the main rotor wake still causes a decrease in dynamic pressure at the tail rotor plane, this effect is overtaken by the out-of-plane velocity component induced by the retreating main rotor blades. The counterclockwise rotation of the main rotor causes a strong downwash that induces the tail rotor in a more severe descent like flow condition, i.e., increased freestream flow going from left to right through the tail rotor when the helicopter is viewed from behind. This significantly leads the tail rotor to produce more thrust for the same tail rotor blade pitch setting. More right pedal is needed to maintain equilibrium, increasing the pedal control margin. Hence, the quartering flight to the left does not represent a threat for running out of pedal scenarios. However, the FAA [54] describes this interference to cause the tail rotor to operate in a turbulent environment. Also, Padfield [114] mentions that it may be characterized by vortex ring flow states. This is another aspect of the loss of tail rotor effectiveness phenomenon and it is explained in the next section.

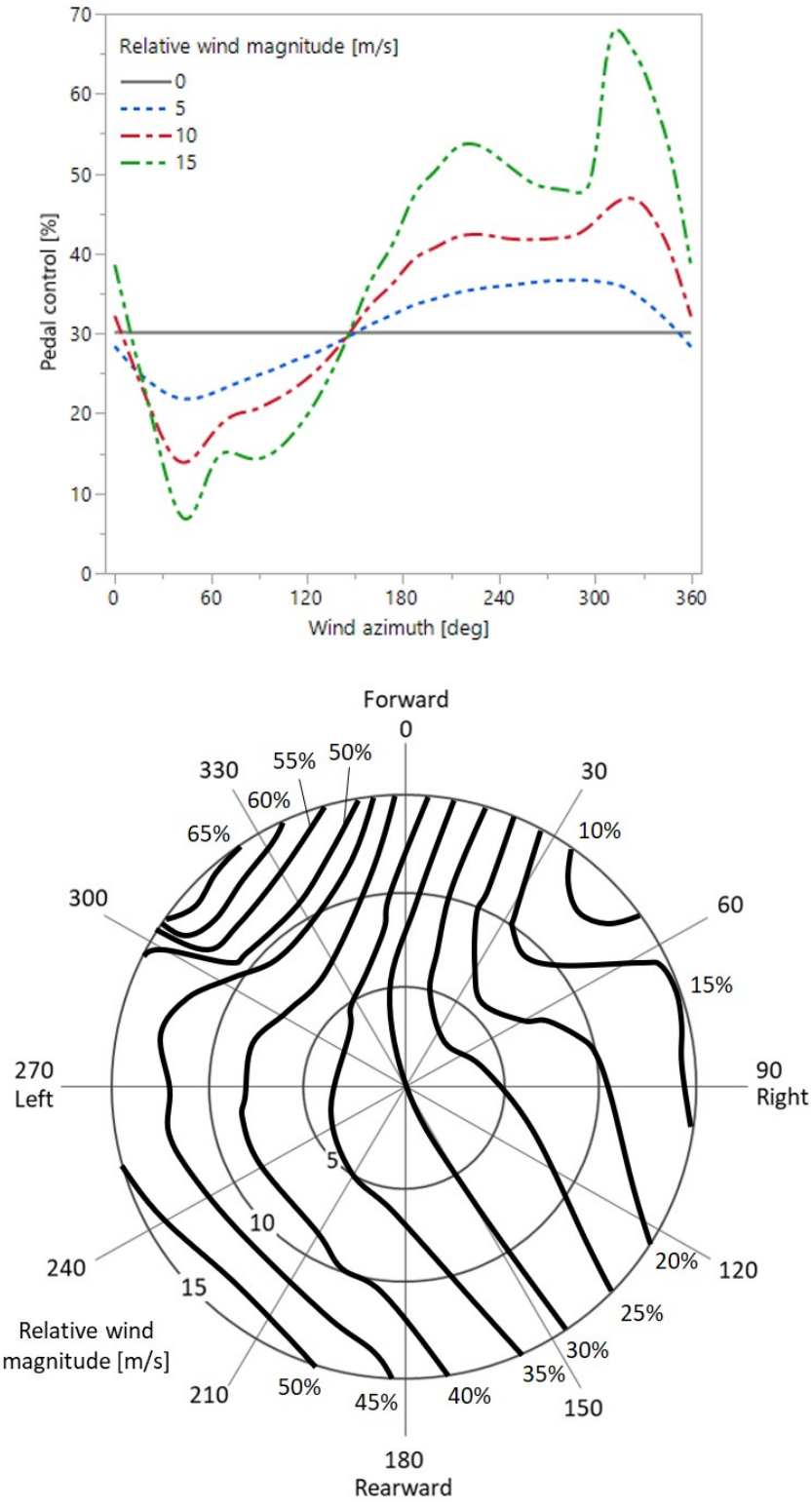

Figure 4.8: Pedal control requirements while using momentum theory augmented with the 3-state main rotor interference (Cartesian and polar visualization).

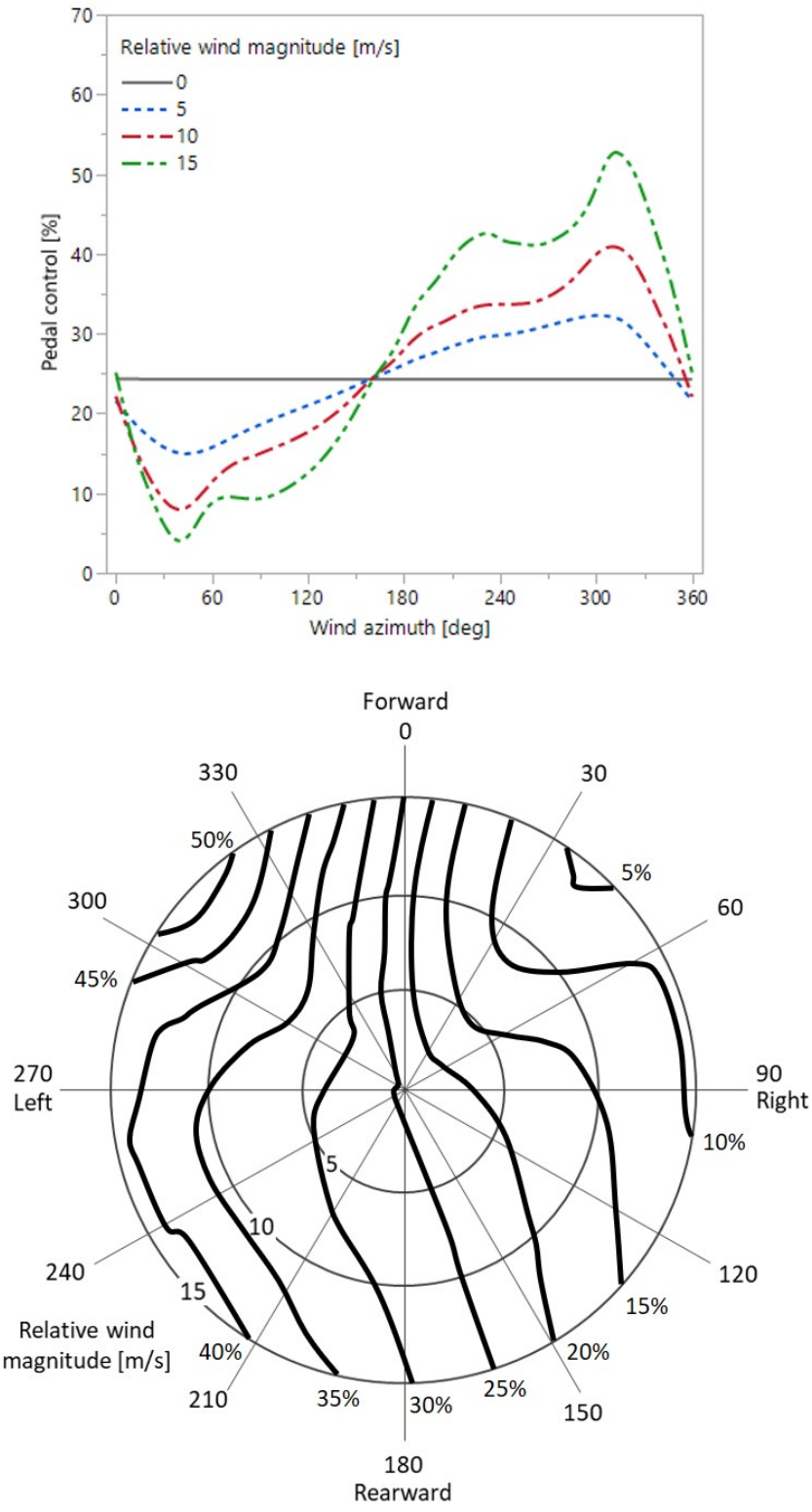

Figure 4.9: Pedal control requirements while using the Pitt-Peters inflow model augmented with the 3-state main rotor wake interference (Cartesian and polar visualization).

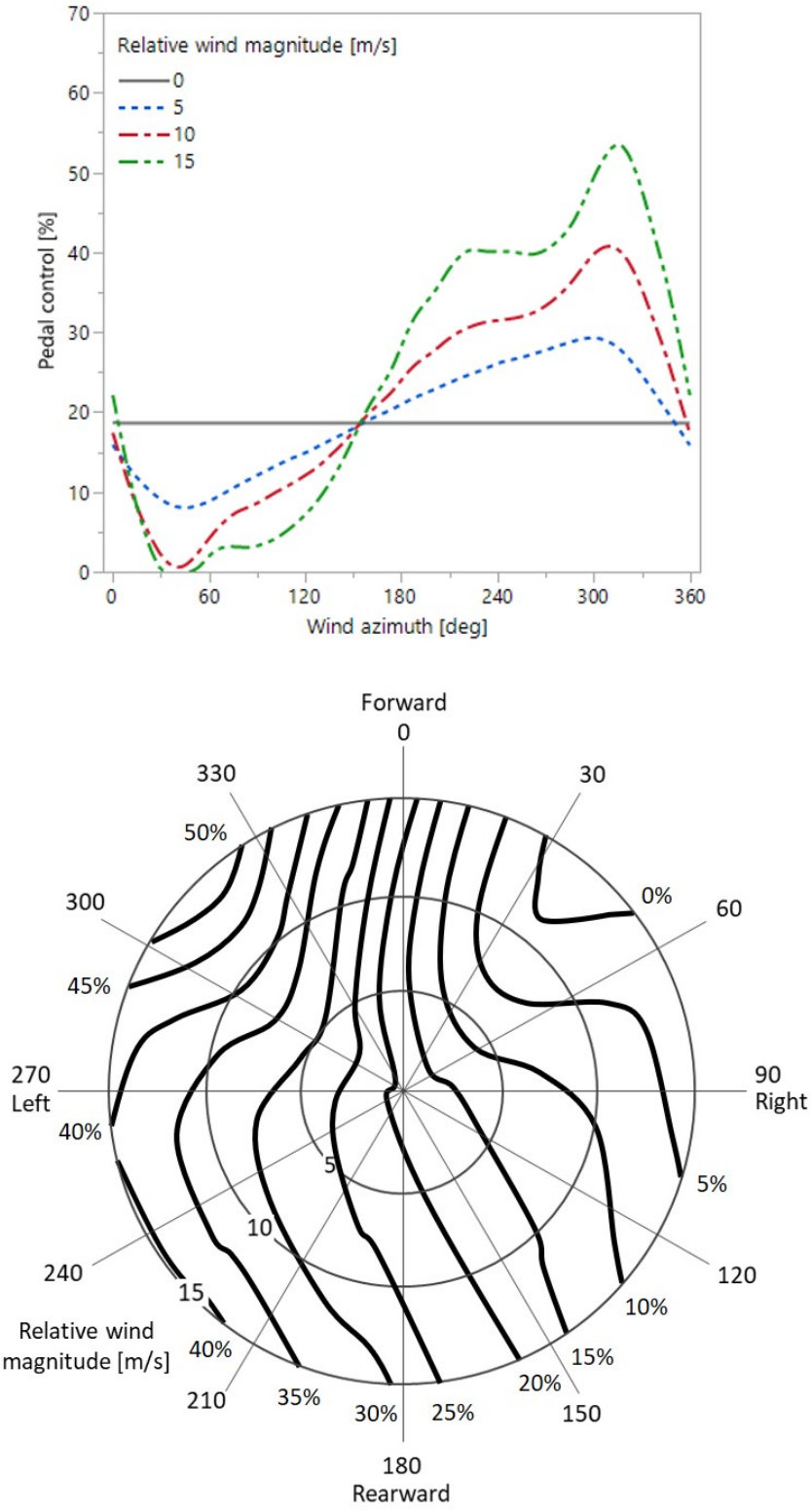

Figure 4.10: Pedal control requirements of a more critical flight scenario while using the Pitt-Peters inflow model augmented with the 3-state main rotor interference (Cartesian and polar visualization).

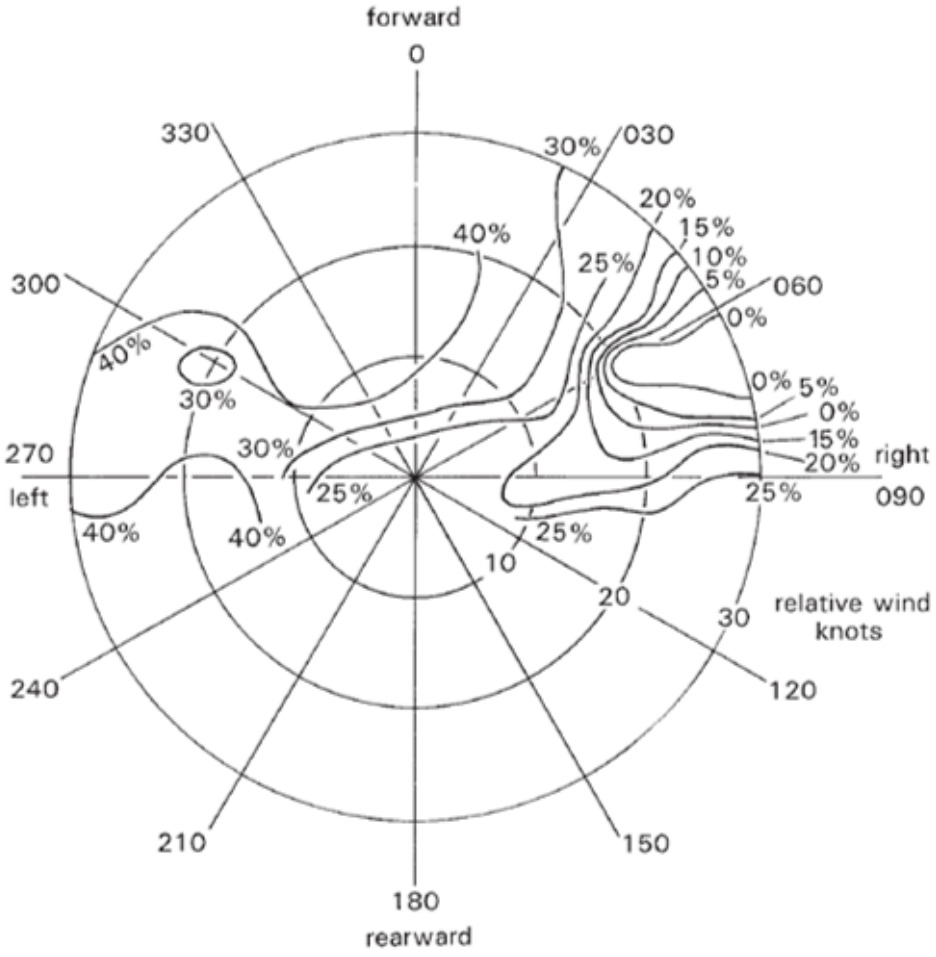

Figure 4.11: Pedal control requirements of Lynx Mk 5 measured during low-speed flight at high weight configuration [114].

4.4 Experiment 3: Simulation of Tail Rotor Vortex Ring State

Tail rotor vortex ring state is a dangerous phenomenon that strongly impacts the tail rotor performance and may lead to loss of directional control. It is essential to fully understand the nature of this flight condition to promote its awareness within the rotorcraft community. Because of the ambiguities surrounding the effectiveness of the tail rotor during this LTE phenomenon, an investigation on the pedal control effectiveness during VRS is needed. The dynamic of an isolated tail rotor in axial sideward motion to the left is modeled using a vortex ring emitter model. After validating the simulation of VRS with the results provided by Brand et al. [18], the existence of the control reversal phenomenon at the tail rotor during a VRS event is investigated.

4.4.1 Experiment Setup

The present investigation considers an isolated rotor with the properties typical of a tail rotor of a medium size helicopter. Table 4.1 lists the tail rotor configuration parameters used.

Table 4.1: Tail rotor configuration.

Tail rotor specification	Unit	Value
Number of blades	-	4
Radius	m	1.67
Rotational speed	rad/s	124.7
Blade airfoil	-	NACA 0012
Blade chord	m	0.24
Lift curve slope	rad^{-1}	5.73
Tip loss factor	%	0.95
Blade twist	rad	0

The rotor thrust is computed coupling the ring emitter model with a blade element model that accounts for 11 blade segments. This investigation neglects the blade motion because of the axisymmetric flow assumption. The blade is assumed to be rigid in bending and torsion. No blade twist has been considered, as the tail rotor blades normally do not include any twist. The ring emitter model assumes that all the blade vorticity is trailed by the blade tip in the form of a vortex ring, neglecting the vortex sheet along the blade span. The vortex core diameter of the toroidal ring cross-section is defined using the empirical recommendation of Scully, i.e., 0.5% of the rotor radius [129].

Appendix B.2 describes the validations that have been carried out to confirm the accuracy of the vortex ring emitter model. First, the vortex ring motion is verified simulating the leapfrogging behavior of two rings. During the analysis it is verified that a second order Runge-Kutta method is an accurate time integration approach to calculate the vortex ring position at each time step. Afterward, the vortex wake development is validated in hover and descent like conditions, coupling the ring emitter model with a blade element model to calculate the rotor performance. After several iterations, it is observed that sufficient wake vorticity is captured through the modeling of 100 vortex rings. Those observations are applied in the final experiment to analyze the effectiveness of pedal control (tail rotor collective) input during a VRS event.

Initially, the tail rotor is set to develop the thrust magnitude necessary to sustain yaw moment equilibrium while the aircraft is in a hover flight scenario. This is identified by the tail rotor thrust coefficient C_{T0}, used to normalize the results. From the trim setting, a series of blade collective pitch reductions of 0.25 deg is applied every 30 s to lead the tail rotor to a VRS encounter. Other than the tail rotor thrust coefficient, the induced velocity and the sideward velocity of the tail rotor are measured throughout the simulation. The resulting velocities are normalized by

the inflow velocity at the tail rotor during a hover like flow condition, i.e., v_h. Two simulations are performed to investigate the effectiveness of the tail rotor during the main phase of the VRS event examining the existence of the control reversal phenomenon. In each simulation an attempted recovery is performed with a sudden increase in collective pitch angle to the initial trim setting. First, an attempted recovery is modeled at the simulation time of 258 seconds. Then, the simulation is repeated applying the collective increase just 1 second after the previous recovery attempt, i.e., 259 seconds.

4.4.2 Results

Successful recovery from VRS

During a sideward motion of the aircraft to the left, the tail rotor is subjected to a descent like flow condition and its wake involves vortex interactions that influence the rotor performance. Figure 4.12 shows that initially at each tail rotor collective pitch reduction, the rotor suffers a thrust loss that is quickly recovered, reaching a new steady-state sideward velocity. A negative value of the sideward velocity represents a translational motion of the tail rotor to the left. The wake self-organization is captured in Figure 4.13, which shows the vortex ring displacement relative to the tail rotor during the flight. Because of the increase of freestream flow from left to right through the rotor, the new ring vortices are propelled towards the left along the wake passing through the rotor plane. This causes blade-vortex interactions that result in stronger vibrations as the left sideward velocity increases. The roughness is visible after $t = 90$ s and significantly rises after $t = 150$ s. The more the left sideward velocity increases, the more the vortex rings are compressed towards the rotor, disrupting the wake slipstream boundary while showing a leapfrogging behavior within different vortex groups. The mutual interactions between the vortex rings cause a radial expansion of the further rings and a weaker ability to propel themselves

towards the left. Hence, the wake vorticity recirculates close to the rotor forming a toroidal structure of corotating vortex rings, which affects the induced velocity at the rotor. This leads to the main phase of the VRS phenomenon, which is triggered at $t = 240$ s by a further reduction in tail rotor collective pitch. A dramatic increase in induced inflow is seen during the accumulation of vorticity in proximity to the rotor. This strongly impacts the aerodynamic environment at each blade element, which experiences a decrease in the effective angle of attack leading to a reduction in rotor thrust. At $t = 258$ s a sudden increase in the tail rotor collective pitch angle is applied. It is observed that the induced inflow value does not reach the highest peak as in a fully developed VRS event, inducing a reduction of thrust that is fully recovered with the increase of blade pitch angle. Figure 4.13 shows that the applied recovery pushes the vortex rings towards the left allowing the wake to reorganize and reach the initial hover like flow conditions in about 10 seconds. The recovery proves to be successful in bringing the rotor out of the VRS condition.

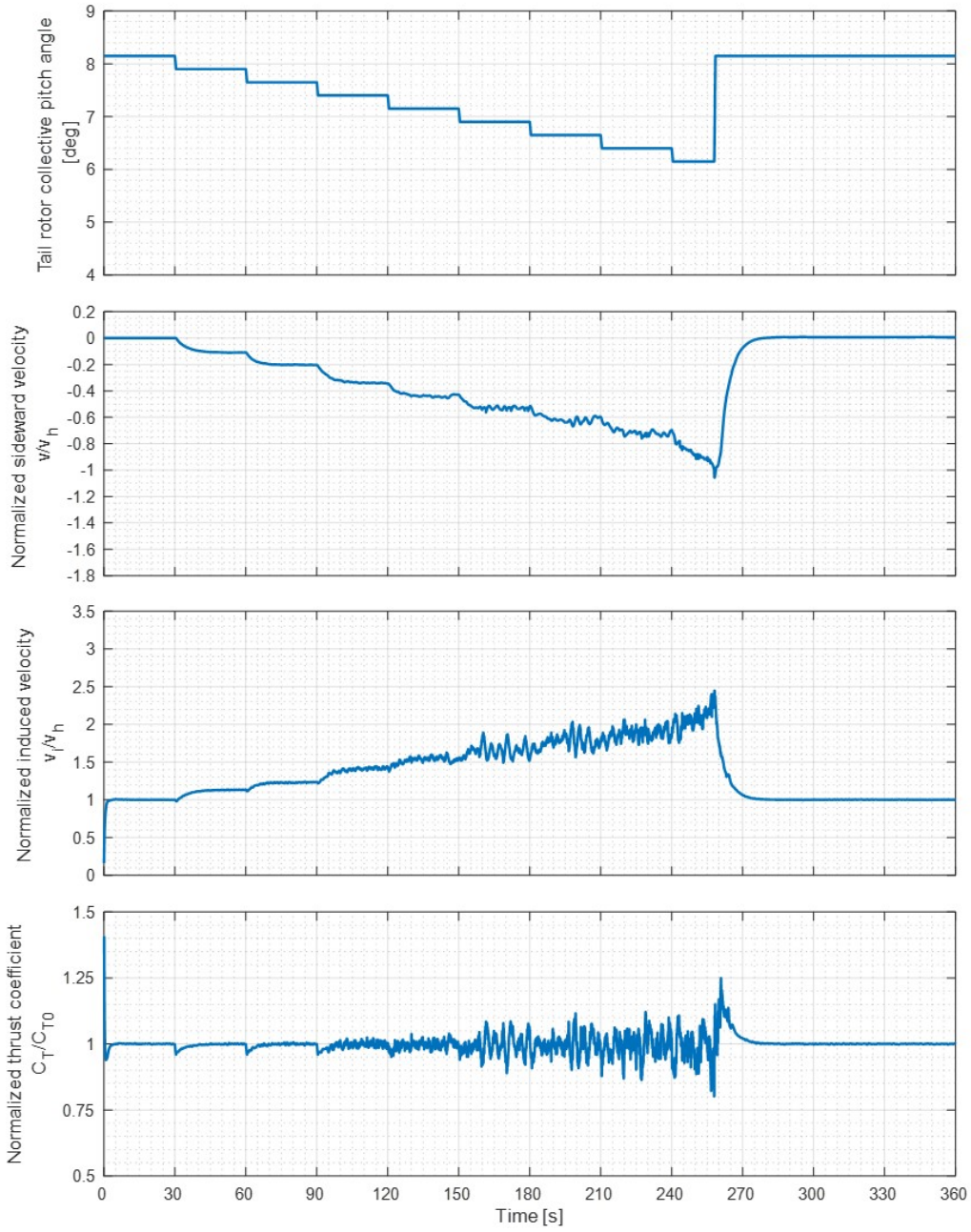

Figure 4.12: Time history of tail rotor variables during a successful recovery from VRS.

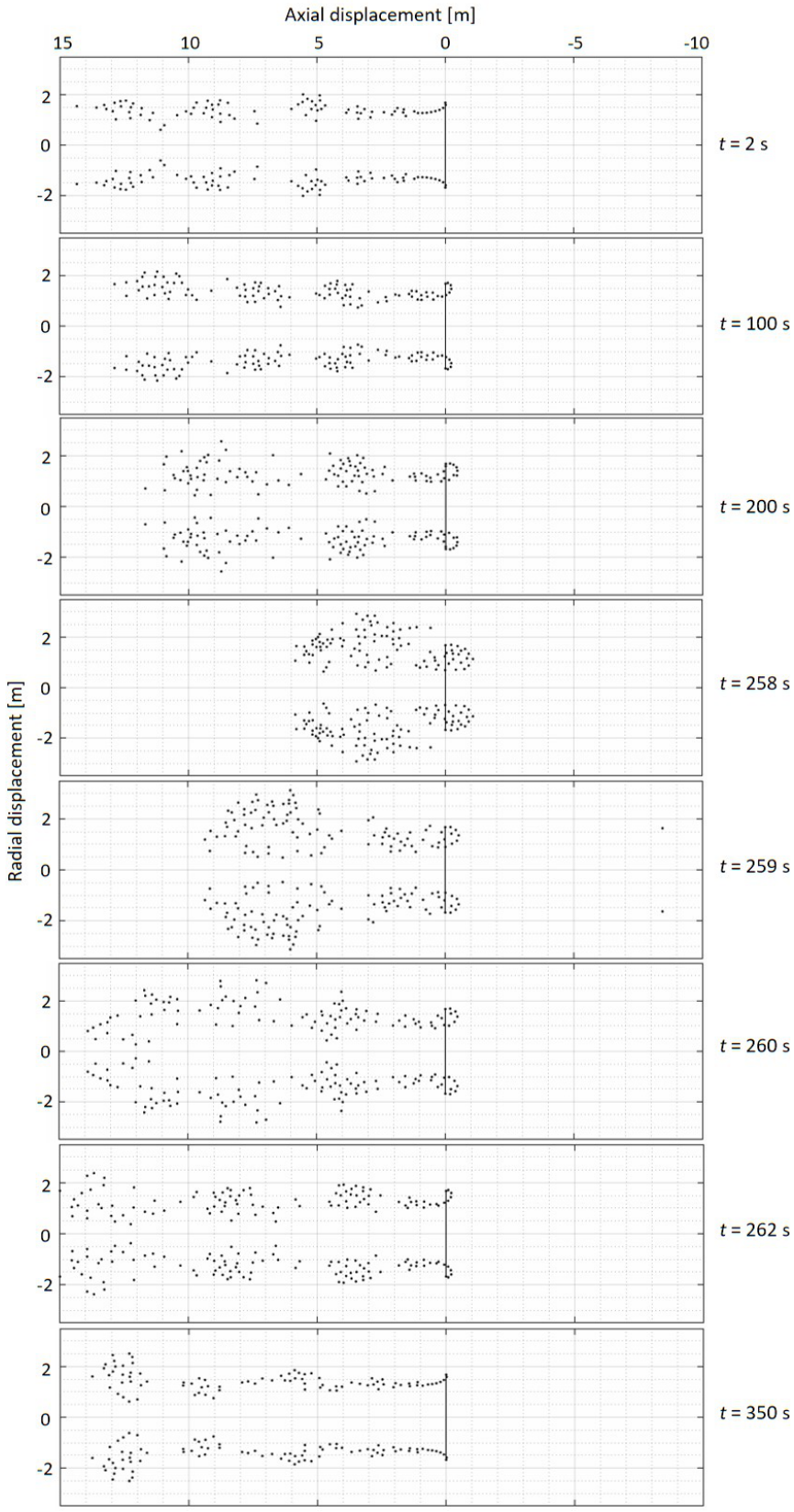

Figure 4.13: Axial displacements of vortex rings emitted by a tail rotor during a successful recovery from VRS.

Failed recovery from VRS

The previous simulation is repeated delaying the recovery of just 1 second. The sudden increase in collective pitch angle is now applied at $t = 259$ s. Figure 4.14 shows how the consequences are much different from the previous test. The recovery is not effective. Despite the attempted recovery, the tail rotor experiences a dramatic rise in induced inflow and suffers a rapid thrust loss that remarkably increases its left sideward velocity. For an aircraft in free flight, this would be perceived by the pilot as a sudden uncommanded right yaw. Figure 4.15 shows that after 1 second from the attempted recovery application the vortex rings organize in a toroidal structure around the rotor. A few seconds later, at $t = 262$ s the vortex rings have already formed a stable vortex structure to the right of the rotor, which is maintained for the rest of the simulation. Even if at trim blade collective pitch setting, the vortex rings are not capable to propel themselves to the left of the rotor because of the stable flow state achieved. When the vortex rings try to reach the rotor from the right, they cause an increase in induced inflow at the rotor. This causes a reduction in thrust that induces the tail rotor into an even faster sideward motion to the left. As seen at $t = 350$ s, the relative position between vortex rings and rotor is maintained. The uninterrupted rotor thrust loss even after a significant increase in collective pitch angle of the tail rotor blades prove the existence of the pedal control reversal phenomenon, validating the hypothesis formulated in Section 3.5.2. The simulation results confirm the ineffectiveness of the tail rotor in reestablishing the equilibrium condition during a VRS event.

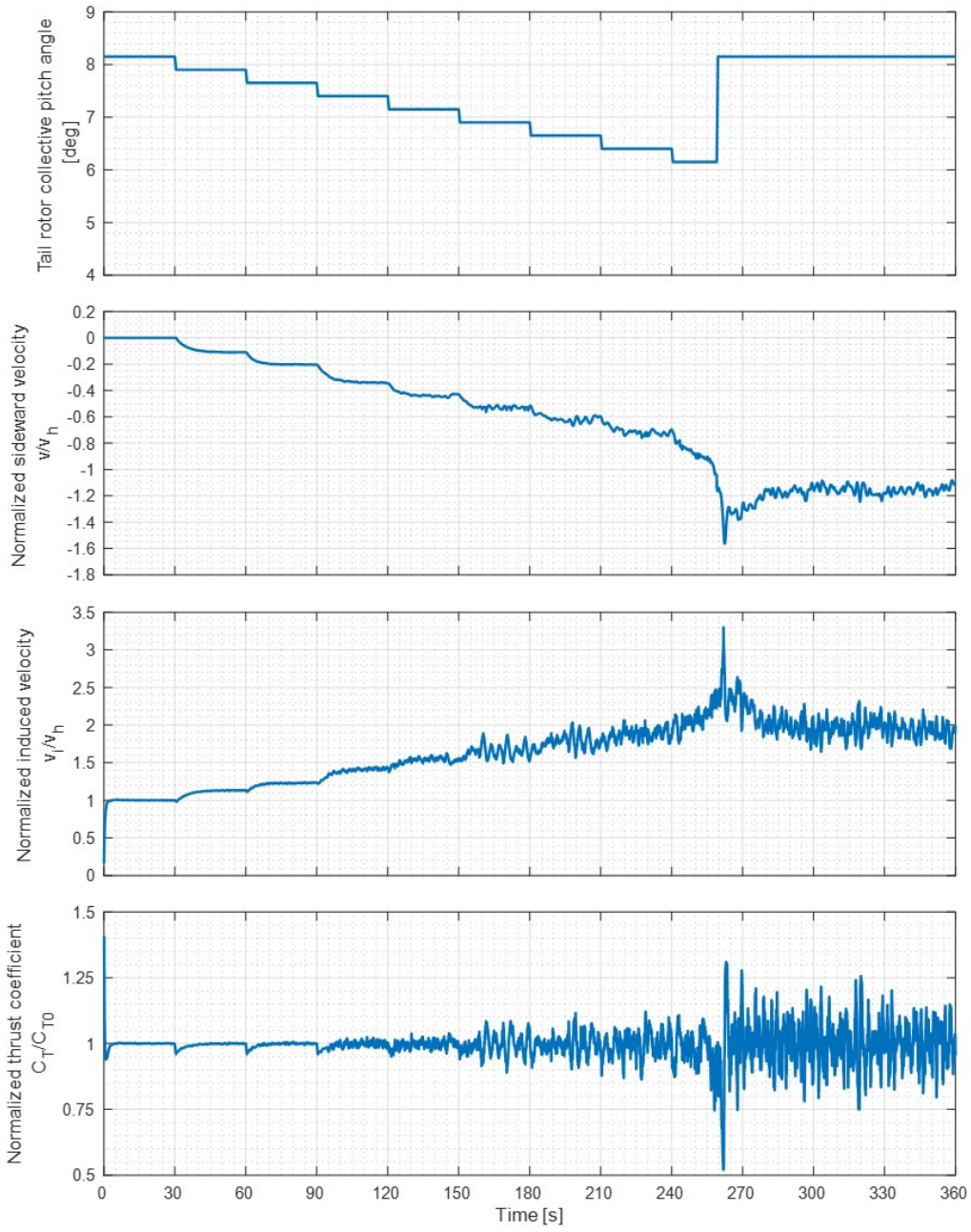

Figure 4.14: Time history of tail rotor variables during a failed recovery from VRS.

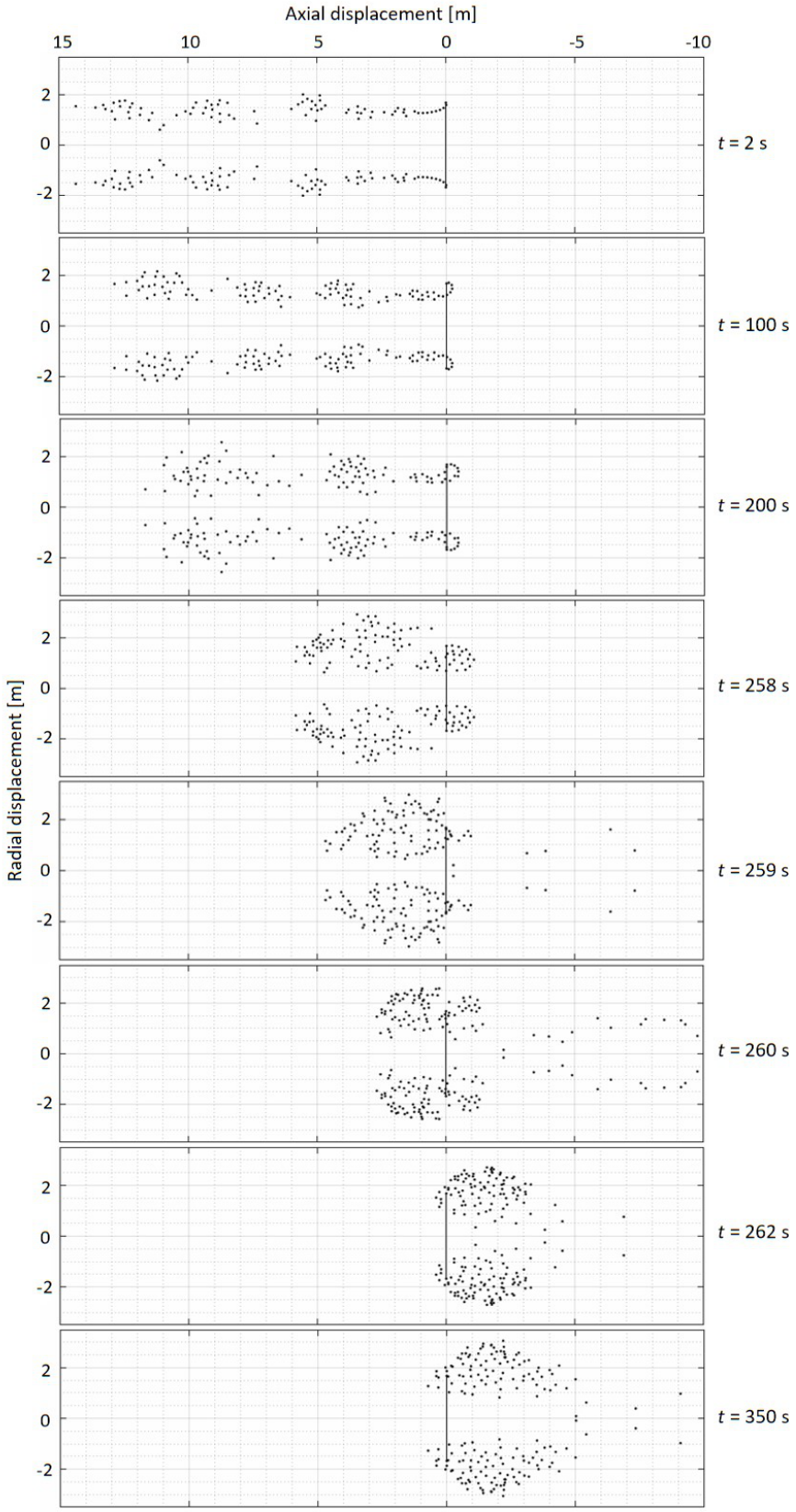

Figure 4.15: Axial displacements of vortex rings emitted by a tail rotor during a failed recovery from VRS.

4.5 Experiment 4: Detection of Loss of Weathercock Stability

The phenomenon of weathercock stability is heavily affected by relative tailwinds, which may lead to LTE like behavior. Hence, the identification of a reliable detection parameter for this flight characteristic is essential to provide an accurate prediction of LTE within flight data. Because of the research gap involving the prediction of the rotorcraft directional stability for flight scenarios with relative tailwinds, an investigation on the directional static stability derivatives of the aircraft is needed. Linear system theory is used to approximate the aircraft stability characteristics for different wind azimuth conditions. The results are notionally validated with the observations made in Experiment 1.

4.5.1 Experiment Setup

The rotorcraft simulation model FLIGHTLAB is used to accomplish this analysis. A generic helicopter configuration with a counterclockwise rotation of the main rotor is modeled. The investigation is carried out through a series of trim and stability analyses. For each equilibrium condition, the helicopter is in a free level flight at standard sea level conditions. The entire range of sideslip angles is explored, including forward and rearward flights, while the yaw attitude of the aircraft is maintained constant. It is noted that equivalent results would be obtained if the simulation involved a hover scenario with winds from different wind azimuths. After several iterations, it was observed that a sideslip angle interval of 5 deg between each simulation provides a good tradeoff between accuracy and computational time. The impact of 5, 10, and 15 m/s airspeeds is investigated. The trim solution is reached numerically to find the minimum of the set of nonlinear equations that define the trim problem within some predefined constraints. The trim convergence criteria were set to be 0.012 m/s^2 in translational acceleration and 0.01 rad/s^2 in angular acceleration. The state vector

used during the stability analysis is defined by the body-axes translational velocities u, v and w; the body-axes angular velocities p, q and r; and the Euler angles ϕ and θ. The normalized stability derivative C_{N_v} is recorded after the system matrix is obtained. The edgewise component of the freestream velocity at the tail rotor normalized by the inflow velocity at the tail rotor during a hover like flow condition, i.e., $V_{x,tr}/v_h$, is used to derive the normalized stability derivative C_{N_β}. Initially, the tail rotor inflow is modeled using the Pitt-Peters inflow model. Then, the model is augmented with the aerodynamic interference from the main rotor wake. The results are notionally validated with the observations made in Experiment 1.

4.5.2 Results

The variation of the weathercock stability of the aircraft has been previously investigated in Experiment 1. A simulation of a wind tunnel test was used to analyze the yaw moment developed by the aircraft for different relative wind conditions. While neglecting the impact of the main rotor wake interference at the tail rotor, it was observed that the most critical directional static instability corresponds to the flight scenarios affected by relative tailwinds. Specifically, in those conditions the aircraft develops a yaw moment reaction that initiates the tendency to yaw away from the equilibrium position. This represents a statically unstable reaction, and it must be associated with a negative static stability derivative. While keeping this in mind, the directional static stability derivatives of the aircraft are first computed neglecting the main rotor-to-tail rotor interaction.

Figure 4.16 shows the normalized stability derivative C_{N_v} calculated for flight scenarios impacted by different relative wind conditions. It is observed that C_{N_v} is positive for all the analyzed flight conditions, providing an unreliable evaluation of the directional static stability of the aircraft during flights affected by relative tailwinds. Figure 4.17 shows the normalized stability derivative C_{N_β} for flight scenarios impacted

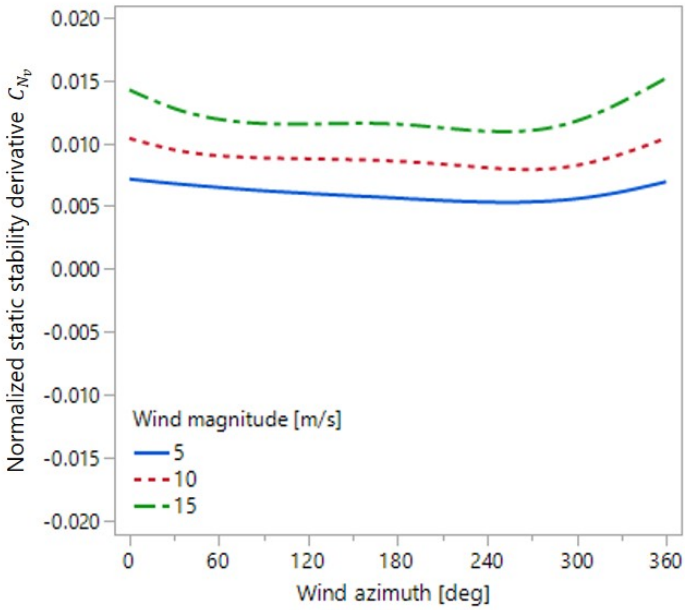

Figure 4.16: Normalized static stability derivative C_{N_v} for trim flight at different relative wind conditions while using the Pitt-Peters inflow model at the tail rotor.

by different relative wind conditions. As expected, the destabilizing effect of the relative tailwinds is represented by a negative value of the directional static stability derivative. Specifically, if the yaw moment reaction from the vehicle to a sideward gust disturbance is such that it tends to reduce the sideslip angle, it is considered as a statically stable reaction and is identified by a positive value of C_{N_β}. On the contrary, if the yaw moment reaction is such that it further accentuates the sideslip angle, it is considered as a statically unstable reaction and it is characterized by a negative value of C_{N_β}.

From the observations made in Experiment 1, the main rotor downwash has a strong impact on the relative wind conditions at the tail rotor plane and must not be neglected. Specifically, the main rotor wake introduces a significant in-plane velocity component at the tail rotor disk during quartering flights. Figure 4.18 shows the resulting values of C_{N_β} while modeling the tail rotor inflow dynamics using the Pitt-Peters inflow model augmented with the aerodynamic interference from the main

rotor wake. Because of the top-forward tail rotor rotation, the normalized edgewise component of the freestream velocity at the tail rotor, i.e., $V_{x,tr}/v_h$, is reduced. This causes the directional static instability to extend over a wider wind azimuth region, also including quartering flight scenarios. This result notionally resembles the findings of Experiment 1, in which the tail rotor inflow is modeled using the Pitt-Peters model augmented by the main rotor wake interference. The negative slope of the yaw moment obtained in Experiment 1 represents the loss of weathercock stability of the aircraft, which is embodied in the present analysis by the negative value of C_{N_β}. However, note that the results of the two experiments cannot be numerically compared, and only a notional validation can be made. While in Experiment 1 the forces and moments acting on the vehicle do not balance each other during the analysis, in the present study each stability analysis is a function of the equilibrium condition and a trim problem must be solved for each flight scenario.

The ability of the parameter N_β to account for the direction of the freestream velocity is the key element for an accurate and more comprehensive representation of the directional static stability of the helicopter. The results validate the hypothesis formulated in Section 3.6.2, confirming the need to compute the directional static stability derivative N_β to obtain a more accurate prediction of the weathercock stability of the helicopter even in presence of flight scenarios with relative tailwinds.

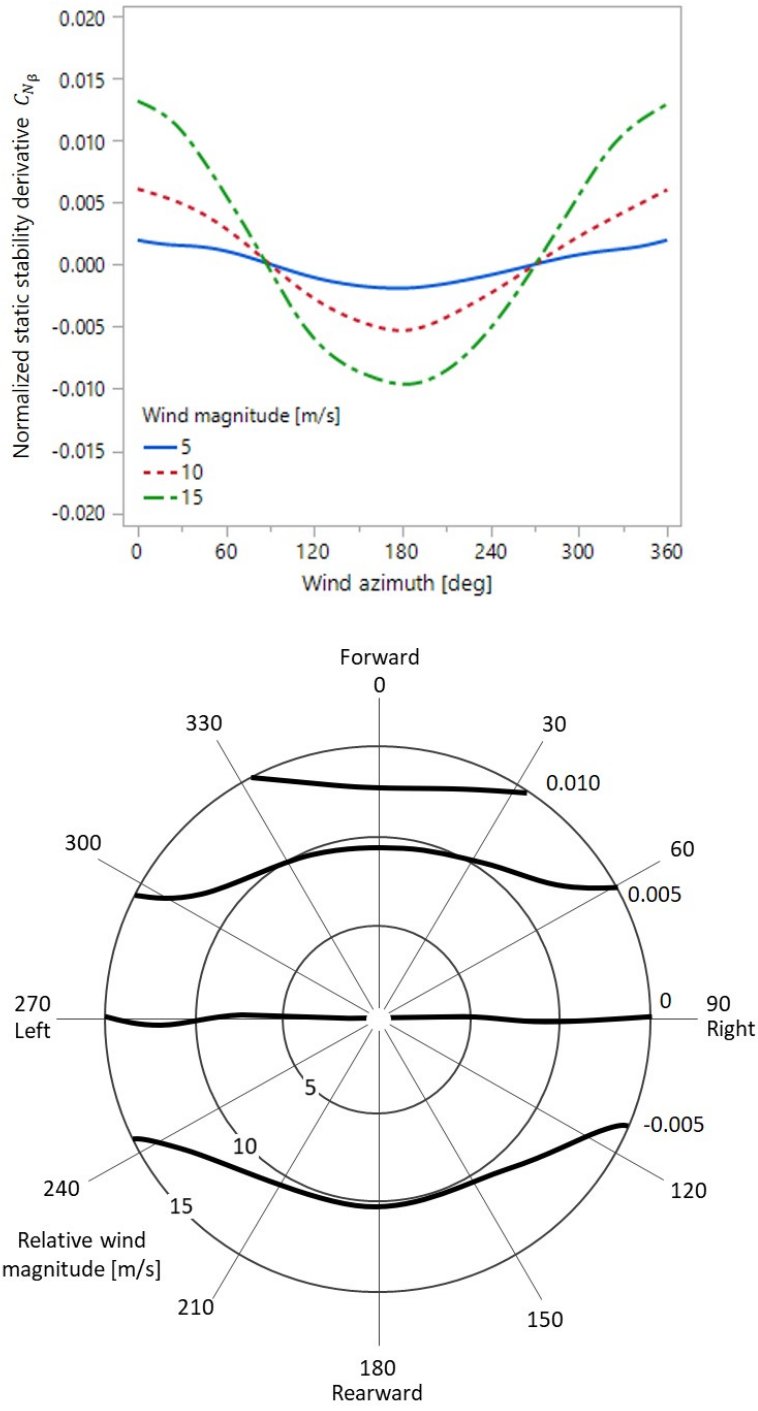

Figure 4.17: Normalized static stability derivative C_{N_β} for trim flight at different relative wind conditions while using the Pitt-Peters inflow model at the tail rotor (Cartesian and polar visualization).

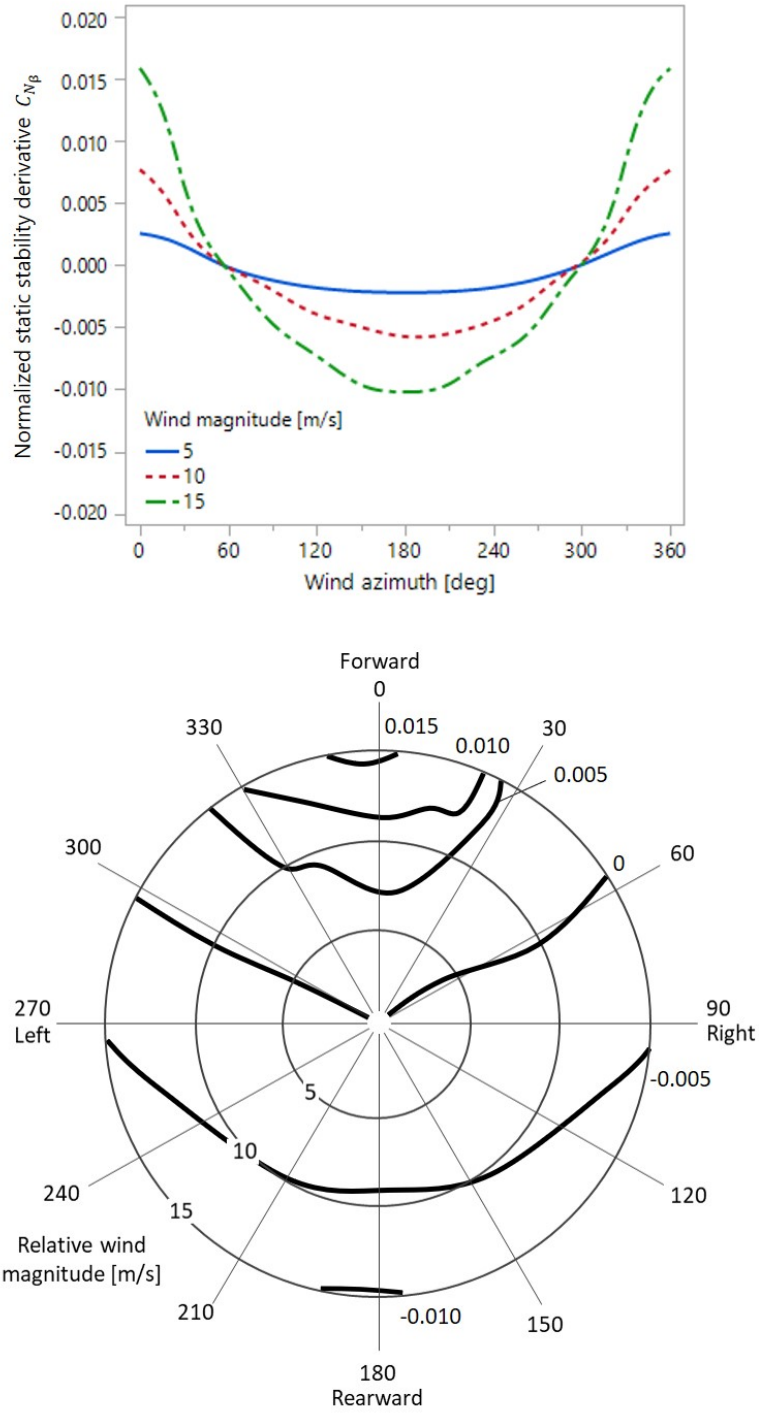

Figure 4.18: Normalized static stability derivative C_{N_β} for trim flight at different relative wind conditions while using the Pitt-Peters inflow model augmented with the 3-state main rotor wake interference (Cartesian and polar visualization).

4.6 Experiment 5: Detection of Tail Rotor Vortex Ring State

The phenomenon of vortex ring state at the tail rotor critically impacts the helicopter directional stability in low-speed flight. It is necessary to provide an accurate estimation of the VRS stability boundary at the tail rotor to ensure accurate safety analyses of flight data. Because of the research gap involving the impact of the main rotor-to-tail rotor interaction on the predicted VRS boundary, an analysis of the inflow model needed to achieve a more reliable VRS detection is necessary. After validating the VRS stability boundary with the results provided by Johnson [81], the impact of the main rotor vortex wake interference on the detection of VRS at the tail rotor is investigated.

4.6.1 Experiment Setup

The rotorcraft simulation model FLIGHTLAB is used to model a generic helicopter configuration with a counterclockwise rotation of the main rotor. The investigation is carried out through a series of trim analyses and uses Johnson's model to detect the VRS events at the tail rotor. Appendix B.1 describes the validation that has been carried out to confirm the accuracy of the VRS stability boundary implementation. For each equilibrium condition, the helicopter is in a free level flight at standard sea level conditions. While the yaw attitude of the aircraft is maintained constant, the range of sideslip angles that induce a freestream inflow going from left to right through the tail rotor is explored. It is noted that equivalent results would be obtained if the simulation involved a hover scenario with winds coming from the left of the aircraft (when the helicopter is viewed from behind). After several iterations, it was observed that a sideslip angle interval of 5 deg between each simulation provides a good tradeoff between accuracy and computational time. The impact of 5, 10, and 15 m/s airspeeds is investigated. The trim solution is reached numerically to find the

minimum of the set of nonlinear equations that define the trim problem within some predefined constraints. The trim convergence criteria were set to be 0.012 m/s^2 in translational acceleration and 0.01 rad/s^2 in angular acceleration. The edgewise and axial components of the freestream inflow at the tail rotor are recorded after each iteration converges. Then, Johnson's model [81] is used to detect the VRS stability boundary at the tail rotor as a function of the freestream inflow components. Initially, the tail rotor inflow is modeled using the Pitt-Peters inflow model. Then, the model is augmented with the aerodynamic interference from the main rotor wake.

4.6.2 Results

The relative wind condition at the tail rotor is the key element needed for the detection of tail rotor VRS events. Figure 4.19 shows the critical flight scenarios that lead to this phenomenon while modeling the tail rotor inflow using the Pitt-Peters inflow model. The results are visualized using the polar coordinate systems, offering an intuitive visualization. The shaded area represents the flight scenarios impacted by the occurrence of tail rotor VRS events. It is observed that the results are symmetric with respect to the relative wind azimuth of 270 deg. During those flight scenarios the tail rotor experiences a remarkable thrust loss that is perceived by the pilot as a sudden uncommanded right yaw. As confirmed by Experiment 3, the tail rotor may be ineffective in reestablishing the equilibrium condition, failing to effectively perform as during normal flight conditions.

The number of flight scenarios impacted by the occurrence of tail rotor VRS events increases when the inflow model used for the tail rotor is augmented with the aerodynamic interference from the main rotor wake. Figure 4.20 shows the detection results obtained using the Pitt-Peters inflow model augmented with the main rotor-to-tail rotor interaction. It is noted that the shaded area is not symmetric anymore with respect to the relative wind azimuth of 270 deg. This was expected as the main

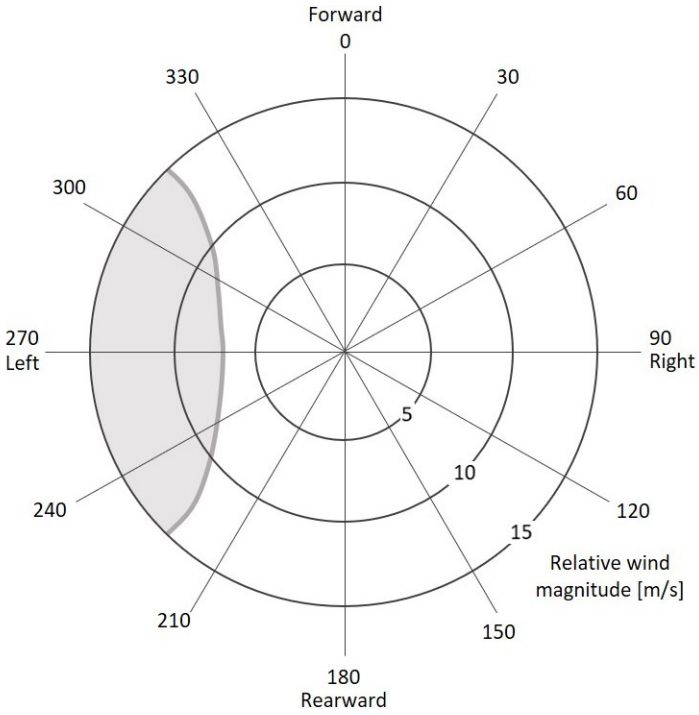

Figure 4.19: Detection of vortex ring state events at the tail rotor while using the Pitt-Peters inflow model.

rotor downwash has a strong impact on the relative wind conditions at the tail rotor plane. Specifically, the main rotor wake introduces a significant in-plane velocity component at the tail rotor disk that causes a decrease in dynamic pressure at the tail rotor plane. Also, the counterclockwise rotation of the main rotor causes a strong downwash that induces the tail rotor in a more severe descent like flow condition, i.e., increased freestream flow going from left to right through the tail rotor when the helicopter is viewed from behind. This interference induces the tail rotor into more severe vortex ring flow states that may cause a rapid loss of directional control. The results validate the hypothesis formulated in Section 3.7.2, confirming that a more accurate detection of tail rotor VRS events is attained when the tail rotor inflow is augmented with the aerodynamic interference from the main rotor vortex wake.

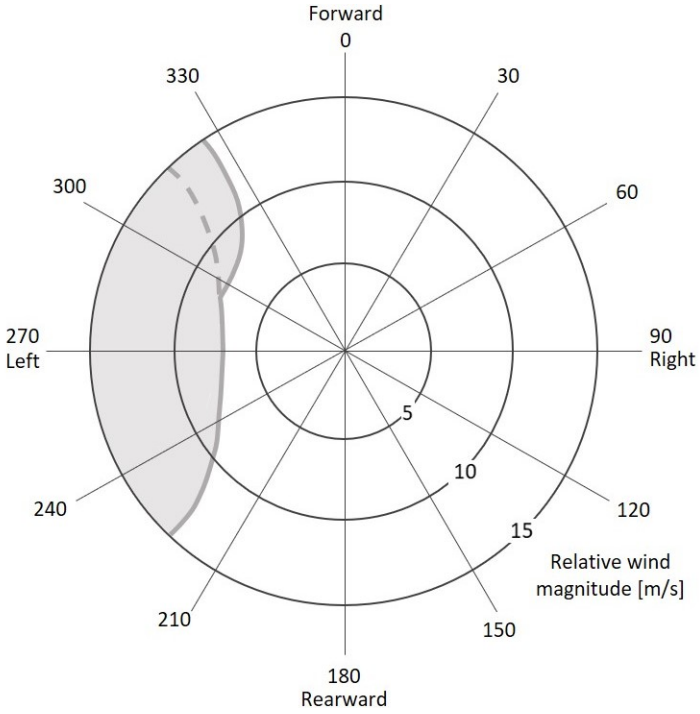

Figure 4.20: Detection of vortex ring state events at the tail rotor while using the Pitt-Peters inflow model augmented with the 3-state main rotor wake interference.

CHAPTER 5
FINAL METHODOLOGY

5.1 Overarching Hypothesis

The results obtained during the experimental phase substantiated the related hypotheses and clarified the research gaps that hindered the direct application of the proposed approach. This leads to the formulation of the final methodology, that aims to develop a more reliable detection of the proximity to LTE within the HFDM program and support the mitigation of helicopter accidents related to this dangerous safety threat. A comprehensive high-level flowchart of the methodology is provided in Figure 5.1. To answer the motivating question of this research and satisfy the research objective stated in Section 2.5, the following overarching hypothesis is formulated:

If the LTE safety metric encompasses the following contributions, then it will yield an improved detection of the proximity to LTE compared to the one currently used within the HFDM program, reducing the number of missed detections to better support the proactive mitigation of helicopter accidents related to LTE:

- *The LTE safety metric comprises the different aspects that can lead to LTE behavior: loss of weathercock stability, running out of pedal (tail rotor collective) for trim, and tail rotor vortex ring state.*

- *The prediction of safety limits for proximity to LTE is achieved using a combination of physics-based simulations, to investigate the aircraft flight envelope, and supervised learning techniques, to develop the predictive models of the three LTE events. (A detailed view of those phases is offered in Figures 5.2 and 5.3, respectively.)*

- *To investigate the aircraft flight envelope, the simulation model includes a linear inflow gradient along the tail rotor blade augmented with the aerodynamic interaction from the main rotor vortex wake.*

- *The phenomenon of running out pedal is detected predicting the pedal control required for yaw balance.*

- *The phenomenon of loss of weathercock stability is detected predicting the directional static stability derivative, N_β.*

- *The phenomenon of tail rotor vortex ring state is detected using a comprehensive VRS stability boundary definition that encloses most of the experimental results available in the literature.*

- *The independent variables used to develop the prediction models of the three LTE phenomena have a relevant impact on the predicted response, are non-dimensional, and are accessible within the operator's flight data.*

- *While the definitions of the three types of LTE events do not change, the proximity to LTE thresholds is left accessible to the operator, to provide flexibility in the risk management of post-flight analyses.*

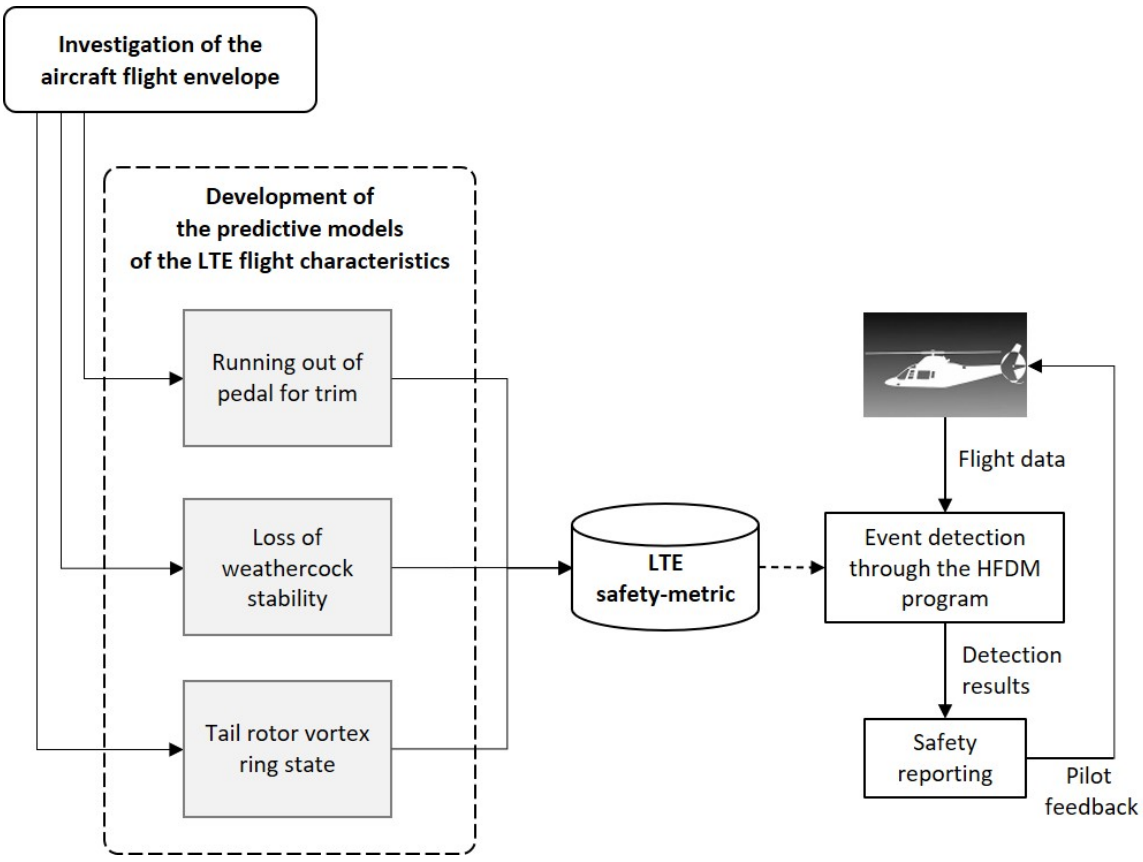

Figure 5.1: High-level flowchart of the final methodology.

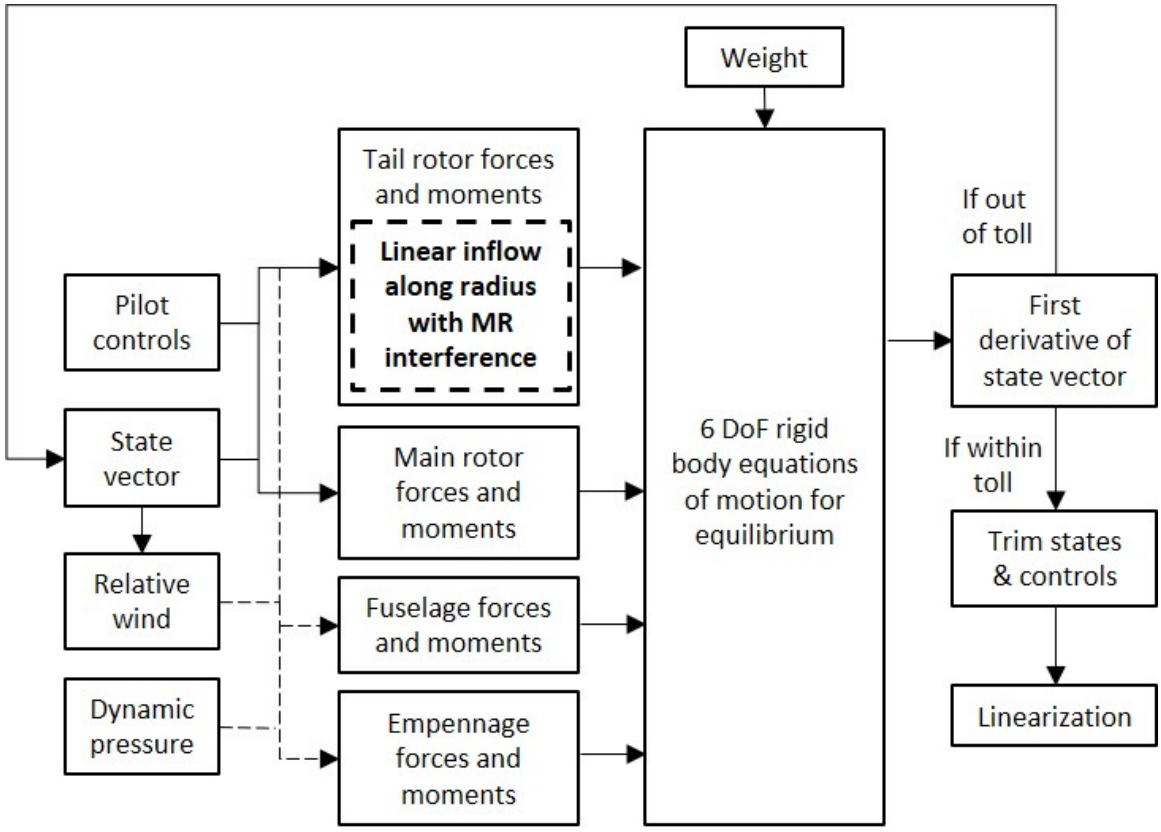

Figure 5.2: Detailed view of the investigation of the aircraft flight envelope.

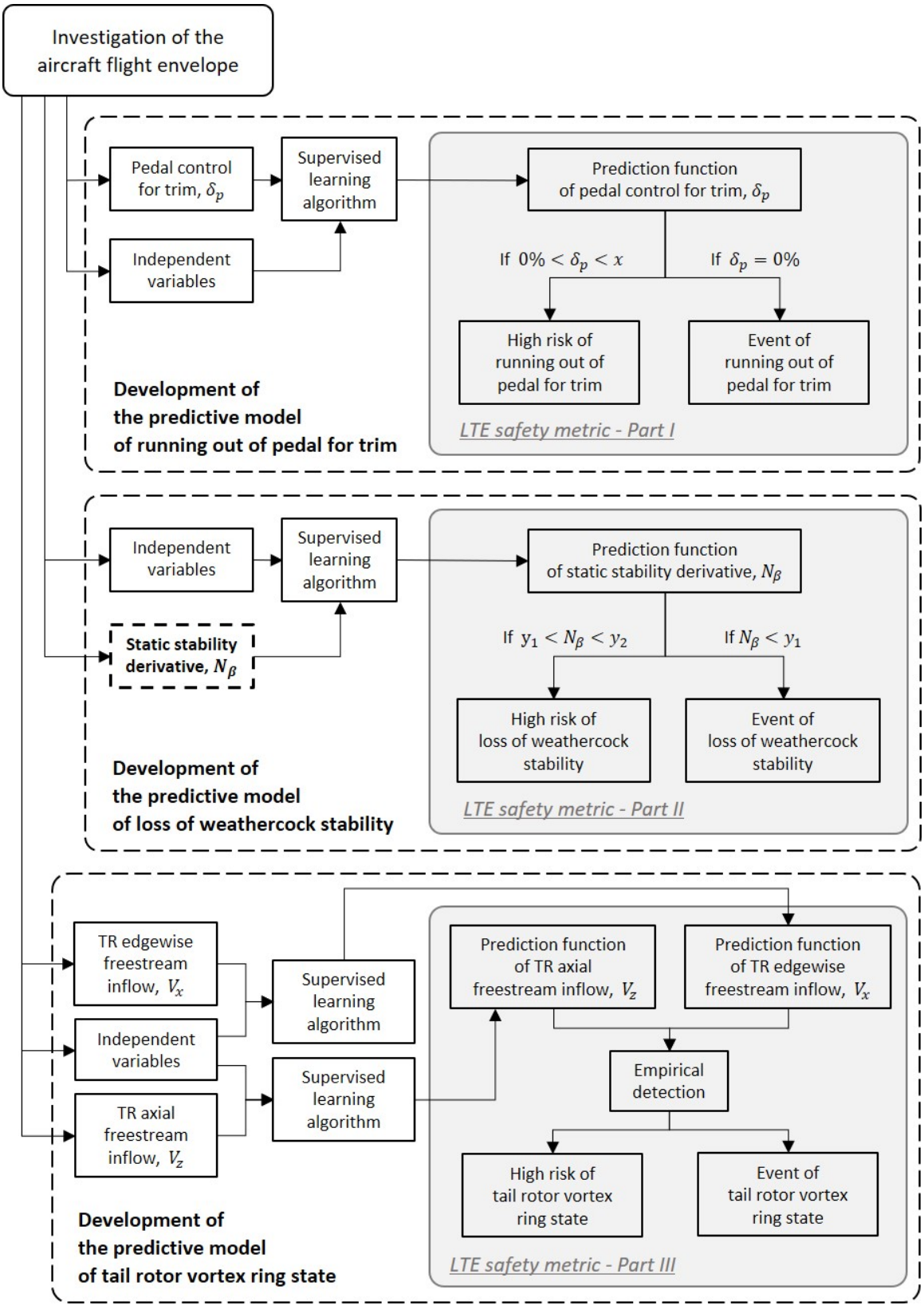

Figure 5.3: Detailed view of the development of the predictive models of the LTE phenomena.

5.2 Methodology Implementation

The approach used to obtain the LTE safety metric can be summarized in two main steps:

- the investigation of the aircraft flight envelope, which involves the selection of the flight scenarios and the computation of the physics-based simulation results;
- the development of the predictive models of the three LTE phenomena, which involves the creation of the prediction functions of the LTE detection parameters and the definition of the proximity to the different LTE events.

The LTE safety metric, i.e., the comprehensive model that predicts LTE events and proximity to LTE, is formed by the collection of the predictive models obtained.

5.2.1 Investigation of the Aircraft Flight Envelope

The rotorcraft simulation model FLIGHTLAB is used to model a generic helicopter configuration with counterclockwise rotation of the main rotor. The modeling of LTE has been described, providing the essential elements needed to accurately simulate the three LTE phenomena, i.e., loss of weathercock stability, running out of pedal (tail rotor collective control) for trim, and tail rotor vortex ring state. Experiments 1, 2, and 5 clarify what inflow model should be used at the tail rotor to appropriately simulate the different LTE events. It is observed that the results significantly improve when the inflow gradient along the tail rotor radius is augmented with the aerodynamic interference from the main rotor wake. Since the same tail rotor inflow representation is needed, the same simulation model is required to accurately represent the three LTE phenomena. Hence a comprehensive set of trim analyses can be designed to include all three LTE events, reducing the overall computational time of the flight envelope investigation. The aircraft mass, the density altitude, the relative airspeed, and the sideslip angle are used as input variables. Since LTE is a low-speed

Table 5.1: Design of experiment for the flight envelope investigation.

Input parameter	Unit	Set of values	Cardinality
Relative wind azimuth	deg	0:10:360	36
Relative wind magnitude	m/s	0:5:20	5
Aircraft mass	kg	5500:625:8000	5
Density altitude	m	0:1125:4500	5

flight characteristic, only a reduced airspeed range is considered, further decreasing the total computational cost of the flight envelope investigation. Table 5.1 lists the parameters and the values used as inputs of the simulation model. After several iterations, it is observed that the set of sideslip angles must have a cardinality much greater than the cardinality of the other sets, to predict with enough accuracy the variation of the LTE detection parameters, in particular, the pedal control (tail rotor collective) for trim.

A trim simulation is performed for each combination of the input variables, followed by a linearization analysis to investigate the weathercock stability of the aircraft. The potential LTE flight envelope of the helicopter is explored through 4500 steady-state simulations with a total computation time of 12 hours and 14 minutes. The parameters recorded after the convergence of each simulation are the variables needed to develop the prediction functions of the detection parameters of the three LTE phenomena, specifically:

1. the advance ratio, μ;
2. the sideslip angle, β;
3. the main rotor blade loading coefficient, C_T/σ;
4. the detection parameter for running out of pedal (tail rotor collective control) for trim, i.e., the pilot's pedal control, δ_p;

5. the detection parameter for loss of weathercock stability, i.e., the directional stability derivative related to the sideslip angle, N_β;

6. the parameters needed for the detection of tail rotor vortex ring state, i.e., the edgewise and axial components of the freestream inflow at the tail rotor normalized by the tail rotor's induced inflow velocity in hover-like flow condition, V_x/v_h and V_z/v_h respectively.

5.2.2 Development of the Predictive Models of the LTE Phenomena

The predictive models of the detection parameters of the three LTE events need to be developed. First, the prediction function of each detection parameter is created through the learning training process of the relationship between the independent variables and the detection parameter of the specific LTE phenomenon. Then, predefined thresholds are set on the predicted parameters to allow for the detection of the LTE events and the proximity to LTE events within flight data.

The prediction functions of the LTE detection parameters are trained with the following independent variables: the advance ratio, the sideslip angle, and the main rotor blade loading coefficient. Those parameters have been chosen because of their relevant influence on the predicted detection parameters, and their low multicollinearity. Their non-dimensional nature accounts for the influence of the relative wind condition, the density altitude, the aircraft weight, and the rotor geometry, extending the application of the safety metric to the flight data of various helicopter sizes while considering the same aircraft configuration. Further, their easy accessibility within the operators' flight data makes the resulting LTE safety metric more applicable within the HFDM environment.

Four prediction functions are created using the data analysis software JMP [127] to enable the detection of the three LTE phenomena. Specifically, those functions predict the LTE detection parameters which are the pilot's pedal control, δ_p, the directional

stability derivative, N_β, and the normalized freestream inflow components at the tail rotor, V_x/v_h and V_z/v_h. To optimize the accuracy of the prediction functions while handling nonlinear relationships between variables, two advanced supervised learning techniques are applied, i.e., boosted decision trees and artificial neural networks. Note that several design choices must be made while selecting each model architecture, however, a complete investigation on the optimal architectures is beyond the scope of this work. In the case of boosted decision trees, 100 layers with 3 splits per tree are used to obtain the four prediction functions. Instead, 2 hidden layers with 10 nodes per layer are used to train each artificial neural network model, employing different activation functions to define the output of each node. Specifically, Gaussian activation functions are used in the case of N_β, V_x/v_h, and V_z/v_h, while hyperbolic tangent activation functions are used for δ_p.

The large dataset of parameters recorded during the investigation of the aircraft flight envelope is partitioned into three sets that are used for the training, validation, and testing of the prediction functions. A partition ratio of 50-25-25 is used because of the large size of the dataset available. Also, note that the synthetic dataset does not include anomalies as only the simulations that successfully converged are considered. While the training dataset is used to fit the model's parameters, the validation dataset allows optimizing the model's hyperparameters increasing the accuracy of the model and preventing overfitting. Finally, the test dataset is used to obtain an unbiased evaluation of the model's predictive ability [77, 88]. Appendix C presents the accuracy measures of the surrogate models used to predict the parameters needed to detect the proximity to the LTE phenomena. It is observed that the artificial neural networks have better flexibility to the nonlinear interactions within the simulation results, outperforming the boosted decision trees.

After ensuring an optimal prediction capability of the LTE detection parameters, the proximity to the three LTE events needs to be defined. The phenomenon of

running out of pedal for trim can be directly identified by the predicted pilot's pedal control for trim, δ_p. Specifically, the event of running out of pedal is detected when $\delta_p = 0$, which represents the ineffectiveness of the tail rotor in providing the necessary thrust for trim. The risk of running out of pedal for trim can be defined by a predefined interval of the detection parameter that approaches the threshold of the running out of pedal for trim event. Hence, a flag for high risk of running out of pedal is detected if $\delta_p < 20\%$.

In the case of loss of weathercock stability, a negative value of the directional stability derivative, N_β, characterizes a statically unstable flight condition which can potentially lead to an LTE like behavior. However, because a small negative value of N_β represents a more neutral behavior of the aircraft in response to external disturbances, the events of loss of weathercock stability are considered to be characterized only by large negative values of N_β. Specifically, the event of loss of weathercock stability is detected if $N_\beta < 0.005$. The risk of loss of weathercock stability can be defined by a predefined interval of the static stability derivative that approaches the threshold of the loss of weathercock stability event. Specifically, a flag for high risk of loss of weathercock stability is detected if $N_\beta < 0$.

Further, post-processing is needed to detect vortex ring state at the tail rotor, using the simple stability boundary defined by Johnson [81]. The freestream inflow components at the tail rotor normalized by the tail rotor induced inflow velocity in hover-like flow conditions, V_x/v_h and V_z/v_h, are used as inputs of the semi-empirical algorithm that allows for the detection of VRS events at the tail rotor. The risk of tail rotor VRS can be defined by a predefined interval of the detection parameters that approaches the threshold of the tail rotor vortex ring state event. The empirical values used for the VRS detection can be tuned to detect the proximity to VRS events. Finally, the LTE safety metric, i.e., the comprehensive model that predicts LTE events and proximity to LTE, is formed by the collection of the predictive models

obtained.

5.3 Overarching Hypothesis Testing

The present methodology was created to support the proactive mitigation of helicopter accidents related to LTE, offering a physics-based detection of proximity to LTE events within the HFDM environment. To test the overarching hypothesis and verify the capabilities of the present approach, the physics-based LTE safety metric needs to be evaluated against the filter-based LTE metric currently used within the HFDM program [158]. An experiment is needed to compare the detection capabilities of both safety metrics and assess if the proposed methodology provides improved detection of the proximity to LTE.

5.3.1 Experiment Setup

The detection results of both LTE safety metrics can be compared considering real flight data, predicting the proximity to LTE at each time step. However, because of the unavailability of flight data that includes the three LTE phenomena of interest, a series of synthetic flight scenarios is used for testing. It is assumed that the only parameters available for each flight scenario are the advance ratio, the sideslip angle, and the main rotor blade loading coefficient. Two sets of flight scenarios are constructed, each including the entire range of sideslip angles and the low-speed range of advance ratios, i.e., [0, 0.09]. Each set is characterized by a different value of the main rotor blade coefficient. A small value of the main rotor blade loading coefficient, i.e., $C_T/\sigma = 0.05$, is used to investigate the detection capability of the safety metrics for normal flight conditions, e.g., low weight configuration at sea level. A large value of the main rotor blade loading coefficient, i.e., $C_T/\sigma = 0.12$, is used to represent more critical flight conditions, e.g., high weight configuration at high density altitude. Both LTE safety metrics are applied on the two sets of synthetic flight data to compare

the detection results of the proximity to LTE.

5.3.2 Results

The detection of the proximity to LTE within flight data depends on the accuracy of the safety metric used. First, the filter-based LTE safety metric employed within the HFDM program is investigated. This metric is based on the definition of critical flight conditions identified by the review of accident reports and experts' opinions. Figure 5.4.a shows the proximity to LTE for flight conditions characterized by a small value of the main rotor blade coefficient at different relative wind conditions. A medium risk level of proximity to LTE is detected for a specific wind azimuth region. Similarly, as shown in Figure 5.4.b, for the set of flight conditions characterized by a large value of the main rotor blade coefficient the metric detects a high-risk level of proximity to LTE for the same wind azimuth region. It is noted that the metric does not recognize the type of LTE phenomenon involved. Also, the unavailability of the control input parameters hinders the detection of LTE events.

The new LTE safety metric offers unique features that are not currently available within the HFDM program. While the filter-based safety metric needed numerous inputs including control parameters that are usually not available within flight data, the new metric presents less severe input requirements enhancing its applicability within the HFDM environment. Specifically, a smaller number of inputs is needed to detect proximity to LTE; the input parameters needed are more accessible within the operators' flight data; the inputs are non-dimensional, extending the application of the safety metric to the flight data of various helicopter sizes while considering the same aircraft configuration. Figures 5.5 - 5.7 show the detection results obtained with the new metric. The detection is based on the physics-based investigation of the LTE phenomena and differentiates the detection of the proximity to LTE into the proximity to running out of pedal for trim, loss of weathercock stability, and tail

rotor vortex ring state. This provides a more comprehensive detection of LTE, better clarifying the causes of the safety threat. The results can be notionally validated with the critical wind azimuth regions published by the FAA and shown in Figures 2.2, 2.3, and 2.5. An enhanced reliability in the detection of the proximity to LTE is observed compared to the results obtained with the filter-based LTE safety metric. It is noted that the FAA [54] and the NTSB [107] do not acknowledge the quartering flight to the right as a critical flight condition. This relates to the phenomenon of running out of pedal for trim, one of the key aspects that characterize LTE. The new LTE metric does not neglect this flight characteristic, promoting a better awareness of LTE within the rotorcraft community. Therefore, the results prove that the present methodology offers an enhanced detection of proximity to LTE compared to the current metric used within the HFDM environment, validating the overarching hypothesis formulated in Section 5.1.

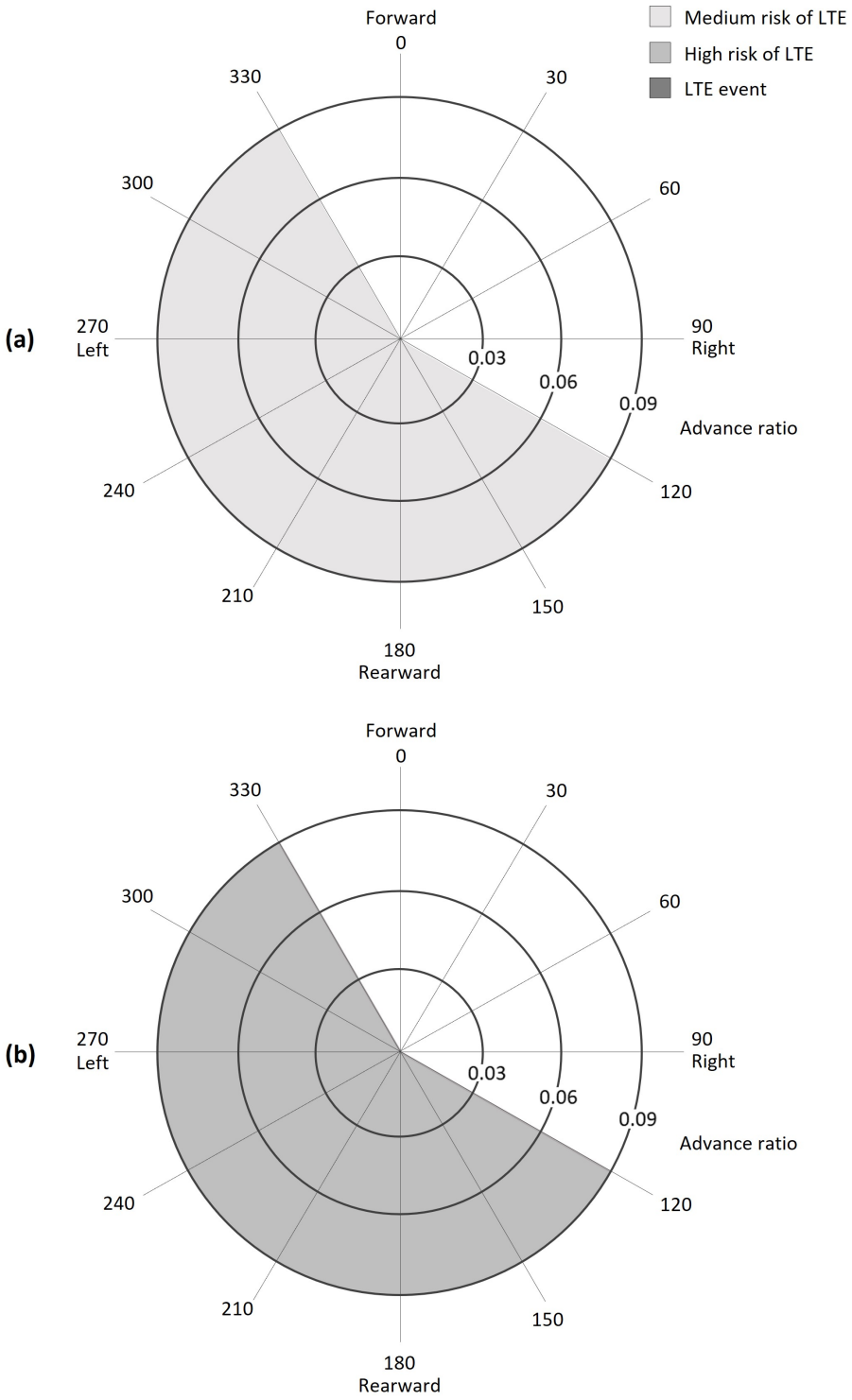

Figure 5.4: Detection results of proximity to LTE provided by the filter-based LTE safety metric. (a) Normal flight conditions with $C_T/\sigma = 0.05$. (b) Critical flight conditions with $C_T/\sigma = 0.12$.

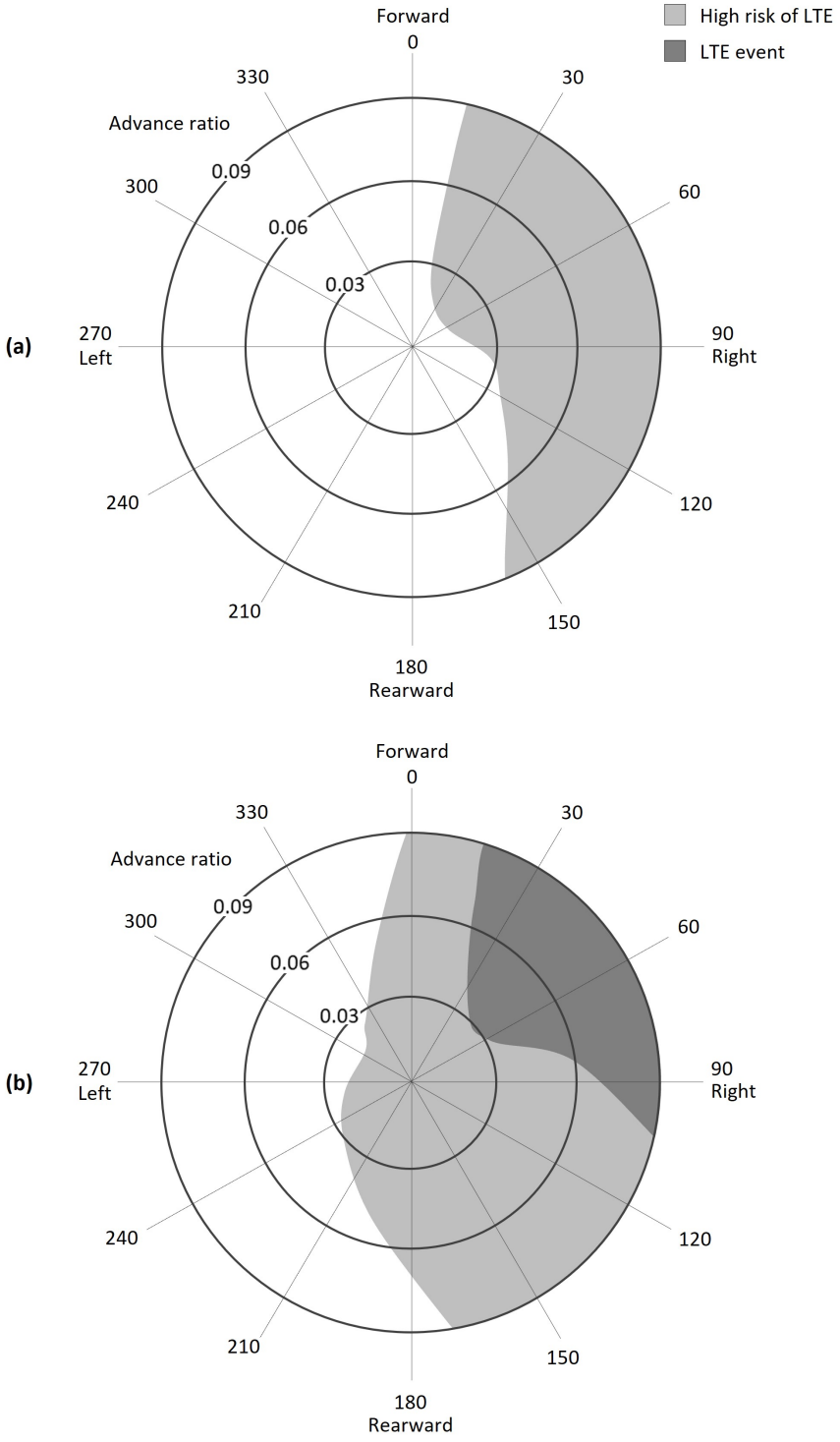

Figure 5.5: Detection results of proximity to running out of pedal for trim provided by the physics-based LTE safety metric. (a) Normal flight conditions with $C_T/\sigma = 0.05$. (b) Critical flight conditions with $C_T/\sigma = 0.12$.

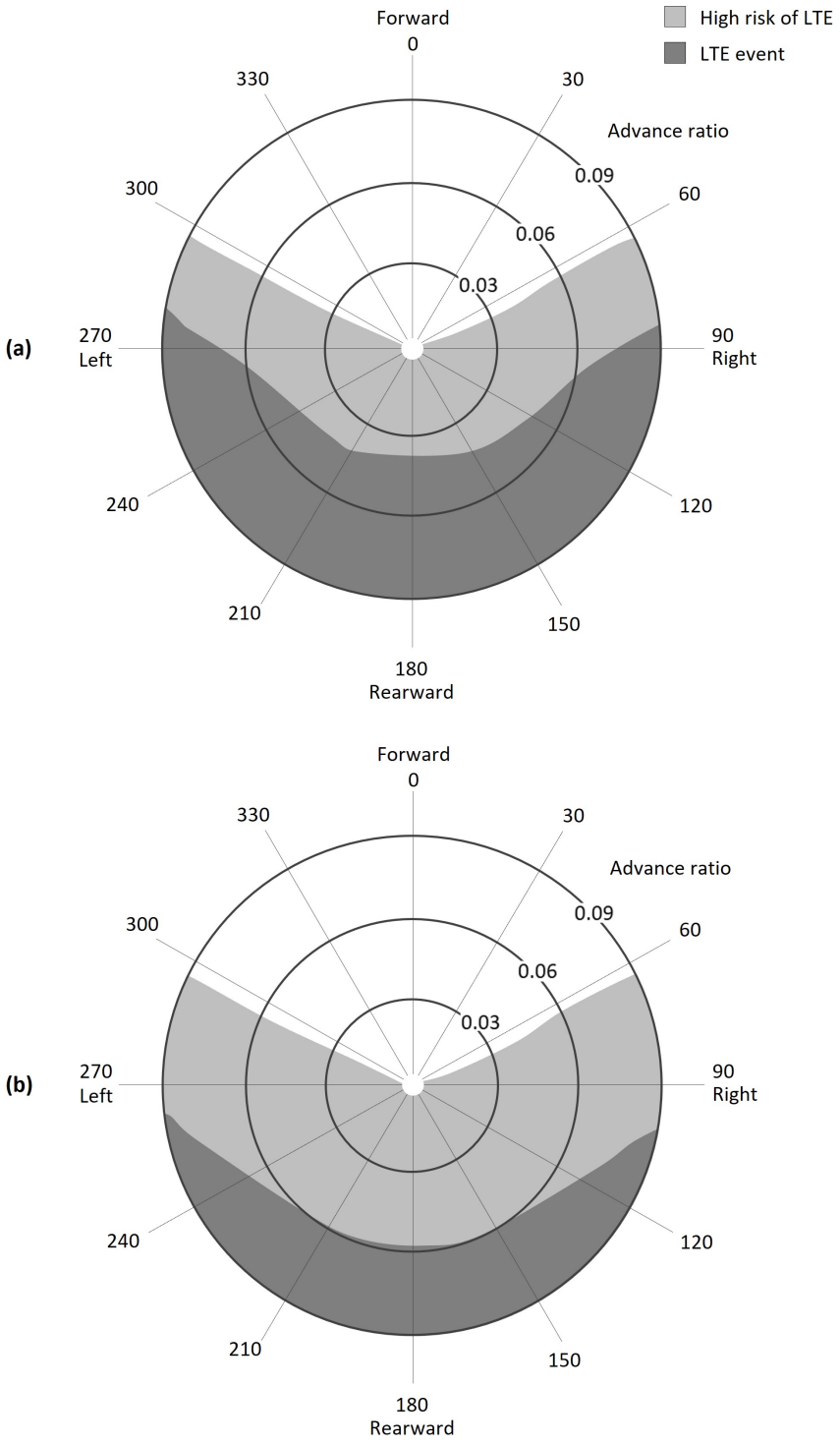

Figure 5.6: Detection results of proximity to loss of weathercock stability provided by the physics-based LTE safety metric. (a) Normal flight conditions with $C_T/\sigma = 0.05$. (b) Critical flight conditions with $C_T/\sigma = 0.12$.

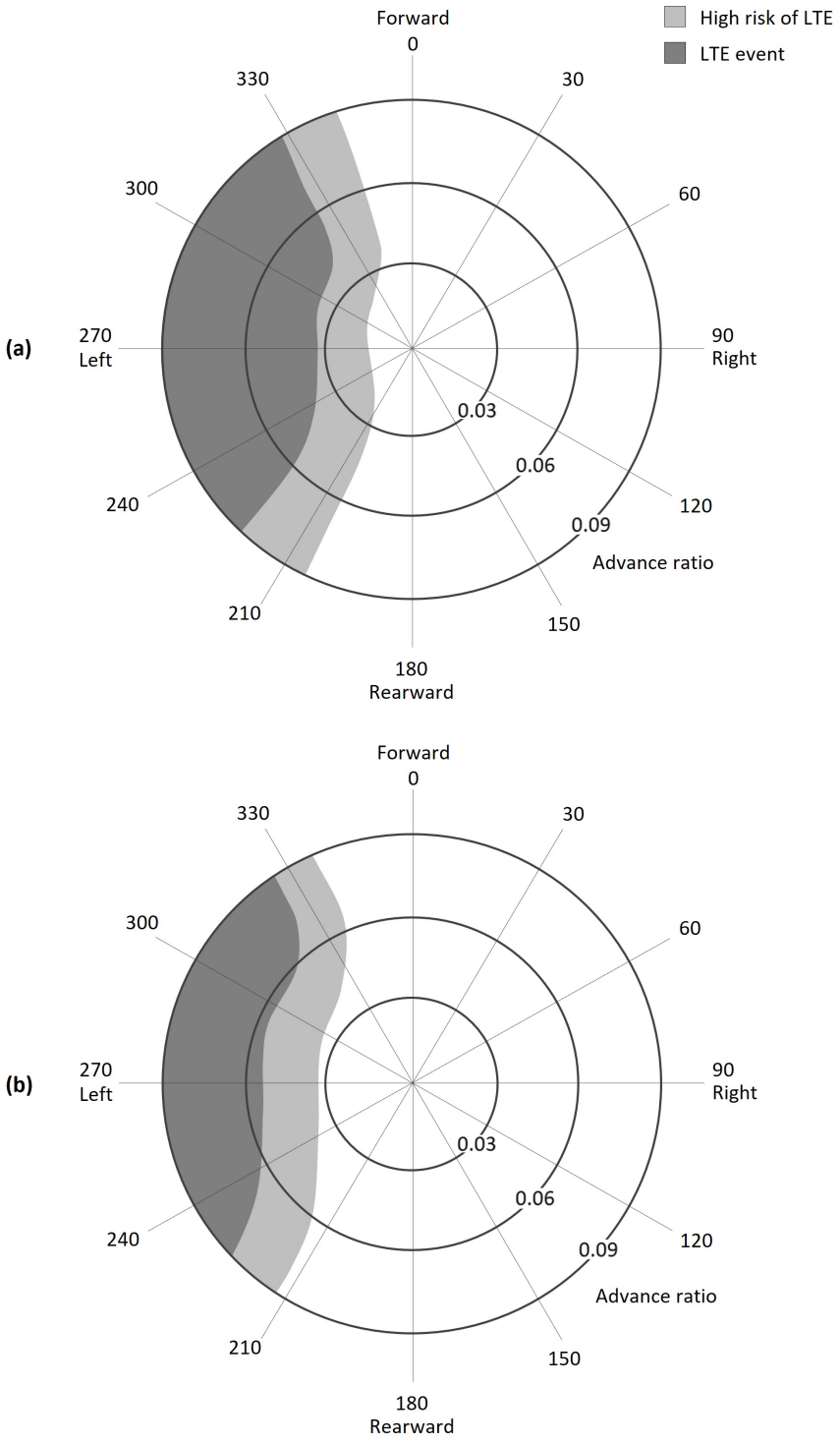

Figure 5.7: Detection results of proximity to tail rotor vortex ring state provided by the physics-based LTE safety metric. (a) Normal flight conditions with $C_T/\sigma = 0.05$. (b) Critical flight conditions with $C_T/\sigma = 0.12$.

CHAPTER 6
CONCLUSIONS AND RECOMMENDATIONS

6.1 Contributions

A methodology was created to improve the detection capability of the proximity to LTE within the HFDM program and support the proactive mitigation of LTE accidents. An alternative approach was used to develop a more reliable LTE safety metric, using a combination of physics-based simulations and machine learning techniques. Initially, a physics-based investigation of LTE was performed to enhance the understanding of the physics of the different LTE events. A more comprehensive definition of LTE was proposed including three different aspects that can lead to LTE behavior, i.e., loss of weathercock stability, running out of pedal (tail rotor collective) for trim, and tail rotor vortex ring state. Each LTE phenomenon was individually modeled and investigated to ensure an accurate physics-based representation of LTE events. The factors that mainly influence the proximity to LTE were identified. Specifically, the following studies and contributions were presented:

- Weathercock stability is related to the yaw moment variation of the aircraft due to a sideward gust. Several inflow models were used during the simulation of a wind tunnel test to compare the accuracy of its representation. It was observed that the results significantly improve when the inflow gradient along the tail rotor radius is augmented with the aerodynamic interference from the main rotor wake. A significant static directional instability is present not only for flights under the impact of relative tailwinds but also while the main rotor vortex wake alters the flow through the tail rotor. Because of this instability, a lateral perturbation will attempt to weathervane the aircraft away from the

initial flight condition, leading to LTE like behavior.

- The running out of pedal phenomenon is related to the yaw moment developed by the tail rotor to maintain directional equilibrium in flight. To appropriately represent this condition, an investigation on the impact of the inflow modeling on the pedal control needed for yaw balance was performed. The distribution of pedal control requirements for trim flight improves when the non-uniform inflow model used for the tail rotor is augmented with the aerodynamic interaction from the main rotor wake. It was observed that the sideward flight to the right significantly reduces the pedal control margin, mostly because of the weathercocking action of the tail rotor. When the pedal control is insufficient to maintain equilibrium, an uncommanded right yaw occurs, confirming the ineffectiveness of the tail rotor in providing the necessary thrust for trim. The quartering flight to the left does not represent a problematic condition with regards to the running out of pedal phenomenon, but it may involve vortex ring flow states.

- The tail rotor may experience vortex ring state while the aircraft is flying sideward to the left. This phenomenon relates to the accumulation of the vortex wake in proximity to the rotor, highly increasing the rotor induced inflow and penalizing its performance. A dynamic simulation was performed using the vortex ring emitter model on an isolated tail rotor while in descent like flow conditions. The results confirm the ineffectiveness of the tail rotor in reestablishing the equilibrium condition during a VRS event because of the reversal of tail rotor control effectiveness. The tail rotor fails to effectively perform as during normal flight conditions, providing a negative thrust variation after an increase in blade collective pitch angle. For an aircraft in free flight, the thrust loss experienced by the tail rotor during VRS would be perceived by the pilot

as a sudden uncommanded right yaw.

After improving the understanding of the fundamental nature of LTE, the parameters that enable the detection of each LTE phenomenon were established to classify LTE events within the simulation results. While the phenomenon of running out of pedal can be easily identified by the pedal control required for yaw balance, further investigation was needed for the other LTE phenomena. Specifically, the following analyses and findings were presented:

- The directional static stability derivatives of the aircraft were investigated applying linear system theory, to establish which parameter accurately predicts the weathercock stability of the helicopter. It was observed that the ability of N_β to account for the change in direction of the freestream velocity caused by the sideward velocity perturbation is the key element for a more comprehensive representation of the directional static stability of the helicopter, even in presence of flight scenarios with relative tailwinds.

- Because of the high computational expense of vortex methods, the empirical VRS stability boundary provided by Johnson [81] was used to provide more affordable but still reliable detection of VRS events. The impact of the aerodynamic interference from the main rotor vortex wake on the tail rotor VRS boundary was investigated. It was observed that this interference induces the tail rotor into more severe vortex ring flow states that may cause a rapid loss of directional control. Hence, when the tail rotor inflow is augmented with the main rotor-to-tail rotor interaction a more accurate detection of VRS events is attained.

The necessity to provide the operator with a tool designed to analyze flight data and easily detect the proximity to LTE without the need for a simulation model urged to find a method that enables the fast and reliable identification of LTE events within

the HFDM environment. After investigating the helicopter flight envelope, supervised learning algorithms were used to develop different prediction functions for each LTE phenomenon. The independent variables used to create the predictive models of the three LTE phenomena were chosen based on their impact on the predicted response and their accessibility within the operator's flight data. Also, they were made non-dimensional, extending the application of the safety metric to the flight data of helicopters with different sizes, while considering the same aircraft configuration. After ensuring an optimal prediction capability of the LTE detection parameters, the proximity to the three LTE events were defined. While the definitions of the three types of LTE events do not change, the boundaries that define the proximity to the LTE phenomena are left accessible to the operator, to provide flexibility in the risk management of post-flight analyses. The LTE safety metric, i.e., the comprehensive model that predicts LTE events and proximity to LTE, is formed by the collection of the three predictive models obtained.

To satisfy the research objective and verify the enhanced capabilities of the final methodology shown in Figure 5.1, the physics-based LTE safety metric was compared against the filter-based LTE metric currently used within the HFDM program. The results confirm the improved detection of the proximity to LTE, validating the overarching hypothesis of this research:

If the LTE safety metric encompasses the following contributions, then it will yield an improved detection of the proximity to LTE compared to the one currently used within the HFDM program, reducing the number of missed detections to better support the proactive mitigation of helicopter accidents related to LTE:

- *The LTE safety metric comprises the different aspects that can lead to LTE behavior: loss of weathercock stability, running out of pedal (tail rotor collective) for trim, and tail rotor vortex ring state.*

- *The prediction of safety limits for proximity to LTE is achieved using a combination of physics-based simulations, to investigate the aircraft flight envelope, and supervised learning techniques, to develop the predictive models of the three LTE phenomena. (A detailed view of those phases is offered in Figures 5.2 and 5.3, respectively.)*

- *To investigate the aircraft flight envelope, the simulation model includes a linear inflow gradient along the tail rotor blade augmented with the aerodynamic interaction from the main rotor vortex wake.*

- *The phenomenon of running out pedal is detected predicting the pedal control required for yaw balance.*

- *The phenomenon of loss of weathercock stability is detected predicting the directional static stability derivative, N_β.*

- *The phenomenon of tail rotor vortex ring state is detected using a comprehensive VRS stability boundary definition that encloses most of the experimental results available in the literature.*

- *The independent variables used to develop the prediction models of the three LTE phenomena have a relevant impact on the predicted response, are non-dimensional, and are accessible within the operator's flight data.*

- *While the definitions of the three types of LTE events do not change, the proximity to LTE thresholds is left accessible to the operator, to provide flexibility in the risk management of post-flight analyses.*

6.2 Recommendations for Future Work

To further advance the methodology developed and better support the mitigation of helicopter accidents related to LTE, the following additional studies are suggested:

- Enhance the LTE safety metric including the prediction of proximity to LTE during flight operations in ground effect. This would also support the implementation of a more reliable LTE flag in simulation models to promote greater awareness within the pilot community.

- Validate with higher fidelity vortex methods the experimental results obtained using the extension of Pitt-Peters inflow model to simulate the main rotor-to-tail rotor interaction. This effort would also further advance the understanding of the impact of the aerodynamic interference from the main rotor vortex wake during the development of the different LTE phenomena.

- Gather experimental data from flight tests and/or wind tunnel investigations to validate the proximity to LTE detection results obtained with the new LTE safety metric and to explore in more detail each LTE event for different rotorcraft configurations. This effort would also further the development of simulation models to enhance the quality of the yaw axis response.

- Investigate the impact of different tail rotor configurations on the development of the LTE phenomena. Results may offer details on the tail rotor designs that are more likely to be affected by this safety threat.

- Develop an onboard LTE warning system to assist in the real time prediction of proximity to LTE during flight. This will facilitate pilots to effectively avoid the critical flight scenarios that may lead to LTE like behavior.

Appendices

APPENDIX A
SUPPLEMENTARY LITERATURE REVIEWS

A.1 Inflow Models for Rotorcraft Flight Dynamics Applications

Several inflow models are available in the literature for the analysis of rotorcraft flight dynamics. Excellent comprehensive reviews are provided by Peters [120], Chen [28], and Gaonkar [60], giving an overview of the historical development of rotor inflow modeling. It is noted that this review includes models applicable for low-speed flight conditions, since loss of tail rotor effectiveness is characterized by low-speed flight scenarios [54], and for out of ground effect flight conditions, because of the assumption made throughout this thesis. Also, because of the need to investigate helicopter flight dynamics, a good tradeoff is required between inflow model accuracy and computational time. Hence, this review excludes the description of vortex methods, because of their relatively high computational expense due to the complex rotor wake modeling [92].

The simplest rotor inflow approximation is offered by momentum theory, which enables the estimation of basic rotor performance through numerous assumptions. The rotor is assumed to be an actuator disc, hence, infinitesimally thin with an infinite number of blades. The flow is assumed to be steady, inviscid, and incompressible with a pressure variation through the rotor flow field. The inflow is assumed to be uniform over the rotor disk and it is computed using basic conservation laws of fluid motion, i.e., conservation laws of mass, linear momentum, and energy. The induced inflow ratio, i.e., the induced inflow velocity normalized by the blade tip speed, is often used because of its nondimensional nature. For forward flight, momentum theory defines

the induced inflow ratio as:

$$\lambda_i = \lambda_0 = \frac{C_T}{2\sqrt{\mu^2 + \lambda^2}} \tag{A.1}$$

The advance ratio, μ, is defined as:

$$\mu = \frac{V_\infty cos\alpha}{V_{tip}} \tag{A.2}$$

where V_∞ is the relative airspeed, α is the angle of attack of the tail rotor disk, and V_{tip} is the rotor blade tip speed. The inflow ratio, λ, includes the components of the freestream inflow and the induced inflow, λ_i, and it is defined by:

$$\lambda = \mu\ tan\alpha + \lambda_\mathrm{i} \tag{A.3}$$

Figure A.1 illustrates the momentum analysis in forward flight. This approach is of-

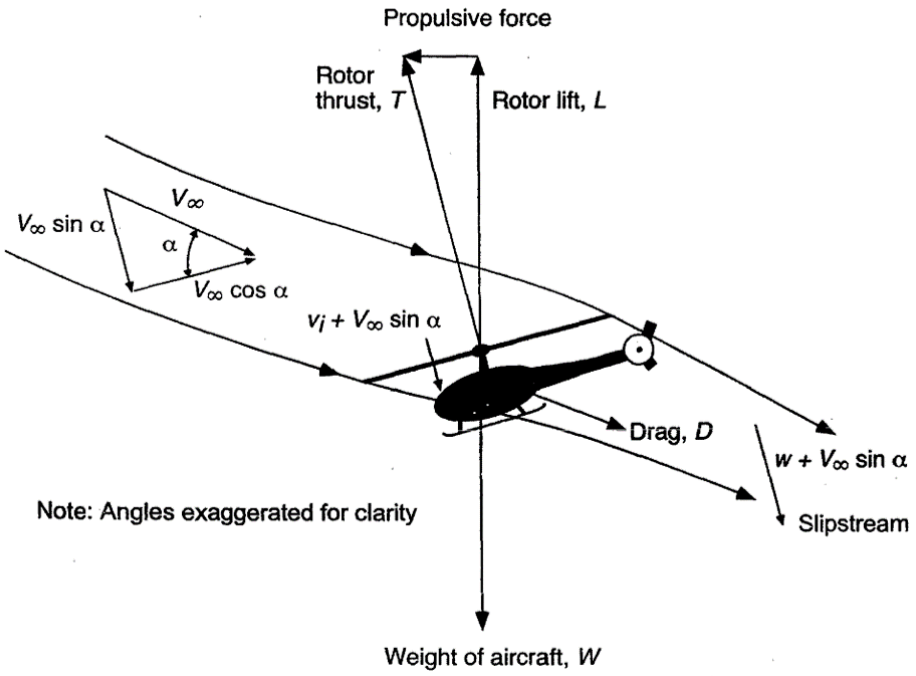

Figure A.1: Momentum analysis for a rotor in forward flight.

ten used because of its simplicity, enabling the calculation of the rotor induced inflow while neglecting the details of the flow environment at each blade section. However, a nonphysical solution is obtained in descent flight when the axial component of the freestream inflow is between 0 and $2v_{\mathrm{i}}$, i.e., $-2v_{\mathrm{i}} < \mu\ tan\alpha < 0$. Under these circumstances, a well-defined slipstream cannot be defined because of the more complex flow patterns involved, e.g. vortex ring flow states, and momentum theory becomes invalid [66]. This flight condition is often analyzed through experimental results or more advanced vortex theories and it is treated in more detail in Appendix A.2.

Several in-flight experiments confirm the nonuniformity of the inflow over the rotor disk [21, 72], revealing the need for a more accurate inflow representation. Based on the experimental results, the variation of the inflow was determined to be approximately linear along the rotor radius. Hence, numerous inflow models have been developed to approximate the linear inflow gradients over the blades. Inflow models that include longitudinal and lateral inflow variations over the rotor disk, as illustrated in Figure A.2, are often adopted. The induced inflow ratio can be calculated using the following equation:

$$\lambda_{\mathrm{i}} = \lambda_0\ (1 + k_x r\ \cos\psi\ + k_y r\ \sin\psi\ ) \tag{A.4}$$

where λ_0 is the mean (average) induced velocity at the rotor disk given by momentum theory, k_x and k_y are the longitudinal and lateral inflow gradients that a uniform model fails to predict, r is the radial position of the blade element normalized by the rotor radius, and phi is the azimuth angle.

Numerous studies focus on the definition of the inflow gradient coefficients, using rigid cylindrical vortex wake theories [34] or momentum theory [80]. Coleman [34] used vortex theory with a uniformly loaded circular disk and determined that:

$$k_x = \tan\left(\frac{\chi}{2}\right) \tag{A.5}$$

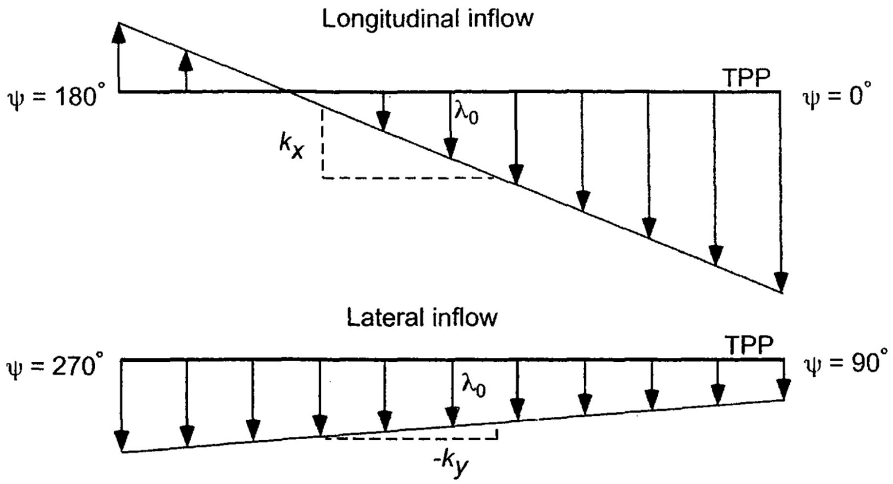

Figure A.2: Linear inflow approximation over the rotor disk.

where χ is the wake skew angle and it is defined as:

$$\chi = \tan^{-1}\left(\frac{\mu}{\mu\ \tan\alpha + \lambda_{\mathrm{i}}}\right) \tag{A.6}$$

Note that the wake skew angle is a function of the advance ratio, the angle of attack at the rotor disk, and the thrust coefficient. This parameter defines the orientation of the rotor wake and has been determined to be a key element in determining an accurate value of the rotor inflow [24].

Drees [40] modified Coleman's model using a different wake geometry and obtained the following weighting coefficients:

$$k_x = \frac{4}{3}\left(\frac{1 - \cos\chi - 1.8\mu^2}{\sin\chi}\right) \tag{A.7}$$

$$k_y = -2\mu \tag{A.8}$$

From the results obtained by Castles and DeLeeuw [24] using a cylindrical wake with uniform disk loading, Payne [115, 89] derived a good estimation of the inflow

Table A.1: Inflow gradient coefficients of various inflow models.

Author	k_x	k_y
Coleman et al. [34]	$\tan(\chi/2\ )$	0
Drees [40]	$(4/3)(1-\cos\chi-1.8\mu^2\ )/\sin\chi$	-2μ
Payne [115]	$(4/3\ \tan\chi\ )/(1.2+\tan\chi\ )$	0
White and Blake [146]	$\sqrt{2}\sin\chi$	0
Howlett [74]	$\sin^2\chi$	0

gradients, i.e.:

$$k_x = \frac{4/3\ \tan\chi}{1.2+\tan\chi} \tag{A.9}$$

Table A.1 provides a summary of the most significant inflow gradient coefficients as functions of the wake skew angle and the advance ratio. Cheeseman and Haddow [26] collected induced velocity data from a low-speed wind tunnel test. It was observed that a good representation of the rotor inflow was provided by the models of Drees [40] and Payne [115], comparing well with the experimental data.

Until this point, the models described assume that the induced velocity varies instantaneously to its new inflow state. However, because of the inertial effects of the mass of air trying to resist flow velocity changes, there is a time lag associated with the buildup in inflow. This is commonly referred to as the apparent mass effect. Dynamic inflow models are defined in terms of a finite number of ordinary differential equations in time, i.e.:

$$[\boldsymbol{M}]\left\{\frac{d\boldsymbol{\lambda}_{\mathrm{n}}}{dt}\right\}+[\boldsymbol{C}]\left\{\boldsymbol{\lambda}_{\mathrm{n}}\right\}=\left\{\boldsymbol{F_m}\right\} \tag{A.10}$$

where $\boldsymbol{\lambda}_{\mathrm{n}}$ are the states that define the flowfield, $\boldsymbol{F_m}$ is the blade loading vector, $\boldsymbol{M}$ is the apparent mass matrix, and $\boldsymbol{C}$ is the influence coefficient matrix.

While poor results were obtained testing forward flight conditions using methods

derived from momentum theory [113, 116], Pitt and Peters developed a model using potential flow theory obtaining excellent correlations with experimental data [121]. The model is based on the study on Mangler and Squire [101] and offers in a closed-form the apparent mass matrix and the inflow influence coefficient matrix to calculate the total induced inflow ratio at any point on the rotor disk. The standard form of the Pitt-Peters model is:

$$[\boldsymbol{M}]\begin{Bmatrix} \dot{\lambda}_0 \\ \dot{\lambda}_y \\ \dot{\lambda}_x \end{Bmatrix} + V[\boldsymbol{L}]^{-1}\begin{Bmatrix} \lambda_0 \\ \lambda_y \\ \lambda_x \end{Bmatrix} = \begin{Bmatrix} C_T \\ -C_L \\ -C_M \end{Bmatrix} \tag{A.11}$$

The apparent mass matrix is given by:

$$\boldsymbol{M} = \begin{bmatrix} \frac{8}{3\pi} & 0 & 0 \\ 0 & \frac{16}{45\pi} & 0 \\ 0 & 0 & \frac{16}{45\pi} \end{bmatrix} \tag{A.12}$$

The mass flow parameter V includes the effect of the wake contraction and is defined as follows:

$$V = \frac{\mu^2 + \lambda\,(\lambda+\lambda_0)}{\sqrt{\mu^2+\lambda^2}} \tag{A.13}$$

The inflow influence coefficient matrix includes the effect of the wake skew angle and

is defined by:

$$\boldsymbol{L} = \begin{bmatrix} \frac{1}{2} & 0 & -\frac{15\pi}{64}\chi \\ 0 & 2(1+\chi^2) & 0 \\ \frac{15\pi}{64}\chi & 0 & 2(1-\chi^2) \end{bmatrix} \tag{A.14}$$

After solving this set of equations, the final induced ratio is computed as follows:

$$\lambda_{\mathrm{i}} = \lambda_0 + \lambda_x r\ \cos\psi\ + \lambda_y r\ \sin\psi \tag{A.15}$$

Pitt-Peters model shows an evident improvement in the prediction of the inflow over the rotor disk, compared to the previous theories [59, 26]. Nowadays it is widely used in many rotorcraft flight simulation models because of its excellent capabilities within the applications involving rotorcraft flight dynamics. Also, it offers a more applicable framework for inflow modeling developments compared to models based on numerical fitting of results obtained from vortex methods.

A significant contribution was provided by Peters and He [117, 118], who extended the potential functions used by Pitt and Peters to provide a more detailed inflow distribution over the rotor disk. In fact, a limitation of the Pitt-Peters model relates to the limited representation of the pressure distribution on the rotor using only two harmonics, i.e., 0^{th} and 1^{st} harmonics, with one or two radial functions of inflow for each harmonic. Instead, Peters and He include all harmonics and all radial distributions of inflow including axial to edgewise values of wake skew angle. The Peters-He generalized wake model offers a finite number of inflow states, including the Pitt-Peters model as a special case (if number of states = 3). The model gives similar results of vortex-lattice methods, avoiding the complex modeling of the true vortex wake while maintaining a more affordable computational analysis. Because the

model uses a higher number of inflow states, it offers a more detailed prediction of the inflow at the rotor which is usually preferred in the study of rotor aeroelasticity [102].

A.2 Tests and Physics-Based Models Related to Vortex Ring State

For more than a century, Vortex Ring State (VRS) has been the subject of challenging aerodynamic investigations. This phenomenon significantly impacts rotor performance and rotorcraft flight dynamics, and it can affect both main and tail rotors [123, 92]. This is intuitive because of the common nature of the flow field around the rotor associated with VRS. A review of the experimental tests and physics-based models is given, to explore the different investigative approaches present in the literature.

A.2.1 Flight Tests and Wind Tunnel Experiments

Several flight tests and wind tunnel experiments have been published, with the intent of furthering the understanding of this complex problem. An excellent summary of the wind tunnel experiments and flight tests performed on VRS has been provided by Johnson [81]. Remarkable flow visualizations, such as Figure A.3, were obtained by Drees et al. [39, 41, 42] while investigating the complex rotor wake behavior of the different working states of a rotor in axial flight. The wind tunnel tests revealed a highly unsteady flow during VRS, due to the periodical vortex break away from the rotor disk. In this region Drees described the behavior of the aircraft as very rough, in attitude and control, with an unsteady increase of power required to maintain altitude. Also, it was observed that VRS was not a problem in forward speed, as the vortices were blown away by the relative wind before they were able to accumulate around the rotor.

Rotor performance is often assessed by the time history measurements of its thrust and torque. Many aerodynamic tests in presence of VRS revealed large fluctuating loads that have been associated with the unsteady nature of VRS. This was not only

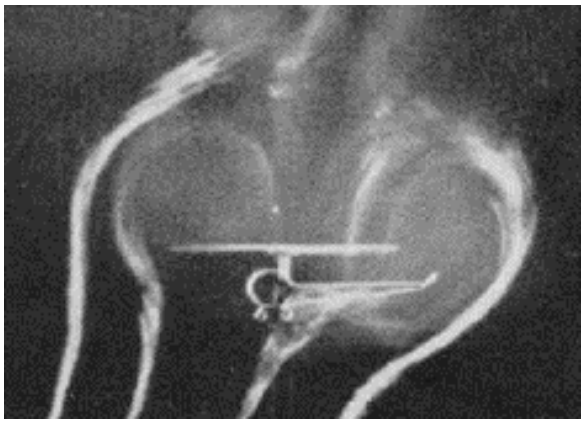

Figure A.3: Flow visualization of rotor operating in vortex ring state [42].

observed in wind tunnel experiments but also during real flight tests. Reeder and Gustafson [125], Brotherhood [21] and Stewart [133] conducted the first flight tests on VRS reported in the literature. The region of roughness described by Drees [42] was experienced in-flight through aperiodic blade flapping, random yawing movements, and significant vibrations. The pilot workload highly increased while approaching VRS. This was noted also by Yeates [156] who described the VRS flight experience in a tandem helicopter, and by Scheiman [128] who investigated VRS for different combinations of descent rate and forward speed. Overall, it was observed that equilibrium flight was difficult to achieve during any VRS event due to the strong vibrations caused by the flow instability.

In the meantime, several studies focused on the different effects of the rotor geometrical properties on the VRS phenomenon. For example, Castles and Grey [25] examined through wind tunnel tests the influence of twist on rotor performance during vertical descent. It was observed that the rotor with twisted blades was affected by larger loads variations and an increase in the rate of descent. Blade twist may have an effect on the position of the tip vortices in the rotor wake and consequently on the distribution of induced velocity over the disk. This has a significant impact on rotor performance, increasing load fluctuations and power required [93].

Similar results were obtained by Yaggy and Mort [155]. Noteworthy is their consideration of relating the unsteady flow field to the rotor disk loading. It was assumed that the amplitude of the fluctuations during VRS was related to the rotor mean thrust. Hence, their study involved the analysis of rotors with different disk loadings. Figure A.4 shows the results collected, revealing no particular difference in thrust variations for low descent rates between rotors with different disk loadings. For all rotors the highest value of thrust fluctuations lies where the magnitudes of downwash and descent rate are approximately equal. However, as the rate of descent increases, a smaller disk loading induces greater unsteadiness during VRS. This suggests how rotors with smaller disk loading are more likely to be affected by this safety threat as a smaller descent velocity is required to initiate the VRS onset.

The test results that have been reviewed above suggest that VRS involves im-

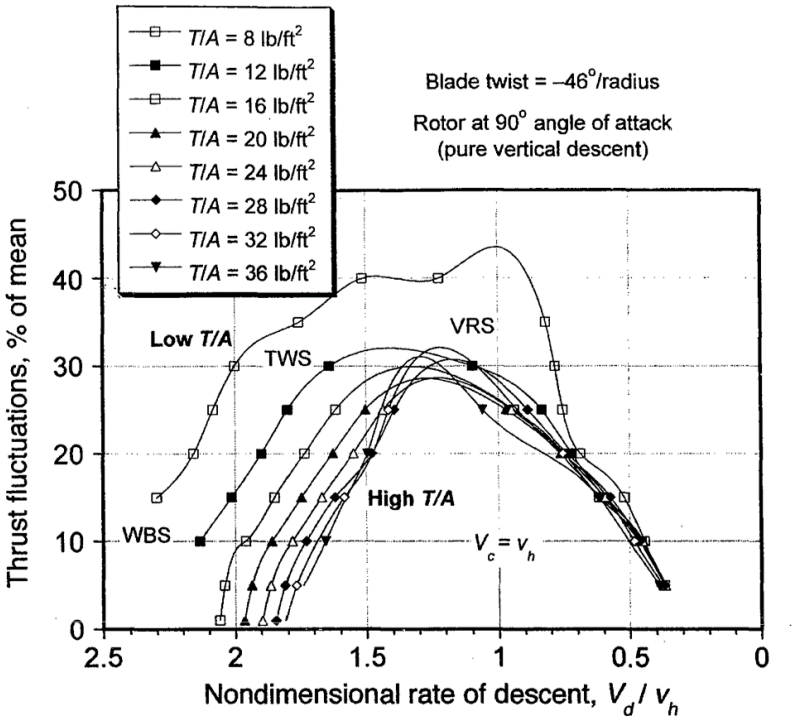

Figure A.4: Yaggy and Mort [155] rotor thrust measurements in axial descent for different values of disk loading [92].

portant aperiodic load fluctuations when the rotor operates at a descent rate that approaches the magnitude of the hover induced inflow. Additionally, Drees [42] and Yaggy [155] also observed that the largest thrust variations occur when a small edge-wise component of the freestream inflow is included. Washizu et al. [145] investigated this aspect calculating the induced inflow of a rotor operating in inclined descending flight, as shown in Figure A.5. The wind tunnel tests involved different angles of attack of the disk, spanning from 90° to 0°, which represent axial descent and forward flight, respectively. It was observed that at angles of attack below 50°, the induced velocity was being well-predicted by momentum theory. Also, he estimated the high power required in steep descents, proving how momentum theory fails to accurately predict rotor performance within the VRS flight regime. The thrust fluctuations were quantified and used to estimate specific VRS boundary criteria, often cited in important VRS related documents [81].

More recent is the experimental study of Stack et al. [132], who describes the large thrust variations during VRS. Excellent flow visualizations were obtained using

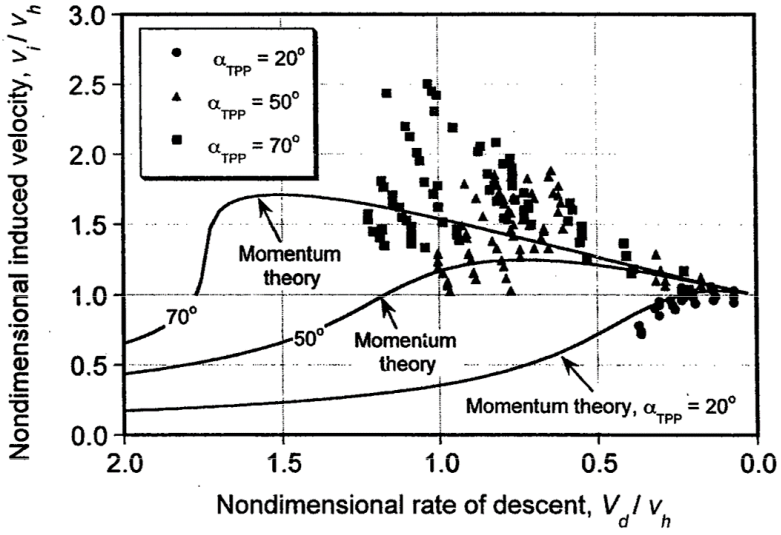

Figure A.5: Washizu et al. [145] measurements of rotor induced velocity in inclined descents [92].

a three bladed rotor operating underwater. The time history of thrust variations was measured for different combinations of descent rates, angles of attack of the disk, and collective pitch angles. The most dramatic peak-to-peak amplitudes of the thrust variations resulted to be up to 95% of the mean thrust, at normalized descent speeds within the range of 1 to 1.5. In presence of the well-developed vortex ring, a severe reduction in thrust was observed, followed by a full thrust recovery after vortex shedding.

Often cited in the literature are the results obtained by the wind tunnel tests of Betzina [9], who studied a relatively highly loaded rotor representative of the one used on a tiltrotor. He observed that the highest thrust oscillations caused by VRS appeared when the angle of attack of the disk was between 50° and 80°. Further, Betzina recognized the importance of the negative damping region, first identified by Gessow [63] in 1954. This region is often recognized as the most important part of VRS. It represents vertical damping instability, where the slope of thrust versus descent rate becomes negative. Here at a fixed collective pitch, if a disturbance initiates an increase in descent rate the rotor responds with a decrease in thrust, which consequently causes a higher descent rate. This flight characteristic is often used to define the entry into a VRS event.

Jimenez et al. [78, 79] and Taghizad et al. [135] performed extensive flight tests through the VRS flight regime and recognized the most distinctive feature of VRS to be the sudden increase in descent rate, even after the application of a collective control input. The VRS boundaries were defined by the vertical velocity drop of the helicopter and the intensity of the fluctuations measured. The types of flight procedures used to investigate the VRS boundaries included a progressive decrease of collective while in forward flight and a progressive decrease of forward speed while in descending flight. A comparison of Taghizad's results with the data obtained by Yeates [156] and Brotherhood [21] is plotted in Figure A.6.

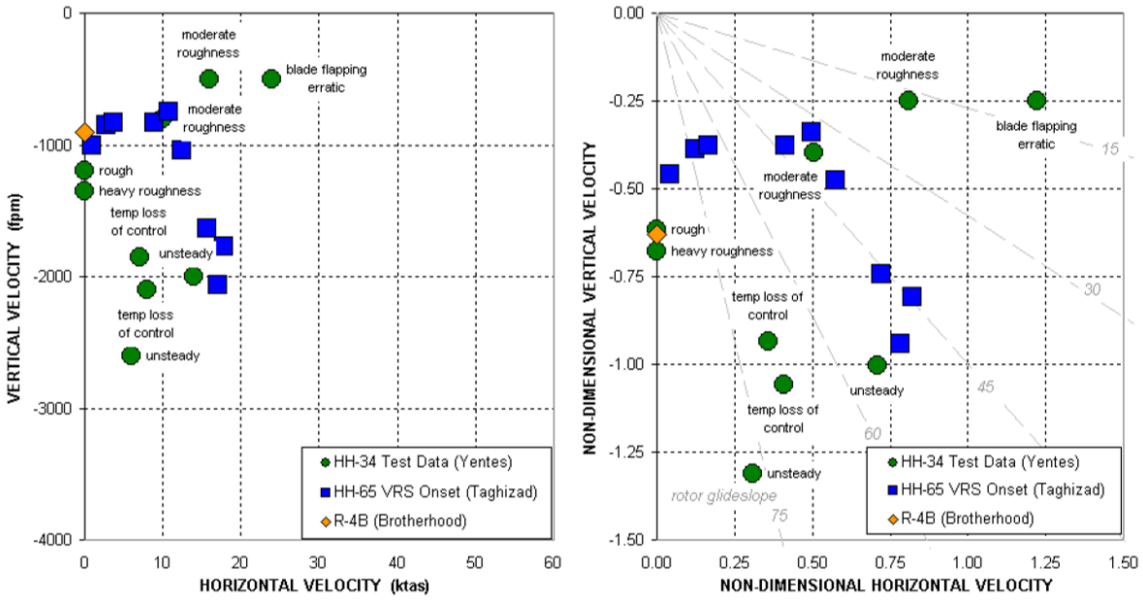

Figure A.6: Published VRS flight data [87].

Very extensive flight tests into fully developed VRS regime have been conducted by the V-22 Integrated Test Team (ITT) [16, 87]. The tests involved steady descents for the investigation of the VRS boundaries and dynamic maneuvers for the exploration of the tiltrotor behavior well beyond typical operational limits. It was observed that the entry into VRS was delayed by the high disk loading of the V-22, in concordance with the results of Yaggy and Mort [155]. Also, contrary to the findings of Castles and Grey [25], it was observed that blade twist did not play an important role in defining the VRS boundaries. Compared to helicopters, tiltrotors have unique handling qualities at the VRS boundary. They experience control degradation in the roll axis and a fast and effective recovery technique is represented by a small rotation of the nacelles. Despite those differences, it was measured that the non-dimensional VRS boundaries are very similar to the ones affecting conventional helicopters. The results obtained by the V-22 ITT provided remarkable insights about portions of the flight envelope never explored before. Throughout the years, each of the above tests progressively enhanced the understanding of this complex safety threat and helped

increase pilot awareness on preventing VRS encounters.

A.2.2 Physics-Based Models and Stability Criteria

As seen in the last section, several flight tests and wind tunnel experiments have been conducted and the results obtained have been essential to make progress in the understanding of the helicopter flight dynamics within the VRS flight envelope. However, because of the difficulty to sustain any form of equilibrium flight, due to the load fluctuations and consequent vibrations, not enough data is available to deeply explore the physical nature of VRS. Also, the investigation of rotors of different geometries often gave inconsistent results leading to misunderstandings in the rotorcraft community. Hence, analytical methods have been used in conjunction with experimental results allowing for improved VRS evaluations. Specifically, two key aspects have been the subject of several studies: the estimation of the rotor induced inflow within the VRS regime and the prediction of the VRS boundaries. Those elements are essential to obtain reliable rotorcraft simulations. While the inflow has a strong impact on the rotor loads and consequently on helicopter performance, the definition of VRS boundaries is important to establish appropriate flags in simulation models.

Glauert [65, 64] was one of the first to conduct a mathematical analysis of the problem, estimating the rotor inflow using the thrust and collective data measured by Lock et al. [98, 99]. He noticed that momentum theory becomes invalid at certain descent velocities because a distinct slipstream boundary ceases to exist [66]. After reviewing the theoretical analyses of Glauert [65, 64], and the test measurements of Lock [99], Brotherhood [21] and Drees [42], Gessow [63] estimated the induced inflow curve in the vortex ring state region as depicted in Figure A.7. Because of the large load fluctuations recorded during the tests, the induced inflow was estimated using a smooth curve fit approximation. Washizu [145] measurements are also shown to emphasize the oscillations recorded within the VRS flight regime. A semi-empirical

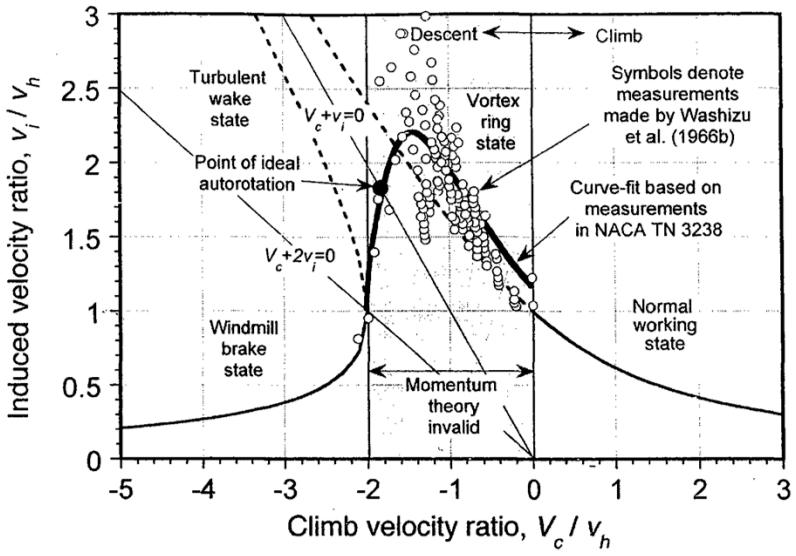

Figure A.7: Induced velocity variation as a function of axial velocity [92].

model was developed by Young [157] linking the normal and windmill working states with linear functions. This approximation proved to match well the laboratory test data of Castles and Grey [25], allowing the estimation of a reliable value of the induced velocity in ideal autorotation.

In 1972 Wolkovitch [153] applied momentum theory to predict the critical speeds and angles of attack of the rotor disk in which VRS is encountered. The induced velocity at the actuator disk is uniform and represented by the value v. Wolkovitch assumed that the slipstream is separated from the relative wind, V, by a series of tip vortices forming a tube of vorticity. Each vortex moves away from the rotor at a rate of descent equal to the mean between upflow and slipstream velocities, as depicted in Figure A.8. The vortex ring state was associated with the breakdown of this protective tube of vorticity. At a critical descent rate, the relative speed of the vortices falls to zero, no longer moving away from the rotor. In this condition a smooth slipstream ceases to exist, as no vortex tube is absorbing the shear velocity differential between upflow and slipstream, leading to unsteady flow. The predicted upper and lower boundaries of VRS are compared with Drees region of roughness

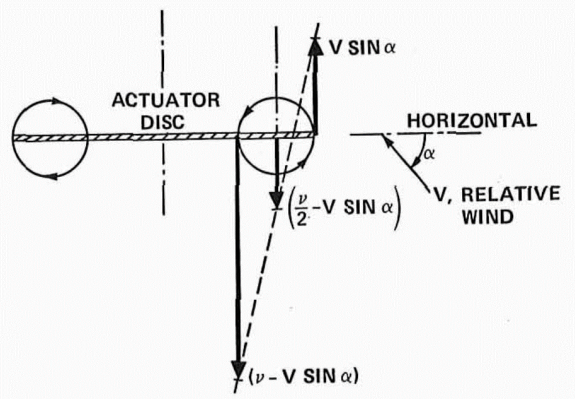

Figure A.8: Wolkovitch's flow model [153].

in Figure A.9. It is noted how the normalized upper boundary in axial descent was calculated to be approximately 0.707. Instead, the lower boundary is less definite as the development of the unsteady flow is less sudden and it is defined as a function of an empirical constant k that takes into account the distance above the rotor where the breakdown of the protective tube of vorticity occurs.

Several studies expanded Wolkovitch's model to further investigate the physics of VRS. For example, Wang [144] used classical vortex theory to find a relation between induced inflow and descent rate in axial flight. Wang noted that the tip vortices

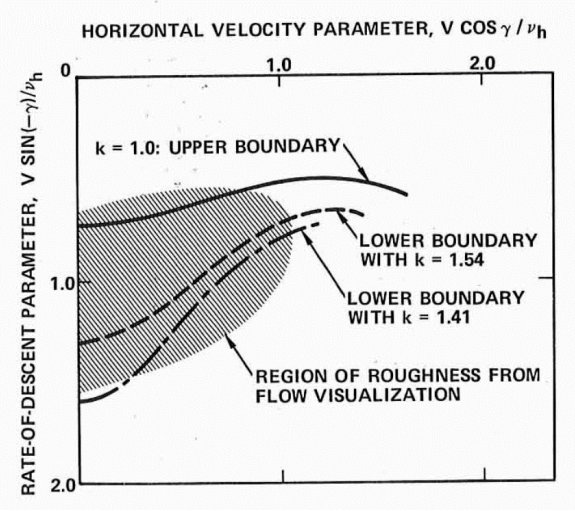

Figure A.9: Wolkovitch's vortex ring state boundaries [153].

dissipate while moving downward along the wake. For this reason, it was assumed that the circulation would decay linearly and would reach the value of zero at a distance proportional to the speed of the trailing vortices. As assumed by Wolkovitch, only axial flight was considered. Also, the VRS condition was defined as the point where the contributions of downwash and freestream upflow cancel each other not allowing the tip vortices to move away from the rotor. A remarkable contribution was given by the predictive capability of the induced inflow as a function of descent rate in the form of a simple set of parametric equations. A good correlation was found between the predicted induced inflow and experimental data.

Another relevant extension of Wolkovitch's theory was performed by Peters and Chen [119] reexamining the VRS boundary criteria while using a more consistent wake model that accounted also for forward flight. Strong correlations between momentum theory, vortex consideration, and dynamic inflow were discussed. An important contribution involved the integration of a wake propagation angle. Wolkovitch assumed the wake to propagate downward with no possible wake skew angle, neglecting the effect of the freestream in-plane velocity component on VRS. While this was not consistent with the experimental tests it provided a good starting point for further analyses. It was found that above the normalized in-plane velocity component of 0.62 the phenomenon of VRS does not exist anymore, as the vortices are being swept away by the forward airspeed in accordance with experimental tests.

After the collection of flight test data, Jimenez et al. [78, 79] and Taghizad et al. [135] developed an empirical inflow model linking the upper and lower branches of momentum theory while accounting for viscous losses. The model was used to improve the response of the Airbus/DLR/ONERA simulator software HOST. The VRS stability boundary was estimated extending Wolkovitch's theory to be valid in

forward flight and it was defined by the criterion:

$$\sqrt{\left(\frac{V_x}{k}\right)^2 + \left(V_z + \frac{v_i}{2}\right)^2} \leq \varepsilon \tag{A.16}$$

The coefficient k was chosen to better match experimental data, while ε represents the intensity of the fluctuations caused by VRS.

An interesting method for VRS boundary estimation and VRS investigation was also proposed by Newman et al. [109]. An interpolation of the limiting cases of momentum theory was used to predict the induced inflow as a function of descent rate for different in-plane velocities, a seen in Figure A.10. Further, simple momentum theory was augmented with physical arguments to derive the onset of the rotor wake breakdown during inclined descents. A balance between the rotor vorticity deposition into the wake and the rate at which the vorticity is swept away was defined as:

$$\frac{v_{WTV}}{v_h} = \sqrt{k^2 \frac{V_x}{v_h} + \left(\frac{V_z}{v_h} + \frac{v_i}{v_h}\right)^2} \tag{A.17}$$

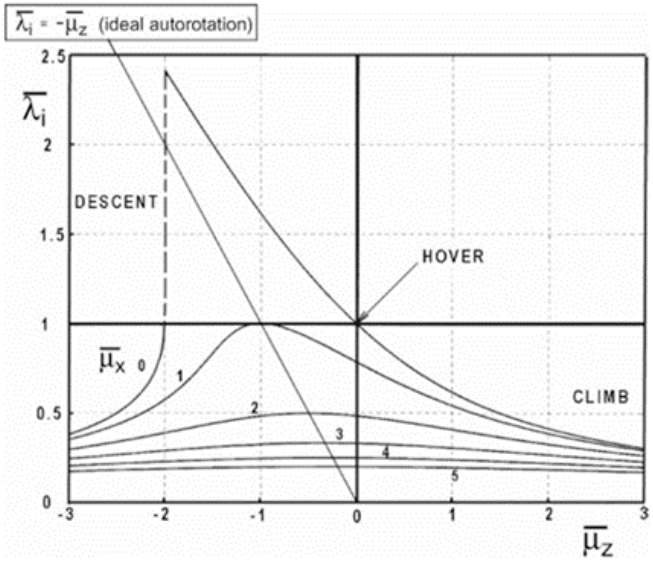

Figure A.10: Inflow model defined by Newman from momentum theory [119].

Below a critical value of this velocity of vorticity transport in the wake, the velocity through the rotor is not sufficient to force the tip vortices away from the rotor leading to VRS. Hence, the combination of descent rates and forward speeds that satisfies the above relationship defines the VRS boundaries in which wake breakdown takes place. An empirical constant k is used to model the lower effect of the in-plane velocity component on the critical velocity of vorticity transport in the wake. The results of this simple model were also supported by a detailed numerical investigation that revealed important physical insights on the wake breakdown during the VRS flight regime. Dynamic effects were investigated, and it was noted how rapid rotor maneuvers may impact VRS development. Also, it was observed that blade parameters may influence the vorticity distribution in the flow affecting the VRS onset. The VRS boundary compares well with the previously published data of Drees [42], Brotherhood [21], Yaggy and Mort [155], and Washizu et al. [145].

In 2004 a remarkable contribution was given by Johnson [81] who developed a uniform inflow model appropriate for VRS flight regimes that allowed for real-time dynamic simulations. The model is an empirical extension of momentum theory and is based on test data available in the literature including the wind tunnel experiments of Castles and Grey [25], Empey and Ormiston [52], Betzina [9] and the flight tests of Taghizad et al. [78, 79, 135]. Deriving the inflow from the test results, Johnson observed that in VRS, at fixed collective, the value of the total inflow curve $(v_z + v_i)$ increases for increasing descent rates, as seen in Figure A.11. Johnson acknowledged how this negative slope in the total inflow is the direct cause of the instability in the vertical motion, confirming Gessow's intuition [63], and included this essential characteristic in his model with the intent of simulating the negative damping of the aircraft seen in real flight tests during VRS. Further, the VRS boundary was estimated such that it would enclose most of the flight test results available, and for convenience it was defined as the locus of points (V_z, V_x) where the slope of the inflow curve is

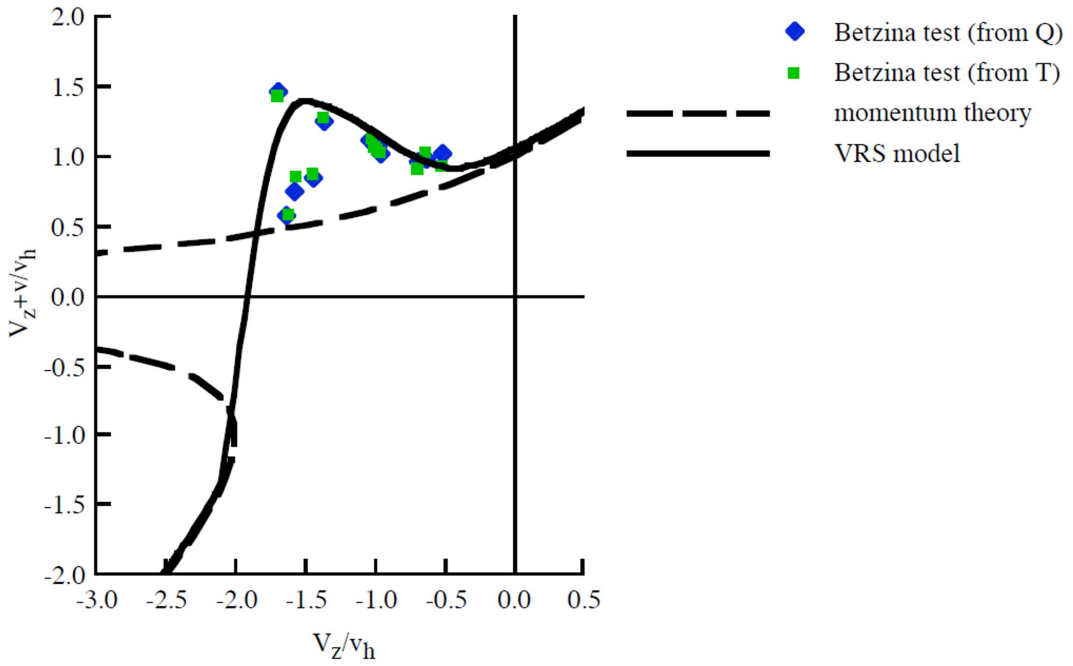

Figure A.11: Comparison between Johnson's model and Betzina wind tunnel tests [81].

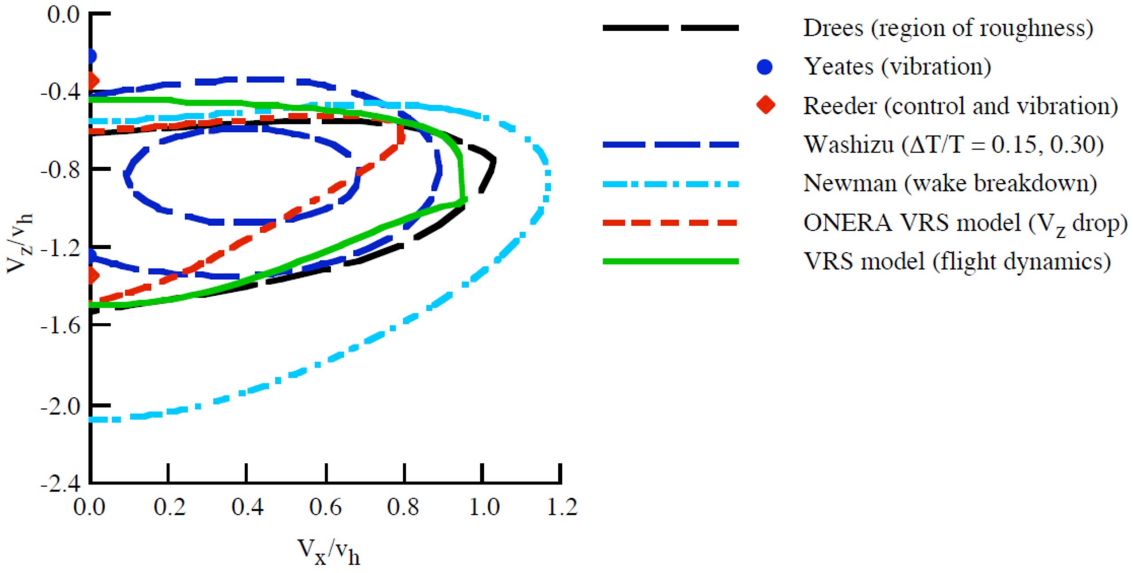

Figure A.12: Existing vortex ring state boundaries [81].

zero. A comparison of the VRS boundaries determined by Johnson with other results obtained from the literature is shown in Figure A.12. For its simplicity and versatility,

this model has been used by various authors to simulate the behavior of both main and tail rotors during VRS conditions. For example, Srinivas et al. [131] developed an isolated tail rotor model using Johnson's inflow model. The thrust variations were predicted for different wind azimuth conditions and a good correlation with wind tunnel data was found. A thrust loss was observed at the critical wind azimuth of about 270° which corresponds to a descent operating condition for the tail rotor.

Johnson's model was acknowledged and discussed also by Brand et al. [18] in a paper focused on the investigation of the physical nature of VRS. It was noted that if the maximum value of the total induced inflow is about 1.5 the hover induced velocity, while the normalized descent rate is about -1.5, then the contribution of the induced inflow is close to 3 times the hover induced inflow. This was a key observation that led the authors to reconsider VRS as a phenomenon involving a stable and organized wake structure. In fact, such a high value of the rotor induced velocity is possible only if the vortex filaments are highly organized in a single vortex ring in proximity to the rotor, dominating the descending inflow field. Hence, a deep investigation of how the blade tip vortices influence the rotor in axial descent was carried out. The ability to capture the organized accumulation of tip vortices in proximity to the rotor is essential to study the fundamental dynamic of VRS. Hence, a simple vortex ring emitter model was developed, to replace the helical wake with a series of vortex rings emitted by each blade at each rotor revolution. This model allowed to obtain significant insights about the nature of VRS, however it was constrained to only axial performance estimations. As depicted in Figure A.13, when the rotor descends into its own wake, the vortices interfere with each other and co-rotate eventually merging into a highly stable vortex ring structure. The induced inflow rapidly increases because of the accumulation of the highly organized vorticity. Blade vortex interactions are caused by the passage of the newborn tip vortices through the rotor plane as they propel downward. While the rotor is approaching the negative damping region of Figure A.11, a rapid thrust loss

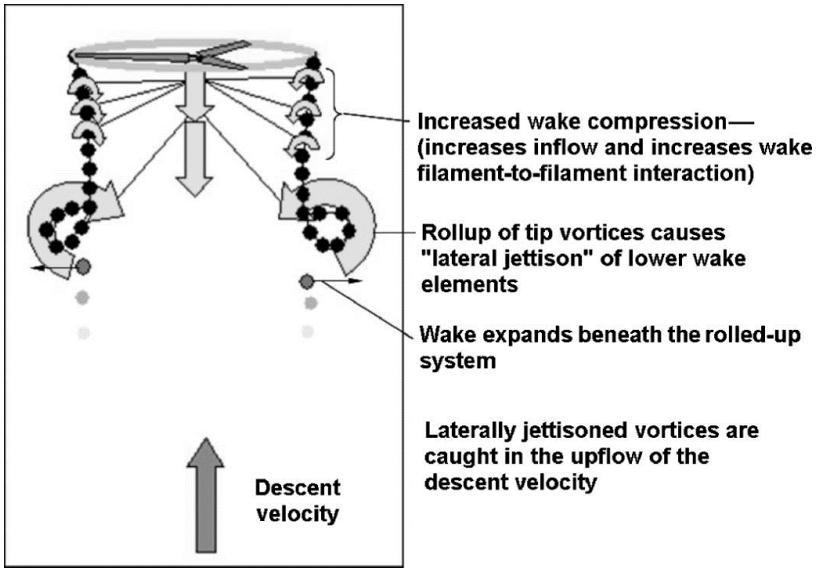

Figure A.13: The fundamental dynamic of vortex ring state [18].

occurs, and the rotor falls through the ring in a stable flow state. From the literature, the several steady descent wind tunnel results, such as the flow visualizations of Drees and Hendal [42], revealed a continuous formation and dissipation of the vortex ring around the rotor associated with high load fluctuations. However, Brand explains how this is not an accurate representation of VRS for a rotor in free flight. Figure A.14 shows the behavior of the newly emitted rings which provide a mechanism that favors

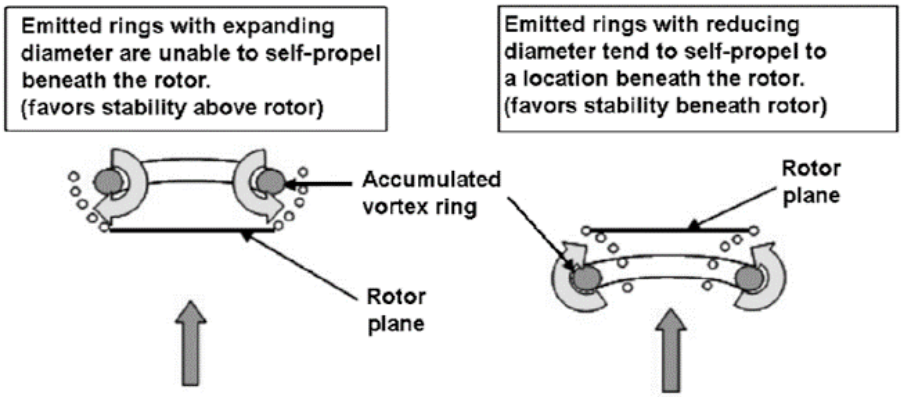

Figure A.14: The accumulated vortex ring influence the diameter of the newborn rings which provide a stable flow state [18].

the accumulated vortex ring to keep a stable position above or below the rotor.

An inflow model that combines the use of a ring vortex model and augmented momentum theory was developed by Chen [27] for a rotor in inclined descent conditions. A ring vortex model was used to account for the strong flow interactions while momentum theory was augmented to create a smooth transition between the normal and windmill states. The VRS boundaries were established based on the uncommanded increase in descent rate. Further, the loss of collective control sensitivity was observed during dynamic simulations in agreement with Johnson's results [81]. Good predictions were obtained with the several experimental data from the literature, such as Washizu et al. [145] and Taghizad et al. [78, 79, 135].

A more accurate investigation of aperiodic wake developments can be computed using free-vortex wake models. Those approaches allow examining in much more detail the effects of rotor geometry and maneuvering flights. The main disadvantage of vortex models is the relatively large computational expense in the calculation of the induced velocity field. At each time step, the numerical integration of the Biot-Savart law must be evaluated over all the elements of each vortex filament, as seen in Figure A.15, which may be discretized in hundreds or thousands of segments. The recent works of Brown [22] and Leishman [93] show good predictive capabilities of the rotor wake breakdown during VRS. To illustrate the effects of the rate of descent on rotor wake development, Figure A.16 captures the time-marching solution when the accumulated vorticity begins to greatly affect the blade loads [93].

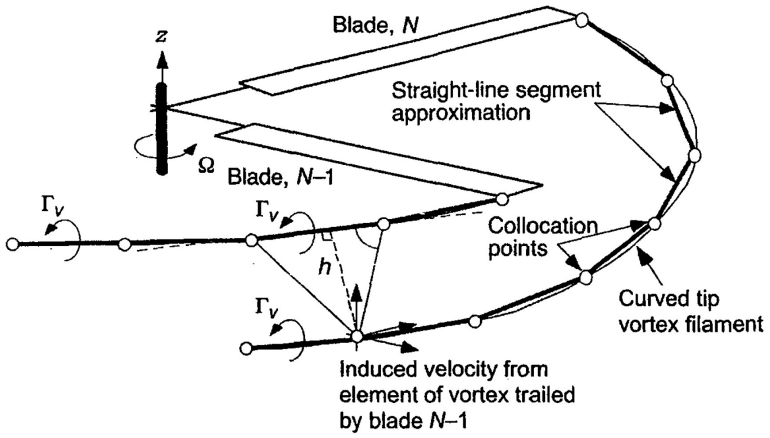

Figure A.15: The discretization of blade tip vortices in the free-vortex wake method [92].

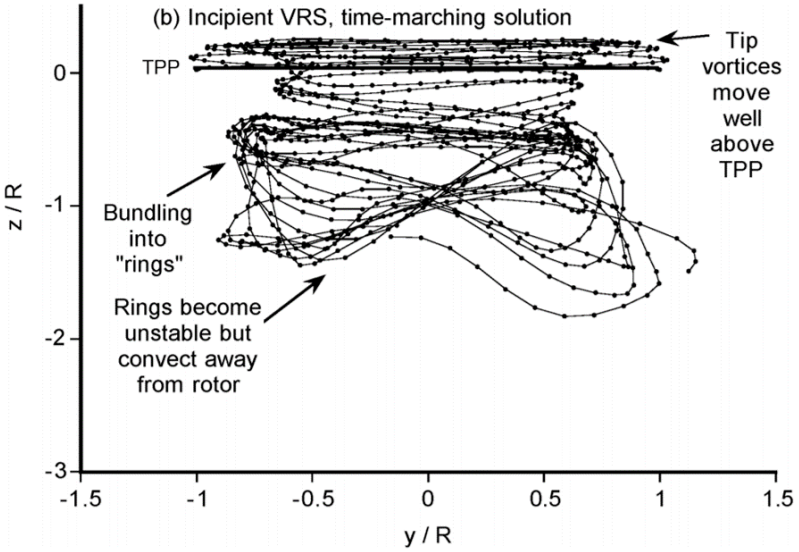

Figure A.16: The aperiodic wake developments during vortex ring state computed by the free-vortex wake analysis [22].

APPENDIX B
VALIDATIONS OF MODELS

B.1 Validation of Johnson's VRS Stability Boundary

This section describes the validation of the VRS stability boundary used to detect the VRS events at the tail rotor. The VRS limits are computed using the model provided by Johnson [81]. Figure B.1 shows the resulting stability boundary as a function of the normalized edgewise component of the freestream inflow, V_x/v_h, and the normalized axial component of the freestream inflow, V_z/v_h. The boundary agrees with Figure B.2, which provides the results published by Johnson [81].

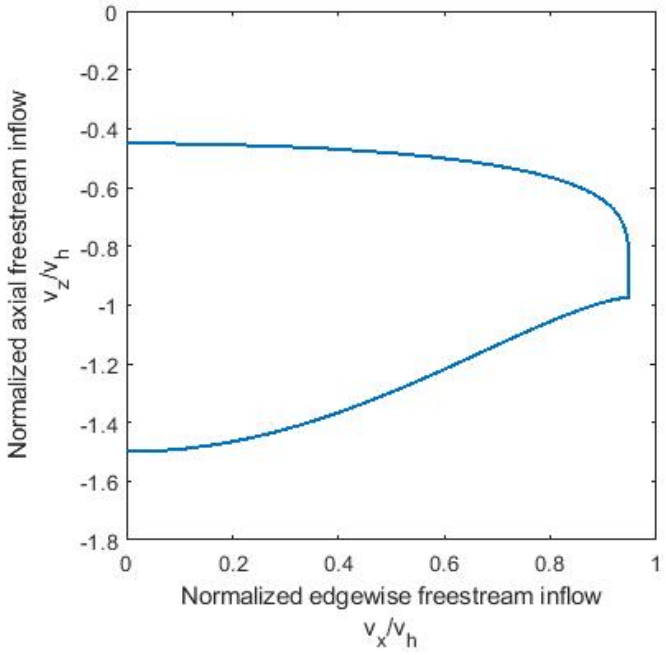

Figure B.1: Vortex ring state stability boundary computed using Johnson's model.

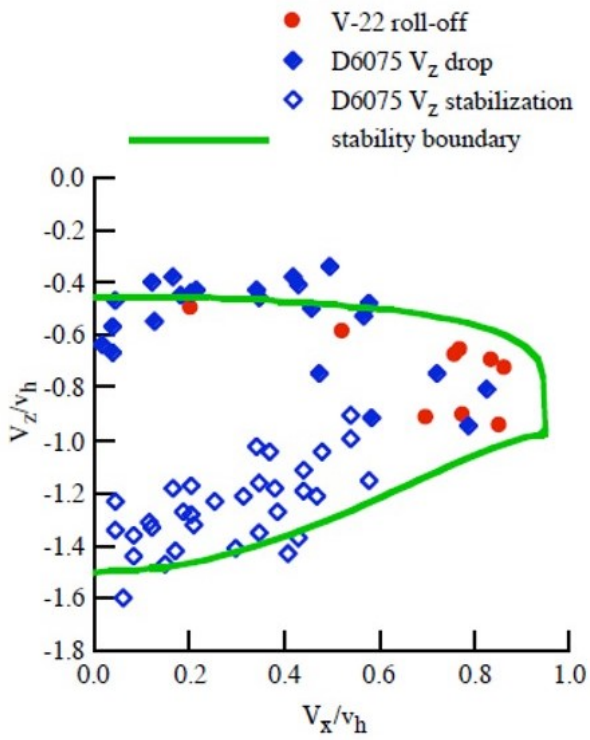

Figure B.2: Vortex ring state stability boundary published by Johnson [81].

B.2 Validations of Vortex Ring Emitter Model

This section describes the validations of the vortex ring emitter model used for the investigation of vortex ring state at the tail rotor. The first validation simulates the motion of 2 vortex rings relative to the rotor and compares the ring behavior with the leapfrogging motion simulated by Niemi et al. [110]. The modeling accuracy of this phenomenon is essential as it has been recognized as a critical element for the VRS initiation [18]. Next, the rotor wake self-organization is validated during a hover flight condition and throughout the different stages of a free-flight axial descent. A fully developed VRS event is carried out and compared with the simulations of Brand et al. [18].

B.2.1 The Dynamics of a Pair of Vortex Rings

A pair of axially aligned vortex rings interact with each other showing a leapfrogging behavior, i.e., alternately passing through each other while moving along a common symmetry axis. Numerous investigations were done on this phenomenon, e.g., the remarkable analytical studies of Dyson et al. [49], and Hicks et al. [73]. Figure B.3 illustrates the phenomenon considering the axial motion of two vortex rings with equal volume. Because the flow is assumed incompressible, the volume of each ring is conserved with time. The upstream ring, i.e., the red ring, induces a radial velocity that tends to widen the downstream ring. For conservation of vorticity, the axial velocity of the downstream ring diminishes. Simultaneously, the downstream ring shrinks the upstream ring, which is accelerated in the axial direction, flowing within the wider ring. Next, the new upstream ring, i.e., the blue ring, widens the downstream ring, and the behavior repeats.

Brand et al. [18] analyzed the behavior of a helicopter rotor wake in axial flight and recognized this mutual interaction between vortices to be a critical element for the VRS initiation. Hence, it is of the utmost importance to accurately model this phenomenon before simulating the dynamics of VRS. During the analysis it was observed that the time integration scheme used had an important impact on the estimation of the vortex ring motion. While the Euler approach generates large numerical instabilities, a second-order Runge-Kutta method allows for an accurate prediction of the leapfrogging behavior. Figure B.4 shows the cross-sections of a pair of vortex rings at different vortex ages after being emitted by an idealized rotor blade.

Figure B.3: The leapfrogging behavior of 2 vortex rings (adapted from [110]).

The rings' cross-section size has been enlarged for clarity. The initial radius of each ring is equivalent to the blade length. The motion of the vortex rings' cross sections confirms the evolution of the leapfrogging phenomenon. The interaction continuously repeats because of the inviscid flow assumption. The results compare well with the simulation results of Niemi et al. [110] given in Figure B.5.

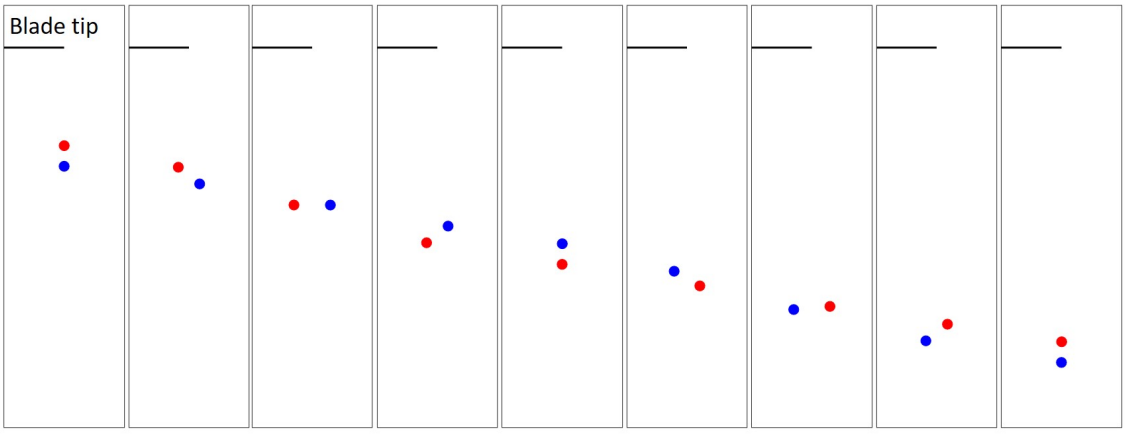

Figure B.4: Simulated motion of a pair of vortex rings' cross sections emitted by an idealized blade.

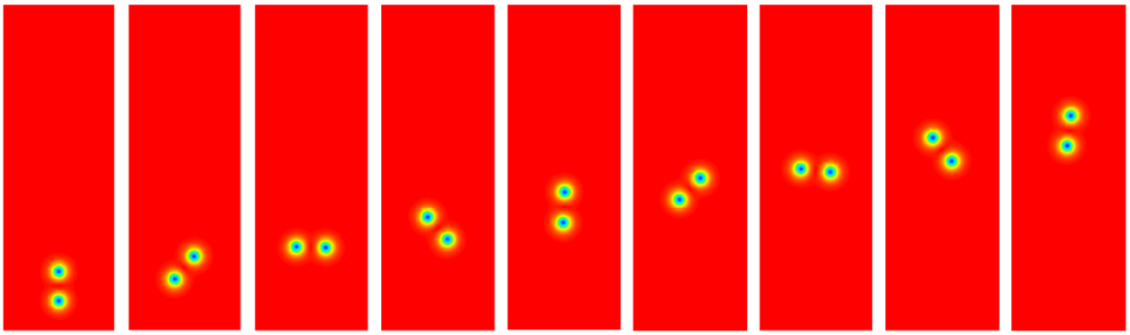

Figure B.5: Simulated motion of a pair of vortex rings' cross sections published by Niemi et al. [110].

B.2.2 The Dynamics of the Rotor Wake in a Free Axial Descent

After ensuring that the motion of a pair of vortex rings is accurately simulated, the ring emitter model is used to replicate a hover flight condition. The motion of 100 vortex rings is analyzed. An isolated rotor is modeled to continuously emit a vortex ring from each blade after every revolution. Figure B.6 shows the stages of the rotor wake development until a stable hover condition is reached. The vortex rings self-organize in a column with a well-defined slipstream boundary near the rotor. The wake contracts below the rotor, in accordance with momentum theory. Further downstream stronger vortex ring interactions occur, disrupting the slipstream boundary. The vortices keep grouping in separate clusters exhibiting a leapfrogging behavior.

Next, the vortex ring emitter model is coupled with the blade element model to compute the rotor loading. An isolated tail rotor in axial descent like flow condition is analyzed, considering a sideward motion of the aircraft to the left. Initially, the tail rotor is set to develop the thrust magnitude necessary to sustain yaw moment

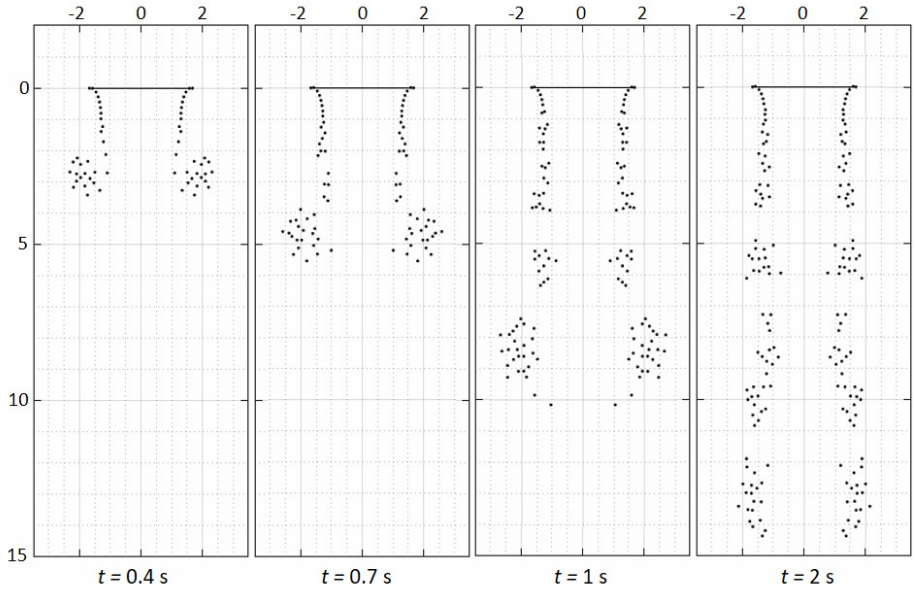

Figure B.6: Vortex wake development of an isolated rotor.

equilibrium while the aircraft is in a hover flight scenario. This is identified by the tail rotor thrust coefficient C_{T0}, used to normalize the results. From the trim setting, a series of controlled collective changes are applied to lead the rotor to a VRS encounter. Figure B.7 shows that initially at each tail rotor collective pitch reduction, the rotor suffers a thrust loss that is quickly recovered, reaching a new steady-state sideward velocity. A negative value of the sideward velocity represents a translational motion of the tail rotor to the left. The wake self-organization is captured in Figure B.8, which shows the vortex ring displacement relative to the tail rotor during the significant moments of the flight. Because of the increase of freestream flow from left to right through the rotor, the new ring vortices are propelled towards the left along the wake passing through the rotor plane. This causes blade-vortex interactions that result in stronger vibrations as the left sideward velocity increases. The roughness is visible after $t = 90$ s and significantly rises after $t = 150$ s.

The more the left sideward velocity increases, the more the vortex rings are compressed towards the rotor, disrupting the wake slipstream boundary while showing a leapfrogging behavior within different vortex groups. The mutual interactions between the vortex rings cause a radial expansion of the further rings and a weaker ability to propel themselves towards the left. Hence, the wake vorticity recirculates close to the rotor forming a toroidal structure of corotating vortex rings, which affects the induced velocity at the rotor. This leads to the main phase of the VRS phenomenon, which is triggered at $t = 240$ s by a further reduction in tail rotor collective pitch. A dramatic increase in induced inflow is seen during the accumulation of vorticity in proximity to the rotor. This strongly impacts the aerodynamic environment at each blade element, which experiences a decrease in the effective angle of attack. This leads to a reduction in rotor thrust that causes a rapid increase in the left sideward velocity, inducing the structure of vortex rings to reorganize to the right of the rotor in just a few seconds. Only when the collective pitch is decreased

further, the vortex ring sheds from the rotor, causing a decrease in inflow and a net thrust recovery. A distinct slipstream boundary expands above the rotor, eventually reaching the windmill brake state in which the rotor is extracting energy from the flow. These results compare well with the simulations of Brand et al. [18], shown in Figure B.9, despite the different rotor configuration used.

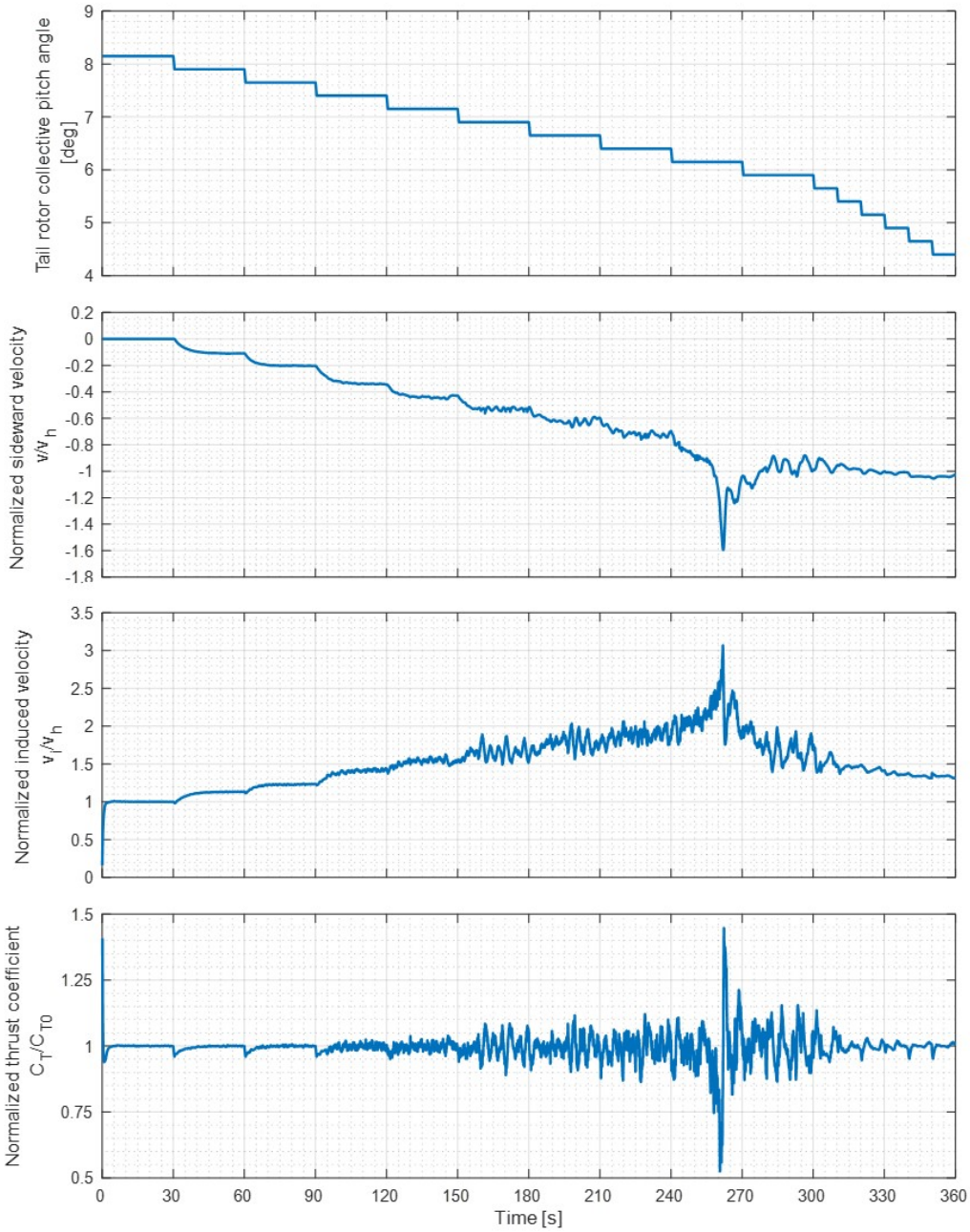

Figure B.7: Time history of tail rotor variables during a free descent that leads to a fully developed VRS event.

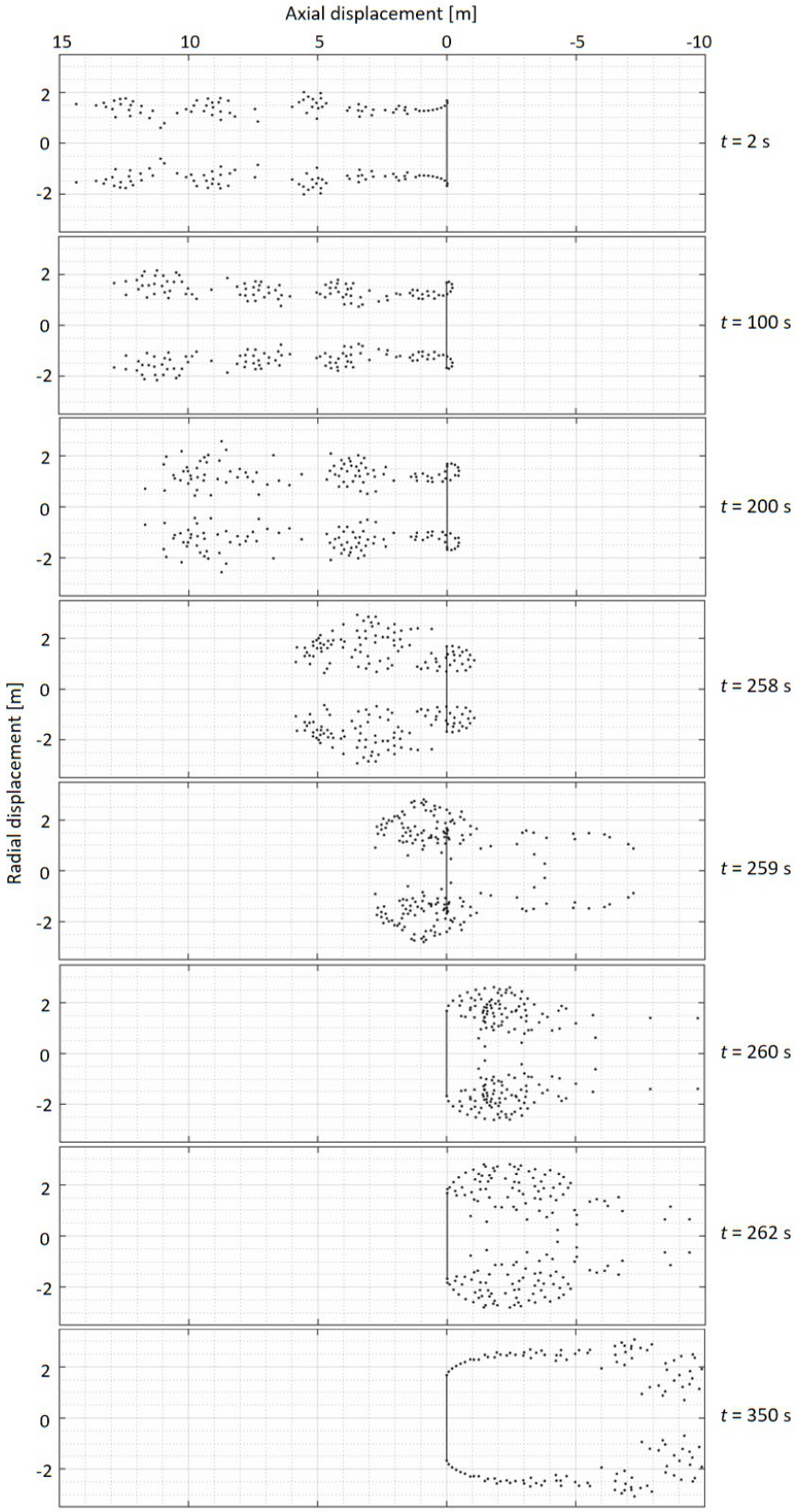

Figure B.8: Axial displacements of vortex rings emitted by a tail rotor during a fully developed VRS event.

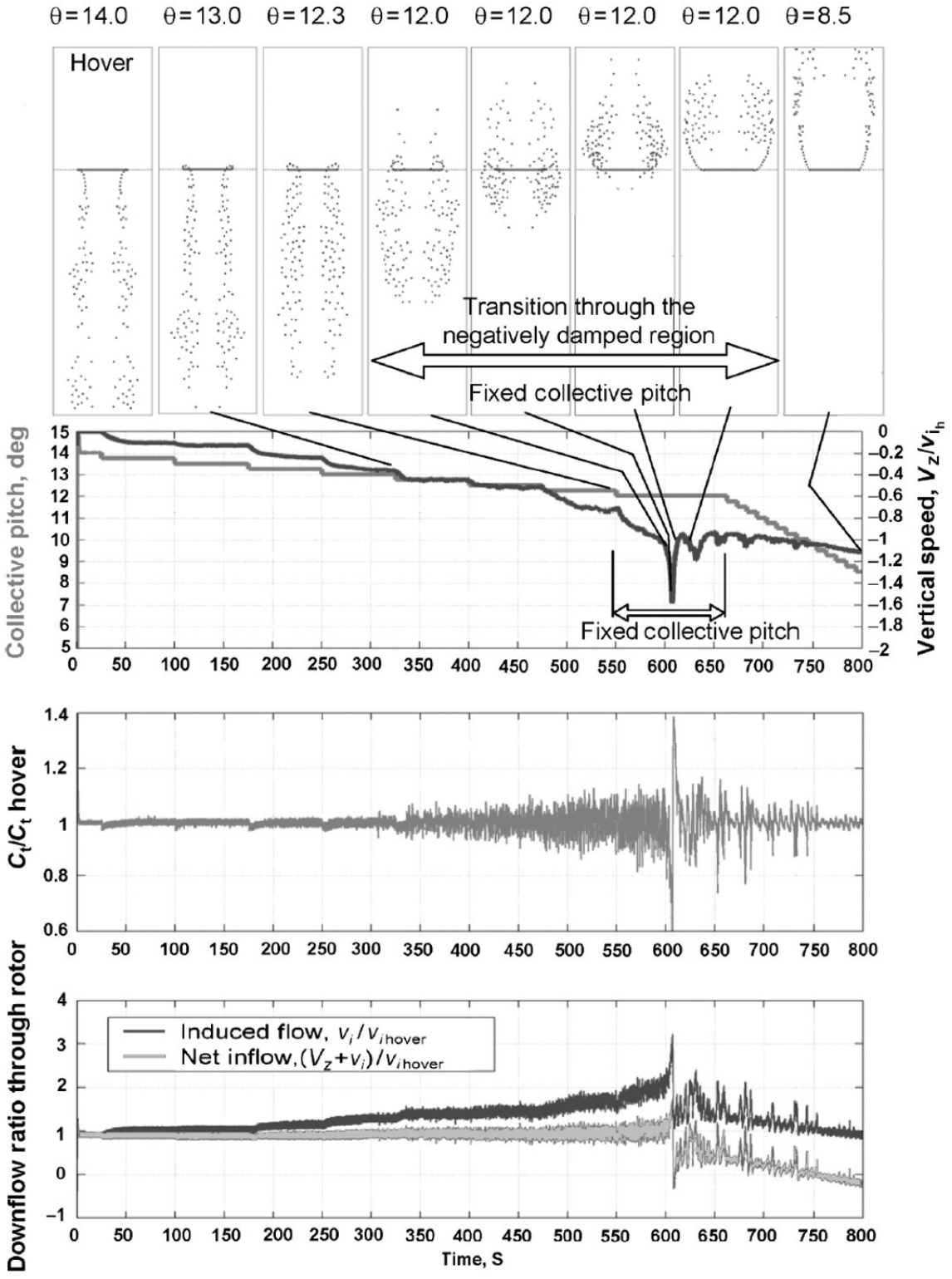

Figure B.9: Time history results of a fully developed VRS event published by Brand et al. [18].

APPENDIX C
TESTING OF SURROGATE MODELS

The prediction functions developed to estimate the LTE detection parameters must provide an adequate approximation of the true system. The LTE detection parameters of interest are the pilot's pedal control, δ_p, the directional stability derivative, N_β, and the normalized freestream inflow components at the tail rotor, V_x/v_h and V_z/v_h. To ensure an adequate prediction of each parameter, this section shows the response adequacy obtained using boosted decision trees and artificial neural networks (see description of model architectures in Section 4.5.5). The goodness-of-fit measures used to check for model accuracy are the coefficient of determination (R^2), the Root Mean Squared Error (RMSE), the actual by predicted plot, and the residual by predicted plot. The coefficient of determination is defined as:

$$R^2 = 1 - \frac{\sum_{i=1}^{i=n} (y_i - \hat{y}_i)^2}{\sum_{i=1}^{i=n} (y_i - \overline{y})^2} \tag{C.1}$$

while the Root Mean Squared Error is estimated as follows:

$$RMSE = \sqrt{\frac{\sum_{i=1}^{i=n} (y_i - \hat{y}_i)^2}{n - p}} \tag{C.2}$$

where y_i is the actual response, $\hat{y}_i$ is the predicted response, $\overline{y}$ is the mean of actual values, n is the number of observations, and p is the number of degrees of freedom. The actual by predicted plot provides a visualization of the actual response y_i versus the predicted response $\hat{y}_i$. The residual by predicted plot presents the residuals e_i versus the predicted response $\hat{y}_i$, where each residual is defined by $e_i = y_i - \hat{y}_i$, $i = 1, 2, \ldots, n$. The surrogate model provides a good prediction when it is characterized

by an R^2 value close to 1, a small RMSE value, an actual versus predicted plot that follows the y = x line, and residual values close to zero and scattered randomly.

Table C.1: Accuracy measures of surrogate models for pedal control (tail rotor collective) for trim.

Predictive model	R^2	RMSE
Boosted decision tree	0.9841	1.8325
Artificial neural network	0.9988	0.3826

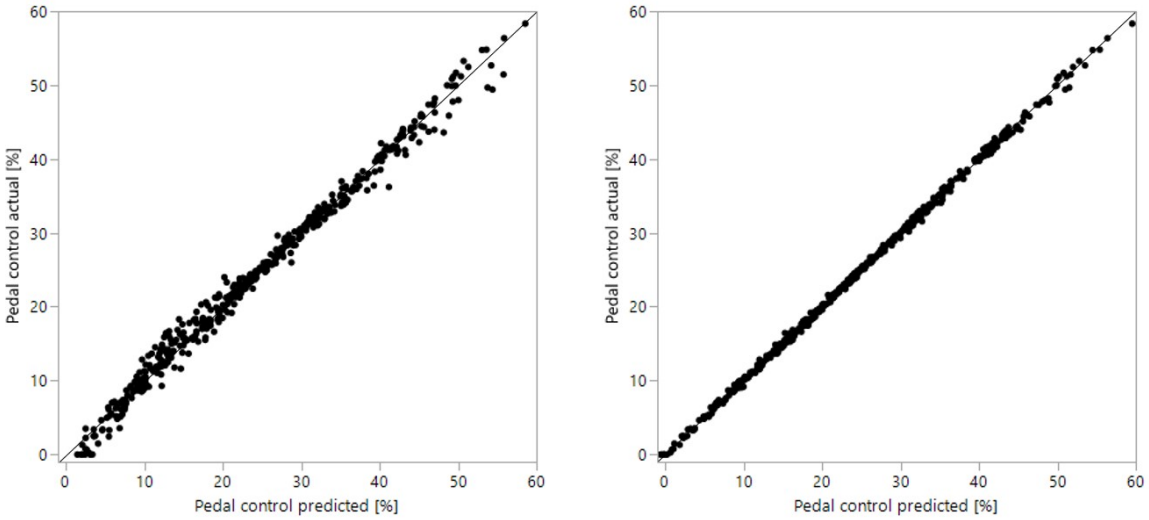

Figure C.1: Actual versus predicted plots of boosted tree model (left) and neural network model (right) for pedal control (tail rotor collective) for trim.

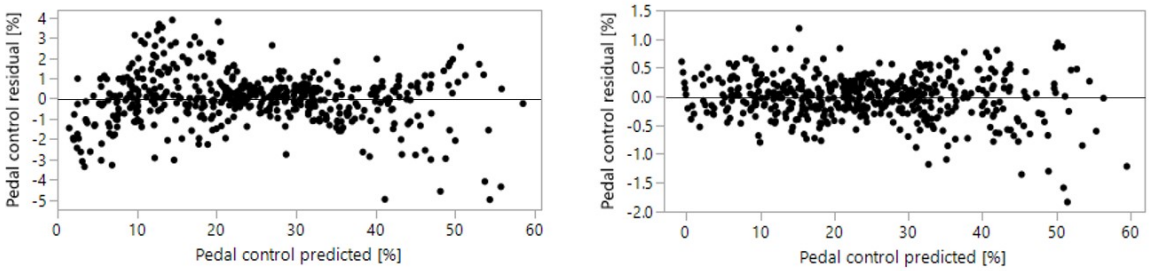

Figure C.2: Residual versus predicted plots of boosted tree model (left) and neural network model (right) for pedal control (tail rotor collective) for trim.

Table C.2: Accuracy measures of surrogate models for static stability derivative.

Predictive model	R^2	RMSE
Boosted decision tree	0.9658	0.0016
Artificial neural network	0.9831	0.0009

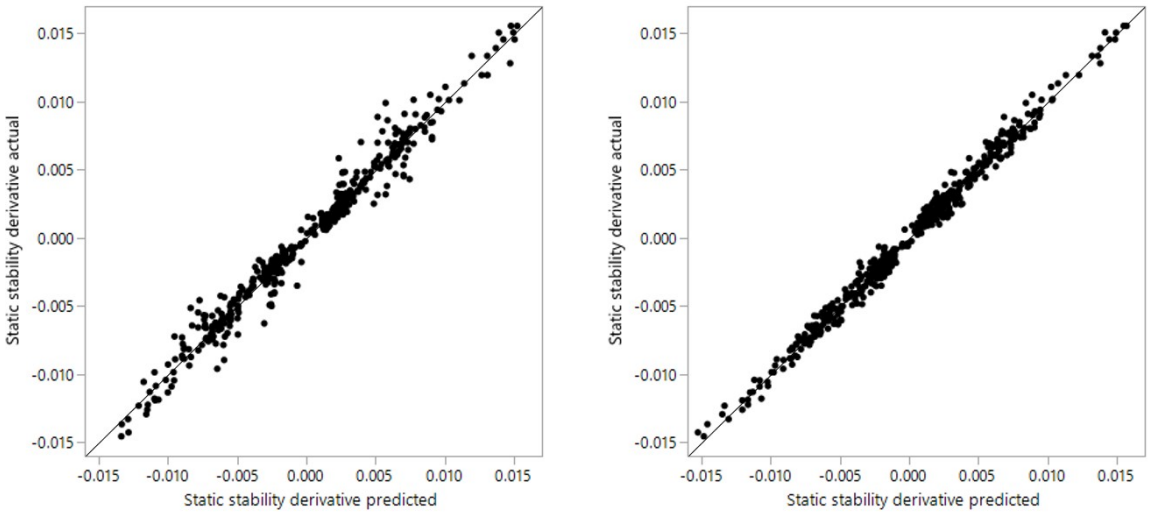

Figure C.3: Actual versus predicted plots of boosted tree model (left) and neural network model (right) for static stability derivative.

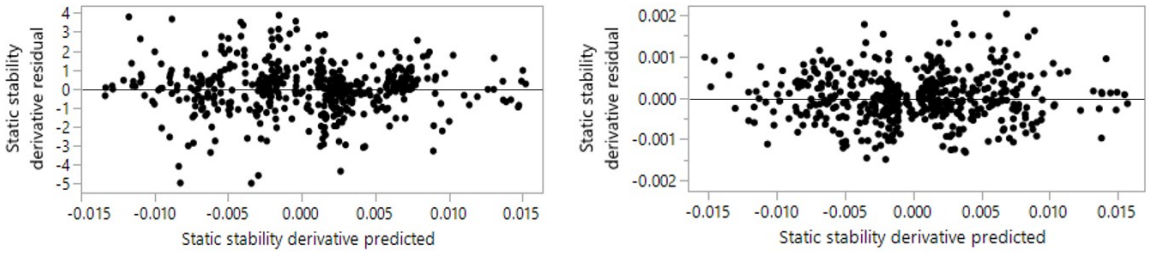

Figure C.4: Residual versus predicted plots of boosted tree model (left) and neural network model (right) for static stability derivative.

Table C.3: Accuracy measures of surrogate models for tail rotor edgewise freestream inflow.

Predictive model	R^2	RMSE
Boosted decision tree	0.9876	0.4725
Artificial neural network	0.9987	0.0954

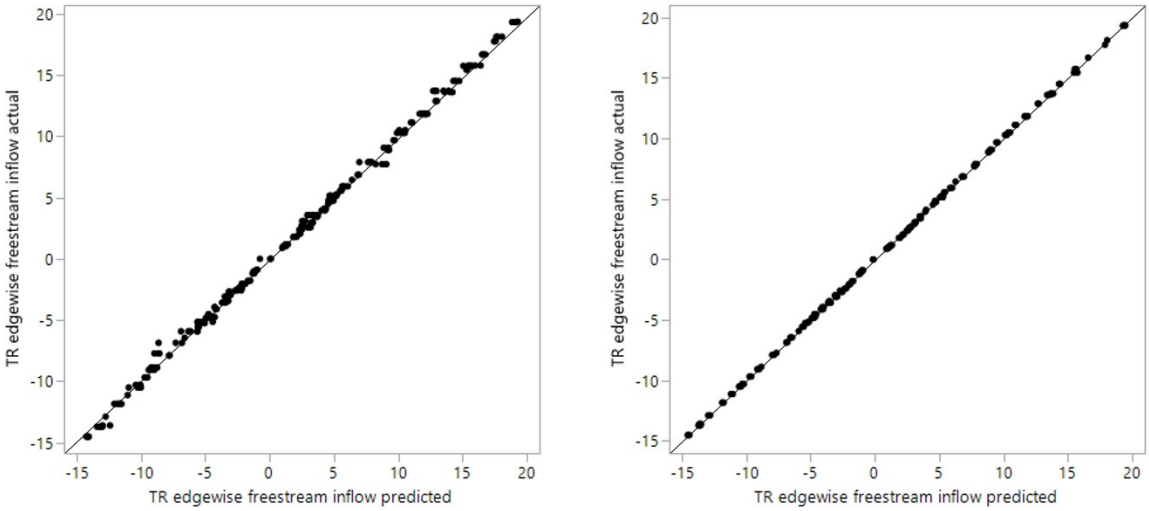

Figure C.5: Actual versus predicted plots of boosted tree model (left) and neural network model (right) for tail rotor edgewise freestream inflow.

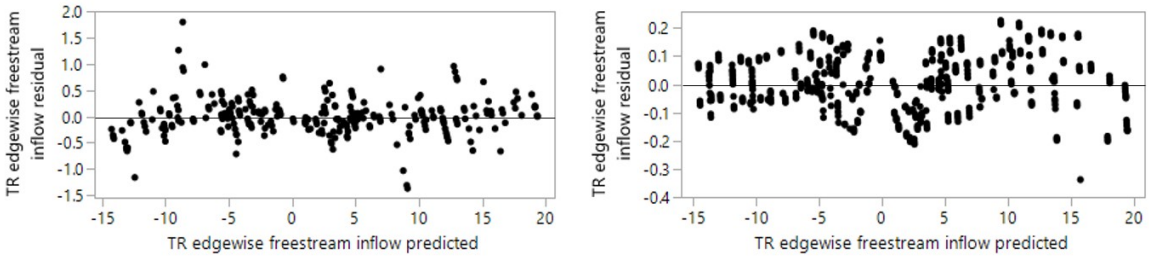

Figure C.6: Residual versus predicted plots of boosted tree model (left) and neural network model (right) for tail rotor edgewise freestream inflow.

Table C.4: Accuracy measures of surrogate models for tail rotor axial freestream inflow.

Predictive model	R^2	RMSE
Boosted decision tree	0.9923	0.3417
Artificial neural network	0.9980	0.1324

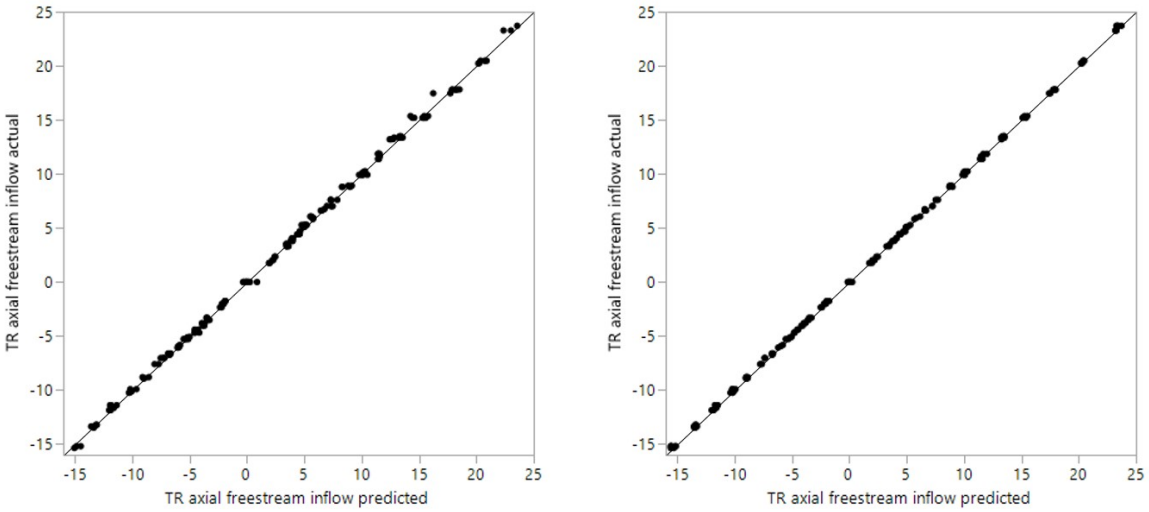

Figure C.7: Actual versus predicted plots of boosted tree model (left) and neural network model (right) for tail rotor axial freestream inflow.

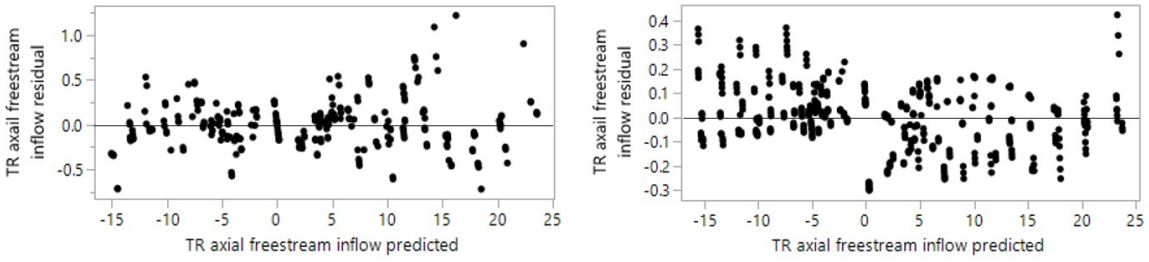

Figure C.8: Residual versus predicted plots of boosted tree model (left) and neural network model (right) for tail rotor axial freestream inflow.

REFERENCES

[1] K. B. Amer and A. Gessow, "Charts for Estimating the Tail-Rotor Contribution to Helicopter Directional Stability and Control in Low-Speed Flight," *NACA Report 1216*, 1955.

[2] F. Babič, L. Alexandra, and J. Paralič, "Descriptive and Predictive Analyses of Data Representing Aviation Accidents," in *Advances in Intelligent Systems and Computing*, vol. 314, 2015.

[3] F. J. Bailey, "A Simplified Theoretical Method of Determining the Characteristics of a Lifting Rotor in Forward Flight," *National Advisory Committee for Aeronautics - Report No. 716*, 1941.

[4] D. A. Balch, "Impact of Main Rotor Tip Geometry on Main Rotor-Tail Rotor Interactions in Hover," in *40th Annual Forum of the American Helicopter Society*, Alexandria, Virginia, 1984.

[5] S. D. Bay and M. Schwabacher, "Mining Distance-Based Outliers in Near Linear Time With Randomization and a Simple Pruning Rule," in *ACM SIGKDD International Conference on Knowledge Discovery and Data Mining*, 2003.

[6] T. S. Beddoes, "A Wake Model for High Resolution Airloads," in *U.S. Army/AHS Conference on Rotorcraft Basic Research*, North Carolina, 1985.

[7] Bell Helicopter Textron Inc., "Supplemental Operating & Emergency Procedures," *Operation Safety Notice 206-83-10*, 1983.

[8] Bell Helicopter Textron Inc., "Low Speed Flight Characteristics Which Can Result in Unanticipated Right Yaw," *Information Letter 206-84-41/206L-84-27*, 1984.

[9] M. D. Betzina, "Tiltrotor Descent Aerodynamics: A Small Scale Experimental Investigation of Vortex Ring State," in *American Helicopter Society 57th Annual Forum Proceedings*, Washington, D.C., 2001.

[10] K. Bhaduri, B. L. Matthews, and C. R. Giannella, "Algorithms for Speeding up Distance-Based Outlier Detection," in *ACM SIGKDD International Conference on Knowledge Discovery and Data Mining*, 2011.

[11] M. J. Bhagwat and J. G. Leishman, "Stability Analysis of Helicopter Rotor Wakes in Axial Flight," *Journal of the American Helicopter Society*, vol. 45, no. 3, 2000.

[12] M. J. Bhagwat and J. G. Leishman, "Stability, Consistency and Convergence of Time-Marching Free-Vortex Rotor Wake Algorithms," *Journal of the American Helicopter Society*, vol. 46, no. 1, 2001.

[13] J. C. Biggers, J. L. McCloud, and P. Patterakis, "Wind-Tunnel Tests of Two Full-Scale Helicopter Fuselages," *NASA Technical Note D-154-8*, 1962.

[14] C. L. Bottasso, G. Maisano, and F. Scorcelletti, "Trajectory Optimization Procedures for Rotorcraft Vehicles Including Pilot Models, With Applications to ADS-33 MTEs, Cat-A and Engine Off Landings," in *American Helicopter Society 65th Annual Forum and Technology Display*, vol. 1, Grapevine, Texas, 2009.

[15] A. R. S. Bramwell, G. Done, and D. Balmford, *Bramwell's Helicopter Dynamics*. Butterworth-Heinemann, 2001.

[16] A. Brand, R. Kisor, R. Blyth, D. Mason, and C. Host, "V-22 High Rate of Descent Test Procedures and Long Record Analysis," in *American Helicopter Society 60th Annual Forum Proceedings*, Baltimore, Maryland, 2004.

[17] A. G. Brand, M. A. Peryea, and T. L. Wood, "Flowfield and Download Measurements and Computation of a Tiltrotor in Hover," in *American Helicopter Society 57th Annual Forum Proceedings*, Washington, D.C., 2001.

[18] A. Brand, M. Dreir, R. Kisor, and T. Wood, "The Nature of Vortex Ring State," *Journal of the American Helicopter Society*, vol. 56, 2011.

[19] A. Brocklehurst, "Main Rotor/Tail Rotor Interactions Near Hover," *Westlands Research Memorandum 535*, 1986.

[20] A Brocklehurst, "Analysis of Tail Rotor Performance in Low Speed Quartering Flight," *GKN-WHL Report RSG/00/0180*, 2000.

[21] P. Brotherhood, "Flow Through a Helicopter Rotor in Vertical Descent," *Aeronautical Research Council, R&M No. 2735*, 1949.

[22] R. E. Brown, J. G. Leishman, S. Newman, and F. J. Perry, "Blade Twist Effects on Rotorcraft Behavior in the Vortex Ring State," in *28th European Rotorcraft Forum*, Bristol, England, 2002.

[23] S Budalakoti, S Budalakoti, A. N. Srivastava, and M. E. Otey, "Anomaly Detection and Diagnosis Algorithms for Discrete Symbol Sequences with Applications to Airline Safety," *IEEE Transactions on Systems, Man, and Cybernetics, Part C (Applications and Reviews)*, vol. 39, no. 1, 2009.

[24] W. J. Castles and J. H. DeLeeuw, "The Normal Component of the Induced Velocity in the Vicinity of a Lifting Rotor and Some Examples of Its Application," *NACA Report 1184*, 1954.

[25] W. J. Castles and R. B. Gray, "Empirical Relation Between Induced Velocity, Thrust, and Rate of Descent of a Helicopter Rotor as Determined by Wind Tunnel Tests on Four Model Rotors," *NACA Technical Note 2427*, 1951.

[26] I. C. Cheeseman and C. Haddow, "An Experimental Investigation of the Downwash Beneath a Lifting Rotor and Low Advance Ratios," in *14th European Rotorcraft Forum*, Milano, Italy, 1988.

[27] C. Chen, "Development of a Simplified Inflow Model for a Helicopter Rotor in Descent Flight," Ph.D. dissertation, Georgia Institute of Technology, 2006.

[28] R. T. N. Chen, "A Survey of Nonuniform Inflow Models for Rotorcraft Flight Dynamics and Control Applications," *NASA Technical Memorandum 102219*, 1989.

[29] H. J. Chin, A. P. Payan, C. Johnson, and D. N. Mavris, "Phases of Flight Identification for Rotorcraft Operations," in *AIAA Scitech 2019 Forum*, San Diego, California, 2019.

[30] Civil Aviation Authority, "Final Report on the Helicopter Operations Monitoring Programme (HOMP) Trial," *CAA Paper 2002/02*, 2002.

[31] Civil Aviation Authority, "Helicopter Tail Rotor Failures," *CAA Paper 2003/1*, 2003.

[32] Civil Aviation Authority, *Requirements and Guidance Material for Operators*. The Stationery Office, 2011, ch. 789.

[33] Civil Aviation Authority, *Flight Data Monitoring*. The Stationery Office, 2013, ch. 739.

[34] R. P. Coleman, A. M. Feingold, and C. Stempin, "Evaluation fo the Induced Velocity Field of an Idealized Helicopter Rotor," *NACA ARR No. L5E10*, 1945.

[35] F. N. Coton, R. A. M. Galbraith, T. Wang, and S. Newman, "Preliminary Results from a Wind Tunnel Based Study of Tail Rotor Blade Vortex Interaction," in *28th European Rotorcraft Forum*, Bristol, England, 2002.

[36] S. Das, L. Li, A. N. Srivastava, and R. John Hansman, "Comparison of Algorithms for Anomaly Detection in Flight Recorder Data of Airline Operations," in *12th AIAA Aviation Technology, Integration and Operations (ATIO) Conference and 14th AIAA/ISSMO Multidisciplinary Analysis and Optimization Conference*, 2012.

[37] S. Das, B. L. Matthews, A. N. Srivastava, and N. C. Oza, "Multiple Kernel Learning for Heterogeneous Anomaly Detection: Algorithm and Aviation Safety Case Study," in *ACM SIGKDD International Conference on Knowledge Discovery and Data Mining*, 2010.

[38] A. M. Dequin, "The Myth of Losing Tail Rotor Effectiveness," in *45th European Rotorcraft Forum*, Warsaw, Poland, 2019.

[39] J. Drees, L. R. Lucassen, and W. P. Hendal, "Airflow Through Helicopter Rotors in Vertical Flight," *National Aeronautical Research Institute, NLL Report V. 1535*, 1949.

[40] J. M. Drees, "A Theory of Airflow Through Rotors and Its Application to Some Helicopter Problems," *Journal of Helicopter Association of Great Britain*, vol. 3, no. 2, 1949.

[41] J. M. Drees and W. P. Hendal, "The Field of Flow Through a Helicopter Rotor Obtained from Wind Tunnel Smoke Tests," *National Aeronautical Research Institute, NLL Report A. 1205*, 1950.

[42] J. M. Drees and W. P. Hendal, "Airflow Patterns in the Neighbourhood of Helicopter Rotors," *Aircraft Engineering*, vol. 23, no. 266, 1951.

[43] M. E. Dreier, *Introduction to Helicopter and Tiltrotor Flight Simulation*. American Institute of Aeronautics and Astronautics, Inc., 2018.

[44] R. W. Du Val, "A Real-Time Blade Element Helicopter Simulation For Handling Qualities Analysis," in *Fifteenth European Rotorcraft Forum*, Amsterdam, The Netherlands, 1989.

[45] R. W. Du Val, "A Low Cost , High Fidelity Real-Time Rotorcraft Simulation for Control and Handling Qualities Analysis," in *HeliJapan 1998: AHS International Meeting on Rotorcraft Technology and Disaster Relief*, Gifu, Japan, 1998.

[46] R. W. Du Val, "A Real-Time Multi-Body Dynamics Architecture for Rotorcraft Simulation," in *American Helicopter Society and Royal Aeronautical Society International Conference on The Challenge of Realistic Rotorcraft Simulation*, London, UK, 2001.

[47] R. W. Du Val and C. He, "Validation of the FLIGHTLAB Virtual Engineering Toolset," *The Aeronautical Journal*, vol. 122, no. 1250, 2018.

[48] R. Du Val and C. He, "FLIGHTLAB TM Modeling for Real-Time Simulation Applications," *International Journal of Modeling, Simulation, and Scientific Computing*, vol. 8, no. 4, 2017.

[49] F. W. Dyson, "The Potential of an Anchor Ring," *Philosophical Transactions of the Royal Society A: Mathematical, Physical and Engineering Sciences*, vol. 184, 1893.

[50] A. D. S. Ellin, "An In-Flight Experimental Investigation of Helicopter Main Rotor/Tail Rotor Interactions," Ph.D. dissertation, University of Glasgow, 1993.

[51] A. D. S. Ellin, "An In-Flight Investigation of Lynx AH Mk 5 Main Rotor/Tail Rotor Interactions," in *19th European Rotorcraft Forum*, Cernobbio, Italy, 1993.

[52] R. W. Empey and R. A. Ormiston, "Tail-Rotor Thrust on a 5.5-Foot Helicopter Model in Ground Effect," in *American Helicopter Society 30th Annual National V/STOL Forum*, Washington, D.C., 1974.

[53] European Helicopter Safety Team, "Safety Considerations: Methods to Improve Helicopter Pilots' Capabilities," Köln, Germany, Tech. Rep., 2010.

[54] Federal Aviation Administration, "Unanticipated Right Yaw in Helicopters," *Advisory Circular 90-95*, 1995.

[55] Federal Aviation Administration, "Flight Operational Quality Assurance," *Advisory Circular 120-82*, 2006.

[56] Federal Aviation Administration, *Helicopter Flying Handbook*. United States Department of Transportation, 2012.

[57] Federal Aviation Administration, "Fact Sheet – Aviation Safety Information Analysis and Sharing (ASIAS) Program," Tech. Rep., 2019.

[58] R. V. Fernandes, "An Analysis of the Potential Benefits to Airlines of Flight Data Monitoring Programmes," *M.Sc. dissertation*, 2002.

[59] G. H. Gaonkar and D. A. Peters, "Effectiveness of Current Dynamic Inflow Models in Hover and Forward Flight," *Journal of the American Helicopter Society*, vol. 31, no. 2, 1986.

[60] G. H. Gaonkar and D. A. Peters, "Review of Dynamic Inflow Modeling for Rotorcraft Flight Dynamics," *27th Structures, Structural Dynamics and Materials Conference*, vol. 12, no. 3, 1988.

[61] A. Gavrilovski, "Predictive Helicopter Flight Data Monitoring for Flight Safety Design," Ph.D. dissertation, Georgia Institute of Technology, 2017.

[62] A. Gavrilovski, H. Jimenez, D. Mavris, A. H. Rao, K. Marais, S. Shin, and I. Hwang, "Challenges and Opportunities in Flight Data Mining: A Review of the State of the Art," in *AIAA Infotech @ Aerospace Conference*, San Diego, California, 2016.

[63] A. Gessow, "Review of Information on Induced Flow of a Lifting Rotor," *NACA Technical Note 3238*, 1954.

[64] H. Glauert, "A General Theory of the Autogyro," *Aeronautical Research Council R&M 1111*, 1926.

[65] H. Glauert, "The Analysis of Experimental Results in the Windmill Brake and Vortex Ring States of an Airscrew," *ARC R&M 1026*, 1926.

[66] H. Glauert, *Airplane Propellers*. Springer Verlag, 1935.

[67] F. D. Harris, "No Accidents—That's the Objective; The 26th Alexander A. Nikolsky Honorary Lectureship," *Journal of the American Helicopter Society*, vol. 52, no. 1, 2007.

[68] F. D. Harris, E. F. Kasper, and L. E. Iseler, "U.S. Civil Rotorcraft Accidents, 1963 Through 1997," *NASA Technical Memorandum-2000-209597*, 2000.

[69] E. D. Harrison, "A Methodology for Predicting and Mitigating Loss of Control Incidents for General Aviation Aircraft," Ph.D. dissertation, 2018.

[70] T. Hastie, R. Tibshirani, and J. Friedman, *The elements of statistical learning*. Springer, 2009.

[71] R. K. Heffley and M. A. Mnich, "Minimum-Complexity Helicopter Simulation Math Model," *NASA Contractor Report 177476*, 1988.

[72] H. H. Heyson and S. Katzoff, "Induced Velocities Near a Lifting Rotor with Nonuniform Disk Loading," *NACA Report 1319*, 1957.

[73] W. M. Hicks, "On the Mutual Threading of Vortex Rings," *Proceedings of the Royal Society A: Mathematical, Physical and Engineering Sciences*, vol. 102, 1922.

[74] J. J. Howlett, "UH-60A Black Hawk Engineering Simulation Program: Vol. I-Mathematical Model," *NASA CR-66309*, 1981.

[75] M. Hurst, T. Cramp, M. Collins, C. Delanghe, S. K. Lau, J. Morgan, M. Pilgrim, M. Price, C. Reed, and S. Tietjen, "Helicopter Flight Data Monitoring - Industry Best Practices," Tech. Rep. April, 2012.

[76] L. Iseler and J. De Maio, "An Analysis of U.S. Civil Rotorcraft Accidents by Cost and Injury (1990-1996)," *NASA Technical Memorandum-2002-209615*, no. May, 2002.

[77] G. James, D. Witten, T. Hastie, and R. Tibshirani, *An Introduction to Statistical Learning*. Springer, 2013.

[78] J. Jimenez, A. Desopper, and A. Taghizad, "Induced Velocity Model in Steep Descent and Vortex-Ring State Prediction," in *27th European Rotorcraft Forum*, Moscow, Russia, 2001.

[79] J. Jimenez, A. Taghizad, and L. Binet, "Helicopter Flight Tests in Steep Descents: Vortex-Ring State Analysis and Induced Velocity Models Improvement," in *CEAS-TRA3 Conference Royal Aeronautical Society*, Cambridge, United Kingdom, 2002.

[80] W. Johnson, *Helicopter Theory*. Dover Publications, Inc., 1994.

[81] W. Johnson, "Model for Vortex Ring State Influence on Rotorcraft Flight Dynamics," *NASA Technical Paper-2005-213477*, 2005.

[82] W. Johnson, "A History of Rotorcraft Comprehensive Analyses," *NASA Technical Paper-2012-216012*, 2012.

[83] K. Kampa, "Heliflow Task 2: Quartering Flight," in *ECD-TN-D/TA2-2000/0005*, 2000.

[84] A. Karpatne, J. Sirohi, S. Mula, and C. Tinney, "Vortex Ring Model of Tip Vortex Aperiodicity in a Hovering Helicopter Rotor," *Journal of Fluids Engineering*, vol. 136, 2014.

[85] I. W. Kaynes, G Preatoni, A Visingardi, N Tino, C Arzoumanian, K Kampa, C Hermans, B. S. M. Renier, F Tchen-Fo, and N Bettschart, "HELIFLOW

Pitch-Up and Quartering Flight Experiments," in *26th European Rotorcraft Forum*, The Hague, The Netherlands, 2000.

[86] H. Khan, G. Rasool, N. C. Bouaynaya, T. Travis, L. Thompson, and C. C. Johnson, "Explainable AI: Rotorcraft Attitude Prediction," in *Vertical Flight Society's 76th Annual Forum and Technology Display*, Virginia Beach, Virginia, 2020.

[87] R. Kisor, R. Blyth, A. Brand, and T. MacDonald, "V-22 High Rate of Descent Test Results," in *American Helicopter Society 60th Annual Forum Proceedings*, Baltimore, Maryland, 2004.

[88] M. Kuhn and K. Johnson, *Applied predictive modeling*. Springer, 2013.

[89] A. J. Landgrebe, "The Wake Geometry of a Hovering Helicopter Rotor and Its Influence on Rotor Performance," *Journal of the American Helicopter Society*, vol. 17, no. 4, 1972.

[90] B. Lanz, *Machine Learning with R*. Packt Publishing, 2015.

[91] A. F. Lehman, "Model Studies of Helicopter Tail Rotor Flow Patterns In and Out of Ground Effect," *USAAVLABS Technical Report 71-12*, 1971.

[92] G. J. Leishman, *Principles of Helicopter Aerodynamics*. Cambridge University Press, 2006.

[93] J. G. Leishman, M. J. Bhagwat, and S. Ananthan, "The Vortex Ring State as a Spatially and Temporally Developing Wake Instability," in *American Helicopter Society International Specialists Meeting on Aerodynamics, Acoustics, and Test and Evaluation*, San Francisco, California, 2002.

[94] J. W. Leverton, J. S. Pollard, and C. R. Wills, "Main Rotor Wake-Tail Interaction," *Vertica*, vol. 1, no. 2, 1977.

[95] S. Lewis and S. Kris, "Lessons Learned from Real World Application of the Bow-tie Method," in *6th Global Congress on Process Safety*, San Antonio, Texas, 2010.

[96] L. Li, S. Das, R. J. Hansman, R. Palacios, and A. N. Srivastava, "Analysis of Flight Data Using Clustering Techniques for Detecting Abnormal Operations," *Journal of Aerospace Information Systems*, vol. 12, no. 9, 2015.

[97] L. Li, M. Gariel, R. J. Hansman, and R. Palacios, "Anomaly Detection in Onboard-Recorded Flight Data Using Cluster Analysis," in *AIAA/IEEE Digital Avionics Systems Conference*, 2011.

[98] C. N. H. Lock and H. Bateman, "Some Experiments on Airscrews at Zero Torque, With Applications to a Helicopter Descending with the Engine "Off," and to the Design of Windmills," *Aeronautical Research Council, R&M No. 885*, 1923.

[99] C. N. H. Lock, H. Bateman, and H. C. H. Townend, "An Extension of the Vortex Theory of Airscrews with Applications to Airscrews of Small Pitch, Including Experimental Results," *Aeronautical Research Counsil, R&M No. 1014*, 1926.

[100] O. Maimon and L. Rokach, *Data mining and knowledge discovery handbook*. Springer Science & Business Media, 2005.

[101] K. W. Mangler and H. B. Squire, "The Induced Velocity Field of a Rotor," *Aeronautical Research Council TR No. 2642*, 1953.

[102] A. H. Modaress-Aval, F. Bakhtiari-Nejad, E. H. Dowell, H. Shahverdi, H. Rostami, and D. A. Peters, "Aeroelastic Analysis of Cantilever Plates Using Peters' Aerodynamic Model, and the Influence of Choosing Beam or Plate Theories as the Structural Model," *Journal of Fluids and Structures*, vol. 96, 2020.

[103] S. Mula, J. Stephenson, C. Tinney, and J. Sirohi, "Dynamical and Evolutionary Characteristics of the Tip Vortex From a Four Bladed Rotor in Hover," in *American Helicopter Society 68th Annual Forum*, Fort Worth, Texas, 2012.

[104] R. H. Myers, D. C. Montgomery, and C. M. Anderson-Cook, *Response surface methodology: process and product optimization using designed experiments*. John Wiley & Sons, 2016.

[105] A. Nanduri and L. Sherry, "Anomaly detection in aircraft data using Recurrent Neural Networks (RNN)," in *ICNS 2016: Securing an Integrated CNS System to Meet Future Challenges*, Herndon, Virginia, 2016.

[106] National Transportation Safety Board, "Expand Use of Recorders to Enhance Transportation Safety," *Most Wanted Trasportation Safety Improvements*, 2016.

[107] National Transportation Safety Board, "Loss of Tail Rotor Effectiveness in Helicopters," Tech. Rep., 2017.

[108] S. Newman, *The Foundations of Helicopter Flight*. Edward Arnold, 1994.

[109] S. Newman, R. Brown, J. Perry, S. Lewis, M. Orchard, and A. Modha, "Predicting the Onset of Wake Breakdown for Rotors in Descending Flight," *Journal of the American Helicopter Society*, vol. 48, no. 1, 2003.

[110] A. J. Niemi and P. Sutcliffe, "Leapfrogging Vortex Rings in the Landau-Lifshitz Equation," *Nonlinearity*, vol. 27, no. 9, 2014.

[111] Y. Okuno and K. Kawachi, "Optimal Control of Helicopters Following Power Failure," *Journal of Guidance, Control, and Dynamics*, vol. 17, no. 1, 1994.

[112] Y. Okuno, K. Kawachi, A. Azuma, and S. Saito, "Analytical Prediction of Height-Velocity Diagram of a Helicopter Using Optimal Control Theory," *Journal of Guidance, Control, and Dynamics*, vol. 14, no. 2, 1991.

[113] R. A. Ormiston and D. A. Peters, "Hingeless Helicopter Response with Nonuniform Inflow and Elastic Blade Bending," *Journal of Aircraft*, vol. 9, no. 10, 1972.

[114] G. D. Padfield, *Helicopter Flight Dynamics Including a Treatment of Tiltrotor Aircraft*. John Wiley & Sons, 2018.

[115] P. R. Payne, *Helicopter Dynamics and Aerodynamics*. Macmillan, 1959.

[116] D. A. Peters, "Hingeless Rotor Frequency Response with Unsteady Aerodynamics," *AHS/NASA Specialists' Meeting on Rotorcraft Dynamics, NASA SP-362*, 1974.

[117] D. A. Peters, D. D. Boyd, and C. J. He, "A Finite-State Induced-Flow Model for Rotors in Hover and Forward Flight," *Journal of the American Helicopter Society*, vol. 34, no. 4, 1989.

[118] D. A. Peters and C. He, "Correlation of Measured Induced Velocities with a Finite-State Wake Model," *Journal of the American Helicopter Society*, vol. 36, no. 3, 1991.

[119] D. A. Peters, "Momentum Theory, Dynamic Inflow, and the Vortex-Ring State," *Journal of the American Helicopter Society*, vol. 27, no. 3, 1982.

[120] D. A. Peters, "How Dynamic Inflow Survives in the Competitive World of Rotorcraft Aerodynamics; The 28th Alexander A. Nikolsky Honorary Lectureship," *Journal of the American Helicopter Society*, vol. 54, no. 1, 2009.

[121] D. M. Pitt and D. A. Peters, "Theoretical Prediction of Dynamic-Inflow Derivatives," *Vertica*, vol. 5, no. 1, 1981.

[122] R. W. Prouty, *Development of the Empennage Configuration of the YAH-64 Advanced Attack Helicopter*. U.S. Army Aviation Research and Development Command, 1983.

[123] R. W. Prouty, *Helicopter Performance, Stability, and Control*. Krieger Publishing Company, 2005.

[124] T. Puranik, E. Harrison, S. Min, H. Jimenezy, and D. Mavrisz, "General Aviation Approach and Landing Analysis Using Flight Data Records," in *16th AIAA Aviation Technology, Integration, and Operations Conference*, 2016.

[125] F. B. Reeder J. P. Gustafson, "On the Flying Qualities of Helicopters," *NACA Technical Note 1799*, 1949.

[126] Royal Australian Air Force, "Bell 206B-1 Directional Control in Low Airspeed Flight," *Report No. ARDU-TI-721*, 1981.

[127] J. Sall, M. Stephens, A. Lehman, and S. Loring, *JMP Start Statistics: A Guide to Statistics and Data Analysis Using JMP*. Sas Institute, 2017.

[128] J. Scheiman, "A Tabulation of Helicopter Rotor-Blade Differential Pressures, Stresses, and Motions as Measured in Flight," *NASA Technical Memorandum-X 952*, 1964.

[129] M. P. Scully, "Computation of Helicopter Rotor Wake Geometry and its Influence on Rotor Harmonic Airloads," Ph.D. dissertation, 1975.

[130] C. D. M. Snellen, "OH-58 Loss of Tail Rotor Effectiveness; Why It Occurs," *United States Army Aviation Digest*, vol. 30, no. 9, 1984.

[131] V. Srinivas, I. Chopra, D. Haas, and K. McCool, "Prediction of Yaw Control Effectiveness and Tail Rotor Loads," in *19th European Rotorcraft Forum*, Cernobbio (Como), Italy, 1993.

[132] J. Stack, F. X. Carradonna, and O. Savas, "Flow Visualization and Extended Thrust Time Histories of Rotor Wakes in Descent," in *4th Decennial Specialists Conference on Aeromechanics*, San Francisco, California, 2004.

[133] W. Stewart, "Helicopter Behaviour in the Vortex-Ring Conditions," *Aeronautical Research Council, R&M No. 3117*, 1951.

[134] A. J. Stolzer and C. Halford, "Data Mining Methods Applied to Flight Operations Quality Assurance Data: A Comparison to Standard Statistical Methods," *Journal of Air Transportation*, vol. 12, no. 1, 2007.

[135] A. Taghizad, J. Jimenez, L. Binet, and D. Heuze, "Experimental and Theoretical Investigations to Develop a Model of Rotor Aerodynamics Adapted to Steep Descents," in *American Helicopter Society 58th Annual Forum Proceedings*, Montreal, Canada, 2002.

[136] P. D. Talbot, B. E. Tinling, W. A. Decker, and R. T. N. Chen, "A Mathematical Model of a Single Main Rotor Helicopter for Piloted Simulation," *NASA Technical Memorandum 84281*, 1982.

[137] P. C. Tarttelin and A. W. Martyn, "In Flight Research with Instrumented Main and Tail Rotor Blades Using the DRA Bedford Aeromechanics Research Lynx Helicopter," *AGARD CP-552*, 1994.

[138] U.S. Army Aviation Engineering Flight Activity, "Preliminary Airworthiness Evaluation OH-58C Helicopter," *USAAEFA Project No. 76-11-1*, 1978.

[139] U.S. Army Aviation Engineering Flight Activity, "Airworthiness and Flight Characteristics Evaluation OH-58C Interim Scout Helicopter," *USAAEFA Project No. 76-11-2*, 1979.

[140] U.S. Army Aviation Engineering Flight Activity, "Loss of Tail Rotor Effectiveness Evaluation of the OH-58C Helicopter with Directional SAS," *USAAEFA Project No. 86-22*, 1988.

[141] U.S. Helicopter Safety Team, "Helicopter Safety Enhancements: Loss of Control – Inflight, Unintended Flight in IMC, and Low-Altitude Operations," Tech. Rep., 2017.

[142] K. Vladislav and E. A. Morelli, *Aircraft system identification: theory and practice*. Ameircan Institute of Aeronautics and Astronautics, 2006.

[143] A. Vuillet, "Rotor and Blade Aerodynamic Design," *AGARD R-781*, 1990.

[144] S. Wang, "Analytical Approach to the Induced Velocity of a Helicopter Rotor in Vertical Descent," *Journal of the American Helicopter Society*, vol. 35, no. 1, 1990.

[145] K. Washizu, A. Azuma, J. Koo, and T. Oka, "Experiments on a Model Helicopter Rotor Operating in the Vortex Ring State," *Journal of Aircraft*, vol. 3, no. 3, 1966.

[146] F. White and B. B. Blake, "Improved Method of Predicting Helicopter Control Response and Gust Sensitivity," in *35th Annual Forum of the American Helicopter Society*, Washington D.C., 1979.

[147] W. Wiesner and G. Kohler, "Design Guidelines for Tail Rotors," *US Army USAAMRDL Report 0210- 10687-1*, 1973.

[148] W. Wiesner and G. Kohler, "Tail Rotor Design Guide," Boeing Vertol Company, Tech. Rep., 1974.

[149] J. E. Wilborn and J. V. Foster, "Defining Commercial Transport Loss-Of-Control: A Quantitative Approach," *AIAA Atmospheric Flight Mechanics Conference*, vol. 1, 2004.

[150] L. Williamson, "Monitoring Flight Operations Using Flight Recorded Data," in *AIAA/AHS/ASEE Aircraft Deisgn, Systems and Operations Conference*, 1989.

[151] J. C Wilson and R. E. Mineck, "Wind-Tunnel Investigation of Helicopter-Rotor Wake Effects on Three Helicopter Fuselage Models," *NASA Technical Memorandum X-3185*, 1975.

[152] I. H. Witten and E. Frank, *Data Mining: Practical machine learning tools and techniques*. 2005.

[153] J. Wolkovitch, "Analytic Prediction of Vortex Ring Boundaries," *Journal of the American Helicopter Society*, vol. 17, no. 3, 1972.

[154] T. Wood, "Fifty Years of Industry Perspective; The 36th Alexander A. Nikolsky Honorary Lectureship," in *AHS International's 72th Annual Forum & Technology Display*, West Palm Beach, Florida, 2016.

[155] P. F. Yaggy and K. W. Mort, "Wind-Tunnel Tests of Two VTOL Propellers in Descent," *NASA Technical Note D-1766*, 1963.

[156] J. E. Yeates, "Flight Measurements of the Vibration Experienced by a Tandem Helicopter in Transition, Vortex-Ring State, Landing Approach, and Yawed Flight," *NACA Technical Note 4409*, 1958.

[157] C. Young, "A Note on the Velocity Induced by a Helicopter Rotor in the Vortex Ring State," *RAE Technical Report 78125*, 1978.

[158] P. Zanella, K. B. Collins, C. C. Johnson, and D. N. Mavris, "Filter-Based Detection of the Proximity to Loss of Tail Rotor Effectiveness Within Helicopter Flight Data Monitoring," in *Vertical Flight Society 75th Annual Forum & Technology Display*, Philadelphia, Pennsylvania, 2019.

[159] P. Zanella, J. V. R. Prasad, C. C. Johnson, and D. N. Mavris, "A Physics-Based Investigation of Loss of Tail Rotor Effectiveness," in *Vertical Flight Society's 77th Annual Forum & Technology Display*, Palm Beach, Florida, 2021.

[160] W. Zhao, F. He, L. Li, and G. Xiao, "An Adaptive Online Learning Model for Flight Data Cluster Analysis," in *IEEE/AIAA 37th Digital Avionics Systems Conference (DASC)*, 2018.